SAPIENZA
UNIVERSITÀ DI ROMA

Strange-metal behavior of cuprates driven by dissipative charge collective modes

Facoltà di Scienze Matematiche, Fisiche e Naturali
Fisica (XXXVI cycle)

Giovanni Mirarchi
ID number 1700140

Advisor
Prof. Sergio Caprara

Academic Year 2022/2023

Strange-metal behavior of cuprates driven by dissipative charge collective modes
PhD thesis. Sapienza University of Rome

This thesis has been typeset by LaTeX and the Sapthesis class.

Version: May 14, 2024

Author's email: giovannimirarchi96@gmail.com

To my family,
in the broadest
sense of the term.

Abstract

This work focuses on the study of high-temperature superconducting copper oxides, commonly known in the literature as *cuprates*. Beyond high-temperature superconductivity, these systems are characterized by a complex phenomenology which shows considerable deviations from the standard theory of metals and whose comprehensive understanding is still an open problem in condensed matter theory. Within our discussion, we will analyze some of the most remarkable physical phenomena observed in the so-called *strange-metal phase* of cuprates, for which there is still no unanimously shared theory that can explain them exhaustively. In the description that we will propose, a central role is played by appropriate short-ranged charge collective modes, recently observed throughout the strange-metal phase thanks to the RIXS experiments. Under suitable hypotheses regarding the Landau damping to which these collective modes are subject, we will show that they are capable of inducing a strange-metal behavior in the systems in which they are present. A discussion on the strongly anisotropic properties observed in the metallic phase of some cuprate thin films is also included.

Contents

Thesis outline

Superconductivity is a fascinating quantum phenomenon whereby the electrical resistivity of certain materials abruptly vanishes below a particular temperature value, commonly known as *critical temperature*. Though this phenomenon was discovered in 1911 by the Dutch physicist Heike Kamerlingh Onnes [1], the first microscopic theory of superconductivity was proposed only in 1957 by John Bardeen, Leon N. Cooper, and Robert Schrieffer, which was named *BCS theory* after them [2]. According to this theory, superconductivity is the result of an attractive coupling between electrons mediated by phonons. This theory describes accurately the behavior of conventional superconductors, whose superconducting properties manifest themselves below the critical temperature. For standard metals, this critical temperature ranges from less than 1 K to about 20 K.

In 1986, Johannes Georg Bednorz and Karl Alexander Müller observed the first example of high-temperature superconductivity in the doped lanthanum barium copper oxide, characterized by a critical temperature of 35 K [3, 4], and it was soon found that the substitution of lanthanum with yttrium raised the critical temperature above 90 K [5]. That was only the first of a long series of copper oxide-based (also known as *cuprates*) superconductors identified during the following decades, characterized by critical temperatures even higher than 100 K. In particular, the highest cuprate critical temperature was observed in 1993 in a sample of mercury iron calcium copper oxide, as high as 135 K [6]. Such high critical temperatures cannot be explained within the standard theory of phonon-mediated superconductivity, moreover a complete theory of superconductivity in these materials has not been developed yet and it is one of the major challenges of theoretical condensed matter physics.

Though high-temperature superconductivity is surely a quite interesting observed phenomenon in cuprates, these systems exhibit anomalous behavior even in their non-superconducting phase, which cannot be explained by the standard paradigm of the Landau theory for the metallic state. These phenomena involve mainly thermodynamic and transport properties, and show sensible deviations from those observed in ordinary metals. This work is aimed exclusively at the study of some of these latter properties, without addressing the issue of high-temperature superconductivity. From the first observation of the anomalous features of cuprates until today, various proposals have been put forward for the explanation of the vast phenomenological landscape which characterize these systems. A point of view which has found a remarkable support within the scientific community identifies some kind of low-energy

collective excitations as mediators of an effective interaction between electrons. Not only these excitations would be responsible of the coupling between electrons that would lead to superconductivity, but they could also provide the explaination to the vastness of phenomena which take place in the so-called *strange-metal phase*. What is still under discussion is the nature of these excitations. According to several theories (including ours), these excitations would be the consequence of the proximity of the system to some ordered state, involving for instance spin or charge degrees of freedom, or circulating currents [7, 8, 9]. It is known that close to an ordered phase strong fluctuations of the degrees of freedom that are going to order appear. These fluctuations assume the form of collective modes that could couple with electrons and effectively mediate an interaction leading to superconductivity. Based on the results of recent resonant X-ray scattering experiments [10], we attribute the role of dominant mediator of the interaction between electrons to dynamic fluctuations of charge density profile taking place near a charge ordered state, and we are going to show how these collective modes can affect the thermodynamic and transport properties of cuprates. Given these premises, the present work will be articulated as follows:

- In the first chapter we will exhibit the main phenomenological properties of cuprates, with particular attention to the experimental observation of the charge order, which will play a central role within our work.
- In chapter 2 we will provide the main theoretical concepts that we will use to describe the physical properties of our interest.
- Chapter 3 is dedicated to the study of a preliminary model to the one we will actually use in the description of cuprates. We are going to show that this model, despite its simplicity, has several interesting physical features which will remain preserved even in the more accurate model that we will adopt in subsequent chapters.
- In chapters 4 and 5 we will deal, respectively, with the anomalous thermodynamic and transport properties observed in the strange-metal phase of cuprates. In the model we will use, a central role will be played by the charge fluctuation modes, which we require to be abnormally damped.
- As a conclusion to the study of the strange-metal phase issue, in chapter 6 we will propose a microscopic mechanism that could induce the required dissipation for our charge modes.
- In chapter 7 we will instead deal with the question of some anisotropic properties observed in suitable cuprate thin films.
- Lastly, in chapter 8, we will make some concluding remarks and discuss the future perspectives of our work.

Although our study is focused on cuprates, it is noteworthy to point out that the strange-metal phenomenology has also been observed in several other types of systems, such as iron-based superconductors [11], heavy fermion metals [12] or twisted bilayer graphene [13]. Many of the ideas we will discuss have a rather broad validity

and can also be extended to other systems. However, since our work takes significant advantage of our collaboration with experimental groups in Milan and Göteborg, with a longstanding experience in transport and x-ray measurements on cuprates, for the sake of concreteness we will always confront experiments carried out on cuprates.

With the exception of chapter 7, the systems we will study are characterized by tetragonal symmetry. For simplicity, we will consider the in-plane lattice spacing a as the reference unit for length, i.e. $a = 1$. We also set $\hbar = 1$, therefore frequency variables have the same dimension as energies, while time variables have the dimension of the reciprocal of an energy. Throughout the discussion, we will treat the terms "energy" and "frequency" essentially as synonyms, we will also do the same with the terms "momentum" and "wave vector" (these latter quantities are dimensionless in our units). The elementary charge e (not to be confused with the Napier's constant e) is expressed in standard SI units, and it's positive (therefore, the electron charge is equal to $-$e). We choose to express also Boltzmann constant k_{B} in its SI units, therefore energy and temperature are dimensionally different. The inverse temperature β is defined as $(k_{\mathrm{B}}T)^{-1}$ and has the dimension of the reciprocal of an energy. We give here our definitions for the Bose and the Fermi functions (respectively) according to our conventions:

$$b(\omega) \coloneqq \frac{1}{e^{\beta\omega} - 1} \qquad f(\omega) \coloneqq \frac{1}{e^{\beta\omega} + 1} \qquad \text{where} \quad \beta \coloneqq \frac{1}{k_{\mathrm{B}}T}$$

Of course, $b(\omega)$ and $f(\omega)$ are functions of both energy ω and temperature T, however to soften the notation we will always leave the temperature dependence implicit. The only argument of these two functions is energy, which is in general a complex quantity. As for the Fourier transforms in time and space variables, we will adopt the following conventions and notations, unless expressly indicated otherwise (further details are given in Appendix A):

$$\mathcal{F}_t\Big[F(t)\Big] \coloneqq \int_{-\infty}^{+\infty} F(t)e^{i\omega t}dt \coloneqq \hat{F}(\omega) \qquad F(t) = \mathcal{F}_\omega^{-1}\Big[\hat{F}(\omega)\Big] \coloneqq \int_{-\infty}^{+\infty} \hat{F}(\omega)e^{-i\omega t}\frac{d\omega}{2\pi}$$

$$\mathcal{F}_{\mathbf{x}}\Big[F(\mathbf{x})\Big] \coloneqq \int_V F(\mathbf{x})e^{-i\mathbf{k}\mathbf{x}}d^{\mathrm{d}}\mathbf{x} \coloneqq \hat{F}(\mathbf{k}) \qquad F(\mathbf{x}) = \mathcal{F}_{\mathbf{k}}^{-1}\Big[\hat{F}(\mathbf{k})\Big] \coloneqq \frac{1}{V}\sum_{\mathbf{k}\in\mathbb{R}^{\mathrm{d}}} \hat{F}(\mathbf{k})e^{i\mathbf{k}\mathbf{x}}$$

As is customary, we use bold letters to denote vectors and distinguish them from scalar quantities (such as t or ω). In particular, we will use $\mathbf{x}$, $\mathbf{y}$ and $\mathbf{r}$ to denote the displacements, while we will use $\mathbf{k}$, $\mathbf{p}$ and $\mathbf{q}$ to denote the wave vectors.

Chapter 1

Phenomenological landscape

1.1 General properties of cuprates

Following the first observation of high-temperature superconductivity in a cuprate compound by Bednorz and Müller in 1986 [3], which earned them the Nobel Prize only the following year, research on these materials surged and many other cuprate superconductors have been identified over the years. In addition to high-temperature superconductivity, all of these compounds share a number of interesting properties that are not yet fully understood.

From a formal point of view, cuprates constitute a class of three-dimensional layered materials, characterized by the alternation of copper oxygen planes (which we will refer to as CuO_2 planes) and layers made of oxygen and other metals. While these latter layers act essentially as charge reservoir for the CuO_2 planes, the most relevant physical process concern precisely these CuO_2 planes, as supported both by theoretical considerations and experiments [14]. In particular, a general property of all cuprate compounds is that the charge carriers reside on the CuO_2 planes. Given the importance of these planes in cuprate physics, these systems are usually classified according to the number of CuO_2 planes per unitary cell, we have for instance:

- Single-layer (for example $La_{2-x}Sr_xCuO_4$, $Nd_{2-x}Ce_xCuO_4$, $Bi_2Sr_2CuO_{6+\delta}$ or $La_{2-x}Ba_xCuO_4$).
- Bilayer (for example $Bi_2Sr_2CaCu_2O_{8+\delta}$, $YBa_2Cu_3O_{7-\delta}$ or $Nd_{1+x}Ba_{2-x}Cu_3O_{7-\delta}$).
- Trilayer (for example $Bi_2Sr_2Ca_2Cu_3O_{10+\delta}$).

This structural characteristic affects several physical properties, including superconductivity. In particular, in each family of cuprates the critical temperature basically increases with the number of CuO_2 planes per unitary cell. For the exemplary case of Bi-based cuprate superconductors, the maximum value of the critical temperature is found at 34 K, 96 K and 110 K respectively for the single-layer, the bilayer and the trilayer compound [15].

Experimentally, it is known not only that the most significant physical processes occur in the CuO_2 planes, but also that the interaction between the different layers is

generally weak. For this reason, cuprates are essentially described as two-dimensional systems [16]. Each of the lattice planes is itself a (clearly two-dimensional) Bravais lattice, and the superposition of these layers defines a three-dimensional Bravais superlattice structure. An interesting property shared by most of cuprate compounds is that the CuO_2 layers have tetragonal symmetry, at least in the bulk state. Only few specific cuprate compounds exhibit a slightly orthorhombic structure, among these the most relevant case is that of $YBa_2Cu_3O_{7-\delta}$, of which many bulk properties are however very similar to those expected from a tetragonal structure [17, 18]. Significant in-plane anisotropy has been observed in thin films, whose physics is dominated by surface and interface properties [19, 20]. For these reasons, except for few particular cases, the two planar directions (henceforth x- and y- directions) can be treated interchangeably for the description of many physical properties. The strong structural anisotropy between the planar direction and the one orthogonal to the layers (henceforth z-direction) is evident from the transport phenomena. The DC resistivity, for instance, is much larger along the z-direction than along the other two directions [16, 21, 22]. Although the description of cuprates as two-dimensional systems is effective and sound, the coupling between the planes, despite being of weak intensity, is responsible for the long-range correlation phenomena, which would be otherwise forbidden in strictly two-dimensional systems at finite temperature due to the Mermin-Wagner theorem [23].

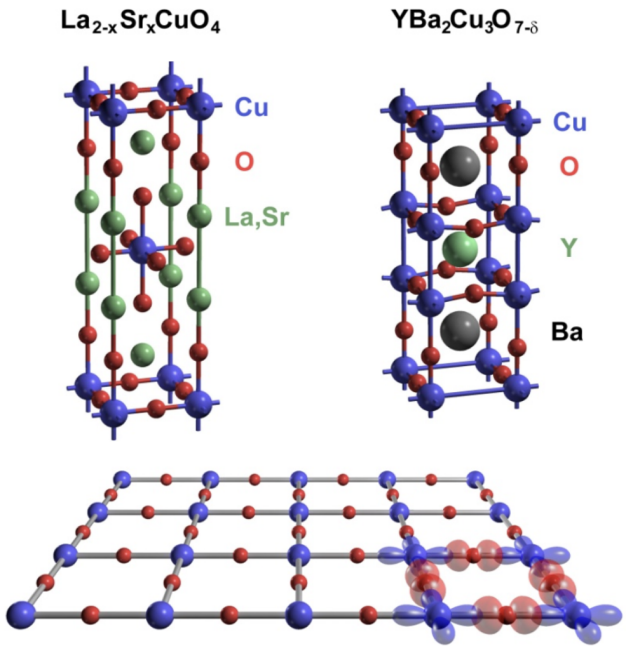

Figure 1.1. From [24], illustration of the unit cells of two cuprate compounds and a CuO_2 layer. The orbitals $d_{x^2-y^2}$ and p_σ, on the Cu and O atoms respectively, are also shown.

In order to illustrate these concepts in a more concrete way, let's consider for instance the $La_{2-x}Sr_xCuO_4$ compound, which is one of the first high-temperature superconductors discovered and which also has one of the simplest lattice structures [15]. In the unit cell, all oxygen atoms are in a O^{2-} valence state, which allows them to complete their p shell. In order to maintain charge neutrality, eight positive charges are required. Six of them come from two lanthanum atoms in a stable La^{3+} valence state configuration, while the remaining two come from the copper atom in its Cu^{2+} state. This results in a hole in the d shell of the copper atom, imparting a net 1/2 spin to it. The copper atom is surrounded by six oxygen atoms, with four belonging to its same

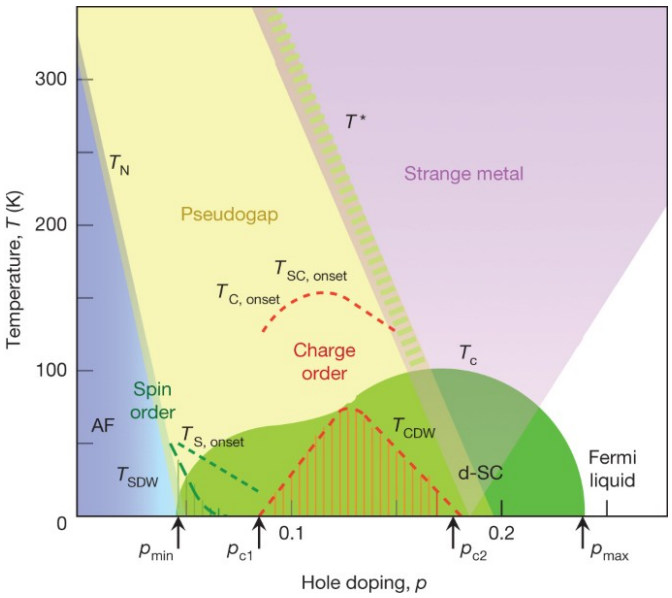

Figure 1.2. From [25], a typical phase diagram of a cuprate superconductor. The blue and green regions indicate antiferromagnetic order and d-wave superconducting order, delimited respectively by Néel temperature T_N and critical temperature T_c. The red striped area, T_{CDW}, indicates the presence of fully developed charge order. The subscript "onset" appearing in the other temperature scales indicates that the order expected at such temperatures is not fully developed.

CuO_2 plane and the other two belonging to the charge reservoir planes. While the distance between the copper atom and the oxygen atoms coplanar to it is approximately 1.9 Å, the distance with the oxygen atoms of the adjacent layers is about 2.4 Å. The interaction in this latter case is therefore weaker and, consequently, less relevant for the various microscopic phenomena. A sketch of the unit cell of the $La_{2-x}Sr_xCuO_4$ compound, as well as a comparison with a $YBa_2Cu_3O_{7-\delta}$ one, is reported in figure 1.1, where the structure of the CuO_2 lattice planes is also illustrated.

As is evident from the chemical structures of the cuprate compounds we have exhibited, these solids are generally non-stoichiometric. The reason is that many of the most interesting phenomenological aspects of these materials are observed in doped compounds. The procedure of doping consists in replacing an element in the charge reservoir layers with an heterovalent one, as for the $La_{2-x}Sr_xCuO_4$ case, or in changing the concentration of interstitial oxygen atoms, as in the case of $YBa_2Cu_3O_{7-\delta}$. We talk about *electron-doped* or *hole-doped* compounds respectly if we increase or decrease the electron concentration in the CuO_2 planes. For instance, in order to get the superconducting compound $La_{2-x}Sr_xCuO_4$ it is necessary to substitute divalent Sr for trivalent La in the stoichiometric compund La_2CuO_4, in this case x denotes the number of holes per Cu atom and therefore it represents the hole-doping level. Although cuprates present a rich and interesting phenomenology in both the electron-doped and hole-doped cases, the most discussed case in the literature is the latter, so much so that the term "doping" is often used as a substitute for "hole-doping" within this context. For brevity, we will also often adopt this terminological convention throughout this thesis.

A typical cuprate phase diagram, as the one shown in figure 1.2, is represented on a Cartesian plane whose x-axis indicates the doping level (usually denoted with p), while the y-axis indicates the temperature. From this diagram, which well describes the behavior of all compounds transversally, the coexistence and competition of

several phases is evident. For instance, a general feature of cuprates is that they are *Mott insulators* at low doping level [26], as a consequence of the fact that the local electron-electron repulsion energy dominates over the bandwidth. By taking for example the already mentioned case of $La_{2-x}Sr_xCuO_4$ compound, we know that in the case $x = 0$ the copper atom in its cell is in a Cu^{2+} state, so it has a single hole in its d shell. The band is therefore half-filled, so a metallic behavior would be expected, but since the local repulsive energy cost needed to put two holes on the same ion is greater than the hole hopping energy the material actually behaves as an insulator. This phase is also characterized by an antiferromagnetic order due to the so-called *superexchange* mechanism [27, 28], which provides a significant energy gain given by the virtual hopping when the spins of neighboring holes are oppositely aligned. By its very nature, this insulating phase is very sensitive to the concentration of charge carriers, and in fact it is easily spoiled upon doping. It is generally sufficient to have a hole concentration between 3% and 5% to suppress the antiferromagnetic order and to make the superconductivity phase appear. This phase is characterized by a doping-dependent critical temperature T_c, which has a maximum point at a particular doping level, commonly known as *critical doping* or *optimal doping* and denoted with p_c. Compounds with doping less or higher than the optimal are respectively called *underdoped* and *overdoped*. Superconductivity in cuprates is known to involve a d-wave pairing, which was predicted by several theoretical models [29, 30, 31] and confirmed by several experiments [32, 33]. A widely shared point of view attributes the origin of superconductivity to some exotic collective excitation which could be responsible for mediating the coupling between electrons, instead of the standard electron-phonon coupling mechanisms at play in conventional superconductivity.

Finally, we observe that the phase diagram represented in figure 1.2, above the superconducting dome, is essentially divided into three regions, denoted as *pseudogap phase*, *strange-metal phase* and *Fermi liquid phase*. This tripartition can be extended below the superconducting dome, as the latter can be removed through the application of strong enough magnetic fields. The two partition lines beneath the superconducting dome seem to converge at the same point at $T = 0$, which is very close to the optimal doping. According to standard theory of critical phenomena [34, 35], these aspects seem to be compatible with a *quantum critical point* scenario. A quantum critical point is a point on the phase diagram in which a second-order phase transition occurs at zero temperature, when an appropriate control parameter (which, in this case, is the doping level) varies. At finite temperature, a so-called "quantum critical region" is established between the two phases (ordered and disordered) which at zero temperature are separated by the critical point. We would like to point out that, regarding the question of the quantum critical point in hole-doped cuprates, there is not yet a unanimously shared point of view among the scientific community. While the idea itself that the phase diagram of cuprates is dominated by a quantum critical point is widely shared, it is not yet entirely clear what the origin of the criticality would be, and therefore what is the value of the doping level that fixes the relevant quantum critical point. The phase diagram itself, shown in figure 1.2, displays several doping level values at which a quantum phase transition may occur. Of these, the most important ones for the purposes of our discussion are two: one is the already mentioned critical doping level p_c, which also signals

the end of the static charge order phase, while the other is the doping level value at which the pseudogap line ends at zero temperature, and it's commonly denoted by p^* (generally $p^* > p_c$). A series of experimental results seems to suggest that the latter is precisely the doping value that determines the quantum criticality in cuprates [36, 37, 38]. The fact that the superconducting phase develops exactly around the quantum critical point may not be accidental, in fact, close to a quantum critical point, low-energy dynamical collective excitations can mediate a strongly doping and temperature dependent interaction among electrons. The latter can become attractive in the d-wave Cooper channel [39] and therefore give rise to superconductivity.

The vast phenomenology of cuprates, even (and especially) outside the superconducting phase, is still strongly debated in the field of theoretical condensed matter physics. Although anomalous behaviors were observed to some extent in all regions of the phase diagram, within this study we will focus exclusively on the phenomenology of the central part of this diagram, i.e. the strange-metal phase.

1.2 Phenomenological aspects of the strange-metal phase

The strange-metal phase, as its name suggests, exhibits an abnormal behavior which cannot be explained by the standard paradigm of the Landau theory for the metallic state. The most significant example of the violation of metallic behavior concerns the trend of resistivity as a function of temperature. In fact, for a standard metal, Landau theory predicts a quadratic behavior at low temperature due to (sufficiently weak) electron-electron interactions. This regime is then followed by a linear temperature dependence, due to the fact that the mediators of scattering between electrons (often phonons) obey semiclassical statistics, in the sense that the Bose function becomes essentially linear in temperature [40]. Finally, at high temperatures the resistivity saturates to a constant value, this saturation is provided by Mott-Ioffe-Regel criterion [41, 42].

What has been observed in cuprates is that, at the critical doping level and in the presence of magnetic fields strong enough to spoil the superconducting order, the temperature trend is perfectly linear starting from very low temperatures up to the highest temperatures ever measured [43, 44, 45]. What is most surprising is that in this solidly linear regime there is no slope variation, which suggests the presence of a robust scattering mechanism that dominates in every temperature range. This behavior, whose full understanding is still an open problem in condensed matter physics, indicates the lack of an intrinsic energy scale, namely a scale-invariant transport. Usually, if the constant of proportionality between the scattering rate and the temperature is $O(1)$ in natural units of $k_B/\hbar$, this behavior is referred to as "Planckian" behavior [46], however we prefer to use the term "strange-metal" behavior throughout this work.

It is still not clear how the physics which lies behind the T-linear resistivity manifests in other transport properties, as for instance the response to an applied magnetic

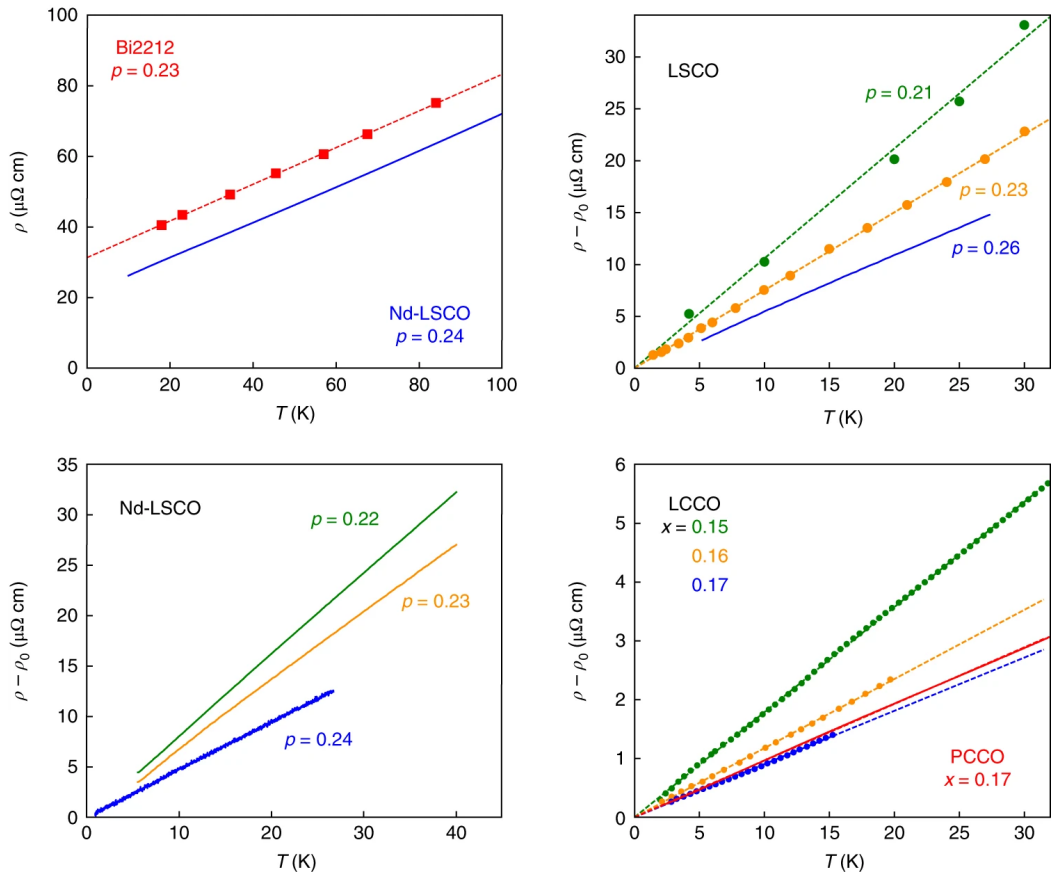

Figure 1.3. From [47], plots of the resistivity as a function of temperature for five different cuprate compounds. The superconducting phase was suppressed through the use of appropriate magnetic fields.

field. For a standard metal, the variation in resistance due to the effect of a transverse magnetic field is expected to be quadratic in the intensity of the field itself [48, 49]. High-field magnetoresistance measurements carried out on some iron pnictide [50] and cuprate [51, 52] superconductors show a resistivity which is linear down to relatively small magnetic fields. These systems seem to obey a good scaling relationship between temperature and magnetic field, which suggests that the two transport phenomena may be deeply connected.

Another abnormal transport phenomenon observed in the strange-metal phase concerns the trend of the Seebeck coefficient as a function of temperature. In fact, right at the critical doping level, the ratio $\mathcal{S}/T$ between the Seebeck coefficient and the temperature is positive and seems to diverge as $\log(1/T)$ in the low temperature limit [54]. This anomalous behavior also has an immediate correspondence in the thermodynamics of the strange-metal phase, in fact the specific heat observed in the same compounds at the same doping level has exactly the same singular trend as a function of temperature [55]. The fact that the Seebeck effect and specific heat are intrinsically linked to each other is a well-known property [56, 57], and for the

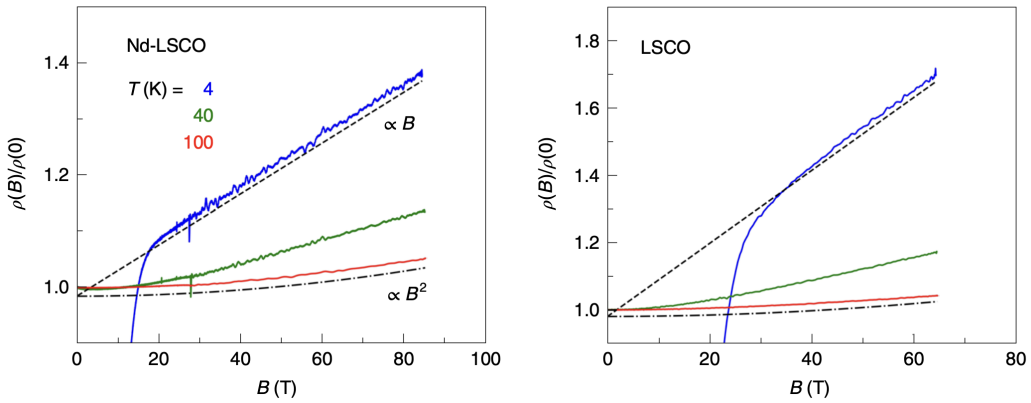

Figure 1.4. From [53], behavior of the in-plane resistivity as a function of the applied transverse magnetic field.

particular case of fermionic contributions to both physical quantities it's possible to show that these two quantities are directly proportional in the low temperature limit [58]. What is still unclear is the origin of this logarithmic divergence. A possible rationale for this singular behavior can be identified, in principle, in a structural singularity. For the case of $La_{1.6-x}Nd_{0.4}Sr_xCuO_4$, for instance, a Van Hove singularity very close to the critical doping level was experimentally observed [59], which would provide a logarithmically divergent density of states in strictly two-dimensional systems. However, as we will show later, the logarithmic divergence given by the Van Hove singularity is strongly smoothed out as soon as a small three-dimensional component in the scattering, or a reasonable scattering rate due to disorder, is considered [55]. Consequently, the fermionic contribution would not be sufficient to explain the singularity observed in the Seebeck coefficient and specific heat.

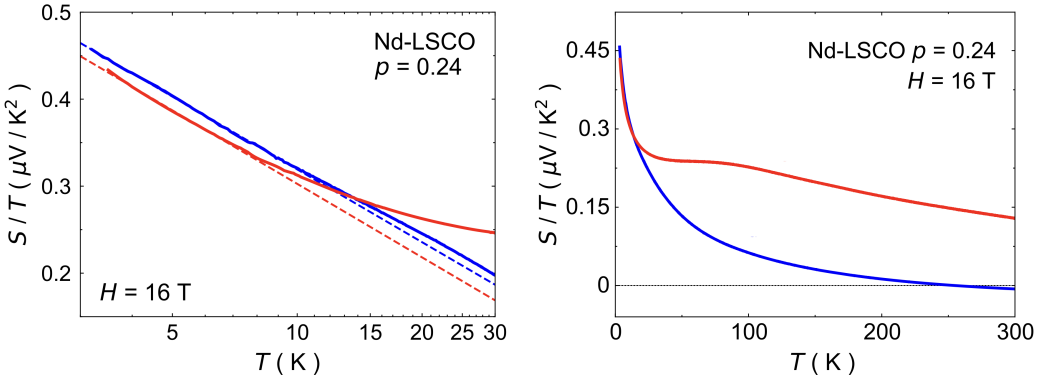

Figure 1.5. From [54], in-plane (blue) and out-of-plane (red) Seebeck coefficients for $La_{1.6-x}Nd_{0.4}Sr_xCuO_4$ in presence of magnetic field.

1.3 Charge density waves in cuprates

As we can see from the phase diagram in figure 1.2, both the pseudogap and superconducting phases exhibit some kind of charge order. This kind of order may not manifest itself as a static modulation of the charge profile, rather in the form of dynamical charge collective modes. One of the first examples of charge ordering within cuprates was detected in 1995 in a $La_{1.6-x}Nd_{0.4}Sr_xCuO_4$ compound, which exhibited a stable stripe-like charge order in its pseudogap phase [60, 61]. By stripe order we mean a state characterized by unidirectional density inhomogeneity, which can involve modulations of the charge density (charge stripe) coexisting with spin density modulations (spin stripe). In the stripe phase the charge carriers introduced with the doping tend to arrange in one-dimensional structures separated by domains which can also exhibit antiferromagnetic correlations.

Around the same time of the first observations of stripe order in cuprates, the idea that another type of charge order was present in these systems, known in the form of incommensurate *charge density waves*, began to emerge. The presence of charge density waves in hole-doped cuprates was initially a theoretical prediction, based on the so-called *frustrated phase separation* mechanism [7, 62, 63]. All relevant details which lie behind this mechanism will be discussed in section 7.3. Nevertheless, for the sake of a qualitative description, frustrated phase separation mechanism is based on the natural tendency to favor a non-homogeneous charge configuration that an electron system would exhibit if subjected to an effective attractive interaction (e.g. mediated by phonons). Of course, this tendency towards charge segregation is normally disadvantaged by Coulomb repulsion, however if the attraction forces are sufficiently strong the system may find a compromise between charge segregation and homogeneity, which would manifest itself precisely in a wavy modulation of the charge density profile. Due to the strong divergence of the unscreened Coulomb repulsion at vanishing momentum, this modulation is expected to have a non-trivial distribution in momentum space, such as to be peaked at a finite critical wave vector or rather at a whole star of wave vectors that are equivalent under point group symmetries of the lattice.

Once the possibility of having charge density waves in cuprates, both in the form of static modulation and dynamic collective modes, as a result of an instability of the Fermi liquid state was ascertained, the search for experimental evidence of their presence began. By their very nature, charge density waves are generally difficult to observe directly, unless particularly favorable conditions take place, such as the establishment of a strongly anharmonic stripe-like order. For this reason, the first experimental observations of this kind of charge order were essentially indirect. Initially, the first traces were sought in the angle resolved photoemission spectra [64, 65], with the idea of observing the alterations of the electronic properties due to their interaction with the charge density waves. Subsequently, experimental evidence of these collective modes began to be looked for in Raman responses [66] and in the interplay between charge and spin degrees of freedom in the underdoped region close to the antiferromagnetic state [67].

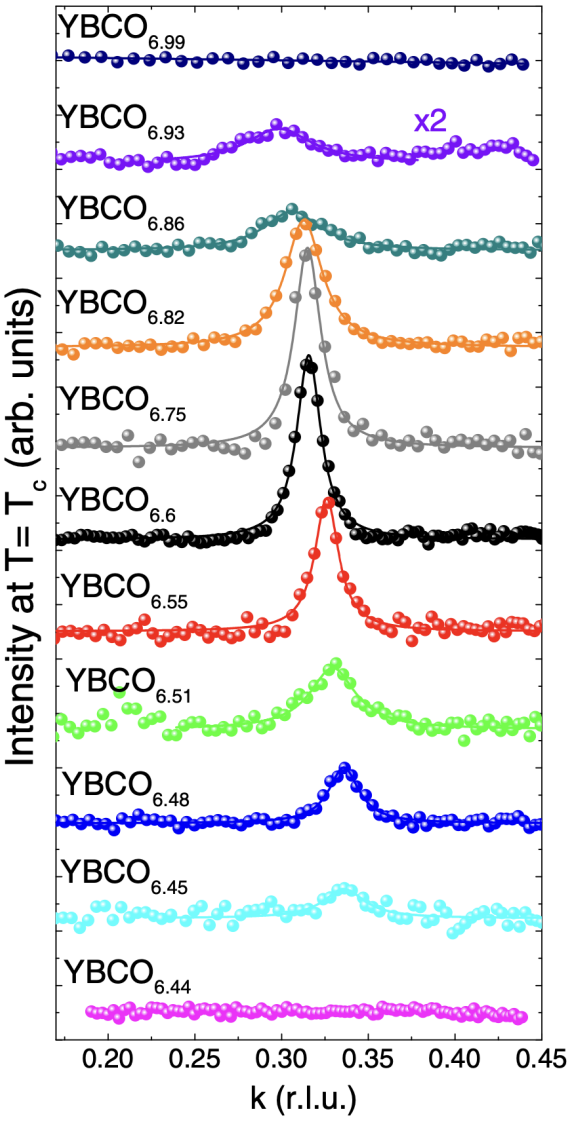

Figure 1.6. From [71], background-subtracted RXS intensity measured along the $(0, 1, 0)$ direction for several $YBa_2Cu_3O_{6+x}$ compounds, with x going from 0.44 ($p = 0.084$) to 0.99 ($p = 0.189$). Solid lines are Lorentzian fits.

An important step forward in this direction has been made thanks to the refinement of resonant intelastic x-ray scattering (RIXS) measurements, until reaching the resolution needed for the direct detection of charge density waves [68, 69, 70, 71]. These experiments not only unambiguously confirmed the presence of charge density waves in essentially all cuprate compounds, but also allowed the parameters characterizing these collective modes to be measured in a relatively accurate way. The experimental observations showed that charge density waves order is established in a slightly underdoped region of the phase diagram (see figure 1.6). Since RIXS experiments, such as those mentioned, are typically performed in the absence of an external magnetic field, they may be sensitive to a possible interplay between superconductivity and charge density waves. Alongside RIXS, experiments on the same systems were carried out with alternative techniques that could be well suited for measurements in the presence of a magnetic field, such as nuclear magnetic resonance spectroscopy [72, 73]. These latter experiments quantitatively confirmed the theoretical prediction that the charge density wave phase should have been dome-shaped and located entirely beneath the superconducting dome.

1.4 Experimental evidence of charge density fluctuations

A more recent breakthrough, also coming in this case from the RIXS experiments, is that the phase diagram of cuprates seems to be permeated by another type of charge collective mode, which presents similarities and differences with standard charge density waves [10].

The overlap of the two collective modes is evident from the fact that the RIXS spectra as a function of the wave vector show a well-marked peak at low temperature and in the underdoped regime, clearly associated with charge density waves, while at higher temperatures and different doping regimes it is observed a peaked but broader profile, well-fitted by a single Lorentzian and therefore interpretable as a well-defined charge collective mode. The narrow profile observed in the charge density waves phase has a slight asymmetry, and can be well fitted with the sum of two Lorentzian distributions, one narrower and the other one broader (see figure 1.7). This second peak is the same one that is also observed outside the charge density waves, the experimental data clearly indicate that this broad peak is not simply part of the high-temperature background as it was initially interpreted [74, 75]. As is common in literature, we will refer to this new collective mode as *charge density fluctuations*, in order to distinguish it from the already known charge density waves.

It is not yet clear why there are two distinct collective modes of charge, however it is reasonable to think that the two have a common origin, indicated by the fact that the two Lorentzian peaks are centered around a similar wave vector (henceforth, *critical* wave vector). As we have already mentioned, the main differences between the two modes is that, while charge density waves are present only in a small region of the phase diagram, charge density fluctuations permeate a much larger part of it, including the entire strange-metal phase. Moreover, while the latter have a quite short correlation length (we are talking about 2 or 3 lattice spacings) the former have a longer correlation length (between 8 or 10 lattice spacings) and can develop long-range order. This difference is a direct consequence of the different widths of the two distributions, as the correlation length of a collective mode is inversely proportional to its spectrum broadness. Another relevant difference between the two modes is their different behavior in the presence of superconductivity. In fact, while it is well-known that charge density waves compete with superconductivity [76, 77, 78], charge density fluctuations seem to be completely indifferent to it [10].

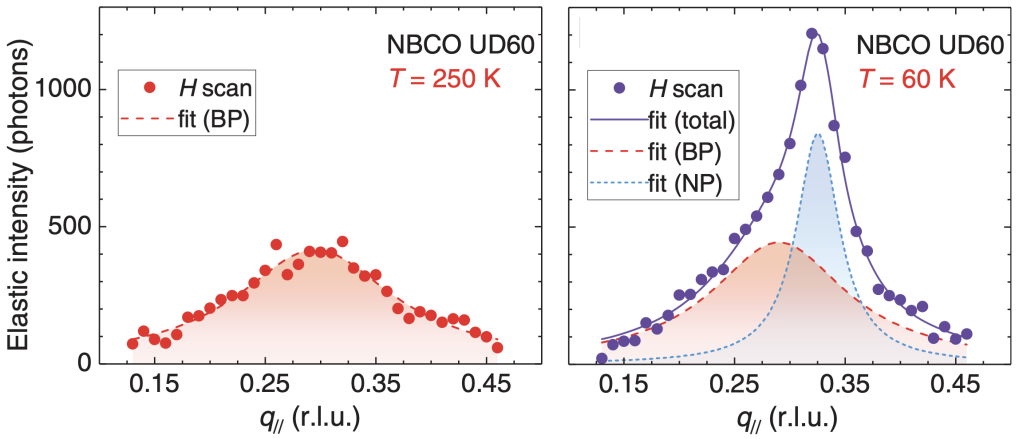

Figure 1.7. From [10], RIXS spectra as a function of the momentum along the antinodal direction for a $Nd_{1+x}Ba_{2-x}Cu_3O_{7-\delta}$ compound at $p \simeq 0.11$, after the removal of the intrinsic background of the signal.

For this reason, we expect that the influence of charge density fluctuations on the superconducting properties of cuprates, such as the mechanisms that determine their critical temperature or the physics of the BCS-BEC crossover in 2D [79], should not be relevant and may be neglected.

The main reason why we believe that the recent observation of charge density fluctuations is so important is that they, unlike charge density waves, make a very good candidate for explaining the linear resistivity and the other strange-metal properties observed in the strange-metal phase. In fact, low-temperature scattering phenomena mediated by charge density fluctuations can only occur between regions of the Fermi surface connected by the critical wave vector (the so-called *hot spots*), as these collective modes are quite narrow in momentum space. This implies that large part of the electrons would retain their standard Fermi liquid behavior, therefore this kind of scattering cannot explain the evident deviation from the Fermi liquid behavior [80]. Charge density fluctuations, on the other hand, being broad in the momentum space, are able to mediate an essentially isotropic scattering on the Fermi surface, and not focused only on specific hot spots [81]. The fact that charge density fluctuations encompass the entire strange-metal phase of cuprates is a further suggestion of the important role they could have in the description of the strange-metal phase.

Based on these premises, our goal is to provide a quantitative description of these collective modes and to illustrate how they can affect the phenomenology of the strange-metal phase of cuprates. In anticipation of the actual description of our model and the comparison with the experimental data, we believe it is useful to exhibit the theory concepts essential for understanding the models that we will use in our discussion. The next chapter is entirely dedicated to this purpose.

Chapter 2

Theoretical framework

In light of what we have exposed so far, it is clear that the problem of the strange-metal phase in cuprates is still open. The experimental evidence of charge density fluctuations seems to be an important piece in understanding the phenomena we have mentioned, we therefore believe that it is worth studying quantitatively how these collective modes can affect (and, possibly, spoil) the Fermi liquid properties of these systems.

In this chapter we will discuss in detail the theoretical tools that we will use in our description, as well as the quantitative details of our model. As we shall see, within our model charge density fluctuations will play the role of the main mediator of scattering between electrons, and will also directly contribute to the thermodynamics of the systems under consideration.

2.1 Landau theory of Fermi liquids

Landau theory is a powerful framework developed with the aim of describing the the emergent properties of a system of interacting fermions at low temperatures. The interactions that are taken into account by the theory are considered strong enough to cause deviations from the ideal behavior of non-interacting fermions, but not so strong that they lead to a completely different state of matter. This is precisely the main feature that defines the concept of Fermi liquid [82, 83].

The starting point for the construction of the Landau theory is the non-interacting Fermi gas. The basic idea is to modify the ideal system by adding a small interaction between electrons, but instead of directly dealing with the complex many-body problem, we are allowed to focus on low-energy excitations close to the Fermi surface, where the physics is dominated by the collective behavior of the so-called electronic *quasiparticles*. These quasiparticles can be viewed as electrons with renormalized properties, such as effective mass and lifetime, but carrying the standard electron quantum numbers. The key concept of Landau theory is that the interacting system is adiabatically connected to its non-interacting counterpart. This means that the states of the ideal Fermi gas are in one-to-one correspondence with the states of the corresponding Fermi liquid, and that the states of the former smoothly transform

into the corresponding states of the latter with the activation of the interaction.

The most suitable formalism for the description of a Fermi liquid is that of many-body physics, which often draws on the methods of quantum field theory. Within this formalism, every quasiparticle, whether it is electronic or a collective mode, is described by an appropriate one-particle Green's function, also referred to as propagator (within this thesis, we will use the expressions "Green's function" and "propagator" essentially interchangeably, as it's common in the context of quantum field theory). For a non-interacting electron system, the expressions in frequency (both real and imaginary) and momentum domain for the one-particle Green's function (henceforth, *bare* Green's function) have a quite simple explicit form [84]:

$$G_R^0(\omega, \mathbf{k}) = \frac{1}{\omega - \xi_{\mathbf{k}} + i0^+} \qquad \mathcal{G}^0(\omega_n, \mathbf{k}) = \frac{1}{i\omega_n - \xi_{\mathbf{k}}}$$

The superscript 0 refers to the fact that these functions describe the non-interacting system, while the subscript R in $G_R^0(\omega, \mathbf{k})$ indicates that this object is actually a "retarded" Green's function, meaning that its poles in ω domain have negative imaginary part and therefore its representation in time domain is different from zero only for positive times. This is not the only possible notion of one-particle Green's function for electrons in the real frequency domain, but in practice, for reasons that will be clarified in the course of this thesis work, it is the only notion we will need to use for our description. The function we denoted with $\xi_{\mathbf{k}}$ is the electronic dispersion, which in our model we will assume to be a two-dimensional tetragonal tight-binding dispersion with never more than three hopping parameters:

$$\xi_{\mathbf{k}} = -2t\big(\cos(k_x) + \cos(k_y)\big) - 4t'\cos(k_x)\cos(k_y) - 2t''\big(\cos(2k_x) + \cos(2k_y)\big) - \mu$$

While the analyticity of $G_R^0(\omega, \mathbf{k})$ in the upper half-plane is guaranteed by construction, from its explicit expression the property $\mathrm{Im}G_R^0(\omega, \mathbf{k}) \leq 0$ for any $\omega \in \mathbb{R}$ is evident. This is a property that also holds in the more general case of an interacting system. In fact, the retarded Green's function for the interacting electron system (which we will also refer to as *dressed* Green's function) is defined in such a way as to be analytic in the upper half-plane, however even in this case it is possible to show that the structure itself of the function, combined with the requirement that it be a retarded function, implies that its imaginary part is always non-positive on the real axis [85]. An even more general property satisfied by the imaginary part of the Green's function, whether bare or dressed, is that it actually represents the single particle spectral density (up to a minus sign and a factor of $1/\pi$), namely the probability density of finding an electron with energy ω and momentum $\mathbf{k}$ as a function of the continuous variable ω. Of course, for the non-interacting case this spectral density is simply a delta function, but in the presence of interaction it takes on a non-trivial form.

There are several ways to express the dressed propagator in terms of the bare one, which are obviously equivalent to each other. The most useful expression for

our purposes is given by Dyson equation [84], which for the case of retarded Green's functions in the real frequency domain takes the following form:

$$G_R(\omega, \mathbf{k}) = \frac{1}{\left[G_R^0(\omega, \mathbf{k})\right]^{-1} - \Sigma_R(\omega, \mathbf{k})} \tag{2.1}$$

The function $\Sigma_R(\omega, \mathbf{k})$ is the (retarded) self-energy of the system, in principle it encodes all the information about the interactions of a particle (in this case, an electron) with the surrounding media. Of course, it depends also on temperature, but for simplicity we leave this dependence implicit. From equation (2.1) we immediately deduce that, if the imaginary part of $\Sigma_R(\omega, \mathbf{k})$ is different from zero, then its sign must be the same as $\mathrm{Im}G_R^0(\omega, \mathbf{k})$, in other words the inequality $\mathrm{Im}\Sigma_R(\omega, \mathbf{k}) \leq 0$ holds for any real ω. Another consequence of the Dyson equation, less evident than the previous one, is that $\Sigma_R(\omega, \mathbf{k})$ is actually a retarded function as its name suggests, in the sense that it is analytic in the upper half-plane [85]. One of the advantages of dealing with a retarded function is that its real and imaginary parts are connected by Kramers-Kronig relations [86, 87]:

$$\mathrm{Re}\Sigma_R(\omega, \mathbf{k}) = \fint_{-\infty}^{+\infty} \frac{\mathrm{Im}\Sigma_R(\omega', \mathbf{k})}{\omega' - \omega} \frac{d\omega'}{\pi} \qquad \mathrm{Im}\Sigma_R(\omega, \mathbf{k}) = -\fint_{-\infty}^{+\infty} \frac{\mathrm{Re}\Sigma_R(\omega', \mathbf{k})}{\omega' - \omega} \frac{d\omega'}{\pi}$$

Where the dashed integral denotes the Cauchy principal value [88]. The subscript R in $\mathrm{Re}\Sigma_R(\omega, \mathbf{k})$ is pleonastic, as the real part of the self-energy does not depend on the prescription for the position of the poles, however we decide to keep it explicit to remind that $\mathrm{Re}\Sigma_R(\omega, \mathbf{k})$ and $\mathrm{Im}\Sigma_R(\omega, \mathbf{k})$ are respectively the real and imaginary parts of the same complex function. The effects that self-energy has on the spectral properties of single particles are multiple. First of all, it shifts the spectral density of the single particle and gives it a finite width, which physically corresponds to a finite lifetime. The crucial hypothesis of Fermi liquid theory is that the lifetime of the quasiparticle is much larger than the reciprocal of its energy in the low energy limit and at zero temperature, so that both the concept of Fermi surface and that of quasiparticle itself are well defined. Mathematically, this is equivalent to requiring that $\mathrm{Im}\Sigma_R(\omega, \mathbf{k})$ at $T = 0$ vanishes faster than linear in ω. More specifically, a Fermi liquid shows the following behavior at low energy and temperature:

$$\mathrm{Im}\Sigma_R(\omega, \mathbf{k}) \quad \sim \quad \alpha_1 \omega^2 + \alpha_2 (k_\mathrm{B} T)^2$$

Where α_1 and α_2 are two constants which do not depend on either ω or T, such that they are of the same order of magnitude with each other. Under this hypothesis, the dressed Green's function at zero temperature has poles in frequency domain, similar to what happened in the non-interacting case. In order to visualize this property, it is convenient to introduce the function $\tilde{\omega}_\mathbf{k}$ and the (generalized) Fermi wave vector $\mathbf{k}_\mathrm{F}$, respectively defined by the following two equations:

$$\tilde{\omega}_\mathbf{k} - \xi_\mathbf{k} - \mathrm{Re}\Sigma_R(\tilde{\omega}_\mathbf{k}, \mathbf{k}) \coloneqq 0 \qquad \xi_{\mathbf{k}_\mathrm{F}} + \mathrm{Re}\Sigma_R(\omega = 0\,, \mathbf{k}_\mathrm{F}) \coloneqq 0$$

In principle, both these quantities depend on temperature, as the self-energy does, nonetheless in many contexts only their zero temperature values are relevant, especially for the second one. From these two definitions immediately follows that

$\tilde{\omega}_{\mathbf{k}_\mathrm{F}} = 0$, we can therefore expand the reciprocal of $G_R(\omega, \mathbf{k})$ around $\omega = 0$ and $\mathbf{k} = \mathbf{k}_\mathrm{F}$. At fixed $T = 0$, this expansion provides:

$$\frac{1}{G_R(\omega, \mathbf{k})} \simeq \left(1 - \frac{\partial \mathrm{Re}\Sigma_R(\omega, \mathbf{k})}{\partial \omega}\bigg|_{\substack{\omega=0 \\ \mathbf{k}=\mathbf{k}_\mathrm{F}}}\right)\omega - \Big(\nabla_{\mathbf{k}}\xi_{\mathbf{k}} + \nabla_{\mathbf{k}}\mathrm{Re}\Sigma_R(\omega, \mathbf{k})\Big)\Big|_{\substack{\omega=0 \\ \mathbf{k}=\mathbf{k}_\mathrm{F}}}(\mathbf{k} - \mathbf{k}_\mathrm{F})$$

Notice that we completely neglected the imaginary part of this function, as it's subleading in ω at zero temperature. In order to express this function in a more compact way, and to generalize it to the finite temperature case, let's introduce the quasiparticle residue $Z_{\mathbf{k}}$ and the quasiparticle lifetime $\tau_{\mathbf{k}}$, whose definitions are the following [85, 89]:

$$Z_{\mathbf{k}} \coloneqq \left(1 - \frac{\partial \mathrm{Re}\Sigma_R(\omega, \mathbf{k})}{\partial \omega}\bigg|_{\omega=\tilde{\omega}_{\mathbf{k}}}\right)^{-1} \qquad \tau_{\mathbf{k}} \coloneqq -\frac{1}{2Z_{\mathbf{k}}\mathrm{Im}\Sigma_R(\tilde{\omega}_{\mathbf{k}}, \mathbf{k})}$$

The quasiparticle lifetime is a physical quantity having the dimension of the reciprocal of an energy, which is linked to the intensity of the scattering to which the quasiparticle is subjected. The presence of the factor $1/2$ in its definition is, in a certain sense, conventional. As we shall see, it will allow us to have a direct comparison with Drude theory in the appropriate limit. The quasiparticle residue is a real number between 0 and 1 which, as we will shortly clarify, characterizes the degree to which an interacting system of particles behaves like a system of non-interacting quasiparticles. This quantity is involved in the following useful identity, which directly follows from the definition of $\tilde{\omega}_{\mathbf{k}}$:

$$\nabla_{\mathbf{k}}\tilde{\omega}_{\mathbf{k}} = Z_{\mathbf{k}}\Big(\nabla_{\mathbf{k}}\xi_{\mathbf{k}} + \nabla_{\mathbf{k}}\mathrm{Re}\Sigma_R(\omega, \mathbf{k})\big|_{\omega=\tilde{\omega}_{\mathbf{k}}}\Big)$$

Both $Z_{\mathbf{k}}$ and $\tau_{\mathbf{k}}$, in addition to being functions of temperature, smoothly depend on $\mathbf{k}$. However, we will be mainly interested in the case where the vector lies on the Fermi surface. We must keep in mind that, in general, even limiting ourselves only to the Fermi surface both functions can still depend on the particular choice of the Fermi vector. Conventionally, if the quantities $Z_{\mathbf{k}_\mathrm{F}}$ or $\tau_{\mathbf{k}_\mathrm{F}}$ do not depend on the specific Fermi vector $\mathbf{k}_\mathrm{F}$ (such as the interesting case of a momentum-independent self-energy) we will simply omit the subscript $\mathbf{k}_\mathrm{F}$, namely we will write $Z_{\mathbf{k}_\mathrm{F}} = Z$ and $\tau_{\mathbf{k}_\mathrm{F}} = \tau$. In the following, we will refer to the quasiparticle residue at the Fermi level as *quasiparticle weight*, as is common in literature. Also notice that, for a Fermi liquid, the quasiparticle lifetime at the Fermi surface diverges as $1/T^2$ in the low temperature limit.

One last concept that should be introduced before proceeding with our discussion is that of *quasiparticle effective mass*. In a non-interacting Fermi system the electron effective mass m_{el} is well defined, it is closely linked to the band structure provided by tight-binding, but does not take interactions into account. The quasiparticle effective mass, denoted by m^*_{el}, is the physical quantity that plays the role of the electronic effective mass in quasiparticle dynamics. Since we are dealing with two-dimensional systems with tetragonal symmetry, we are allowed to treat the electron effective mass as a scalar quantity. In order to exhibit a relationship between

m_{el} and m^*_{el}, we require that the effective mass is inversely proportional to the Fermi velocity in both the interacting and non-interacting cases. More specifically:

$$\frac{m^*_{el}}{m_{el}} = \frac{1}{Z_{\mathbf{k}_\mathrm{F}}} \left[\lim_{\mathbf{k}\to\mathbf{k}_\mathrm{F}} \frac{\Big(\nabla_{\mathbf{k}}\xi_{\mathbf{k}}\Big)(\mathbf{k}-\mathbf{k}_\mathrm{F})}{\Big(\nabla_{\mathbf{k}}\xi_{\mathbf{k}} + \nabla_{\mathbf{k}}\mathrm{Re}\Sigma_R(\omega=0,\mathbf{k})\Big)(\mathbf{k}-\mathbf{k}_\mathrm{F})} \right]$$

Where, of course, $\mathbf{k}_\mathrm{F}$ is a vector belonging to the renormalized Fermi surface. In most cases $m^*_{el} > m_{el}$, this inequality is certainly true in the exemplary case of a momentum-independent self-energy, for which we simply have $m^*_{el} = m_{el}/Z$. We shall see that the ratio m^*_{el}/m_{el} will play an important role in the calculation of the specific heat. Collecting the notions we have exposed so far, we can compactly express the Green's function expansion close to $\omega = 0$ and $\mathbf{k} = \mathbf{k}_\mathrm{F}$ in the two following equivalent ways:

$$\frac{1}{G_R(\omega,\mathbf{k})} \simeq \frac{\omega - \Big(\nabla_{\mathbf{k}}\tilde{\omega}_{\mathbf{k}}\big|_{\mathbf{k}=\mathbf{k}_\mathrm{F}}\Big)(\mathbf{k}-\mathbf{k}_\mathrm{F})}{Z_{\mathbf{k}_\mathrm{F}}} \qquad \frac{1}{G_R(\omega,\mathbf{k})} \simeq \frac{\omega - \dfrac{m_{el}}{m^*_{el}}\Big(\nabla_{\mathbf{k}}\xi_{\mathbf{k}}\big|_{\mathbf{k}=\mathbf{k}_\mathrm{F}}\Big)(\mathbf{k}-\mathbf{k}_\mathrm{F})}{Z_{\mathbf{k}_\mathrm{F}}}$$

Again, both expressions are to be considered valid only at zero temperature, in case we consider a low but finite temperature we should include a small imaginary part proportional to T^2. Let's consider a path contained in the Brillouin zone that crosses the Fermi surface at exactly one point. We have just seen that the Green's function becomes singular at this point, however we can separate the singular part from the regular background:

$$G^{coh}_R(\omega,\mathbf{k}) \coloneqq \frac{Z_{\mathbf{k}_\mathrm{F}}}{\omega - \Big(\nabla_{\mathbf{k}}\tilde{\omega}_{\mathbf{k}}\big|_{\mathbf{k}=\mathbf{k}_\mathrm{F}}\Big)(\mathbf{k}-\mathbf{k}_\mathrm{F}) + i0^+} \qquad G^{inc}_R(\omega,\mathbf{k}) \coloneqq G_R(\omega,\mathbf{k}) - G^{coh}_R(\omega,\mathbf{k})$$

The two functions we have just defined are known respectively as the "coherent" part and the "incoherent" part of the Green's function $G_R(\omega,\mathbf{k})$. The coherent part is formally identical to the free electron Green's function expanded around $\mathbf{k}_\mathrm{F}$, with the only difference that it is multiplied by a positive prefactor less than 1. It is clearly associated with electronic quasiparticles, which can therefore be treated as free electrons but with physical characteristics different from the usual ones.

A similar decomposition is obviously valid also for the spectral density, as it is directly proportional to the imaginary part of $G_R(\omega,\mathbf{k})$. However, since the spectral density is a probability density in ω that depends parametrically on $\mathbf{k}$, in this case it is convenient to first fix a vector $\mathbf{k}$ (not necessarily on the Fermi surface) and then expand $1/G_R(\omega,\mathbf{k})$ around $\omega = \tilde{\omega}_{\mathbf{k}}$. By carrying out steps similar to those we have already exhibited, it is possible to show that the spectral density of the interacting electron can be decomposed as the sum of a Lorentzian peak (very narrow for $\mathbf{k}$ close to the Fermi surface) and a background part, identifiable respectively as the coherent and incoherent parts of the function. Also notice that, for $\mathbf{k} \neq \mathbf{k}_\mathrm{F}$, we have that $\mathrm{Im}G_R(\omega=0,\mathbf{k}) = 0$ at zero temperature. The graphical difference between the spectral density of an ideal Fermi gas and that of a Fermi liquid, at fixed $\mathbf{k}$ close to (but not lying on) the Fermi surface is sketched in figure 2.1.

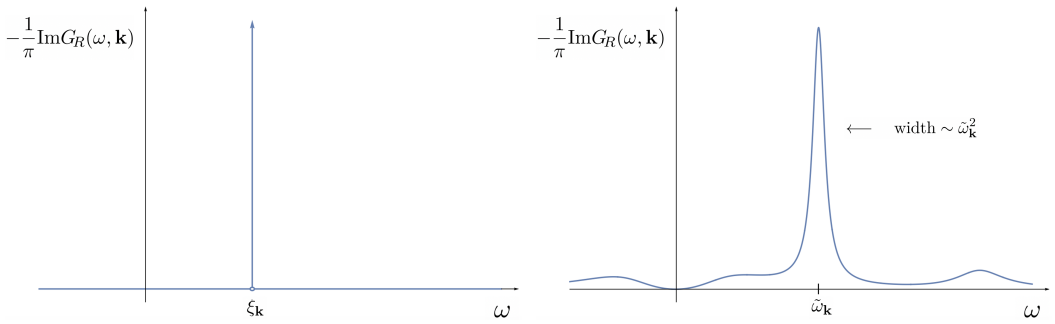

Figure 2.1. Plots of the spectral density at fixed $\mathbf{k} \neq \mathbf{k}_\mathrm{F}$ for a non-interacting Fermi system (left panel) and for a Fermi liquid (right panel).

The decomposition between the coherent and incoherent part, both in the case of propagators and spectral densities, is obviously also valid at a finite temperature, the difference is that at finite temperature the quasiparticle lifetime is always reduced. In particular, it is never divergent, so the coherent part of the spectral function is never δ-like, not even on the Fermi surface.

2.2 Collective modes

Within Landau theory, a fundamental role in describing the low-energy properties of Fermi liquids is played by the already mentioned collective modes. These modes are collective excitations of the system that involve the coordinated motion of many particles and can themselves be described as full-fledged quasiparticles. In particular, collective modes can also be described through appropriate propagators. As we have mentioned, within our study we will focus mainly on a single bosonic collective mode, namely that of charge density fluctuations, whose propagator is the following:

$$D_R(\omega,\mathbf{k}) = \frac{1}{m_{\mathbf{k}} - i\gamma\omega - \dfrac{\omega^2}{\Omega}} \qquad \mathcal{D}(\omega_n,\mathbf{k}) = \frac{1}{m_{\mathbf{k}} + \gamma|\omega_n| + \dfrac{\omega_n^2}{\Omega}} \tag{2.2}$$

This propagator, which takes essentially the standard Ginzburg-Landau form in the Gaussian approximation, was proposed long ago for the description of charge density waves [7, 90, 91, 92], what distinguishes the propagators of the two collective modes are the numerical values of the involved parameters. As we have already emphasized, the main characteristics of charge density fluctuations propagator are the Landau damping, quantitatively described by γ parameter, and the weak dependence on $\mathbf{k}$ in the $m_{\mathbf{k}}$ function. The frequency scale Ω is simply an ultraviolet cutoff. The precise shape of $m_{\mathbf{k}}$, as well as the value of Ω, can be inferred from RIXS spectra. We know that $m_{\mathbf{k}}$ must have absolute minima at a star of four critical wave vectors, which can be expressed in the form of $\mathbb{R}^2$ vectors as follows:

$$\mathbf{q}_c^{I} = \begin{pmatrix} q_c \\ 0 \end{pmatrix} \qquad \mathbf{q}_c^{II} = \begin{pmatrix} 0 \\ q_c \end{pmatrix} \qquad \mathbf{q}_c^{III} = \begin{pmatrix} -q_c \\ 0 \end{pmatrix} \qquad \mathbf{q}_c^{IV} = \begin{pmatrix} 0 \\ -q_c \end{pmatrix}$$

Where q_c is a dimensionless constant (in lattice spacings units) between 0 and π, also determinable from RIXS spectra, of course it represents the magnitude of each of the four $\mathbf{q}_c$ wave vectors. Then, it is useful to define the function $\eta_\iota(\mathbf{q})$ as follows:

$$\eta_\iota(\mathbf{q}) := 4 - 2\cos(q_x - q^\iota_{c,x}) - 2\cos(q_y - q^\iota_{c,y})$$

Here, the index ι labels the particular critical wave vector, namely $\iota = I, II, III, IV$. In the cases where we are not interested in the precise critical vector among the four ones, this will simply be denoted by $\mathbf{q}_c$. Finally, we can express $m_\mathbf{k}$ as follows:

$$m_\mathbf{k} = m_c + \frac{\nu}{\big(2 - 2\cos(2q_c)\big)\big(4 - 4\cos(q_c)\big)^2} \prod_{\iota=I}^{IV} \eta_\iota(\mathbf{k})$$

This is a smooth function of $\mathbf{k}$ which satisfies the right symmetries of the lattice, it works well if q_c is far enough from 0. A plot of this function is shown in figure 2.2. The parameter m_c is the mass of the fluctuations, and measures the distance from the criticality, while ν is the energy scale which sets the curvature at the bottom of the dispersion law. If $\mathbf{k}$ is close to one of the four critical wave vectors, the following approximate expression is valid:

$$m_\mathbf{k} = m_c + \nu|\mathbf{k} - \mathbf{q}_c|^2$$

Notice that, for $\omega = 0$ and $\mathbf{k} \simeq \mathbf{q}_c$, $D_R(\omega, \mathbf{k})$ takes the standard Ornstein-Zernike form of the static susceptibility [93]. The correlation length ξ of the collective mode (not to be confused with the electronic dispersion $\xi_\mathbf{k}$) is given by $\sqrt{\nu/m_c}$. The values of the parameters m_c and ν can, in general, depend on temperature. The temperature dependence of m_c, for example, is important near a (classical) phase transition in the case of a critical collective mode. Experimentally, it is known that these parameters depend very weakly on temperature in the case of charge density fluctuations, this implies that ξ itself is essentially constant throughout the phase diagram. On the basis of this experimental evidence, throughout our discussion we will treat all bosonic parameters as strictly temperature-independent except

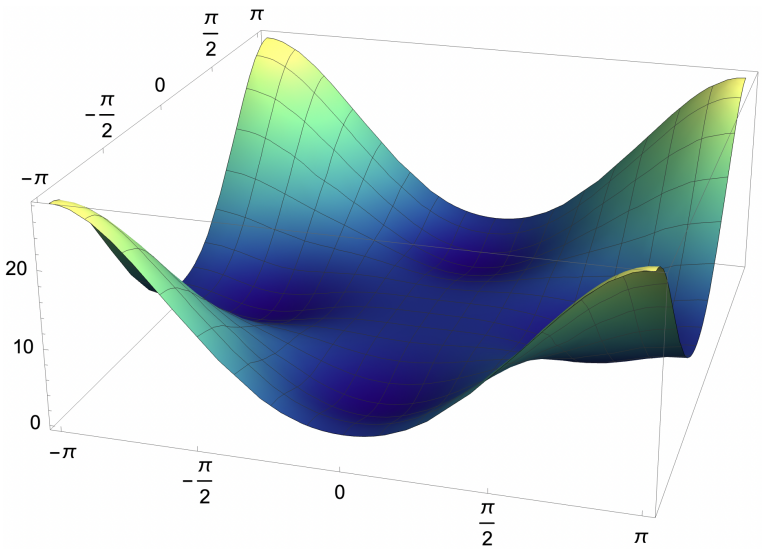

Figure 2.2. Plot of the function $m_\mathbf{k}$ with $m_c = 1$ and $\nu = 4$ (which corresponds to $\xi = 2$) over the First Brillouin zone. Here we set $q_c = 2$.

for γ, whose temperature dependence will in any case be assumed to be weak (at most proportional to $\log(1/T)$). Just to give an idea of the orders of magnitude of these parameters, we report the estimated values for $Nd_{1+x}Ba_{2-x}Cu_3O_{7-\delta}$ and $YBa_2Cu_3O_{7-\delta}$ compounds [81]:

$$m_c = 15\,\text{meV} \quad \nu = 1.4\,\text{eV}/(\text{r.l.u.})^2 \simeq 35\,\text{meV} \quad q_c = 0.3\,\text{r.l.u.} \simeq 1.9 \quad \Omega = 30\,\text{meV}$$

Here, r.l.u. denotes the *reciprocal lattice units*, defined in such a way that 1 r.l.u. equals to $2\pi/a$ (with the lattice spacing a made explicit), it is an often convenient unit for comparison with experimental data. It should be stressed that the values we just exhibited are only estimates, besides compound-dependent. For this reason, sometimes in the numerical analyzes that we will carry out we will replace these values with slight different ones, if this can help to have a better agreement with the experimental data. In most cases, our description of the systems under consideration will be based on the interaction between electrons and charge density fluctuations, and on the direct contribution of the latter on thermodynamics and transport. Therefore, whenever we refer to a bosonic collective mode we will always mean that it is a charge density fluctuations mode, except where differently indicated.

The charge density fluctuations propagator encodes all the quantitative information about the collective mode, and will be the basis of all our theoretical calculations. In particular, it plays a central role in the calculation of electronic self-energy, which will be a fundamental object for the determination of the most relevant physical quantities we are interested in. Since we are in a weak coupling regime, we adopt a perturbative approach. In particular, for our self-energy we apply the so-called *Fock approximation*, which from a diagrammatic point of view can be represented as follows [94]:

$\Sigma(\omega, \mathbf{k}) \simeq$

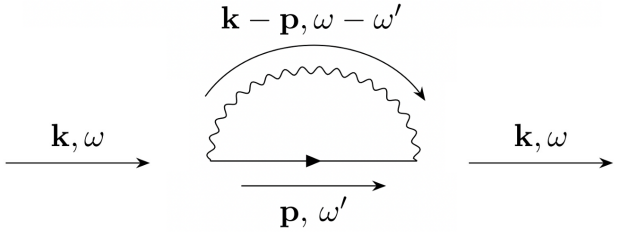

(2.3)

Where the continuous line represents a bare electron, while the wavy line represents the collective mode. The sum over frequencies can be performed exactly, the result is the following [95, 96]:

$$\text{Im}\Sigma_R(\omega, \mathbf{k}) = -\frac{g^2}{N}\sum_{\mathbf{p}} \text{Im}D_R(\xi_{\mathbf{p}} - \omega, \mathbf{p} + \mathbf{k})\big[f(\xi_{\mathbf{p}}) + b(\xi_{\mathbf{p}} - \omega)\big] \tag{2.4}$$

The energy scale we denoted with g is simply the coupling constant between electrons and charge density fluctuations, whose value is estimated to be between 150 meV and 200 meV [81]. As discussed in Appendix A, the sum over momenta should be multiplied by a factor of $1/v_{\text{uc}}$ in order to take also transverse momenta into account, where v_{uc} is the volume of the three-dimensional unit cell (which is equal to the interplane distance d according to our units). However, to soften the notation, we

include this factor inside the definition of g. Of course, the real part of the self-energy can be obtained by applying the Kramers-Kronig relation to expression (2.4). All the details on the explicit computation of this function will be provided in the following chapters. However, it is worth pointing out here that if $D_R(\omega, \mathbf{k})$ does not depend on $\mathbf{k}$, the same will be true also for self-energy. Within our model $D_R(\omega, \mathbf{k})$ has a momentum dependence, but we know it is weak. Therefore, in the following we will apply the approximation of considering self-energy as momentum-independent. For simplicity, if the self-energy does not depend on momentum (or if this dependence is negligible) we will omit the latter from the arguments of the function, i.e. we will express $\Sigma_R(\omega, \mathbf{k})$ simply as $\Sigma_R(\omega)$. Under this assumption, both the quasiparticle residue and the quasiparticle lifetime depend on $\mathbf{k}$ only through $\xi_{\mathbf{k}}$:

$$Z_{\mathbf{k}} = \left(1 - \frac{\partial \mathrm{Re}\Sigma_R(\omega)}{\partial \omega}\Big|_{\omega=\tilde{\omega}_{\mathbf{k}}}\right)^{-1} \qquad \tau_{\mathbf{k}} = -\frac{1}{2Z_{\mathbf{k}}\mathrm{Im}\Sigma_R(\tilde{\omega}_{\mathbf{k}})} \tag{2.5}$$

Where $\tilde{\omega}_{\mathbf{k}} - \mathrm{Re}\Sigma_R(\tilde{\omega}_{\mathbf{k}}) = \xi_{\mathbf{k}}$ by definition.

2.3 Linear Response Theory

Some of the physical quantities of our interest, such as the electrical conductivity or the Seebeck coefficient, are generally related to the response shown by a physical system to some external agent. The general problem we want to address is therefore to understand how a system, whose equilibrium behavior is well known, reacts to these external agents, customarily known as *sources*. This is commonly a difficult problem to solve, and there are various theories and techniques to address the issue, each of which has its own domain of applicability.

The framework we exhibit within this section is based on the hypothesis that the sources are small enough to allow the use of a perturbative approach. This is the regime of validity of *Linear Response Theory*, which is built precisely on the assumption that the response of the system to a perturbative source can be considered linear in the source itself. A canonical example of the application of this theory, which will be of great relevance for this thesis work, is the linear response exhibited by a system subjected to both an electrostatic field and a thermal gradient. Such a system is described by the following equations [97]:

$$\begin{cases} \langle \mathbf{J}^N \rangle_{\text{n.e.}} = -\Gamma_{11}\nabla(\mu + \mathrm{e}\phi) - \Gamma_{12}\dfrac{\nabla T}{T} \\ \\ \langle \mathbf{J}^Q \rangle_{\text{n.e.}} = -\Gamma_{12}\nabla(\mu + \mathrm{e}\phi) - \Gamma_{22}\dfrac{\nabla T}{T} \end{cases} \tag{2.6}$$

On the left sides of the two equations we have, respectively, the expectation values of the particle current and the heat current, where the average takes the external perturbation into account (of course, the subscript stands for "non-equilibrium"). Since our study is limited to two-dimensional systems, such currents have to be understood as two-component vectors. The coefficients we denoted with Γ_{11}, Γ_{12} and Γ_{22} are actually 2×2 matrices, but in the presence of tetragonal symmetry and

in the absence of magnetic fields they reduce to scalar quantities. In most cases, both these hypotheses are valid for the systems we aim to analyze. In particular, the formalism we are describing in this section will be always applied to physical systems for which both assumptions are actually satisfied, therefore we will always treat these three coefficients as scalar quantities. Further details about their calculation, as well as their physical meaning, will be provided later. Here we simply provide the expressions for electrical conductivity σ, Seebeck coefficient $\mathcal{S}$ and thermal conductivity κ in this notation [98]:

$$\sigma = \mathrm{e}^2\Gamma_{11} \qquad \mathcal{S} = -\frac{1}{\mathrm{e}T}\frac{\Gamma_{12}}{\Gamma_{11}} \qquad \kappa = \frac{1}{T}\left(\Gamma_{22} - \frac{\Gamma_{12}^2}{\Gamma_{11}}\right)$$

The general problem of linear response theory can be stated by expressing the full Hamiltonian of the system as the sum of an unperturbed part and a time-dependent perturbation:

$$H = H_0 + \delta H(t)$$

Where the unperturbed Hamiltonian must be considered within grand canonical ensemble. The general expression for the perturbative part is:

$$\delta H(t) = -\sum_{\mathrm{i}} \int_{\mathbb{R}^{\mathrm{d}}} A_{\mathrm{i}}(\mathbf{r}) v_{\mathrm{i}}(\mathbf{r}, t) d^{\mathrm{d}}\mathbf{r} \tag{2.7}$$

We are using the notation $v_{\mathrm{i}}(\mathbf{r}, t)$ to indicate the sources of the perturbation, which can be considered as classical quantities, while $A_{\mathrm{i}}(\mathbf{r})$ are the operators which represent the observables that couple to the former. Our hypothesis is that the sources $v_{\mathrm{i}}(\mathbf{r}, t)$ are "small". So far, we are working within Schrödinger picture, consequently operators do not evolve in time. As is well known from time-dependent perturbation theory [99], the reason why $\delta H(t)$ depends on time while expressed in Schrödinger picture is that its time dependence emerges from an external potential, so its dynamics is not related to the Hamiltonian. Another example of an operator that evolves over time within Schrödinger picture is the density operator $\hat{\rho}(t)$, which we will discuss in more detail in Appendix C.

With the exception of operators $\delta H(t)$ and $\hat{\rho}(t)$, the use of the Schrödinger picture or the interaction picture is conventionally signaled, respectively, by the absence or presence of the time variable as operator's argument. For instance, if $\mathcal{O}$ is a generic operator expressed in the Schrödinger picture, its counterpart within interaction picture is simply expressed as $\mathcal{O}(t)$, and is related to the former by the following equations:

$$\mathcal{O}(t) = e^{iH_0 t}\mathcal{O}e^{-iH_0 t} \qquad \mathcal{O}(\tau) = e^{H_0 \tau}\mathcal{O}e^{-H_0 \tau}$$

Where the latter is the imaginary time evolution. It is convenient to define also the perturbation of the observables due to the external sources:

$$\delta\langle A_{\mathrm{i}}(\mathbf{r}, t)\rangle \coloneqq \langle A_{\mathrm{i}}(\mathbf{r}, t)\rangle_{\mathrm{n.e.}} - \langle A_{\mathrm{i}}(\mathbf{r})\rangle \tag{2.8}$$

Where $\langle A_{\mathrm{i}}(\mathbf{r})\rangle$ and $\langle A_{\mathrm{i}}(\mathbf{r}, t)\rangle_{\mathrm{n.e.}}$ are the thermal averages of the operator $A_{\mathrm{i}}(\mathbf{r})$ obtained, respectively, through the density matrix of the non-interacting system and that of the complete one. Of course, thermal averages do not depend on the scheme

we choose to use. If we look only at the linear response, and by assuming that the system is translationally invariant, we can define the response function $\chi_{ij}(\mathbf{r}, t)$ as follows:

$$\delta\langle A_i(\mathbf{r}, t)\rangle \coloneqq \sum_j \int_{\mathbb{R}^{d+1}} \chi_{ij}(\mathbf{r} - \mathbf{r}', t - t') v_j(\mathbf{r}', t') d^d\mathbf{r}' dt' \tag{2.9}$$

The $\chi_{ij}(\mathbf{r}, t)$ response functions contain a lot of information about the systems under consideration and will play a central role throughout our study. Within linear response theory it is possible to exhibit an explicit expression for the response function, by means of the famous *Kubo formula* [100, 101]. For a complete derivation of this formula we refer to Appendix C, here we report its expression in its best-known form:

$$\chi_{ij}(\mathbf{r}, t) = i\theta(t)\big\langle \big[A_i(\mathbf{r}, t), A_j(\mathbf{0}, 0)\big]\big\rangle \tag{2.10}$$

The great advantage of this equation is that its right-hand side can be perturbatively calculated using the diagrammatic theory. In fact, correlation functions of the form (2.10) are graphically represented by two-vertex bubble-like diagrams, which can be computed explicitly at an arbitrary perturbative order by applying Feynman's rules [84]. For instance, in the case of fermionic correlation functions, self-energy and vertex corrections will explicitly enter into the calculation of the diagrams.

The Kubo formalism is also suitable for the description of transport phenomena, namely all those processes that tend to naturally bring a physical system back to its equilibrium configuration whenever it is brought out of equilibrium due to external agents. The currents emerge as a natural consequence of these restoration processes. In order to describe transport phenomena within this formalism, it is therefore necessary to introduce current operators, which we indicate generically with $J_\alpha(\mathbf{r})$, where the subscript α conventionally indicates both the nature and the space component of the current. Of course, Kubo formula also works for current-current response functions, it is possible for example to obtain the function $\chi_{\alpha\beta}(\mathbf{r}, t)$ simply by inserting the current operators $J_\alpha(\mathbf{r}, t)$ and $J_\beta(\mathbf{0}, 0)$ in the commutator which appears on the right-hand side of (2.10). However, due to their very nature, it is less straightforward to describe the effect of the currents as a perturbation of the Hamiltonian due to coupling with appropriate sources. For this particular class of phenomena, it is convenient to adopt a slightly different formalism, whose starting point is the entropy production rate instead of the direct perturbation of the Hamiltonian. Within this description, the role of the sources is played by the so-called *conjugated forces*, i.e. those external agents which produce the non-equilibrium conditions, and which possibly force the system to keep that configuration permanently. Let's consider a stationary system, in which neither the currents nor the conjugate forces depend on time. In accordance with the most used notation in the literature, the irreversible entropy production rate is expressed as:

$$\frac{\partial S_{\text{irr}}}{\partial t} = k_B \sum_\alpha \int_{\mathbb{R}^d} \langle J_\alpha(\mathbf{r})\rangle_{\text{n.e.}} X_\alpha(\mathbf{r}) d^d\mathbf{r}$$

Where $\langle J_\alpha(\mathbf{r})\rangle_{\text{n.e.}}$ is just a short notation for $\langle J_\alpha(\mathbf{r},0)\rangle_{\text{n.e.}}$, of course setting $t=0$ in the current term is fine as this quantity is constant as a function of time. The relation we have just shown defines the conjugate force $X_\alpha(\mathbf{r})$ for a stationary system, which is a classical quantity. Within the linear response regime, under the hypothesis of translational invariance, we also have that:

$$\langle J_\alpha(\mathbf{r})\rangle_{\text{n.e.}} = \sum_\beta \int_{\mathbb{R}^\text{d}} Z_{\alpha\beta}(\mathbf{r}-\mathbf{r}')X_\beta(\mathbf{r}')d^\text{d}\mathbf{r}'$$

The functions $Z_{\alpha\beta}(\mathbf{r})$ are known as *Onsager coefficients*. Given this relation, the entropy production rate actually becomes a quadratic form of the conjugate forces, which is entirely determined by Onsager coefficients. Of course, this quadratic form must be positive (semi)definite. The case of major interest is the one in which the external forces are homogeneous in space. In this case, the currents are homogeneous too and are proportional to the integral over the entire space of the Onsager coefficients (namely, calculated at $\mathbf{q}=\mathbf{0}$ in the momentum space), which for simplicity we denote with $Z_{\alpha\beta}$ (with no arguments):

$$Z_{\alpha\beta} \coloneqq \int_{\mathbb{R}^\text{d}} Z_{\alpha\beta}(\mathbf{r})d^\text{d}\mathbf{r}$$

Although these coefficients are *not* the response functions, in a certain sense they play a role analogous to them, just as the conjugate forces play the role of the sources. The equation equivalent to Kubo formula for Onsager coefficients is the following:

$$Z_{\alpha\beta} = \lim_{\epsilon\to 0^+}\frac{1}{\beta}\int_{-\infty}^{0} e^{\epsilon t}\left[\int_0^\beta\left(\int_{\mathbb{R}^\text{d}}\langle J_\alpha(\mathbf{r},-t-i\lambda)J_\beta(\mathbf{0},0)\rangle d^\text{d}\mathbf{r}\right)d\lambda\right]dt \tag{2.11}$$

Within this work, we will always and only deal with currents $J_\alpha(\mathbf{r})$ and $J_\beta(\mathbf{r})$ such that their product is even under time-reversal symmetry. Under this assumption, it is possible to show that these coefficients satisfy the *Onsager relations* in the form $Z_{\beta\alpha}=Z_{\alpha\beta}$ (see refs. [102, 103] or Appendix B for further details). Moreover, the same symmetry implies the following relation connecting Onsager coefficients to the corresponding response functions:

$$Z_{\alpha\beta} = \frac{1}{\beta}\lim_{\omega\to 0}\frac{\text{Im}\chi_{\alpha\beta}(\mathbf{q}=\mathbf{0},\omega)}{\omega} \tag{2.12}$$

Where $\text{Im}\chi_{\alpha\beta}(\mathbf{q}=\mathbf{0},\omega)$ is directly given by the actual Kubo formula. All the details about the derivation of relations (2.11) and (2.12) are provided in Appendix C. We want to point out that, in accordance with the most used notation in the literature, the first argument of the response function is the moment while the second is the frequency, unlike propagators and self-energy for which the opposite convention is instead valid. Finally, we introduce the $\Gamma_{\alpha\beta}$ coefficients by simply rescaling the Onsager coefficients by the temperature, namely $\Gamma_{\alpha\beta}\coloneqq\beta Z_{\alpha\beta}$. The coefficients $\Gamma_{\alpha\beta}$ are exactly the ones which appear in the system of equations (2.6), in that case the subscript 1 represents the x-component of a particle current, while the subscript 2 represents the x-component of a heat current. Of course, by hypothesis of tetragonal symmetry, the same result is obtained by choosing the y-components for all the currents.

2.4 Boltzmann Transport Theory

An alternative formulation to Kubo theory for the study of transport phenomena is *Boltzmann Transport Theory* [40]. This theory describes electron dynamics semiclassically, in the sense that it associates *both* a displacement vector $\mathbf{r}$ and a wave vector $\mathbf{k}$ with each electronic wave packet, and both vectors depend on time. This approximation works under two hypotheses:

- The broadness of the electronic wave function must be small compared with the dimension of the Brillouin zone. This is equivalent to requiring the same wave function, in position domain, to be spread over many primitive cells.
- The external fields acting on electrons vary very slowly over the dimension of an electronic wavepacket, except for the periodic field provided by the ionic lattice, for which a quantum description always applies.

In principle, each electron is described not only by the vectors $\mathbf{r}$ and $\mathbf{k}$, but also by its band index. However, since in the course of this work we will only deal with single-band systems, for simplicity we will omit this quantum number. In absence of collisions, the dynamics of electrons is uniquely determined by their band dispersion and the external forces to which they are subjected, which we will always assume to be conservative. Given these quantities as a starting point, the semiclassical equations of motion are the following:

$$\frac{d\mathbf{r}}{dt} = \nabla_{\mathbf{k}}\xi_{\mathbf{k}} \qquad \frac{d\mathbf{k}}{dt} = \mathbf{F}_{\text{ext}}(\mathbf{r},\mathbf{k})$$

It should be stressed that the wave vector $\mathbf{k}$ does not represent the full momentum of an electron, but only its crystal momentum. For this reason, the force exerted by the periodic field of the lattice must not be included in the term of external forces that appears in the equation for $\mathbf{k}$.

The main idea behind Boltzmann formalism is to encode all the information about the dynamics of the electron system in a suitable distribution function $\tilde{f}(\mathbf{r},\mathbf{k},t)$, after that the goal is therefore to find an explicit expression for this function (if possible) given the microscopic details of the model. This distribution function is defined as the function that expresses the infinitesimal number of electrons present in an infinitesimal volume of phase space around the point identified by the coordinates $\mathbf{r}$ and $\mathbf{k}$ at time t:

$$dN \coloneqq 2\tilde{f}(\mathbf{r},\mathbf{k},t)\frac{d^{\mathrm{d}}\mathbf{r}\, d^{\mathrm{d}}\mathbf{k}}{(2\pi)^{\mathrm{d}}}$$

Where we included a factor of 2 accounting for spin degeneracy. At equilibrium, this function simply reduces to the Fermi function evalued at $\xi_{\mathbf{k}}$, for given local and instantaneous values of the chemical potential $\mu = \mu(\mathbf{r},t)$ and temperature $T = T(\mathbf{r},t)$. Under arbitrary non-equilibrium conditions, the equation that governs the time evolution of the distribution function $\tilde{f}(\mathbf{r},\mathbf{k},t)$ is the famous *Boltzmann equation*, whose most general form is:

$$\frac{d\tilde{f}}{dt} = \mathcal{I}_{\text{coll}}[\tilde{f}]$$

On the left-hand side of the equation we have the total derivative of $\tilde{f}(\mathbf{r}, \mathbf{k}, t)$, which of course takes into account also the time dependence of the variables $\mathbf{r}$ and $\mathbf{k}$. The term $\mathcal{I}_{\text{coll}}[\tilde{f}]$ that appears on the right-hand side is the so-called *collision integral*, a non-linear functional of $\tilde{f}(\mathbf{r}, \mathbf{k}, t)$ which takes into account, at least formally, all the collision phenomena of the system. Of course, the trivial case $\mathcal{I}_{\text{coll}}[\tilde{f}] = 0$ simply describes a collisionless time evolution (ideal Fermi gas), in this case Boltzmann equation reproduces Liouville's theorem [104], as we expect since we are describing the time evolution of the distribution function of a Hamiltonian system. However, in the general case, the collision integral has a complicated expression and makes Boltzmann equation difficult to solve. A useful approximation for the collision integral, which works well in many circumstances, especially when the system is weakly out of equilibrium, is the so-called *relaxation time approximation* [105, 106], whose mathematical formulation is:

$$\mathcal{I}_{\text{coll}}[\tilde{f}] = -\frac{\tilde{f}(\mathbf{r}, \mathbf{k}, t) - f(\xi_{\mathbf{k}})}{\tau(\mathbf{r}, \mathbf{k})}$$

Here, $\tau(\mathbf{r}, \mathbf{k})$ is the relaxation time, and within this approximation it is the only relevant time scale that comes into play in scattering processes. In the case of homogeneous systems (on a scale much larger than lattice spacing), this time scale depends only on the moment, in which case we will simply write $\tau(\mathbf{r}, \mathbf{k}) = \tau(\mathbf{k})$. The relaxation time in Boltzmann theory plays the same role as the quasiparticle lifetime $\tau_{\mathbf{k}}$ in Fermi liquid theory. This is not the only point of contact between the two theories. However, since within Boltzmann description there is no concept analogous to the quasiparticle effective mass, if we want to describe a purely Fermi liquid system with Boltzmann theory we need to insert this concept manually into the latter. For instance, if we want to replicate the coefficients introduced within linear response theory through equation (2.6) we have to take care to modify the linear system as follows:

$$\begin{cases} Z\langle \mathbf{J}^N \rangle_{\text{n.e.}} = -Z\Gamma_{11}^{\text{B}} \nabla(\mu + \text{e}\phi) - \Gamma_{12}^{\text{B}} \dfrac{\nabla T}{T} \\ \\ Z^2\langle \mathbf{J}^Q \rangle_{\text{n.e.}} = -Z\Gamma_{12}^{\text{B}} \nabla(\mu + \text{e}\phi) - \Gamma_{22}^{\text{B}} \dfrac{\nabla T}{T} \end{cases}$$

Where we simply considered $Z = m_{el}/m_{el}^*$, according to the idea that the self-energy within Kubo counterpart is assumed to be momentum-independent, and that $Z_{\mathbf{k}_{\text{F}}}$ does not depend on the specific wave vector of the Fermi surface. The superscript appearing in the $\Gamma_{\alpha\beta}^{\text{B}}$ coefficients denotes that they are calculated within Boltzmann formalism. From the comparison with system (2.6) the following relationships are evident:

$$\Gamma_{11} = \Gamma_{11}^{\text{B}} \qquad \Gamma_{12} = \Gamma_{12}^{\text{B}}/Z \qquad \Gamma_{22} = \Gamma_{22}^{\text{B}}/Z^2$$

As we shall see in more detail in chapter 5, in the calculation of $\Gamma_{\alpha\beta}$ coefficients for fermionic responses terms proportional to the square of $\mathrm{Im}G_R(\omega,\mathbf{k})$ will often appear. The bridge with the $\Gamma^{\mathrm{B}}_{\alpha\beta}$ coefficients of the Boltzmann formalism is given by the following identification [54]:

$$\frac{1}{\pi}\left[\mathrm{Im}G_R(\omega,\mathbf{k})\right]^2 \simeq \frac{\delta(\omega-\xi_{\mathbf{k}}-\mathrm{Re}\Sigma_R(\omega,\mathbf{k}))}{2\,\mathrm{Im}\Sigma_R(\omega,\mathbf{k})}$$

Notice that, for a purely Fermi liquid system, the quantity on the right-hand side can be expressed as $Z^2\delta(\omega-\tilde{\omega}_{\mathbf{k}})\,\tau_{\mathbf{k}}$.

2.5 Thermodynamics

In addition to the transport properties, for which we have exhibited the main elements of theory that we are going to use, another physical quantity of interest for the purposes of this work is the specific heat. It is a fundamental thermodynamic quantity, and its calculation can be carried out by exploiting elementary relations of statistical mechanics. The subtlety behind the calculations we are going to make lies in the fact that we are dealing with dissipative systems. Consequently, strictly speaking, a Hamiltonian approach may not be a good starting point to describe the thermodynamic properties of the systems we aim to study, and it is therefore necessary to rely on more general tools. A good starting point is the expression of the partition function of the system in terms of the field propagator as functional integrals [107]:

$$\mathcal{Z}^f_G = \int e^{-\beta\sum_{\mathbf{k},\sigma}\sum_{n\,\mathrm{odd}}\overline{\psi}_{-\omega_n,-\mathbf{k}}\mathcal{G}^{-1}(\omega_n,\mathbf{k})\,\psi_{\omega_n,\mathbf{k}}} d[\overline{\psi}]d[\psi] = \prod_{\mathbf{k},\sigma}\prod_{n\,\mathrm{odd}}\beta\mathcal{G}^{-1}(\omega_n,\mathbf{k})$$

$$\mathcal{Z}^b_G = \int e^{-\beta\sum_{\mathbf{k}}\sum_{n\,\mathrm{even}}\phi_{-\omega_n,-\mathbf{k}}\mathcal{D}^{-1}(\omega_n,\mathbf{k})\,\phi_{\omega_n,\mathbf{k}}} d[\phi] = \prod_{\mathbf{k}}\prod_{n\,\mathrm{even}}\sqrt{\frac{\pi}{\beta\mathcal{D}^{-1}(\omega_n,\mathbf{k})}}$$

Of course, $\mathcal{Z}^f_G$ refers to a fermionic field while $\mathcal{Z}^b_G$ refers to a (real and spinless) bosonic one. The fields we have denoted with $\psi_{\omega_n,\mathbf{k}}$ and $\phi_{\omega_n,\mathbf{k}}$ are to be understood as the Fourier transforms of the fields $\psi(\tau,\mathbf{r})$ and $\phi(\tau,\mathbf{r})$ respectively, nonetheless choosing a normalization similar to the one commonly used to express the creation and destruction operators in terms of field operators. Note that, for the bosonic propagator, we used the same notation that we had chosen for charge density fluctuations propagator, however we want to point out that the expression of $\mathcal{Z}^b_G$ we have shown is valid for any real bosonic field. The advantage of starting from the partition functions instead of the internal energy is that they are well defined even for a non-conservative system. There is a temptation to state that the total partition function $\mathcal{Z}^{tot}_G$ of a system of fermions and bosons is the product between $\mathcal{Z}^f_G$ and $\mathcal{Z}^b_G$, which would be true for instance in the case of a system in which electrons

and bosonic collective modes do not interact. If the two degrees of freedom interact with each other, the exact partition function of the system cannot be factorized into a fermionic and a bosonic part [108, 109]. In principle, factorizing the partition function for the interacting system would lead to a problem of double-counting of some contributions. However, in section 3.6 we will show that the most important contribution to the thermodynamics in our systems comes only from the bosonic part and is therefore not double-counted. This allows us to safely approximate $\mathcal{Z}_G^{tot}$ as $\mathcal{Z}_G^f \mathcal{Z}_G^b$ without overestimating the leading term to the calculation of thermodynamic properties of the systems we are going to study.

With that being said, starting from the partition function of the system we can formally express the Helmholtz free energy, the internal energy and the entropy, respectively, as follows:

$$F = -\frac{1}{\beta} \log \mathcal{Z}_G \qquad U = \frac{\partial}{\partial \beta} (\beta F) \qquad S = -k_{\mathrm{B}} (\beta F - \beta U)$$

It should be stressed that, in presence of dissipation, the thermodynamic potentials expressed by these three equations may not be well-defined. However, we will always assume the validity of these three equations, with the eventuality that the physical quantities they describe have to be understood as a sort of "generalized" version of the quantities they are supposed to be. In any case, the first thermodynamic potential that we need to calculate is F, for which the following expressions are valid:

$$F_f = -\frac{1}{\beta} \sum_{\mathbf{k},\sigma} \sum_{n\,\mathrm{odd}} \log \left(\beta \mathcal{G}^{-1}(\omega_n, \mathbf{k}) \right) \qquad F_b = \frac{1}{2\beta} \sum_{\mathbf{k}} \sum_{n\,\mathrm{even}} \log \left(\frac{\beta \mathcal{D}^{-1}(\omega_n, \mathbf{k})}{\pi} \right) \tag{2.13}$$

The Matsubara sums are formally divergent, nevertheless it is possible to regularize them by means of standard quantum field theory techniques and to calculate them exactly in the cases of our interest.

In the context of this thesis, by "specific heat" we will always mean the heat capacity at constant volume normalized to the total number of unit cells of the system. As discussed in Appendix A, if a three-dimensional system exhibits a trivial behavior along the z-axis it can be treated as a full-fledged two-dimensional system, with the only precaution of entering the factor $1/v_{\mathrm{uc}}$ manually to take into account the possible normalization of a $\mathbf{k}$-sum with respect to the three-dimensional volume of the system. Since we are normalizing the specific heat with respect to the total number of unit cells we do not have to take this factor into account, so just as the $\mathbf{k}$-sums are extended to a two-dimensional domain, the total number of sites considered is that of the single lattice plane. We remind that we are considering a system of units for which the lattice spacing on the plane is taken as unit, so normalizing by the total number of sites is equivalent to normalizing by the total (two-dimensional) volume. Our expression for the specific heat is therefore:

$$c_V := \frac{1}{N} \frac{\partial U}{\partial T} = -k_{\mathrm{B}} \frac{\beta^2}{N} \frac{\partial U}{\partial \beta} \tag{2.14}$$

In addition the calculation of the specific heat, in section 5.3 we will use the generalized expressions of the thermodynamic potentials in the presence of damping to provide a possible definition of the heat current transported by charge density fluctuations. That expression will play an important role in the calculation of the Seebeck coefficient.

The calculation scheme we have introduced for specific heat is completely general and works in every temperature range. However, for the particular case of the fermionic contribution at low temperature it is often convenient to perform the calculation via the Sommerfeld expansion. In the case of a non-interacting Fermi gas, this technique allows the specific heat to be expressed in a compact form:

$$c_V^f = \frac{\pi^2}{3} k_B^2 T N_0 \tag{2.15}$$

Where N_ω is the density of states for the non-interacting electron system (or *bare* density of states), in this case evaluated at $\omega = 0$. The corresponding function in the case of an interacting system (or *dressed* density of states) will be denoted by N_ω^{int}, in order to distinguish it from the former. The definitions of these two functions are the following:

$$N_\omega := \frac{1}{N} \sum_{\mathbf{k},\sigma} \delta(\omega - \xi_{\mathbf{k}}) \qquad N_\omega^{int} := \frac{1}{N} \sum_{\mathbf{k},\sigma} \left(-\frac{1}{\pi} \mathrm{Im} G_R(\omega, \mathbf{k}) \right) \tag{2.16}$$

By definition, both functions are normalized with respect to spin multiplicity, which is 2. Of course, the second of these two expressions becomes equal to the first one if the Green's function is that of the non-interacting system. In order to generalize our expression for c_V^f to the interacting case, the first thing that comes to mind is to simply replace N_0 with N_0^{int}. This would be fine if the self-energy that describes the interactions does not depend on temperature. If the temperature dependence of self-energy is not negligible, the issue is more delicate. In the particular case of a Fermi liquid system, for which the temperature dependence of the self-energy is actually important, Landau theory states that the complete asymptotic expression of the specific heat at low temperature is obtained simply by rescaling the expression given by Sommerfeld expansion by the constant term m_{el}^*/m_{el}, already introduced in section 2.1 [110]:

$$c_V^f = \frac{\pi^2}{3} k_B^2 T \frac{m_{el}^*}{m_{el}} N_0^{int} \tag{2.17}$$

Where the assumption that N_0^{int} is evaluated at zero temperature is implicit. It is worth noting that, for a purely Fermi liquid system, the expression of N_0^{int} is very similar to the corresponding expression in the non-interacting case. In fact:

$$N_0 = \frac{1}{N} \sum_{\mathbf{k},\sigma} \delta(\xi_{\mathbf{k}}) \qquad N_0^{int} = \frac{1}{N} \sum_{\mathbf{k},\sigma} \delta(\xi_{\mathbf{k}} + \mathrm{Re}\Sigma_R(0, \mathbf{k}))$$

For the particular case of a momentum-independent self-energy, the effect of the Fermi-liquid interaction on the specific heat consists in a simple uniform shift of the chemical potential in the density of states. If instead we have $\mathrm{Re}\Sigma_R(0, \mathbf{k}) = 0$ at any $\mathbf{k}$, the two densities of the states coincide at $\omega = 0$.

Another interesting case, which will also be particularly relevant in this thesis work, is the one in which the electronic interaction is provided by a constant elastic scattering, provided for instance by impurities. It can be described by a self-energy of the form $\Sigma_R(\omega, \mathbf{k}) = -i\Sigma_0$, where Σ_0 is a real and positive term having the dimension of an energy. In this case, the dressed density of states is simply a convolution between the bare density of states and a Lorentzian distribution:

$$N_\omega^{int} = \frac{1}{N}\sum_{\mathbf{k},\sigma}\frac{1}{\pi}\frac{\Sigma_0}{(\omega-\xi_\mathbf{k})^2+\Sigma_0^2} = \int_{-\infty}^{+\infty}\frac{1}{\pi}\frac{\Sigma_0}{(\omega-\xi)^2+\Sigma_0^2}\,N_\xi\,d\xi$$

The reason why this kind of interaction is particularly interesting is that it removes and flattens any singularities in the density of states. It should be stressed that this self-energy is in conflict with the hypotheses that characterize a Fermi liquid. However, as this is a particularly simple interaction to deal with, it is easy to include this effect within a purely Fermi liquid description. In the calculation of the specific heat for a system in which the self-energy is given by the superposition of a Fermi liquid and a constant impurity scattering component, the terms coming from the derivative of N_ω^{int} with respect to temperature provide corrections of order $k_\mathrm{B}T/\Sigma_0$ to the ratio c_V^f/T provided by Sommerfeld expansion, therefore they are negligible at low temperature, provided that by "low temperature" it is meant that $k_\mathrm{B}T$ is much lower than Σ_0 (as well as much lower than the Fermi energy, as is required in the usual Sommerfeld expansion). For this reason, the term m_{el}^*/m_{el} should not be included in the Sommerfeld expression for c_V^f. In this case, the full expression for N_ω^{int} would become:

$$N_\omega^{int} = \frac{1}{N}\sum_{\mathbf{k},\sigma}\frac{1}{\pi}\frac{-\mathrm{Im}\Sigma_R(\omega,\mathbf{k})}{\left(\omega-\xi_\mathbf{k}-\mathrm{Re}\Sigma_R(\omega,\mathbf{k})\right)^2+\mathrm{Im}\Sigma_R(\omega,\mathbf{k})^2}$$

Where $\mathrm{Im}\Sigma_R(\omega,\mathbf{k})$ is given by the sum of $-\Sigma_0$ and a Fermi liquid self-energy term. Nevertheless, in the same temperature regime, the whole imaginary part of $\Sigma_R(\omega,\mathbf{k})$ is dominated by the impurity scattering term, therefore the approximation $\mathrm{Im}\Sigma_R(\omega,\mathbf{k}) \simeq -\Sigma_0$ is valid. The real part of $\Sigma_R(\omega,\mathbf{k})$ remains explicit in the complete expression for N_ω^{int}, however it is exactly the same as that obtained from the purely Fermi liquid case, as the addition of the term $-\Sigma_0$ to $\mathrm{Im}\Sigma_R(\omega,\mathbf{k})$ does not contribute to the Kramers-Kronig relation for $\mathrm{Re}\Sigma_R(\omega,\mathbf{k})$. Based on these observations, the specific heat for the described system should have the following expression:

$$c_V^f = \frac{\pi^2}{3}k_\mathrm{B}^2 T N_0^{int} \qquad \text{where} \quad N_0^{int} = \frac{1}{N}\sum_{\mathbf{k},\sigma}\frac{1}{\pi}\frac{\Sigma_0}{\left(\xi_\mathbf{k}+\mathrm{Re}\Sigma_R(0,\mathbf{k})\right)^2+\Sigma_0^2} \tag{2.18}$$

Where, again, $\mathrm{Re}\Sigma_R(0,\mathbf{k})$ is evalued at zero temperature. Even here, if we consider the particular case of a momentum-independent self-energy, N_0^{int} is simply given by the convolution between N_ξ and the same Lorentzian distribution exhibited previously:

$$N_0^{int} = \int_{-\infty}^{+\infty} \frac{1}{\pi} \frac{\Sigma_0}{\left(\xi + \mathrm{Re}\Sigma_R(0)\right)^2 + \Sigma_0^2} N_\xi \, d\xi$$

The only difference with the previous case is that the chemical potential is shifted due to the real part of the self-energy evaluated at $\omega = 0$. We stress that the chemical potential renormalization is not a peculiar effect of the Fermi-liquid theory but applies to more general forms of interactions, including the one we are considering now. However, since in this case the effect of Σ_0 is to attenuate the profile of the bare density of states, the effect of the chemical potential shift is rather slight as long as Σ_0 is sufficiently large.

Starting from the theoretical concepts that we have exposed so far, we are able to build the models that we will use for the purposes of this thesis work. Before addressing the question of charge density fluctuations in the strange-metal phase of cuprates, we will start by considering a preliminary model, which shares all the essential characteristics with the charge density fluctuations model. For reasons that will become clear throughout the discussion, we will refer to the behavior that emerges from this particular model as *Shrinking Fermi liquid* [111].

Chapter 3

Preliminary model for Shrinking Fermi liquid behavior

As we have already highlighted, a central role for the purposes of our study is played by the electronic self-energy, therefore one of the first problems we want to address is the explicit calculation of this function. According to equation (2.4), the momentum dependence of self-energy is directly determined by that of the charge density fluctuations propagator. Within our description, we know that the latter is weak, this allows us to treat the self-energy essentially as momentum-independent.

Although we can neglect its momentum dependence, the dependence of the self-energy on frequency and temperature is, in general, important and rather difficult to treat. The complete calculation can only be performed numerically, and we will exhibit all the details in the next chapter. Instead, in this chapter we are going to consider a simpler model, in which the collective mode considered is that of a damped Holstein phonon, while the electronic density of states is taken as constant.

3.1 Self-energy provided by a damped dispersionless collective mode

The propagator of the damped Holstein phonon has essentially the same form as that of the charge density fluctuations shown in equation (2.2), with the only difference that it is strictly dispersionless (or local) [112], so the dispersion $m_{\mathbf{k}}$ is replaced by the constant value M. Similarly to the case of charge density fluctuations, we denote this propagator by $D_R(\omega)$, where $\mathbf{k}$ obviously no longer appears as argument of the function:

$$D_R(\omega) = \frac{1}{M - i\gamma\omega - \dfrac{\omega^2}{\Omega}} \qquad \mathrm{Im}D_R(\omega) = \frac{1}{\gamma}\frac{\omega}{\left(\dfrac{M}{\gamma} - \dfrac{\omega^2}{\gamma\Omega}\right)^2 + \omega^2}$$

This is simply the retarded Green's function associated with a one-dimensional damped harmonic oscillator. Exceptionally for this chapter, the bosonic propagator $D_R(\omega)$ will be used to describe only the damped Holstein phonon mode, and any

mention to a bosonic collective mode will always be understood as referring to this particular phonon mode. For the sake of concreteness, we will attribute to M and Ω values similar to those experimentally known for charge density fluctuations, while we leave γ as a variable parameter. Just to be able to adapt our simplified model to the description of charge density fluctuations, at the appropriate moment we will introduce a slight temperature dependence for this last parameter. Another assumption of this model is that the density of states is constant, we denote its value by N_0 (not to be confused with the total number of sites N) according to the notation introduced in equation (2.16). The effect of a finite bandwidth can be mimicked by manually introducing an ultraviolet cutoff of the same order of magnitude as the bandwidth itself, however for the purposes of our discussion we do not need to include this effect. In light of what we have said so far, we can express the imaginary part of the self-energy as follows:

$$\mathrm{Im}\Sigma_R(\omega,T) = -\frac{g^2 N_0}{M}\frac{M}{\gamma}\int_{-\infty}^{+\infty} \frac{\xi}{\left(\frac{M}{\gamma}-\frac{\xi^2}{\gamma\Omega}\right)^2+\xi^2}\frac{\cosh\left(\frac{\beta\omega}{2}\right)}{2\cosh\left(\frac{\beta(\xi+\omega)}{2}\right)\sinh\left(\frac{\beta\xi}{2}\right)}d\xi \tag{3.1}$$

Since in this study we will focus on the temperature and frequency dependencies of this object, we decided to explicitly insert the temperature as second argument of the function (therefore not to be confused with the momentum $\mathbf{k}$, which in this case is absent). The reason we expressed the prefactor of the integral that way is that we can identify the ratio g^2N_0/M as a dimensionless coupling constant, which we will denote by λ. We shall assume that λ is significantly less than one in order to justify a perturbative approach, for the concrete case of charge density fluctuations observed in slightly overdoped cuprates it has been shown that $\lambda \simeq 0.3 - 0.5$ [81], so it seems reasonable to adopt this kind of approach. Notice that this expression for $\mathrm{Im}\Sigma_R(\omega,T)$ is negative definite, as we expect since it is the imaginary part of a retarded function, and that it is an odd function of ω. This latter property implies that $\mathrm{Re}\Sigma_R(\omega=0,T)=0$, therefore this model does not provide any renormalization of the chemical potential at any temperature.

Expression (3.1) can be taken as the starting point for the deduction of all quantitative aspects of our model. Unfortunately, the integral which appears in this expression cannot be analitically solved for any frequency and temperature, however it is possible to obtain interesting analytical results restricted to suitable physical regimes.

3.2 Temperature behavior at zero frequency

First of all, let's explore the temperature dependence of the imaginary part of self-energy at fixed $\omega = 0$:

$$\mathrm{Im}\Sigma_R(\omega=0,T) = -\lambda\frac{M}{\gamma}\int_{-\infty}^{+\infty} \frac{\xi}{\left(\frac{M}{\gamma}-\frac{\xi^2}{\gamma\Omega}\right)^2+\xi^2}\frac{1}{\sinh(\beta\xi)}d\xi \tag{3.2}$$

This integral is not analytically solvable, however it is possible to identify two limit regimes as a function of temperature:

$$\mathrm{Im}\Sigma_R(\omega=0,T) \simeq \begin{cases} -\dfrac{\lambda}{2}\dfrac{M}{\gamma}\left(\pi\dfrac{\gamma k_{\mathrm{B}}T}{M}\right)^2 & \text{for } k_{\mathrm{B}}T \ll \dfrac{M}{\gamma} \\ -\lambda\pi k_{\mathrm{B}}T & \text{for } k_{\mathrm{B}}T \gg \dfrac{M}{\gamma} \end{cases}$$

Notice that our expression for $\mathrm{Im}\Sigma_R(\omega = 0, T)$ predicts a crossover between a quadratic and a linear regime, and that this crossover is only ruled by the parameter M/γ. What is most remarkable is that the slope of the linear regime does not depend on γ. These features are particularly interesting as they seem to accurately describe the behavior of resistivity in the strange-metal phase. In fact, for an isotropic scattering mechanism, the DC resistivity is essentially proportional to $|\mathrm{Im}\Sigma_R(\omega = 0, T)|$, therefore according to our model we get a Fermi liquid resistivity at low enough temperature and a linear regime at higher temperature. The effect of increasing γ (at a fixed M) is to extend the linear regime to increasingly lower temperatures without affecting the slope at high temperature. From here on out, we will refer to this kind of behavior as *Shrinking Fermi liquid*. We stress that the damped Holstein model we are discussing is not necessarily the only possible realization of this shrinking Fermi liquid behavior. Nevertheless, we chose this model as an exemplary case both for its simplicity and for the srong analogy between damped dispersionless phonon and charge density fluctuations.

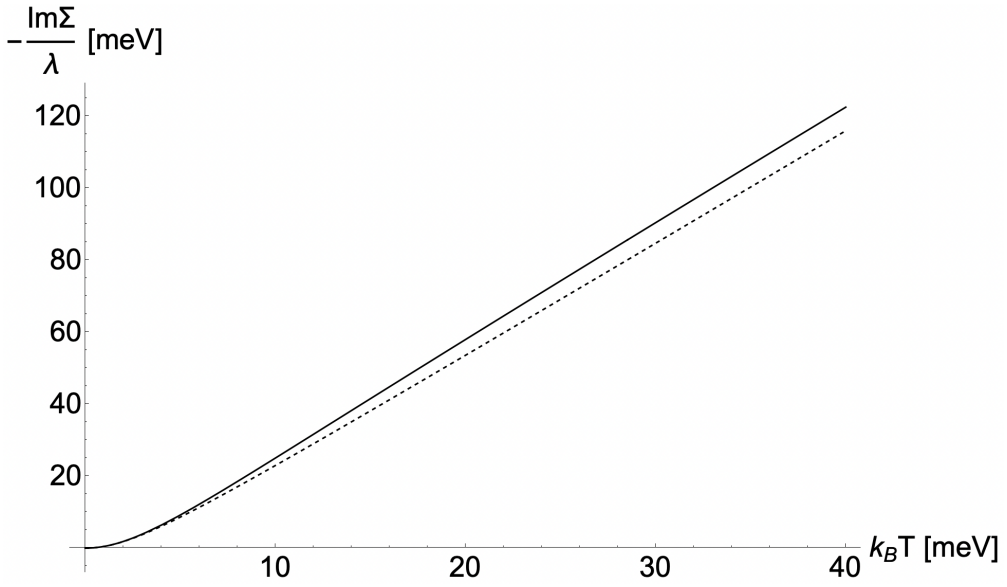

Figure 3.1. From [111], graphical comparison between the exact expression of $\mathrm{Im}\Sigma_R(\omega = 0, T)$ provided by equation (3.2) (solid lines) and the approximate expression given by (3.3) (dashed lines), we fixed $M = 10\,\mathrm{meV}$, $\gamma = 1$ and $\Omega = 30\,\mathrm{meV}$.

A possible fitting expression for $\mathrm{Im}\Sigma_R(\omega = 0, T)$ that works well at any temperature range is the following:

$$\mathrm{Im}\Sigma_R(\omega = 0, T) \simeq -\lambda \frac{M}{\gamma} \left[\sqrt{1 + \left(\pi \frac{\gamma k_\mathrm{B} T}{M} \right)^2} - 1 \right] \tag{3.3}$$

3.3 Energy behavior at zero temperature

According to (3.1), the zero temperature expression for $\mathrm{Im}\Sigma_R(\omega, T)$ is:

$$\mathrm{Im}\Sigma_R(\omega, T = 0) = -\lambda \frac{M}{\gamma} \int_0^\omega \frac{\xi}{\left(\frac{M}{\gamma} - \frac{\xi^2}{\gamma \Omega} \right)^2 + \xi^2} d\xi \tag{3.4}$$

This integral has an exact expression in terms of elementary functions, however the complete expression is not enlightening for understanding the physics behind it. It is instead interesting to observe the behavior of this expression in appropriate regimes. The only two energy scales relevant to this function can both be expressed as the product between the energy scale M/γ and a dimensionless function of the parameter $\phi \coloneqq \gamma^2 \Omega / M$. We denote these two energy scales by ω_infl and ω_sat, and their definitions are the following:

$$\omega_\mathrm{infl} \coloneqq \frac{M}{\gamma} \sqrt{\phi \frac{\sqrt{(\phi - 2)^2 + 12} - (\phi - 2)}{6}} \qquad \omega_\mathrm{sat} \coloneqq \max\left(\frac{M}{\gamma} \phi \,,\, \omega_\mathrm{infl} \right)$$

By definition of these two scales, we always have the inequality $\omega_\mathrm{sat} \geq \omega_\mathrm{infl}$, it can also be shown that this inequality becomes strict for $\phi > (1 + \sqrt{5})/4$. The function $\mathrm{Im}\Sigma_R(\omega, T = 0)$ goes as ω^2 at small ω and saturates to a constant value at large ω. In the intermediate frequency regime there is an extended inflection in which an approximately linear regime can be observed. The frequency ω_infl is defined precisely as the inflection point of this function, while ω_sat is the approximate scale beyond which the saturation regime is observed. Given these, we have the following approximate behaviors:

$$\mathrm{Im}\Sigma_R(\omega, T = 0) \simeq \begin{cases} -\dfrac{\lambda}{2} \dfrac{M}{\gamma} \left(\dfrac{\gamma \omega}{M} \right)^2 & \text{for } \omega \ll \omega_\mathrm{infl} \\ -\lambda \dfrac{\Lambda_\phi}{2} \omega & \text{for } \omega \simeq \omega_\mathrm{infl} \\ \mathrm{Im}\Sigma_R(\omega \to \infty, T = 0) & \text{for } \omega \gg \omega_\mathrm{sat} \end{cases}$$

Where Λ_ϕ is defined in such a way as to replicate the correct slope of $\mathrm{Im}\Sigma_R(\omega, T = 0)$ at the inflection point, its expression as a function of ϕ is the following:

$$\Lambda_\phi = \frac{2\sqrt{\phi\dfrac{\sqrt{(\phi-2)^2+12}-(\phi-2)}{6}}}{\left(1-\dfrac{\sqrt{(\phi-2)^2+12}-(\phi-2)}{6}\right)^2+\phi\dfrac{\sqrt{(\phi-2)^2+12}-(\phi-2)}{6}}$$

This is a monotonic decreasing function of ϕ which approaches 1 in the limit $\phi \to \infty$ and goes as $2/\sqrt{\phi}$ when ϕ goes to zero. The qualitative trend of $\mathrm{Im}\Sigma_R(\omega, T=0)$ is more complicated than what we found for the complementary case $\mathrm{Im}\Sigma_R(\omega=0,T)$ and cannot be fitted with an expression similar to (3.3) in all frequency regimes. However, we can exhibit a rather simple fitting expression limited to the $\omega \leq \omega_{\mathrm{infl}}$ regime:

$$\begin{cases} \mathrm{Im}\Sigma_R(\omega, T=0) \simeq -\lambda\dfrac{M}{\gamma}\left[\sqrt{1+\left(\dfrac{4+\Lambda_\phi^2}{4\Lambda_\phi}\dfrac{\gamma\omega}{M}\right)^2}-\sqrt{1+\left(\dfrac{4-\Lambda_\phi^2}{4\Lambda_\phi}\dfrac{\gamma\omega}{M}\right)^2}\right] \\ 1 \leq \Lambda_\phi \leq 2 \end{cases} \tag{3.5}$$

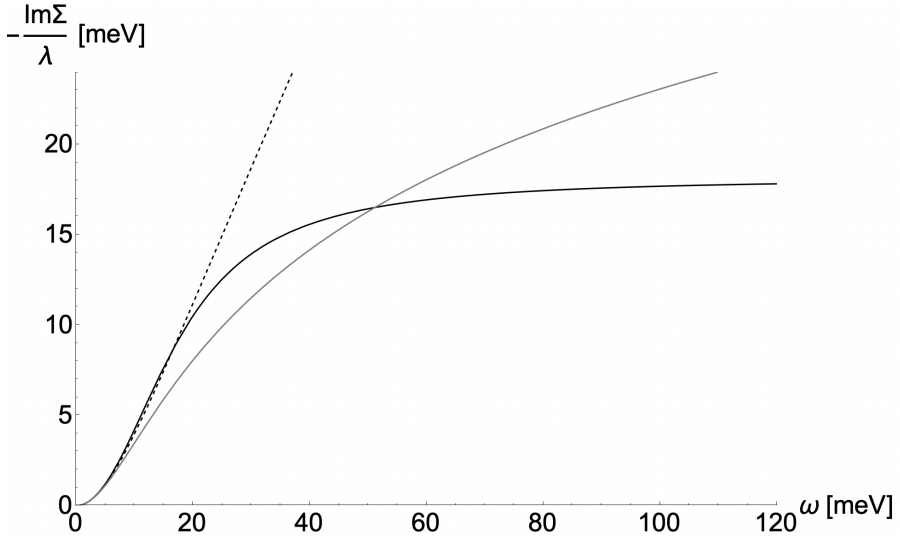

Figure 3.2. From [111], graphical comparison between the exact expression of $\mathrm{Im}\Sigma_R(\omega, T=0)$ provided by equation (3.4) (solid lines) and the approximate expression given by (3.5), we fixed $M = 10\,\mathrm{meV}$, $\gamma = 1$ and $\Omega = 30\,\mathrm{meV}$ (which provide $\phi = 3$ and $\Lambda_\phi \simeq 1.407$). The solid grey line is a plot of expression (3.4) in the case $\Omega \to \infty$.

3.4 Quasiparticle weight at zero temperature

As discussed in section 2.5, the electronic contribution to the specific heat for a Fermi liquid at low temperature is given by the standard Sommerfeld expansion, provided that the standard expression is multiplied by the factor m^*_{el}/m_{el} evalued

at zero temperature. Since we are considering a momentum-independent self-energy, this ratio is simply equal to $1/Z$, where Z does not depend on the choice of the specific Fermi surface wave vector. This latter quantity is connected to the derivative of the real part of the self-energy at $T = 0$ and $\omega = 0$, which is:

$$\frac{\partial \mathrm{Re}\Sigma_R(\omega, T=0)}{\partial \omega}\Big|_{\omega=0} = \int_0^\infty \frac{1}{\omega}\left[\frac{\partial \mathrm{Im}\Sigma_R(\omega', T=0)}{\partial \omega'}\Big|_{\omega'=\omega} + \right.$$
$$\left. -\frac{\partial \mathrm{Im}\Sigma_R(\omega', T=0)}{\partial \omega'}\Big|_{\omega'=-\omega}\right]\frac{d\omega}{\pi} = -\lambda\int_{-\infty}^{\infty}\frac{M}{\gamma}\frac{1}{\left(\frac{M}{\gamma}-\frac{\omega^2}{\gamma\Omega}\right)^2+\omega^2}\frac{d\omega}{\pi} = -\lambda$$

And the corresponding quasiparticle weight is:

$$Z = \left(1 - \frac{\partial \mathrm{Re}\Sigma(\omega, T=0)}{\partial \omega}\Big|_{\omega=0}\right)^{-1} = \frac{1}{1+\lambda}$$

Which is a particularly interesting result as it shows that the quasiparticle weight is completely independent of γ and Ω, and that it's always regular as the coupling constant λ is finite (and small) by hypothesis. In particular, this would imply that the fermionic specific heat is not renormalized by γ at low temperature, and that it's always finite (non-critical). This is a consequence of the fact that our system, at sufficiently low energy, always behaves like a standard Fermi liquid, therefore there is no reason to expect a singular mass renormalization. The effect of an ultraviolet cutoff ω_c would be to introduce Z corrections of order $M/(\gamma\omega_c)$, which vanish when this latter quantity goes to zero and of course are irrelevant for our purposes.

3.5 Comparison with Marginal Fermi liquid theory

Based on what we have shown so far, our model seems to have some interesting points of contact with the Marginal Fermi liquid theory. This theory is based on the phenomenological assumption that the imaginary part of the electronic self-energy is proportional to $\min(\omega, \pi k_B T)$ or, equivalently, to $\sqrt{\omega^2 + (\pi k_B T)^2}$, with no momentum dependence [113]. This implies that the quasiparticle residue at zero temperature diverges logarithmically as we approach the Fermi surface. This means that the single particle occupation function is continuous as a function of $\mathbf{k}$, but it has a point of non-differentiability, therefore the concept of Fermi surface is still well-defined both in frequency and in momentum space [110]. For this reason, Marginal Fermi liquid is in a sense the weakest way to violate the standard Fermi liquid.

In order to have an immediate comparison between our self-energy and the self-energy of a Marginal Fermi liquid, we choose to express the imaginary part of the latter as follows:

$$\mathrm{Im}\Sigma_R(\omega, T)_{MFL} = -\lambda\sqrt{\left(\frac{\Lambda_\phi}{2}\omega\right)^2 + (\pi k_B T)^2} \tag{3.6}$$

The prefactor of ω was placed by hand, it ensures that the high frequency behavior of this expression is the very same as the one provided by (3.5), in order to have a more immediate comparison with our model. Strictly speaking, this expression describes a Marginal Fermi liquid only for $\Lambda_\phi = 2$, but since the prefactor we included is of order 1 this is an irrelevant detail for our discussion. What is most relevant is that the perfect ω/T scaling that characterizes the Marginal Fermi liquid remains preserved.

If we put together the two approximate expressions (3.3) and (3.5) we obtain the following fitting expression for the imaginary part of our self-energy:

$$\mathrm{Im}\Sigma_R(\omega, T) \simeq -\lambda \left[\sqrt{\left(\frac{M}{\gamma}\right)^2 + \left(\frac{4+\Lambda_\phi^2}{4\Lambda_\phi}\omega\right)^2 + (\pi k_\mathrm{B} T)^2} - \sqrt{\left(\frac{M}{\gamma}\right)^2 + \left(\frac{4-\Lambda_\phi^2}{4\Lambda_\phi}\omega\right)^2} \right] \tag{3.7}$$

We need to include two constraints on this expression:

$$1 \leq \Lambda_\phi \leq 2 \quad \wedge \quad k_\mathrm{B} T < \frac{4\Lambda_\phi \sqrt{2(16+\Lambda_\phi^4)}}{\pi(4-\Lambda_\phi^2)^2} \frac{M}{\gamma}$$

The first of these two constraints comes directly from (3.5), and is necessary for the slope of the linear part of the original function to be correctly fitted. The second constraint ensures that the fitting expression we have proposed is always an increasing function of ω, and that its behavior at low ω is effectively quadratic. This expression becomes particularly similar to the one we proposed for $\mathrm{Im}\Sigma_R(\omega, T)_{MFL}$ in the case $\Lambda_\phi = 2$, and of course this is not the only point of contact between the two schemes.

In light of what has been shown so far, we note that our Shrinking Fermi liquid has several interesting similarities and differences with the Marginal Fermi liquid. First of all, while Marginal Fermi liquid exhibits an exact ω/T scaling, within our model this scaling is violated due to the M/γ term, however an approximate scaling can be recovered at sufficiently high temperatures and frequencies. The absence of an exact scaling in our model is a consequence of the different origin for the linear regimes in ω and in T, however the fact that the scaling is only approximate may account for for the small scaling violations at low frequencies in slightly overdoped cuprates observed in optical experiments [114]. The most interesting connection between the two scenarios is probably the temperature dependence of the self-energy imaginary part. In fact, our approximate expression for $\mathrm{Im}\Sigma_R(\omega = 0, T)$ works in any temperature range, and it perfectly simulates the Marginal Fermi liquid case (i.e. it becomes linear in temperature) if temperature is sufficiently larger than the scale M/γ. As we mentioned, this implies that the resistivity of a Shrinking Fermi liquid becomes a linear function of temperature, and that the energy scale at which this regime begins is exactly M/γ. If, for some reason, γ slightly depends on temperature, in such a way as to be a decreasing function of T when the latter is low, the range of validity of the Fermi liquid regime *shrinks* by decreasing the temperature. In ref. [115] we proposed the following phenomenological expression

for γ as a function of temperature and doping level in order to reproduce specific heat data for $La_{1.8-x}Eu_{0.2}Sr_xCuO_4$ and $La_{1.6-x}Nd_{0.4}Sr_xCuO_4$ compounds [55]:

$$\gamma = \gamma(T,p) = \frac{1}{\left[\gamma_0 \log\left(1 + \frac{T_0}{\min(T, T_{\mathrm{sat}})}\right)\right]^{-1} + \upsilon\,|p - p^*|} \tag{3.8}$$

Where p^* is the pseudogap critical doping level, which we identify with the value of doping at which γ may diverge, while the temperature scale T_{sat} is simply the scale above which the temperature dependence of γ becomes negligible. For instance, if we want to impose that γ is never less than 1 for $p = p^*$, we must set $T_{\mathrm{sat}} = T_0/(e^{1/\gamma_0} - 1)$. It should be stressed that, in the application of this model to the specific case of charge density fluctuations in cuprates, p^* should not be identified with the critical doping level p_c [96]. The distance between the two points is generally finite and compound-dependent, for our description to be meaningful we only need the two points to not be very far apart. The requirement that p^* not be too far from p_c is to ensure that the collective mode in question has sufficiently low energy, however for it to be sufficiently broad in momentum space the strict inequality $p^* > p_c$ must hold.

In figure 3.3 we show a comparison between expressions (3.7) and (3.6) in the two cases in which we have, respectively, $\gamma = 1$ and $\gamma = \gamma(T) = \log(20\,\mathrm{meV}/(k_{\mathrm{B}}T))$, the latter is just a simplified version of expression (3.8), which still captures the Shrinking Fermi liquid behavior at low temperature and at the critical doping level (the scale of 20 meV is essentially arbitrary). From this plot the relationship between the increase of γ and the narrowing of the window in which the Fermi liquid regime holds is clear, as well as the similarity with Marginal Fermi liquid.

A remarkable difference between the two scenarios is the behavior of the quasiparticle weight, and its effect on the electronic contirbution to the specific heat. In fact, while Marginal Fermi liquid theory would provide a logarithmically divergent quasiparticle effective mass as temperature goes to zero, and therefore a singular behavior for the specific heat [110], within our model the fermionic contribution to the specific heat is perfectly regular. Nevertheless, as the microscopic origin of the Shrinking Fermi liquid behavior within this model is provided by damped dispersionless phonon modes, the latter can give a direct contribution to the specific heat of the system. Therefore, the total specific heat of this system is provided by the sum of the renormalized fermionic contribution, which is essentially given by equation (2.17) with $m^*_{el}/m_{el} = 1 + \lambda$ and $N_0^{int} = N_0$, and the direct bosonic contribution.

3.6 Direct contribution of collective modes to the specific heat

In the previous sections we discussed how our model does not predict anomalies in fermionic specific heat renormalization. Nonetheless, since our collective modes can provide a direct contribution to the specific heat, it is worth trying to quantify this

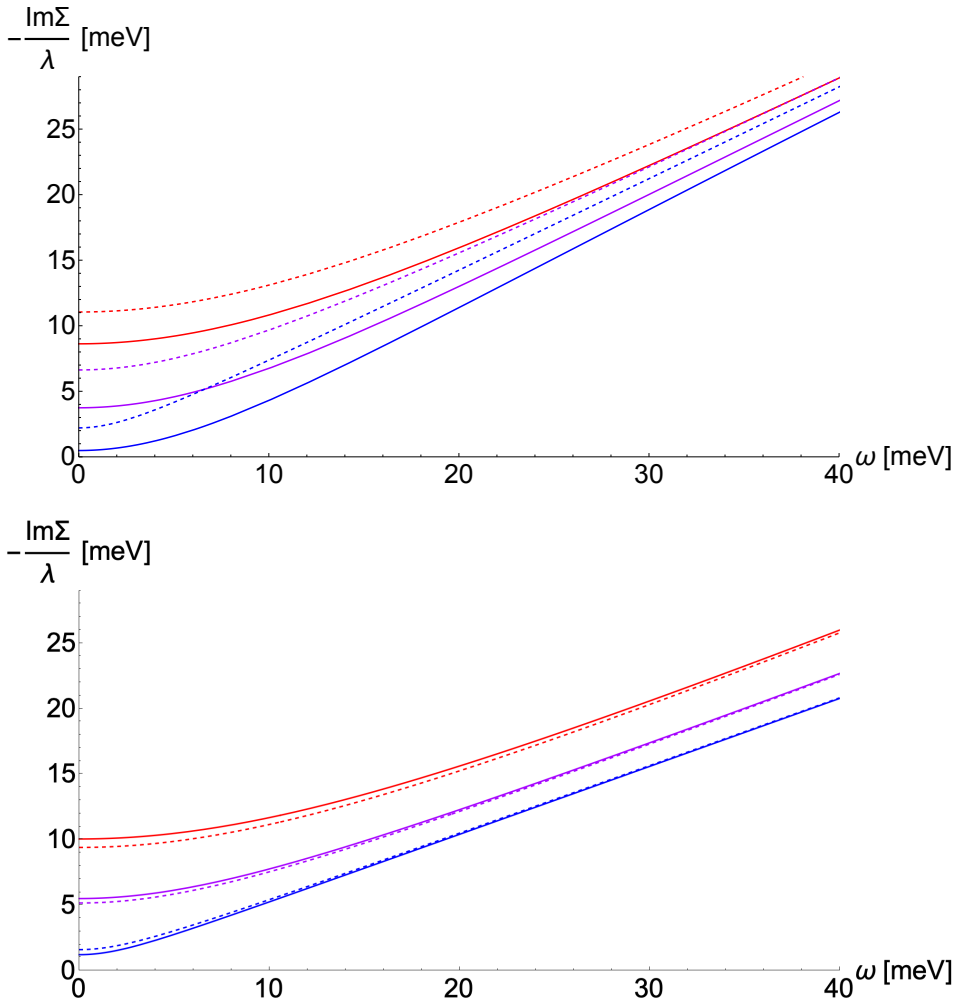

Figure 3.3. From [111], frequency dependence of the approximate SFL expression given in (3.7) (solid lines), in comparison with the MFL given in (3.6) (dotted lines). The values of the parameters are $M = 10\,\mathrm{meV}$ and $\Omega = 30\,\mathrm{meV}$, while γ is fixed to 1 in the upper panel while it is set to $\log(20\,\mathrm{meV}/(k_{\mathrm{B}}T))$ in the lower panel; the three different colors represent three different temperatures: $k_{\mathrm{B}}T = 1\,\mathrm{meV}$ (blue curves), $k_{\mathrm{B}}T = 3\,\mathrm{meV}$ (magenta curves) and $k_{\mathrm{B}}T = 5\,\mathrm{meV}$ (red curves).

contribution and compare it with that known for dressed fermions. Our calculation will follow the steps we described in section 2.5, so the starting point is the expression for the damped Holstein propagator within Matsubara domain:

$$\mathcal{D}(\omega_n) = \frac{1}{M + \gamma|\omega_n| + \dfrac{\omega_n^2}{\Omega}}$$

As discussed in section 2.5, the total Helmholtz free energy for the system of collective modes is uniquely determined given the expression of the propagator. In order to regularize the Matsubara sums we follow the discussion exhibited in Appendix D, in this section we show only the most relevant results. Our bosonic free energy has the form provided by equation (2.13):

$$\beta F_b = \frac{N}{2} \sum_{n\,\text{even}} \log\left(\frac{\beta \mathcal{D}^{-1}(\omega_n)}{\pi}\right)$$
$$= N \log\left(\beta\sqrt{\Omega M}\right) + N \sum_{n=1}^{\infty} \log[(2\pi n)^2 + \beta\gamma\Omega 2\pi n + \beta^2 \Omega M]$$

The quantity inside square brackets can be decomposed as $(2\pi n + i\beta\omega_+)(2\pi n - i\beta\omega_-)$, where ω_+ and ω_- are defined as the poles of $D_R(\omega)$, with a conventional overall minus sign in the definition of the second pole. For the standard damped regime ($\gamma^2 < 4M/\Omega$), they are defined as follows:

$$\omega_+ := \sqrt{\Omega M - \frac{\gamma^2\Omega^2}{4}} - i\frac{\gamma\Omega}{2} \qquad \omega_- := \sqrt{\Omega M - \frac{\gamma^2\Omega^2}{4}} + i\frac{\gamma\Omega}{2} \tag{3.9}$$

Note that, for this regime, $i\omega_+$ and $-i\omega_-$ are the complex conjugate of each other. For the overdamped regime ($\gamma^2 > 4M/\Omega$) it is more useful to use the following form:

$$i\omega_+ = \frac{\gamma\overline{\Omega}}{2}\left(1 - \sqrt{1 - \frac{4M}{\gamma^2\Omega}}\right) \qquad i\omega_- = -\frac{\gamma\Omega}{2}\left(1 + \sqrt{1 - \frac{4M}{\gamma^2\Omega}}\right) \tag{3.10}$$

Notice that, regardless of the damping regime, the quantities $i\omega_+$ and $-i\omega_-$ always have non-negative real part. The advantage of choosing to use exactly these two quantities is that they both play the role of the phonon frequency in Holstein model. In fact, in absence of damping, they both take on the same value, given by the following limits:

$$\lim_{\gamma\to 0^+} \omega_+ = \lim_{\gamma\to 0^+} \omega_- = \sqrt{\Omega M}$$

By introducing the parameters ω_+ and ω_-, we can calculate the sum that appears in the expression of F_b as follows:

$$\frac{\beta F_b}{N} = \log\left(\beta\sqrt{\omega_+\omega_-}\right) + \sum_{n=1}^{\infty} \log(2\pi n + i\beta\omega_+) + \sum_{n=1}^{\infty} \log(2\pi n - i\beta\omega_-)$$
$$= \log\left(\beta\sqrt{\omega_+\omega_-}\right) - \log\left(\Gamma\left(1 + i\frac{\beta\omega_+}{2\pi}\right)\Gamma\left(1 - i\frac{\beta\omega_-}{2\pi}\right)\right) +$$
$$+ i\frac{\beta\omega_+}{2\pi}\left(\log\left(i\frac{\beta\omega_+}{2\pi}\right) - 1\right) - i\frac{\beta\omega_-}{2\pi}\left(\log\left(-i\frac{\beta\omega_-}{2\pi}\right) - 1\right)$$

Where we exploited the fact that $\omega_+\omega_- = \Omega M$, furthermore when carrying out this sum we have already removed the zero-point energy term. Note that this expression is always real, regardless of the damping regime. Moreover, in the limit $\gamma\to 0^+$ it tends to the expression of the free energy for an ideal dispersionless phonon gas. To calculate the internal energy it is sufficient to take the derivative with respect to β of this last expression:

$$\frac{U_b}{N} = \frac{1}{\beta} + \frac{i\omega_+}{2\pi}\left[\log\left(i\frac{\beta\omega_+}{2\pi}\right) - \psi\left(1 + i\frac{\beta\omega_+}{2\pi}\right)\right] - \frac{i\omega_-}{2\pi}\left[\log\left(-i\frac{\beta\omega_-}{2\pi}\right) - \psi\left(1 - i\frac{\beta\omega_-}{2\pi}\right)\right]$$

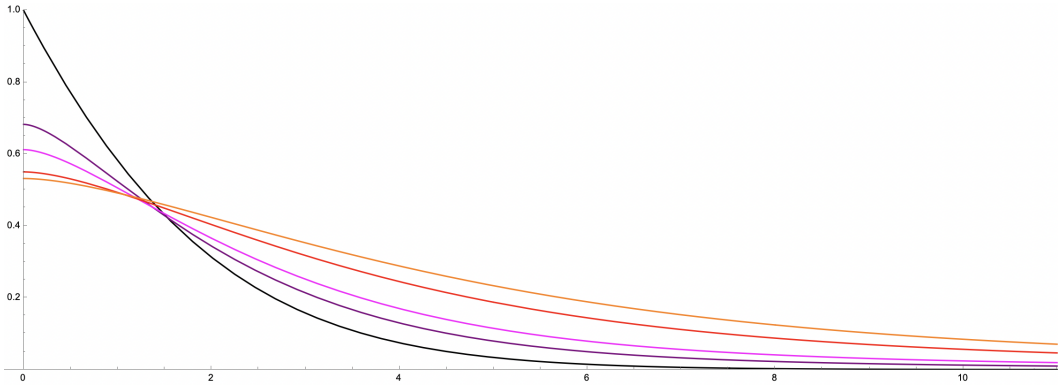

Figure 3.4. Plots of U_b/N as a function of the energy variable $\sqrt{\Omega M}$ for different values of γ (here we fixed $\beta = 1$). The black curve corresponds to $\gamma = 0^+$, while the colored curves correspond to increasing values of γ. Notice that, by increasing γ, the curves tend to fall at low energies and rise at high energies, with continuity in γ. Of course, the actual energy scales ω_+ and ω_- are not uniquely determined by the value of $\sqrt{\Omega M}$, and in particular they do not necessarily go to zero for $\sqrt{\Omega M} \to 0^+$.

Where $\psi(z)$ is the logarithmic derivative of the gamma function (commonly known as *digamma function*). This expression seems to be quite far from the one commonly known for standard phonons, however we point out the validity of the following limit:

$$\lim_{\gamma \to 0^+} \frac{U_b}{N} = \frac{\sqrt{\Omega M}}{e^{\beta\sqrt{\Omega M}} - 1}$$

This implies that our expression it is continuously connected to the well-known case of the undamped dispersionless phonon gas. Note that in applying the derivative with respect to β in the transition from F_b to U_b we assumed that all parameters of the theory were independent of temperature. Actually, within our model γ is allowed to have a slight temperature dependence, in particular we assume that γ is proportional to $\log(T_0/T)$ in the low temperature limit, where T_0 is an arbitrary temperature scale. However, since it is in fact a very weak dependence, the terms proportional to $\partial\gamma/\partial\beta$ always give a subleading contribution compared to the others, so we will neglect them throughout our discussion.

Finally, for the specific heat calculation we can exploit relation (2.14), which leads to the following result:

$$c_V^b = k_{\mathrm{B}} \left[1 + \left(i\frac{\beta\omega_+}{2\pi} \right)^2 \psi'\left(1 + i\frac{\beta\omega_+}{2\pi} \right) - i\frac{\beta\omega_+}{2\pi} + \left(-i\frac{\beta\omega_-}{2\pi} \right)^2 \psi'\left(1 - i\frac{\beta\omega_-}{2\pi} \right) + i\frac{\beta\omega_-}{2\pi} \right]$$

In the high temperature limit ($\beta \to 0$) we simply get $c_V^b = k_{\mathrm{B}}$, which is the standard Dulong-Petit law for the one-dimensional Einstein model. To evaluate the low temperature limit ($\beta \to \infty$) it is useful to rely on the following asymptotic trend for the derivative of the digamma function [117]:

$$z^2\psi'(1+z) - z + \frac{1}{2} = \frac{1}{6z} + O\left(\frac{1}{z^3}\right) \qquad \text{for} \quad |z| \to \infty \quad \wedge \quad |\mathrm{Arg}(z)| < \pi - 0^+$$

By applying this expansion to our expression for the specific heat, we get the following low temperature behavior:

$$c_V^b = \frac{\pi^2}{3} k_B^2 T \frac{\gamma}{\pi M} \tag{3.11}$$

Which is formally the same expression known for the fermionic specific heat, with the only difference that the quasiparticle density of states is replaced by a factor proportional to γ/M. This is a non-trivial result, as usually the contribution of a dispersionless optical phonon mode to specific heat drops exponentially. The presence of damping drastically changes the low temperature trend of this contribution, and even makes it comparable with the fermionic one. The difference in the qualitative temperature trends between the fermionic and the bosonic contributions to specific heat is that, in this second case, the purely linear trend has a logarithmic correction due to the temperature dependence of γ. Therefore its temperature behavior retraces the Marginal Fermi liquid one. Again, we stress that this singular behavior does not come from fermionic degrees of freedom (as actually happens for the Marginal Fermi liquid) but from the bosonic ones. We would like to point out that in our calculation we considered the fermionic and bosonic degrees of freedom as separate, and that in both we took mutual interaction into account, at least at the leading order. As we mentioned, this could lead to double-counting the interaction. However, since the anomalous behavior of the specific heat comes exclusively from the bosonic part, it is evident that this contribution cannot come from the mutual interaction of the two, and therefore it is clearly not double-counted. For this reason, the approximation $\mathcal{Z}_G^{tot} \simeq \mathcal{Z}_G^f \mathcal{Z}_G^b$ we discussed in section 2.5 is able to capture the most relevant thermodynamic properties of the systems we set out to study. A similar separation of fermionic and bosonic degrees of freedom will also be applied in the calculation of the overall contribution of charge density fluctuations to the specific heat.

Despite its simplicity, the model we have described exhibits a non-trivial phenomenology, which may be suitable for the description of the strange-metal behavior in cuprates. Having established the essential ingredients for the development of the Shrinking Fermi liquid scenario, as well as its main characteristics, we therefore proceed with the description of the actual charge density fluctuations model, starting with thermodynamics. Given the deep analogy between damped Holstein phonons and charge density fluctuations, it is reasonable to think that the latter may be a good candidate for the realization of a Shrinking Fermi liquid phenomenology in cuprates.

Chapter 4

Thermodynamic properties

From the study of the damped Holstein model it clearly emerged that a strong damping of the collective mode and a sufficiently weak dependence on momentum are sufficient elements for the implementation of a Shrinking Fermi liquid behavior. As we have seen, this model is able to take into account two important aspects that characterize the strange-metal phase of cuprates, namely the linear resistivity and the logarithmic divergence of the specific heat, where the latter emerges as a consequence of the temperature dependence of γ.

Since charge density fluctuations are very similar to the damped dispersionless phonons that we discussed in the previous chapter, we expect that they are able to reproduce a phenomenology similar to that of the Shrinking Fermi liquid. The purpose of this chapter is precisely to describe the overall effect of charge density fluctuations on the specific heat of cuprates. In particular, we are going to show that it is possible to explain the seeming divergence of the specific heat recently observed in $La_{1.6-x}Nd_{0.4}Sr_xCuO_4$ and $La_{1.8-x}Eu_{0.2}Sr_xCuO_4$ compunds [55] by means of the functional form of $\gamma = \gamma(T, p)$ exhibited in (3.8).

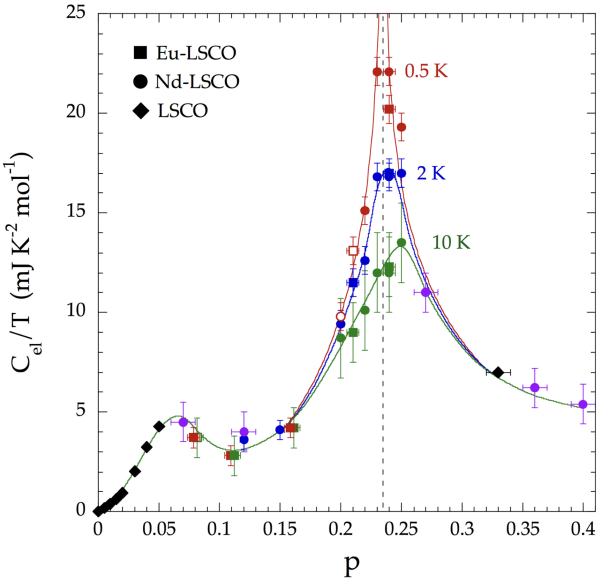

Figure 4.1. From [55], ratio between the specific heat and the temperature as a function of the doping level, for several cuprate compounds. The plotted data are obtained by subtracting the nucleic and phononic contribution from the total specific heat measured, so it is supposed to include only the fermionic contribution.

4.1 Fermionic contribution to the specific heat

Exactly as in the case of the damped Holstein model, the collective modes have a dual effect on the specific heat: on the one hand they are able to alter the contribution of the electronic quasiparticles, on the other they themselves provide a direct contribution. Let us therefore start by calculating the fermionic contribution, which at low temperatures is simply the result of the Sommerfeld expansion. The only caution we must take is to use the quasiparticle density of states instead of the usual one. For this purpose it is therefore necessary to introduce the self-energy of our system. From the resistivity experimental data (which will be discussed in detail in the next chapter) an isotropic elastic component in the electronic scattering is evident, the origin of which can be identified in the quenched impurities of the systems under examination. As we mentioned in section 2.5, this scattering component can be mimicked by manually adding a constant term in the imaginary part of the self-energy. In order to keep these two contributions to self-energy well separated we express the retarded Green's function as follows:

$$G_R(\omega, \mathbf{k}) = \frac{1}{\omega - \xi_{\mathbf{k}} - \Sigma_R(\omega, \mathbf{k}) + i\Sigma_0}$$

From now on we will always apply this explicit separation. The imaginary part of the self-energy $\Sigma_R(\omega, \mathbf{k})$ is again provided by (2.4), where in this case, as in the rest of this thesis, $D_R(\omega, \mathbf{k})$ once again has the role of propagator of charge density fluctuations, i.e. the one expressed by equation (2.2). Again, the real part of the total self-energy is provided by the Kramers-Kronig relation applied only on the term $\mathrm{Im}\Sigma_R(\omega, \mathbf{k})$, as the term Σ_0 that we have just added to the imaginary part does not alter the real part in any way. As we have already discussed, we will neglect the momentum-dependence of our self energy, namely $\Sigma_R(\omega, \mathbf{k}) \simeq \Sigma_R(\omega)$ (for the sake of practicality, we will compute $\Sigma_R(\omega)$ by evaluating expression (2.4) at the nodal Fermi vector). Under this assumption, the electronic Green's function depends on $\mathbf{k}$ only through dispersion $\xi_{\mathbf{k}}$, for this reason henceforth we will use the handier notation $G_R(\omega, \xi_{\mathbf{k}})$ to denote the Green's function instead of $G_R(\omega, \mathbf{k})$:

$$G_R(\omega, \xi_{\mathbf{k}}) \coloneqq \frac{1}{\omega - \xi_{\mathbf{k}} - \Sigma_R(\omega) + i\Sigma_0} \tag{4.1}$$

If on the one hand it is true that the critical point of the strange-metal phase is close to a singular point in the density of states and therefore corrections to the chemical potential may be relevant, on the other hand we know that cuprates are generally rather disordered systems, in the sense that the value of Σ_0 is relatively high (according to [81], the order of magnitude is that of few tens of meV). Consequently, accordingly to equation (2.18), the quasiparticle density of states at low temperature will essentially be a convolution between the bare density of states and a Lorentz distribution with scale parameter Σ_0. Even assuming that the electron dispersion in cuprates is strictly two-dimensional, the Van-Hove singularity that would occur would be at most logarithmic, and therefore it's easily suppressed by disorder [55]. The result is a density of states that varies weakly even around optimal doping, and which presents a slight peak at approximately the same value as the doping level at

which the logarithmic singularity would occur in the absence of disorder. Within our analysis, we are interested in understanding how the fermionic contribution to the specific heat depends on the doping level. This dependence is implicit within the (bare) chemical potential $\mu = \mu(p)$, and is given by the following relation:

$$\frac{2}{N}\sum_{\mathbf{k}} f(\xi_{\mathbf{k}}) = 1 - p$$

Where the spin multiplicity has been taken into account. Of course, the value of the chemical potential affects N_0^{int} even if $\omega = 0$ is fixed. In order to estimate the fermionic contribution to the specific heat, first of all we need to fix the hopping parameters for the system. A possible choice of these parameters, in accordance with the estimate provided by reference [116], is the following:

$$t = 435\,\text{meV} \qquad t' = -50\,\text{meV} \qquad t'' = 38\,\text{meV}$$

With this set of parameters we get a Van Hove singularity at $p = 0.24$ and $\mu \simeq -350\,\text{meV}$. In order to evaluate the effect of the interactions, we also have to fix the remaining relevant parameters of the theory:

$$m_c = 15\,\text{meV} \qquad \nu = 1.4\,\text{eV}/(\text{r.l.u.})^2 \qquad q_c = 1.95 \qquad \gamma = 1$$
$$\Omega = 30\,\text{meV} \qquad g = 160\,\text{meV} \qquad \Sigma_0 = 15\,\text{meV}$$

Here we show, as an example, a plot of the fermionic specific heat both in the presence and absence of interactions:

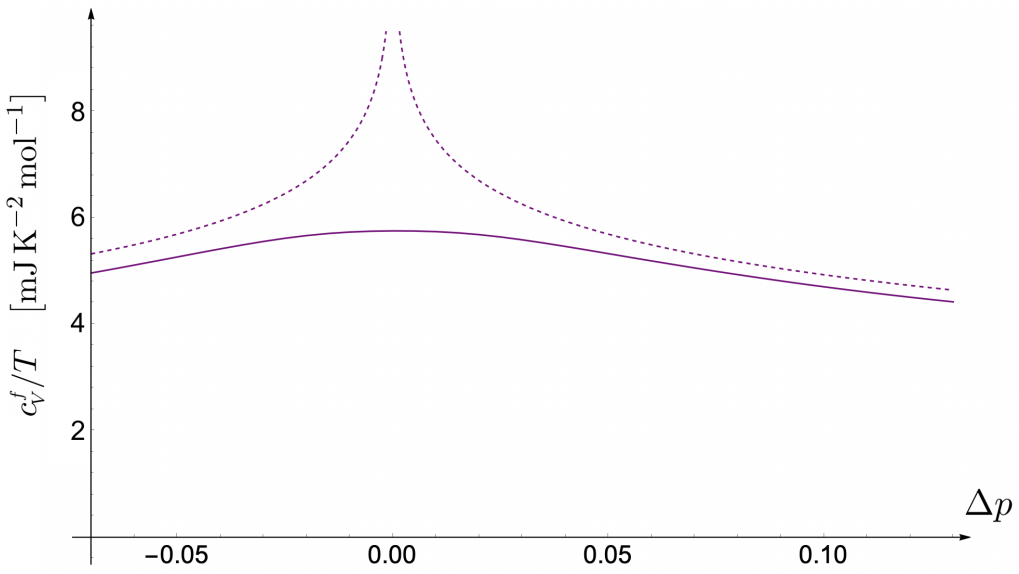

Figure 4.2. Fermionic contribution to the specific heat, both in absence (dashed lines) and in presence (solid lines) of interactions, according to equations (2.15) and (2.18) respectively. For simplicity we considered only two hopping parameters, namely $t = 250\,\text{meV}$ and $t' = -50\,\text{meV}$, while for the other parameters we stuck to the ones we exhibited above. These fermionic parameters provide a Van Hove singularity at $p = 0.17$ and $\mu \simeq -200\,\text{meV}$. On the x-axis we report the difference between the doping level p and the doping value at which the Van Hove singularity occurs.

The set of parameters we exhibited is quite general, and therefore for simplicity we will consider the same parameter values for the description of both $La_{1.8-x}Eu_{0.2}Sr_xCuO_4$ and $La_{1.6-x}Nd_{0.4}Sr_xCuO_4$. The result of our calculation, reproduced on the plot in figure 4.2, clearly shows that disorder strongly flattens the logarithmic singularity of the bare density of states, as we expected. Changing the values of the hopping parameters can (slightly) affect the numerical value of the specific heat, but not the qualitative trend. As we anticipated, we attribute the apparent singularity of the specific heat observed to the direct contribution of charge density fluctuations.

4.2 Bosonic contribution to the specific heat

In order to calculate the direct contribution of charge density fluctuations to the specific heat we can, in principle, follow the same steps that we exhibited in section 3.6 for the dispersionless case. The only difference is that the energy scale M is replaced by the function $m_{\mathbf{k}}$, so the poles of the propagator depend on $\mathbf{k}$. In analogy to the case that we analyzed in the previous chapter, we call these poles $\omega^+_{\mathbf{k}}$ and $\omega^-_{\mathbf{k}}$, they play exactly the same role as ω_+ and ω_- respectively, and are defined by relations completely analogous to (3.9) or (3.10) with the only difference that M is replaced by $m_{\mathbf{k}}$ in both expressions. In particular, the two following limits hold:

$$\lim_{\gamma\to 0^+} \omega^+_{\mathbf{k}} = \lim_{\gamma\to 0^+} \omega^-_{\mathbf{k}} = \sqrt{\Omega m_{\mathbf{k}}}$$

Although the approach we have already shown for calculating the bosonic specific heat also works well in this context, in order to carry out the sum over momenta it may be useful to use a slightly different approach. As explained in detail in Appendix D, the Matsubara sums can be reduced to suitable integrals over frequencies by means of the residue theorem. The result for internal energy, for instance, is the following:

$$U_b = \sum_{\mathbf{k}} \int_0^\infty \frac{1}{e^{\beta\omega}-1} \frac{\gamma\omega\left(m_{\mathbf{k}} + \dfrac{\omega^2}{\Omega}\right)}{\left(m_{\mathbf{k}} - \dfrac{\omega^2}{\Omega}\right)^2 + \gamma^2\omega^2} \frac{d\omega}{\pi}$$

We immediately note that, within the integrand function, it is possible to factorize a Bose function and an ω term, so everything else (including the $\mathbf{k}$ sum) can be interpreted as an effective density of states for charge density fluctuations.

$$\frac{U_b}{N} = \int_{-\infty}^{+\infty} \frac{\omega}{e^{\beta\omega}-1} N_\omega^{CDF} d\omega \qquad N_\omega^{CDF} := \frac{1}{N}\sum_{\mathbf{k}} \frac{1}{\pi} \frac{\gamma\left(m_{\mathbf{k}} + \dfrac{\omega^2}{\Omega}\right)}{\left(m_{\mathbf{k}} - \dfrac{\omega^2}{\Omega}\right)^2 + \gamma^2\omega^2} \theta(\omega) \quad (4.2)$$

The definition of this density of states is very similar to the definition of N_ω^{int} provided by equation (2.16). It is possible to show, by explicitely integrating N_ω^{CDF} in $d\omega$ over the whole real axis that the effective density of states N_ω^{CDF} is itself already normalized to 1, as we would expect for a spinless mode. Moreover, each of the addends of the sum tends to $\delta(\omega - \sqrt{\Omega m_{\mathbf{k}}})$ in the limit $\gamma \to 0^+$. This clearly shows

that our model, in the undamped limit, exactly reproduces the thermodynamics of a phonon gas with dispersion $\sqrt{\Omega m_{\mathbf{k}}}$. Since each of the addends of the $\mathbf{k}$ sum within N_ω^{CDF} depends on $\mathbf{k}$ only through $m_{\mathbf{k}}$, the sum over momenta can be converted into an integral by introducing a suitable density of states for the bosonic dispersion:

$$\varrho(\varepsilon) \coloneqq \frac{1}{N}\sum_{\mathbf{q}} \delta(\varepsilon + m_c - m_{\mathbf{q}})$$

In order to perform the sum in $\mathbf{q}$ we exploit the fact that, close to any of the four critical wave vectors $\mathbf{q}_c$, the dispersion can be approximated as $m_{\mathbf{q}} \simeq m_c + \nu|\mathbf{q}-\mathbf{q}_c|^2$. Therefore, we divide the Brillouin zone into four regions, separated from each other by the two diagonals of the square. Then we approximate each of the quarters of the Brillouin zone with a circle centered in $\mathbf{q}_c$, with an area equal to one quarter of the Brillouin zone. The overall density of states will be given by the sum of these four contributions, the expression found is the following (see Appendix E for the details on the calculation):

$$\varrho(\varepsilon) \simeq \frac{\theta(\varepsilon)\,\theta(\pi\nu - \varepsilon)}{\pi\nu}$$

Of course, the approximation we have applied is such as to preserve the normalization of $\varrho(\varepsilon)$, this property in turn guarantees the correct normalization of N_ω^{CDF}. Also notice that, in the $\nu \to 0^+$ limit, $\varrho(\varepsilon)$ becomes a Dirac delta distribution and our approximation becomes exact, therefore in this limit we find exactly the already discussed case of the dispersionless boson system. Within this approximation, the charge density fluctuations density of states N_ω^{CDF} can be computed exactly at any frequency. However, if we consider a range of temperatures low enough such that both $k_\mathrm{B}T \ll \sqrt{\Omega m_{\mathbf{k}}}$ and $\gamma k_\mathrm{B}T \ll m_{\mathbf{k}}$ hold, it is possible to calculate the specific heat through an approach completely analogous to the Sommerfeld expansion. The asymptotic expression is:

$$c_V^b = \frac{2\pi^2}{3} k_\mathrm{B}^2 T N_0^{CDF} \qquad \text{where} \quad N_0^{CDF} = \frac{1}{2}\frac{\gamma}{\pi^2\nu}\log\Big(1 + \frac{\pi\nu}{m_c}\Big) \tag{4.3}$$

Notice that this result does not depend on q_c nor on Ω. The factor of 2 of difference with the usual Sommerfeld specific heat expression for fermions is due to the fact that the Fermi function is replaced by the Bose function in the integral over the entire real axis which defines the specific heat. However, this factor of 2 is compensated by the factor of $\theta(0) = 1/2$ which appears in the effective density of states. An alternative way of looking at this is to define the effective density of states without the theta function and restrict the integral over the positive real semi-axis by hand (as required by the original expression for U_b), in this case the numerical prefactor of c_V^b would be $\pi^2/3$ while there would be no prefactor $1/2$ in the expression for N_0^{CDF}. From a purely formal point of view, this second interpretation is more correct, and the reason is that a Sommerfeld-like expansion is valid only if the function that we expand is smooth around $\omega = 0$, while N_ω^{CDF} actually is not. Despite that, we prefer to stick to the first formulation, namely the one described by equations (4.3), as it provides the proper normalization for the effective density of states and correctly reproduces the case of the ideal phonon gas in the $\gamma \to 0^+$ limit.

The most remarkable aspect about the expressions we found for specific heat, both in the dispersionless model and in the case of charge density fluctuations, is that they have a linear dependence on both T and γ. This means that the c_V^b/T ratio as a function of temperature, at least in the low temperature regime, mimics the temperature behavior of γ with a good approximation. Again, it is worth noting that our expression for c_V^b given by (4.3) reproduces the one provided by equation (3.11) in the $\nu \to 0^+$ limit, with identification $m_c = M$.

In order to estimate the bosonic specific heat from experimental data, we first consider a doping level window around the value at which the divergence was observed (which we have denoted by p^*). We then subtract from the experimental values of the presumed fermionic specific heat those that we have estimated with our calculation, making the doping level value at which our c_V^f reaches its maximum as a function of p coincide with p^*. Finally, we apply equation (4.3) with the expression of $\gamma(T, p)$ given by (3.8) in order to fit the data obtained from this subtraction. In principle, the fact that we have fixed $\gamma = 1$ in the calculation of the fermionic contribution would make this procedure not self-consistent, but this is not a problem as γ does not play a relevant role in our previous calculation because of the strong disorder.

With the expression we have chosen for $\gamma(T, p)$, it is possible to quantitatively fit the bosonic component of the specific heat estimated from the experimental data. However, as we have discussed extensively in references [96] and [115], the values of γ that provide a quantitative fit of the specific heat are too small to explain the deviation from Fermi liquid behavior observed in the transport properties. Consequently, a correct reproduction of resistivity data inevitably involves an overestimation of the specific heat. Our fit for the specific heat is able to capture only the qualitative trend of the observed curves, but this value is amplified uniformly over all temperatures. In particular, by consistently fitting the resistivity and specific heat data, we found $T_0 = 37\,\mathrm{K}$, $p^* = 0.232$, $\gamma_0 = 8.55$, $\upsilon = 2.84$ for $La_{1.8-x}Eu_{0.2}Sr_xCuO_4$, and $T_0 = 50\,\mathrm{K}$, $p^* = 0.235$, $\gamma_0 = 17.86$ and $\upsilon = 0.87$ for $La_{1.6-x}Nd_{0.4}Sr_xCuO_4$. The results of our fits are reported in figure 4.3, the overall amplification that we obtained from our calculation compared to the experimental data is a factor of 11 for $La_{1.8-x}Eu_{0.2}Sr_xCuO_4$ and a factor of 30 for $La_{1.6-x}Nd_{0.4}Sr_xCuO_4$. We believe that the most plausible origin of this overestimation is due to the fact that charge density fluctuation modes may live on a coarse-grained lattice with larger effective spacing, so the total number of collective modes in the system could be significantly smaller than the actual number of lattice sites and therefore their contribution to the thermodynamics would be significantly reduced [115].

4.3 Effect of a three-dimensional dispersion

Although cuprates can be well described as two-dimensional systems, we know that a weak coupling between lattice planes must exist, and that it is partly responsible for the long-range correlation phenomena at finite temperature, otherwise forbidden by Mermin-Wagner theorem. It may be interesting to evaluate the effect of a dispersion

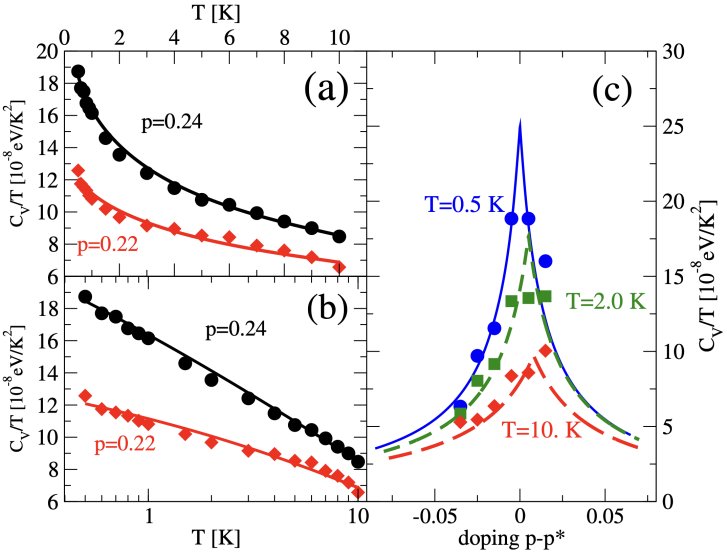

Figure 4.3. From [115], temperature and doping dependence of the bosonic contribution to the specific heat for $La_{1.6-x}Nd_{0.4}Sr_xCuO_4$ compound. The points represent the experimental data (taken from [55]) after the subtraction of the fermionic component we estimated, while the solid lines are the result of our theoretical calculation. The latter are scaled by a factor of 1/30, in accordance with our discussion.

along the z-axis. For this purpose, we replace the dispersion $m_{\mathbf{q}}$ with a more general dispersion $m_{\mathbf{q},q_z}$ which also depends on q_z and which respects the correct periodicity given by the three-dimensional lattice. In analogy to the two-dimensional case, the approximate form of this dispersion close to a critical wave vector $\mathbf{q}_c$ is $m_{\mathbf{q},q_z} \simeq m_c + \nu|\mathbf{q}-\mathbf{q}_c|^2 + \nu_\perp q_z^2$. We can compute $\varrho(\varepsilon)$ in a formally identical way to that applied in the case $\nu_\perp = 0$, but this time we obtain the following result:

$$\pi\nu\varrho(\varepsilon) \simeq \begin{cases} \sqrt{\varepsilon/E} & \text{for } 0 < \varepsilon \leq E \\ 1 & \text{for } E < \varepsilon \leq \pi\nu \\ 1 - \sqrt{(\varepsilon - \pi\nu)/E} & \text{for } \pi\nu < \varepsilon \leq E + \pi\nu \\ 0 & \text{elsewhere} \end{cases}$$

Where $E \coloneqq \pi^2\nu_\perp/d^2$ and d is the interplane distance (here expressed in lattice spacing units). Of course, in order for this expression to make sense, the condition $E < \pi\nu$ must hold, which can be expressed as $\nu_\perp < \nu_\perp^{\max}$, where $\nu_\perp^{\max} \coloneqq \nu_\perp d^2/\pi$. Experimentally, we know that $\nu_\perp \ll \nu_\perp^{\max}$, but it may be interesting to evaluate the trend of the specific heat as the parameter varies within its entire validity domain, which is what we show in figure 4.4.

Even in this case, the integral in $d\varepsilon$ which defines a closed form for N_ω^{CDF} at any frequency can be solved analytically. Nonetheless, since we are interested once again in the low temperature regime, we limit ourselves to exhibiting only its zero frequency value:

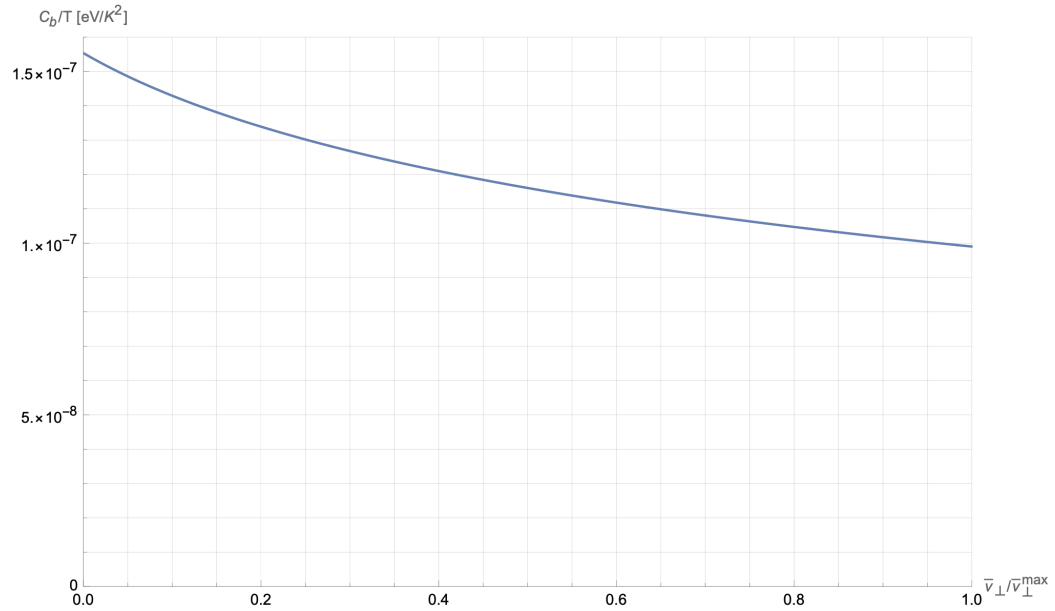

Figure 4.4. From [96], plot of c_V^b/T as a function of $\nu_\perp$, expressed in units of $\nu_\perp^{\max}$. Parameter values are $m_c = 15\,\text{meV}$, $\nu = 1.3\,\text{eV/(r.l.u.)}^2$, $\gamma = 1$ and $d = 11$.

$$N_0^{CDF} = \frac{\gamma}{\pi^2\nu}\left[\frac{1}{2}\log\left(1+\frac{\pi\nu}{m_c+E}\right) - \sqrt{\frac{m_c}{E}}\arctan\left(\sqrt{\frac{E}{m_c}}\right) + \right.$$
$$\left. + \sqrt{\frac{m_c+\pi\nu}{E}}\arctan\left(\sqrt{\frac{E}{m_c+\pi\nu}}\right)\right]$$

It is immediate to note that this new expression tends to the one we found in the case $\nu_\perp = 0$ in the limit $E \to 0$, as expected. Of course, also within this approximation, a linear relation between c_V^b/T and γ is obtained, which is analogous to equation (4.3). As we can see from the plot in figure 4.4, the effect of a dispersion along z-axis is to reduce specific heat, but since $\nu_\perp \ll \nu_\perp^{\max}$, this effect is essentially negligible. These observations justify our choice to treat charge density fluctuations as two-dimensional objects.

Just as in the case of the overdamped Holstein model, the collective mode affects not only thermodynamics but also transport phenomena in the systems in which they are present. The next chapter will be dedicated to the discussion on this topic.

Chapter 5

Transport properties

In the previous chapter we have seen how charge density fluctuation modes can affect the thermodynamic properties of the systems in which they are present. In particular, we have seen that our model is potentially able to take into account the abnormal behavior of specific heat observed in the strange-metal phase, to the only cost of having to modify a single parameter of the theory appropriately, taking that it has a precise functional dependence on temperature and doping level.

In this chapter, instead, we will deal with the problem of transport. Based on our preliminary study of the damped Holstein model, we are going to show how charge density fluctuations are able to take into account the most remarkable phenomena observed in the srange-metal phase.

5.1 Resistivity

According to Ohm's law, he electrical conductivity σ of a system is simply the proportionality tensor between the applied electric field to the system and the electric current that is generated as a response. As we mentioned, for two-dimensional systems with tetragonal symmetry in absence of magnetic field, σ is simply a scalar quantity, in this case the resistivity ρ is simply its reciprocal. As discussed in section 2.3, resistivity within Kubo formalism is directly connected to the Γ_{11} coefficient, which is simply the Onsager coefficient associated to two particle currents along the same direction, rescaled by temperature. Within our model, the calculation of this coefficient must take into account both the electrons and the charge density fluctuations. However, since we are interested in a static response and charge density fluctuations are neutral collective modes, the latter cannot provide a direct contribution to charge transport. The collective mode will enter indirectly by renormalizing the fermionic response. The Feynman diagram associated with this coefficient is the following:

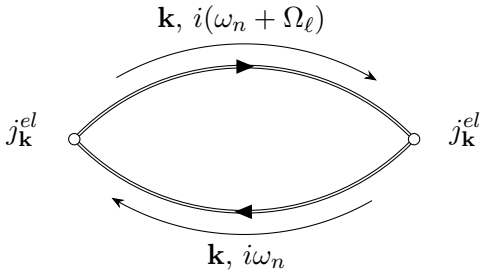

(5.1)

The entering momentum is set to zero, while we are keeping explicit the dependence on the entering bosonic frequency $i\Omega_\ell$. Commonly, the frequencies that enter into the calculation of a bubble diagram like this at finite temperature, including the external frequency, are Matsubara frequencies. As discussed in Appendix B, in order to return to real frequency domain it is sufficient to make the substitution $i\Omega_\ell \to \omega + i0^+$ at the end of the calculation. The doubled lines represent renormalized electrons, therefore they are associated with the dressed Green's functions. The vertex terms $j^{el}_{\mathbf{k}}$, graphically associated with white dots, represent the particle current functions, namely the x-component of the group velocity of the mode with momentum $\mathbf{k}$:

$$j^{el}_{\mathbf{k}} = v_{\mathbf{k},x} = \frac{\partial \xi_{\mathbf{k}}}{\partial k_x}$$

The effect of the interactions is taken into account through the renormalization of the fermionic lines. In principle, it would be appropriate to also include vertex corrections. Nevertheless, Ward-Takahashi identities imply that the magnitude of the vertex corrections is proportional to the derivative of the self-energy with respect to the momentum [118, 119], and in particular they vanish in the case of momentum-independent self-energy. Since we are neglecting the momentum dependence of self-energy in our model, we are allowed to neglect the vertex corrections as well. The expression of the coefficient Γ_{11} provided by diagram (5.1) is the following:

$$\Gamma_{11} = \frac{1}{v_{\text{uc}}} \frac{1}{N} \sum_{\mathbf{k},\sigma} \left(j^{el}_{\mathbf{k}}\right)^2 \int_{-\infty}^{+\infty} \left[\text{Im}G_R(\omega, \xi_{\mathbf{k}})\right]^2 \left(-\frac{\partial f(\omega)}{\partial \omega}\right) \frac{d\omega}{\pi}$$

We want to clarify, as we already mentioned, that the presence of the factor $1/v_{\text{uc}}$ emerges a consequence of the fact that the sum over momenta in the loop should be normalized to the total three-dimensional volume, but the summand functions does not depend on the z-component of the momentum (see Appendix A for further details). Notice that we used convention (4.1) to express the momentum-dependence of the Green's function. Since the momentum-dependence of the function inside the $\mathbf{k}$-sum is only inside the $v^2_{\mathbf{k},x}$ prefactor and in the $\xi_{\mathbf{k}}$ function, it is convenient to convert the sum into an integral by introducing the following function:

$$\widetilde{N}_\xi := \frac{1}{N} \sum_{\mathbf{k},\,\sigma} v^2_{\mathbf{k},x} \delta(\xi - \xi_{\mathbf{k}} - \text{Re}\Sigma_R(0)) = \frac{2}{N} \sum_{\mathbf{k}} \frac{\partial^2 \xi_{\mathbf{k}}}{\partial k_x^2} \theta(\xi - \xi_{\mathbf{k}} - \text{Re}\Sigma_R(0)) \tag{5.2}$$

By comparison with definition (2.16), we clearly see that our $\widetilde{N}_\xi$ function is very similar to the bare density of states N_ξ, the only relevant difference between the two

functions lies in the presence of the weighting terms $v_{\mathbf{k},x}^2$ in the $\mathbf{k}$-sum which defines $\widetilde{N}_\xi$. This implies that, within our units, while N_ξ has the dimension of the reciprocal of an energy, $\widetilde{N}_\xi$ has the dimension of an energy. For simplicity, we have explicitly included the chemical potential shift in the definition of this function. With the help of $\widetilde{N}_\xi$, we can express Γ_{11} as follows:

$$\Gamma_{11} = \frac{1}{v_{\mathrm{uc}}} \int_{-\infty}^{+\infty} \left[\int_{-\infty}^{+\infty} \widetilde{N}_\xi \left[\mathrm{Im} G_R(\omega, \xi) \right]^2 \frac{d\xi}{\pi} \right] \left(-\frac{\partial f(\omega)}{\partial \omega} \right) d\omega$$

The integral in $d\xi$ can be calculated by means of Allen approximation [120], leading to the following result (further details are provided in Appendix F):

$$\Gamma_{11} = \frac{\widetilde{N}_0}{v_{\mathrm{uc}}} \int_{-\infty}^{+\infty} \frac{1}{2\left(\Sigma_0 - \mathrm{Im}\Sigma_R(\omega)\right)} \left(-\frac{\partial f(\omega)}{\partial \omega} \right) d\omega \tag{5.3}$$

It is worth noting that this expression is essentially a generalization of Drude formula for electrical conductivity. In fact, within our formalism the electrical conductivity σ is $\mathrm{e}^2\Gamma_{11}$, the factor $\widetilde{N}_0/v_{\mathrm{uc}}$ in expression (5.3) is the ratio between the electron density and the mass, while the integral in $d\omega$ represents the mean scattering time. In particular, in the case in which the entire imaginary part of the self-energy is constituted by the constant term Σ_0 only, we get $\Gamma_{11} = \widetilde{N}_0/(2\Sigma_0 v_{\mathrm{uc}})$, therefore the Drude scattering time has to be identified with $1/(2\Sigma_0)$. This latter observation justifies the presence of the factor $1/2$ in the definition of $\tau_{\mathbf{k}}$ provided in section 2.1. Since $\mathrm{Im}\Sigma_R(\omega)$ goes to zero for $T = 0$ and $\omega = 0$, the zero temperature expressions for Γ_{11} and the resistivity are given by:

$$\Gamma_{11}\big|_{T=0} = \frac{1}{2\Sigma_0} \frac{\widetilde{N}_0}{v_{\mathrm{uc}}} \qquad\qquad \rho(T=0) = \frac{1}{\mathrm{e}^2\,\Gamma_{11}}\Big|_{T=0} = 2\Sigma_0 \frac{v_{\mathrm{uc}}}{\mathrm{e}^2 \widetilde{N}_0}$$

The fact that the experimental resistivity curves go to a finite value at zero temperature therefore allows us to deduce that Σ_0 is different from zero, according to our expression for $\rho(T=0)$. The same curves also allow a quantitative estimate of Σ_0 for several compunds. In agreement with [81], the value of Σ_0 should lie between 10 meV and 20 meV. Within our calculation, we will treat Σ_0 as a fit parameter, taking however into account this constraint dictated by the experimental data.

While the value of Σ_0 sets the zero temperature value of $\rho(T)$, the temperature and frequency dependencies of $-\mathrm{Im}\Sigma_R(\omega)$ determine the temperature dependence of the resistivity. As usual, our expression for the self-energy is that provided by (2.4) at the nodal Fermi vector. We know that this self-energy describes a Shrinking Fermi liquid system, therefore we expect that γ establishes the boundary between quadratic and linear behavior, while the value of m_c controls the slope of the linear part.

In accordance with what was discussed in detail in section 4.2, the very same set of parameters that allowed us to fit the specific heat data for $La_{1.8-x}Eu_{0.2}Sr_xCuO_4$ and $La_{1.6-x}Nd_{0.4}Sr_xCuO_4$ (up to an overall amplification factor) also allowed us to fit the experimental resistivity curves. Of course, this set includes also the parameters T_0, p^*, γ_0 and υ, which appear in the phenomenological expression of $\gamma(T, p)$ provided

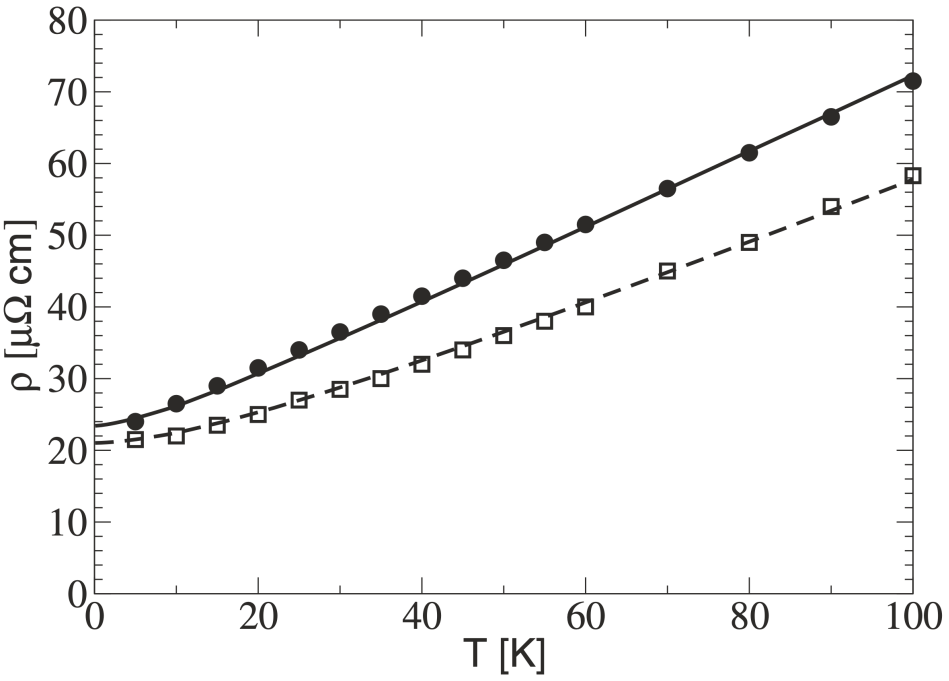

Figure 5.1. From [115], resistivity calculations for a $La_{1.6-x}Nd_{0.4}Sr_xCuO_4$ sample (black solid line) and for a $La_{1.8-x}Eu_{0.2}Sr_xCuO_4$ (black dashed line), both with $p = 0.24$. The symbols refer to the experimental data taken from reference [55]. We used g and Σ_0 as fitting parameters to get the theoretical curves, in particular we fixed $g = 212\,\text{meV}$ and $\Sigma_0 = 13.7\,\text{meV}$ for $La_{1.6-x}Nd_{0.4}Sr_xCuO_4$, and $g = 204\,\text{meV}$ and $\Sigma_0 = 12.3\,\text{meV}$ for $La_{1.8-x}Eu_{0.2}Sr_xCuO_4$. Moreover, $a = 3.8\,\text{Å}$ and $d = 13.3\,\text{Å}$ are set.

by equation (3.8). The only parameters that we did not take from the set shown in section 4.1 are those of g and Σ_0, as to have a good fit of the data it was necessary to choose different values for the two compounds. Moreover, in order to reproduce resistivity data we also need to fix the value of v_{uc}, which played no role in the calculation we made for the specific heat (in the considered case of no dispersion along z-axis). For the case of $La_{1.6-x}Nd_{0.4}Sr_xCuO_4$, a reasonable estimate of the lattice parameters in the considered doping range is $a \simeq 3.8\,\text{Å}$ and $d \simeq 13.3\,\text{Å}$ [121, 122], these values are essentially unchanged for the description of $La_{1.8-x}Eu_{0.2}Sr_xCuO_4$ compound [123]. Therefore, we choose to take 3.5 as the dimensionless value of d for both compounds, which is thus the value of v_{uc}. The result of our calculation is reported in figure 5.1, note that the dimensional value of a is necessary in order to express the theoretical resistivity in SI units.

Although the set of parameters (both fermionic and bosonic) that we chose allowed us to correctly fit the resistivity as a function of temperature for both compounds, not all the values of the set are suitable for fitting the Seebeck coefficient data. As we shall see, the problem lies in the value of q_c. In fact, in order to get the correct sign of the Seebeck coefficient we have to choose a value for q_c significantly lower than that observed experimentally. Since we have adopted the momentum-independent self-energy approximation, our resistivity calculation is not influenced in any way

by the value of q_c, so the results we have exhibited so far remain valid even by significantly changing this value. What is remarkable is that the range of values for q_c which guarantees the correct sign of the Seebeck effect and good linearity in γ is consistent with the value obtained from the theoretical calculation for the charge instability. We will address the issue in detail in chapter 7, for the moment we limit ourselves to treating q_c as a fitting parameter of the theory.

5.2 Fermionic contribution to Seebeck coefficient

In order to calculate the Seebeck coefficient we need both the Γ_{11} coefficient, which we have already calculated, and the Γ_{12} coefficient. We have seen that charge density fluctuations, not carrying electric charge, do not give a direct contribution to the coefficient Γ_{11}. However they carry energy, therefore they can contribute to the coefficient Γ_{12} through the heat current channel even at $\omega = 0$, in complete analogy to the well-known phonon drag mechanism [124, 125]. It is convenient to express Γ_{12} as $\Gamma_{12}^{el} + \Gamma_{12}^{drag}$, in order to keep the electronic contribution well separated from that of charge density fluctuations. For the calculation of Γ_{12}^{el}, we have to consider a diagram fully analogous to (5.1), but with an electron heat current in place of a particle current (graphically represented by a black dot):

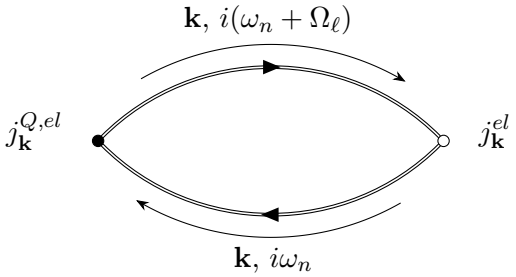

(5.4)

The question of the general definition of a microscopic heat current is thorough and widely debated, however it is generally agreed that any definition of such a current is based on energy conservation arguments [126, 127, 128, 129]. This approach works well for conservative systems, but it may fail in the presence of dissipation. For the case of electron heat current we do not have this kind of problem, in this case the choice for heat current $j_{\mathbf{k}}^{Q,el}$ simply reduces to the product between the electron dispersion referring to (renormalized) chemical potential and the (x-component of the) electron group velocity [98, 130]:

$$j_{\mathbf{k}}^{Q,el} \;=\; \left(\xi_{\mathbf{k}} + \mathrm{Re}\Sigma_R(0)\right) \frac{\partial \xi_{\mathbf{k}}}{\partial k_x}$$

The calculation of the coefficient Γ_{12}^{el} is performed in a completely analogous way to that done for the coefficient Γ_{11}, the result we get is the following:

$$\Gamma_{12}^{el} = \frac{1}{v_{\mathrm{uc}}} \int_{-\infty}^{+\infty} \left[\int_{-\infty}^{+\infty} \widetilde{N}_\xi \, \xi \left[\mathrm{Im} G_R(\omega, \xi) \right]^2 \frac{d\xi}{\pi} \right] \left(-\frac{\partial f(\omega)}{\partial \omega} \right) d\omega$$

Again, we can solve the integral in $d\xi$ by means of Allen approximation, the resulting expression is the following:

$$\Gamma_{12}^{el} = \frac{\widetilde{N}_0}{v_{\rm uc}} \int_{-\infty}^{+\infty} \frac{\omega - {\rm Re}\Sigma_R(\omega) + {\rm Re}\Sigma_R(0)}{2\left(\Sigma_0 - {\rm Im}\Sigma_R(\omega)\right)} \left(-\frac{\partial f(\omega)}{\partial \omega}\right) d\omega \tag{5.5}$$

We immediately notice that, if the entire self-energy was made up of the $-i\Sigma_0$ term alone, this expression would go identically to zero. More generally, this expression vanishes if ${\rm Im}\Sigma_R(\omega)$ is an even function of ω and ${\rm Re}\Sigma_R(\omega)$ is odd. This is due to the fact that this form for the self-energy, combined with the $\widetilde{N}_\xi \simeq \widetilde{N}_0$ approximation, guarantees a perfect particle-hole symmetry for the system. In fact, a general property of the electronic Seebeck coefficient is that it directly provides a measure of the particle-hole asymmetry of the system. In particular, it is positive for a hole-like band structure, negative for an electron-like one and zero for a particle-hole symmetric system [131]. The $\widetilde{N}_\xi \simeq \widetilde{N}_0$ approximation is equivalent to neglecting all the asymmetry effects coming from the band structure. Therefore, the only source of asymmetry in our model is given by the interaction between electrons and charge density fluctuations. It should be stressed that, in absence of interactions, it would be meaningless to treat the function $\widetilde{N}_\xi$ as a constant, as the Seebeck coefficient would be completely determined by the ξ-dependence of this function. According to expression (5.5), in the low temperature limit Γ_{12}^{el} goes to zero as T^2, the coefficient is the following:

$$\frac{\Gamma_{12}^{el}}{T^2}\Big|_{T=0} = \frac{\widetilde{N}_0}{v_{\rm uc}} \frac{1}{2\Sigma_0} \frac{\pi^2}{3} k_{\rm B}^2 \left(-\frac{1}{2} \frac{\partial^2 {\rm Re}\Sigma_R(\omega)}{\partial \omega^2}\Big|_{\substack{\omega=0 \\ T=0}}\right)$$

Our calculation clearly shows that the ratio $\Gamma_{12}^{el}/\Gamma_{11}$ vanishes as T^2 in the low temperature limit, therefore the electronic contribution to the Seebeck coefficient $\mathcal{S}_{el}$ vanishes linearly in temperature:

$$\mathcal{S}_{el} \coloneqq -\frac{1}{{\rm e}T} \frac{\Gamma_{12}^{el}}{\Gamma_{11}} \simeq -\frac{\pi^2}{3} \frac{k_{\rm B}^2 T}{\rm e} \left(-\frac{1}{2} \frac{\partial^2 {\rm Re}\Sigma_R(\omega)}{\partial \omega^2}\Big|_{\substack{\omega=0 \\ T=0}}\right)$$

This asymptotic expression is very similar to the standard *Mott formula* for thermopower in metals [132]:

$$\mathcal{S}_{el} \simeq -\frac{\pi^2}{3} \frac{k_{\rm B}^2 T}{\rm e} \frac{\sigma'(\xi=0)}{\sigma(\xi=0)} \qquad \text{where} \quad \sigma(\xi) \coloneqq \frac{{\rm e}^2}{v_{\rm uc}} \frac{1}{N} \sum_{\mathbf{k},\,\sigma} \tau(\mathbf{k}) v_{\mathbf{k},x}^2 \delta(\xi - \xi_{\mathbf{k}})$$

The quantity we denoted with $\sigma(\xi)$ is the energy-dependent electrical conductivity, while $\tau(\mathbf{k})$ is the relaxation time of the Boltzmann description, under the assumption that it does not depend on the position. Of course, it is possible to introduce a quantity analogous to $\sigma(\xi)$ within Kubo formalism and make a comparison with Boltzmann theory, provided that the (possible) Z factors and the chemical potential shift are put appropriately by hand in the latter. The term $\sigma'(\xi=0)/\sigma(\xi=0)$ in Mott formula, in principle, takes into account both the band structure and the collision effects. Of course, also in this case it is possible to hide the structure effects by applying an Allen-like approximation.

A feature of our expression for $\mathcal{S}_{el}$ is that it does not depend on the value of Σ_0, so apparently it would be possible to state that it is also valid in the $\Sigma_0 \to 0^+$ limit. This would not be correct as the asymptotic expressions we have exhibited for Γ_{11} and Γ_{12}^{el} are valid only if $k_B T$ is much smaller than Σ_0, a regime that would never occur for $\Sigma_0 = 0$. However, it can be shown that even in the case $\Sigma_0 = 0$ there is linearity between $\mathcal{S}_{el}$ and T. The reason is that the asymptotic trends of Γ_{11} and Γ_{12}^{el} at low temperature wolud be $\Gamma_{11} \sim T^{-2}$ and $\Gamma_{12}^{el} \sim const.$, so the trend of their ratio would remain unchanged.

In order to fit experimental data, we choose a slightly different set of parameters than the one used for resistivity and specific heat. As for the fermionic set we have:

$$t = 300\,\text{meV} \qquad t' = -82\,\text{meV} \qquad t'' = 17\,\text{meV} \qquad p = 0.24$$

Which provide a value for the bare chemical potential very similar to that found with the previous set of parameters, namely $\mu \simeq -350\,\text{meV}$. The bosonic parameters we choose are the following:

$$m_c = 15\,\text{meV} \qquad \nu = 1.3\,\text{eV}/(\text{r.l.u.})^2 \qquad \Omega = 30\,\text{meV}$$
$$g = 320\,\text{meV} \qquad \Sigma_0 = 20\,\text{meV}$$

For the moment, we have not set the values of γ and q_c. Within the momentum-independent self-energy approximation, the value of q_c plays no role in our expression for $\mathcal{S}_{el}$, therefore it is not necessary to define it at present. As for γ, we keep it as a variable parameter, in accordance with our model. The numerical calculation of the full expression of $\mathcal{S}_{el}$, where Γ_{12}^{el} are computed respectively by means of equations (5.3) and (5.5), confirms the approximate linearity in temperature and also provides a slight dependence on the γ parameter, at least if γ varies between 5 and 10. The result is shown in figure 5.2. Our approximate expression would predict that these curves are constant in temperature, while the figure shows a basin at a temperature of around 8 K. While this dependence appears to be non-negligible if limited to the $\mathcal{S}_{el}$ term alone, we will see that it will be negligible when considering the sum with the drag contribution. Therefore, by neglecting the residual temperature dependence of $\mathcal{S}_{el}/T$, we can express its dependence on γ as follows:

$$\frac{\mathcal{S}_{el}}{T} \simeq (7.40 - 0.40\,\gamma) \times 10^{-8}\,\text{V/K}^2$$

5.3 Bosonic contribution to Seebeck coefficient

The Seebeck coefficient in metals provided by Mott formula would be linear in temperature, relatively small (less than $1\,\mu\text{V K}^{-1}$ at $T = 10\,\text{K}$) and with the same sign as the carriers' charge. These are not the features that are usually observed in many standard metals. The main reason of this discrepancy is that Mott formula is valid only under the Bloch conditions, i.e. when the phonons are assumed to be at equilibrium. Instead, at low enough temperatures (below the Debye temperature) the effects of non-equilibrium phonons become appreciable and, in many cases,

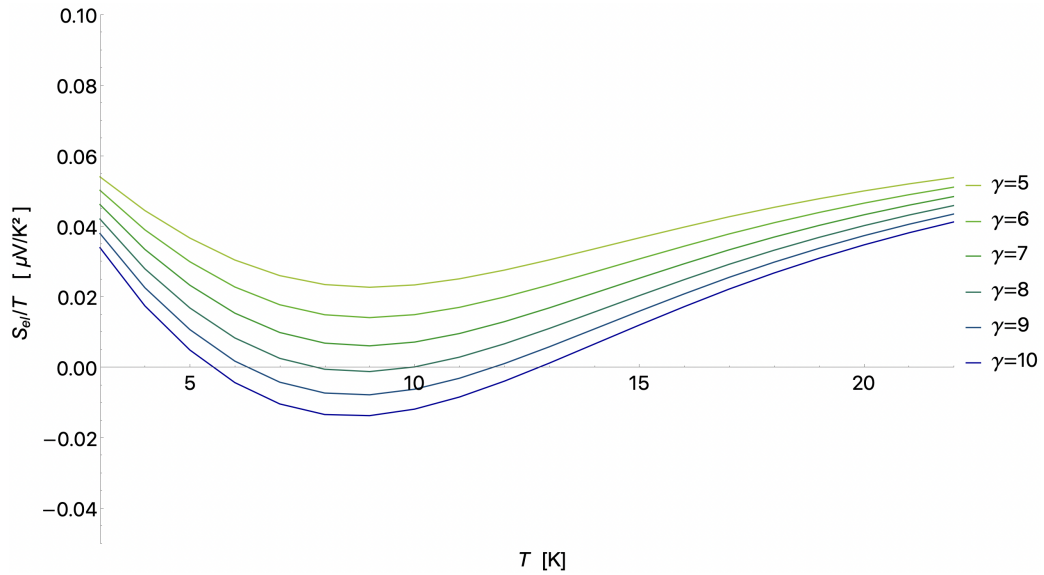

Figure 5.2. Plots of the ratio $\mathcal{S}_{el}/T$ as a function of temperature for different values of γ.

they can become dominant [133, 134]. This leads precisely to the aforementioned mechanism of phonon drag. What we are going to propose is a mechanism analogous to phonon drag, with the difference that the role of the phonons is played by the charge density fluctuations modes [135]. Henceforth, we will refer to this mechanism as *charge density fluctuations drag*, or more simply *CDF drag*. Within diagram theory, the diagram associated with the standard phonon drag at the lowest order of perturbation is [136]:

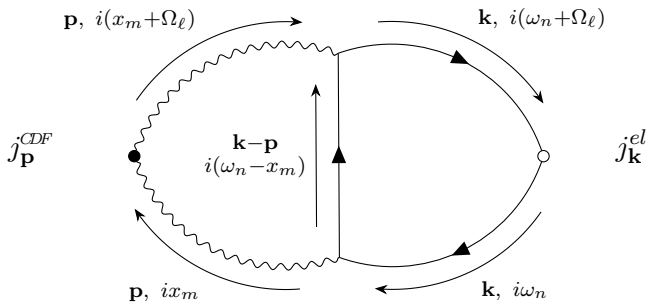

(5.6)

This is the diagram that we will use to calculate the coefficient Γ_{12}^{drag}, where $j^{CDF}_{\mathbf{p}}$ is the bosonic heat current due to the charge density fluctuations, while the wavy lines are associated to their propagators. The Matsubara sums in the loops of diagram (5.6) can be analitically performed, the result can be compactly expressed as follows (all the details on the calculation are shown in Appendix G):

$$\Gamma_{12}^{drag} = \frac{1}{v_{\mathrm{uc}}} \frac{2g^2}{N^2} \sum_{\mathbf{k},\mathbf{p}} j^{CDF}_{\mathbf{p}} j^{el}_{\mathbf{k}} \big(f(\xi_{\mathbf{k}}) - f(\xi_{\mathbf{k}-\mathbf{p}})\big)\big(I^a_{\mathbf{k},\mathbf{p}} + I^b_{\mathbf{k},\mathbf{p}}\big) \tag{5.7}$$

The reason why this expression contains only one factor $1/v_{\mathrm{uc}}$, despite the sum over the momenta being double, is that one of the two factors is included in the

definition of the coupling constant g, as we have already discussed when calculating the self-energy within Fock approximation. The quantities $I^a_{\mathbf{k},\mathbf{p}}$ and $I^b_{\mathbf{k},\mathbf{p}}$ are defined as follows:

$$I^a_{\mathbf{k},\mathbf{p}} \coloneqq -\fint_{-\infty}^{+\infty} \frac{\dfrac{\partial}{\partial x}\left[\Big(\mathrm{Im}D_R(x,\mathbf{p})\Big)^2 b'(x)\right]}{x-(\xi_{\mathbf{k}}-\xi_{\mathbf{k}-\mathbf{p}})}\frac{dx}{\pi}$$

$$I^b_{\mathbf{k},\mathbf{p}} \coloneqq \left.\frac{\dfrac{\partial}{\partial \xi}\left[\Big(\mathrm{Im}D_R(\xi,\mathbf{p})\Big)^2 b'(\xi)\right]}{\mathrm{Im}D_R(\xi,\mathbf{p})}\right|_{\xi=\xi_{\mathbf{k}}-\xi_{\mathbf{k}-\mathbf{p}}} \fint_{-\infty}^{+\infty} \frac{\mathrm{Im}D_R(x,\mathbf{p})}{x-(\xi_{\mathbf{k}}-\xi_{\mathbf{k}-\mathbf{p}})}\frac{dx}{\pi}$$

Unlike the fermionic case, the problem of defining the heat current for a system of damped collective modes is very subtle and far from trivial, and the reason lies precisely in the damping term. In order to find a reasonable expression for $j^{CDF}_{\mathbf{p}}$ which can account for the damping we will apply an inductive procedure. Instead of deriving the expression for the heat current from the beginning, we will start from the standard case of the undamped phonon and generalize it. First of all, let's recall the general form in which a current operator is expressed within second quantization formalism:

$$J_\alpha(\mathbf{q}) = \sum_{\mathbf{k}\,\sigma} j^\alpha_{\mathbf{k},\mathbf{k}+\mathbf{q},\sigma,\sigma'} \hat{a}^\dagger_{\mathbf{k},\sigma}\hat{a}_{\mathbf{k}+\mathbf{q},\sigma'} \qquad \text{with} \quad \langle 0|\hat{a}_{\mathbf{k},\sigma}\, J_\alpha(\mathbf{q})\, \hat{a}^\dagger_{\mathbf{k}',\sigma'}|0\rangle = j^\alpha_{\mathbf{k},\mathbf{k}',\sigma,\sigma'}\delta_{\mathbf{k}',\,\mathbf{k}+\mathbf{q}}$$

Where $\hat{a}^\dagger_{\mathbf{k},\sigma}$ and $\hat{a}_{\mathbf{k},\sigma}$ are, respectively, the creation and the annihilation operators of the particle which carries the current (with momentum $\mathbf{k}$ and spin σ). Coherently with the notation adopted in section 2.3, the subscript α denotes both the nature and the space component of the current, the latter will always be the one along the x-direction without loss of generality. The action of the operator $J_\alpha(\mathbf{q})$ is fully determined by the coefficients $j^\alpha_{\mathbf{k},\mathbf{k}',\sigma,\sigma'}$. We are interested in the case in which the current operator is evalued at $\mathbf{q}=\mathbf{0}$, and in which it does not act on spin degrees of freedom. This latter request is equivalent to take $j^\alpha_{\mathbf{k},\mathbf{k}',\sigma,\sigma'}$ in the form $j^\alpha_{\mathbf{k},\mathbf{k}'}\delta^\sigma_{\sigma'}$. Moreover, to soften the notation, when the term $j^\alpha_{\mathbf{k},\mathbf{k}'}$ is evalued at $\mathbf{k}=\mathbf{k}'$ we will omit one of the two momenta among the arguments, namely $j^\alpha_{\mathbf{k}} \coloneqq j^\alpha_{\mathbf{k},\mathbf{k}}$. Under these conditions, the operator of our interest takes on the following simple form:

$$J^\alpha(\mathbf{q}=\mathbf{0}) = \sum_{\mathbf{k}\,\sigma} j^\alpha_{\mathbf{k}}\hat{a}^\dagger_{\mathbf{k},\sigma}\hat{a}_{\mathbf{k},\sigma} = \sum_{\mathbf{k}\,\sigma} j^\alpha_{\mathbf{k}}\hat{n}_{\mathbf{k},\sigma}$$

In our case, the coefficients $j_{\mathbf{k}}$ are precisely the currents $j^{CDF}_{\mathbf{p}}$, and they are the object for which we are going to find an explicit expression. Let's begin with the simple case of a single-band undamped phonon gas, with dispersion $\omega_{\mathbf{k}}$. For such a system, the internal energy at thermal equilibrium is given by the sum of the energies of the individual modes, each weighted with the Bose function. The total equilibrium heat current can be expressed as a sum over the modes too, but each of the terms must be the product of the Bose function, the energy carried by the mode and its group velocity. In other words, we have the following two equations:

$$U_b = \sum_{\mathbf{k}} b(\omega_{\mathbf{k}})\,\omega_{\mathbf{k}} \qquad \langle J_Q^{ph}\rangle = \sum_{\mathbf{k}} b(\omega_{\mathbf{k}})\,\omega_{\mathbf{k}}\frac{\partial\omega_{\mathbf{k}}}{\partial k_x}$$

Notice that the second sum is trivially equal to zero by virtue of divergence theorem, as it should be since there must be no current in equilibrium conditions. In writing the full expression of $\langle J_Q^{ph}\rangle$ we used the well-known expression of the microscopic phonon heat current [126, 137], usually written in a vector form:

$$\mathbf{j}_{\mathbf{k}}^{ph} = \omega_{\mathbf{k}}\nabla_{\mathbf{k}}\omega_{\mathbf{k}}$$

In order to generalize this expression to the charge density fluctuations case, our starting point is the (generalized) expression of the internal energy of such a system. Our hope is to be able to express the internal energy of the system as the sum over all modes of the product between the energy transported by the single mode, its group velocity and a factor representing the statistical occupancy of that mode at thermal equilibrium. Moreover, it is necessary to take into account the fact that, in the presence of damping, the poles of the bosonic propagator are no longer simply equal and opposite, but become linearly independent of each other. This would result in an effective splitting of the dispersion, which must be taken into account in the final expressions. Essentially, the expressions we are looking for are in the following forms:

$$U_b = \sum_{\mathbf{k},s} c_s\, n_s(\omega_{\mathbf{k},s})\,\omega_{\mathbf{k},s} \qquad \langle J_Q^{CDF}\rangle = \sum_{\mathbf{k},s} c_s\, n_s(\omega_{\mathbf{k},s})\,\omega_{\mathbf{k},s}\frac{\partial\omega_{\mathbf{k},s}}{\partial k_x} \tag{5.8}$$

The s index labels the splitted dispersions, $n_s(\omega_{\mathbf{k},s})$ is the statistical occupation function (which essentially plays the same role as the Bose function for the undamped phonon gas) and c_s is simply a weighting coefficient. In order for the quantities appearing in these two equations to be defined without ambiguity, we require the following constraints to hold:

$$\sum_s c_s = 1 \qquad \lim_{\omega\to 0^+} n_s(\omega)\,\omega = \frac{1}{\beta}$$

The first one simply allows us to interpret the numbers c_s as wieghting coefficients, while the second one ensures that the $n_s(\omega)$ functions behave as Bose functions at low frequency, when the effect of the damping becomes irrelevant. If we are able to express U_b and $\langle J_Q^{CDF}\rangle$ in the forms we have exhibited above, then we choose the following expression for the charge density fluctuations heat current:

$$\mathbf{j}_{\mathbf{k}}^{CDF} = \sum_s c_s\,\omega_{\mathbf{k},s}\nabla_{\mathbf{k}}\omega_{\mathbf{k},s}$$

It should be stressed that this argument, as well as the final expression we found for $\mathbf{j}_{\mathbf{k}}^{CDF}$, is not necessarily exclusive to charge density fluctuations but can be applied essentially to any damped collective mode. For the specific case of charge density fluctuations, we know that the expression for the generalized internal energy is analogous to that exhibited in section 3.6, with the only difference that the poles of the bosonic propagator are momenutm-dependent (see also equation (D.8) in Appendix D):

$$U_b = \frac{1}{2}\sum_{\mathbf{k}}\Big(n_+(\omega_{\mathbf{k}}^+)\,\omega_{\mathbf{k}}^+ + n_-(\omega_{\mathbf{k}}^-)\,\omega_{\mathbf{k}}^-\Big)$$

$$\text{where} \qquad n_\pm(\omega) \coloneqq \frac{1}{\beta\omega} \pm \frac{\psi\Big(1 \pm i\frac{\beta\omega}{2\pi}\Big) - \log\Big(\pm i\frac{\beta\omega}{2\pi}\Big)}{i\pi}$$

This expression is coherent with the generic form exhibited in (5.8). In this case, the dispersion of the undamped limit is splitted into two effective "bands", which are $\omega_{\mathbf{k}}^+$ and $\omega_{\mathbf{k}}^-$. For each of these two, the weighting coefficient is $1/2$, while the statistical terms are given respectively by $n_+(\omega_{\mathbf{k}}^+)$ and $n_-(\omega_{\mathbf{k}}^-)$. According with our discussion in section 3.6, the $\gamma \to 0^+$ limit of U_b precisely provides the sum over all momenta of the quantity $b(\omega_{\mathbf{k}})\,\omega_{\mathbf{k}}$, with $\omega_{\mathbf{k}} = \sqrt{\Omega m_{\mathbf{k}}}$, consistently with the known result for the undamped case. In particular, the average mean of $n_+(\omega)$ and $n_-(\omega)$, when ω is real and positive, is precisely the Bose function $b(\omega)$, moreover both functions separately satisfy the required $\omega \to 0^+$ limit. Also notice that the two pieces into which the total internal energy is split, each taken separately, could give a complex contribution, only the sum of the two guarantees that U_b is actually real. For this reason, the interpretation of $\omega_{\mathbf{k}}^+$ and $\omega_{\mathbf{k}}^-$ as two separate bands is only formal, it is instead necessary to always consider them together to obtain sensible physical results.

The deviation from the pure phonon case due to damping within this description is therefore expressed in two distinct effects: on the one hand there is the splitting of the energy $\omega_{\mathbf{k}}$ into $\omega_{\mathbf{k}}^+$ and $\omega_{\mathbf{k}}^-$, each of which however gives half a contribution to the termodynamics of the system, on the other we have a modification of the statistical occupation function, which would usually be the Bose function. This second effect does not affect the current vertex expression, it is therefore not considered in our calculation. We take into account the first effect by simply considering the arithmetic mean of the vertices given separately by the two frequencies:

$$\mathbf{j}_{\mathbf{k}}^{CDF} = \frac{1}{2}(\omega_{\mathbf{k}}^+\nabla_{\mathbf{k}}\omega_{\mathbf{k}}^+ + \omega_{\mathbf{k}}^-\nabla_{\mathbf{k}}\omega_{\mathbf{k}}^-) = \frac{1}{2}\,\Omega\,\nabla_{\mathbf{k}} m_{\mathbf{k}}$$

It is worth noting that γ simplifies perfectly in this calculation, so we deduce that the current we find in the charge density fluctuations case is the same as in the case of undamped phonons with dispersion $\omega_{\mathbf{k}} = \sqrt{\Omega m_{\mathbf{k}}}$. In conclusion, the expression we propose for the coefficient $j_{\mathbf{k}}^{CDF}$ is the following:

$$j_{\mathbf{k}}^{CDF} = \frac{\Omega}{2}\frac{\partial m_{\mathbf{k}}}{\partial k_x}$$

Given this expression, we are ready to compute the coefficient Γ_{12}^{drag}. Basically, we need to study the behavior of expression (5.7) as a function of temperature and some selected bosonic parameters. Numerically, it is possible to show that, within the same range of parameters introduced in the previous section (including the considered range of values for γ), Γ_{12}^{drag} is linear in γ and quadratic in T in the low temperature limit. In other words, we have the approximate proportionality $\Gamma_{12}^{drag} \propto \gamma\, T^2$, where the proportionality coefficient depends significantly on the parameters of the theory. In particular, we observed that this coefficient depends crucially on the value of

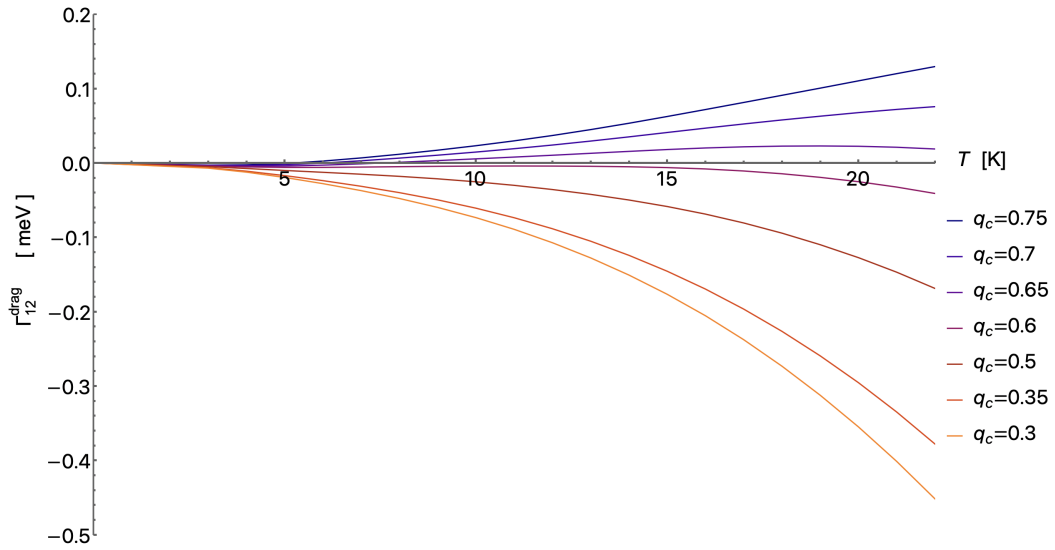

Figure 5.3. Plots of the coefficient Γ_{12}^{drag} as a function of temperature at fixed $\gamma = 10$ for different values of q_c. For simplicity, we fixed $v_{\mathrm{uc}} = 1$.

q_c, which also determines the sign of Γ_{12}^{drag} (and, consequently, the sign of the Seebeck coefficient, having the latter sign opposite to Γ_{12}^{drag}). Therefore, our first step is to fix a reasonable value for this parameter. In figure 5.3 we show the plot of Γ_{12}^{drag} as a function of temperature for several values of q_c at fixed $\gamma = 10$, obtained by evaluating numerically expression (5.7). We see that, for $q_c \lesssim 0.35$, the approximate low-temperature behavior $\Gamma_{12}^{drag} \propto \gamma T^2$ works quite well, and that the proportionality constant is negative. Since this is exactly the regime we are interested in, we fix $q_c = 0.3$ in the following calculations. Of course, the very same asymptotic behavior is also valid for the ratio $\Gamma_{12}^{drag}/\Gamma_{11}$, as Γ_{11} tends to a finite value at zero temperature, which is independent of γ. By taking these observations into account, and by observing that $\Gamma_{12}^{drag}/\Gamma_{11}$ has the dimension of an energy, we can define a positive γ-dependent energy scale $\tilde{\varepsilon}(\gamma)$ such as to satisfy the following relation:

$$\frac{\Gamma_{12}^{drag}}{\Gamma_{11}} \simeq -\frac{1}{\beta^2 \tilde{\varepsilon}(\gamma)}$$

In principle, this relation can be made exact by defining $\tilde{\varepsilon}(\gamma)$ in an appropriate way, the approximation lies in considering $\tilde{\varepsilon}(\gamma)$ independent of temperature. In view of the above, we expect that $\tilde{\varepsilon}(\gamma)$ is approximately proportional to $1/\gamma$ for a reasonable range of parameters. If we denote the drag contribution to Seebeck coefficient as $\mathcal{S}_{drag}$, we have:

$$\mathcal{S}_{drag} \coloneqq -\frac{1}{\mathrm{e}T}\frac{\Gamma_{12}^{drag}}{\Gamma_{11}} \simeq \frac{k_{\mathrm{B}}^2 T}{\mathrm{e}}\frac{1}{\tilde{\varepsilon}(\gamma)}$$

The complete calculation of $\mathcal{S}_{drag}$ as a function of temperature and of γ, carried out by numerically evaluating the complete expressions for Γ_{11} and Γ_{12}^{drag}, confirms the qualitative trend that we expected. We show the result in figure 5.4. Even here, our

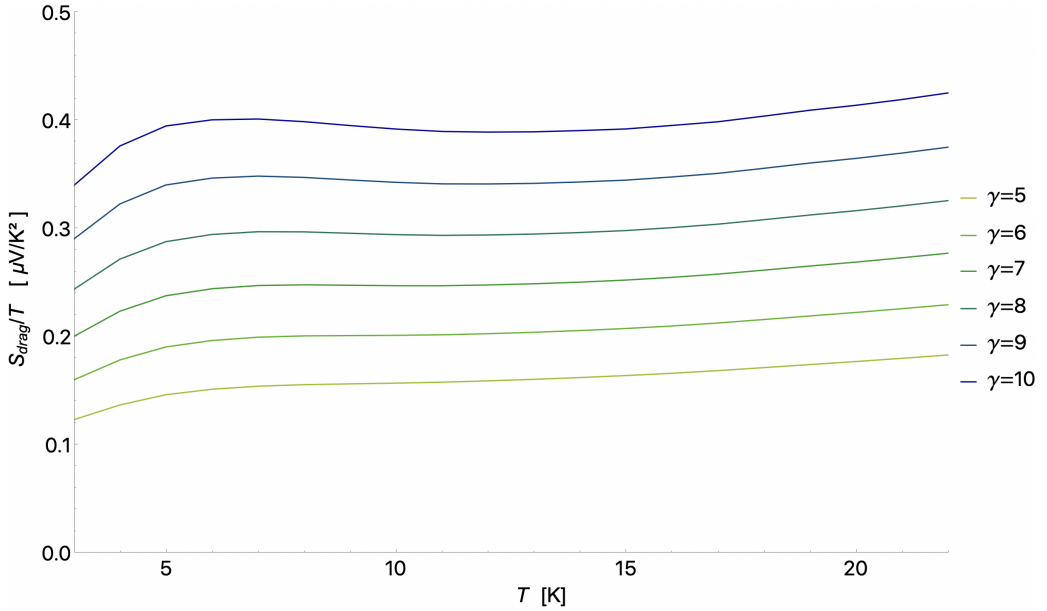

Figure 5.4. Plots of the ratio $\mathcal{S}_{drag}/T$ as a function of temperature for different values of γ. Note that, differently from figure 5.2, these curves increase as a function of γ.

approximation would be equivalent to considering these curves as constants, which is completely reasonable within the range of temperature and γ we are considering. From the figure it is clear that the order of magnitude of $\mathcal{S}_{drag}/T$ varies between $0.1\,\mu V\,\mathrm{K}^{-2}$ and $0.4\,\mu V\,\mathrm{K}^{-2}$, while the deviation from a constant behavior observed in the curves for $\mathcal{S}_{el}/T$ in figure 5.2 was a few hundredths of a $\mu V\,\mathrm{K}^{-2}$, this confirms that it was reasonable to neglect this effect in view of the fact that the two contributions will be added. The approximate γ dependence for the ratio $\Gamma_{12}^{drag}/\Gamma_{11}$ is the following:

$$\frac{\mathcal{S}_{drag}}{T} \simeq (-8.83 + 4.85\,\gamma) \times 10^{-8}\,\mathrm{V/K^2}$$

The sum of the electronic and the drag contributions provides the following result:

$$\frac{\mathcal{S}}{T} = \frac{\mathcal{S}_{el} + \mathcal{S}_{drag}}{T} \simeq (-1.43 + 4.45\,\gamma) \times 10^{-8}\,\mathrm{V/K^2}$$

Within our model, the whole temperature dependence of $\mathcal{S}/T$ lies in $\gamma = \gamma(T)$. For simplicity, we fix $p = p^*$ and consider a simplified version of (3.8), namely $\gamma(T) = \max(\gamma_0 \log(T_0/T)\,, 1)$. The experimental data can be accurately fitted for $\gamma_0 = 2.66$ and $T_0 = 170\,\mathrm{K}$. With these parameters, γ varies approximately within 5 and 10, which is precisely the range of values that we considered within our study. Moreover, in this range for γ, the energy scale $\tilde{\varepsilon}(\gamma)$ varies approximately between 15 meV and 45 meV, which is a range comparable with the other bosonic energy scales of the model. In figure 5.5 we show the result of our fit.

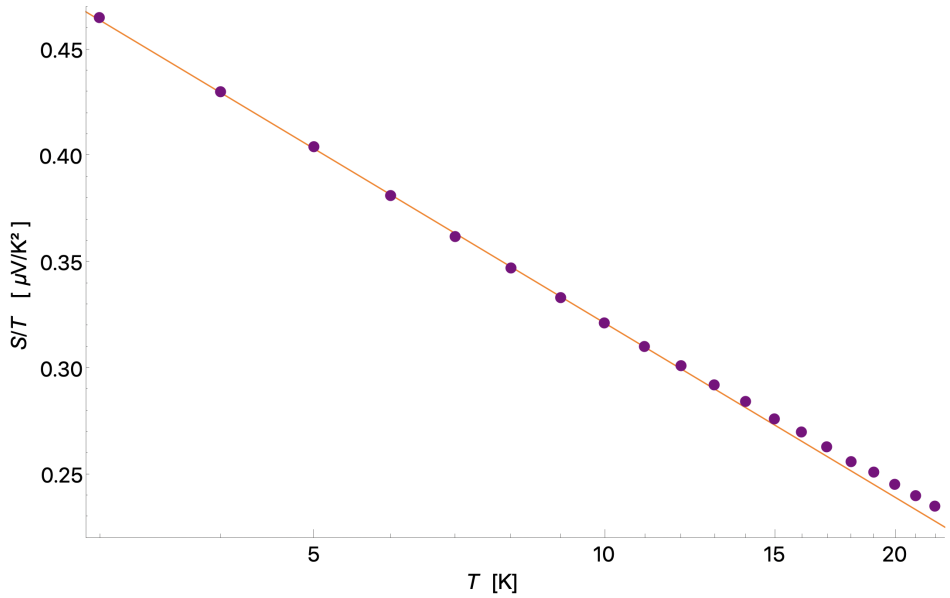

Figure 5.5. Comparison between experimental data for $La_{1.6-x}Nd_{0.4}Sr_xCuO_4$ taken from reference [54] (purple dots) and our theoretical calculation with the chosen parameters (orange line).

5.4 Magnetoresistance

On the basis of the analysis we carried out on our Shrinking Fermi liquid model, and then confirmed by the study of charge density fluctuations, the linear trend of resistivity as a function of temperature observed in optimal doped cuprates is not due to a perfect scaling between ω and T in self-energy, which in our model is only approximately reproduced. As we have discussed, this violation of scaling is due to the fact that the dependencies of self-energy on these two variables have a clearly different origin, only in an appropriate range for the two parameters is it possible to recover an apparent scaling. In the same vein, we expect that even the apparent scaling between temperature and magnetic field observed in magnetoresistance measurements is only approximate.

In reference [53] it was explicitly shown that, in order to obtain a linear relationship between the in-plane resistivity and the transverse magnetic field, it is sufficient that the elastic scattering component is anisotropic enough on the Fermi surface. Angle-resolved photoemission spectroscopy experiments carried out on $La_{1.6-x}Nd_{0.4}Sr_xCuO_4$ show that, at 24% doping level, the scattering rate along the Fermi surface is strongly anisotropic and peaked at the nodal points [138], which is likely due to the proximity to the Van Hove Singularity [139]. So far, within our work we have only explored the inelastic (i.e. temperature-dependent) contribution to scattering due to collective modes, which is weakly momentum-dependent. At present, we still don't know how our model is able to take into account the seeming linearity of the magnetoresistance, however a preliminary study we have carried out seems to confirm the claim that a linear magnetoresistance can be produced by

anisotropic elastic scattering [140]. In particular, we considered an angle-dependent elastic scattering rate on the Fermi function of the same form given in reference [53]:

$$\frac{1}{\tau(\mathbf{k}_\mathrm{F})} = \frac{1}{\tau_\mathrm{is}} + \frac{1}{\tau_\mathrm{an}}|\cos(2\varphi_{\mathbf{k}_\mathrm{F}})|^\nu \tag{5.9}$$

Where $\varphi_{\mathbf{k}_\mathrm{F}}$ denotes the angle that the Fermi surface vector $\mathbf{k}_\mathrm{F}$ makes with the positive x-semiaxis in the first Brillouin zone. In the presence of a transverse magnetic field, the electrical conductivity is no longer a scalar but becomes a 2×2 matrix. However, tetragonal symmetry ensures that the two diagonal components are equal to each other, as are the two off-diagonal components, therefore the conductivity tensor is determined by only the two components diagonal and off-diagonal, which we indicate with σ_{xx} and σ_{xy} respectively. In order to determine the magnetic field dependence of these two quantities, in a non-perturbative way, we use the Chambers' solution to the Boltzmann equation [40, 141]:

$$\sigma_{xx}(B) = \frac{2\mathrm{e}^2}{v_\mathrm{uc}} \oint_{FS} v_{\mathbf{k}_\mathrm{F}(0),x} \left(\int_{-\infty}^{0} e^{-\int_t^0 \frac{dt'}{\tau(\mathbf{k}_\mathrm{F}(t'))}} \frac{v_{\mathbf{k}_\mathrm{F}(t),x}}{v_{\mathbf{k}_\mathrm{F}(t)}} \, dt \right) \frac{dk}{4\pi^2}$$

$$\sigma_{xy}(B) = \frac{2\mathrm{e}^2}{v_\mathrm{uc}} \oint_{FS} v_{\mathbf{k}_\mathrm{F}(0),x} \left(\int_{-\infty}^{0} e^{-\int_t^0 \frac{dt'}{\tau(\mathbf{k}_\mathrm{F}(t'))}} \frac{v_{\mathbf{k}_\mathrm{F}(t),y}}{v_{\mathbf{k}_\mathrm{F}(t)}} \, dt \right) \frac{dk}{4\pi^2}$$

Where B is the z-component of the transverse magnetic field $\mathbf{B}$, while $v_\mathbf{k}$ is the magnitude of the electron group velocity $\mathbf{v}_\mathbf{k}$ (the notations $v_{\mathbf{k},x}$ and $v_{\mathbf{k},y}$, the former of which has already been used in section 5.1, refer instead to the two components of $\mathbf{v}_\mathbf{k}$). Within our expressions for $\sigma_{xx}(B)$ and $\sigma_{xy}(B)$ the function $\mathbf{k}_\mathrm{F}(t)$ appears, it is precisely through this function that the dependence on the magnetic field comes into play. In order to get the time evolution of $\mathbf{k}_\mathrm{F}(t)$ we need to integrate the standard equation of motion for an electron in an uniform electric and magnetic field:

$$\frac{d\mathbf{k}}{dt} = -\mathrm{e}(\mathbf{E} + \mathbf{v}_\mathbf{k} \times \mathbf{B})$$

Where $\mathbf{k}$, $\mathbf{E}$ and $\mathbf{v}_\mathbf{k}$ lie on the lattice plane, while $\mathbf{B}$ is orthogonal. However, since we are not interested in non-linear effects in the electrostatic field, we can set $\mathbf{E} = \mathbf{0}$. The equation we find can be expressed either in Cartesian coordinates or in polar coordinates as follows:

$$\begin{cases} \dfrac{dk_x}{dt} = -\mathrm{e}Bv_y \\ \dfrac{dk_y}{dt} = \mathrm{e}Bv_x \end{cases} \qquad \begin{cases} \dfrac{1}{k}\dfrac{dk}{dt} = -\mathrm{e}B\dfrac{k_x v_y - k_y v_x}{k_x^2 + k_y^2} \\ \dfrac{d\varphi}{dt} = \mathrm{e}B\dfrac{k_x v_x + k_y v_y}{k_x^2 + k_y^2} \end{cases}$$

Since the integral that defines the electrical conductivity is restricted to the Fermi surface, the various vectors that appear are uniquely identified by their angle with respect to the origin of the first Brillouin zone. Consequently, the only relevant equation of motion is the one for φ. Of course, in absence of magnetic field, φ is constant in time. It is straightforward to show that, in this case, σ_{xx} and σ_{xy} assume the standard expressions foreseen by Boltzmann theory (in particular $\sigma_{xy} = 0$) [49]. We define the magnetoresistance such that it vanishes at $B = 0$:

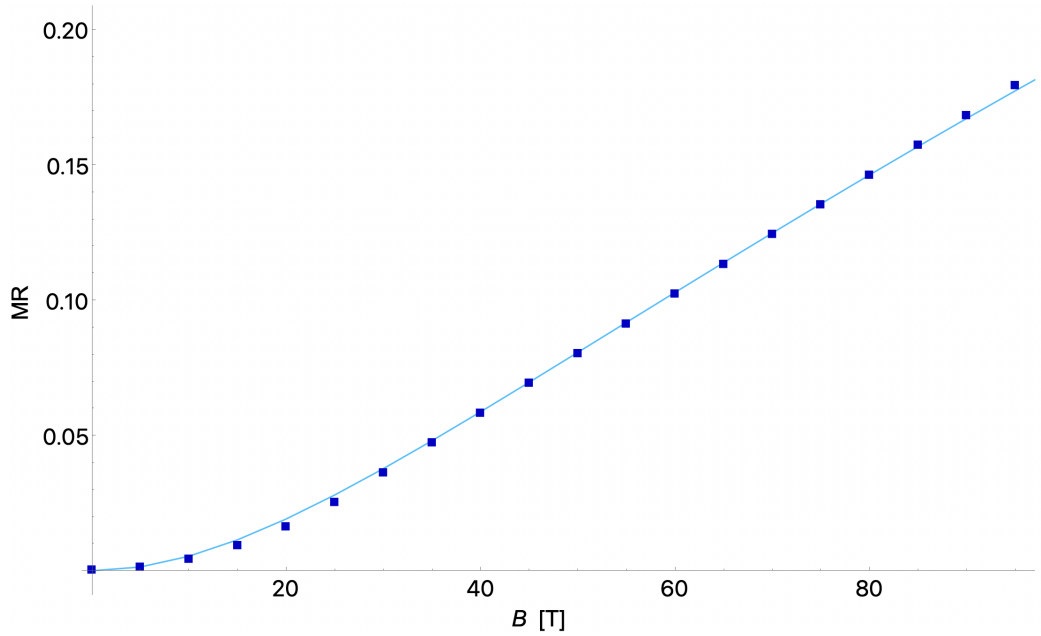

Figure 5.6. Plots of the magnetoresistence experimental data (dots) and theoretical fit (solid line) for $La_{1.6-x}Nd_{0.4}Sr_xCuO_4$, at $p = 0.24$ and $T = 30\,\mathrm{K}$. The experimental data are taken from reference [53].

$$\mathrm{MR}\,(B) \coloneqq \frac{\sigma_{xx}(0)}{\sigma_{xx}(B)} - 1 = \frac{\rho_{xx}(B)}{\rho_{xx}(0)} - 1$$

It is worth noting that, according to our units, the quantity eB is dimensionless. It can be expressed as the ratio between B and the magnetic field scale B_0, whose definition in SI units is the following:

$$B_0 \coloneqq \frac{\hbar}{e\,a^2} \simeq \frac{65\,821.2\,\mathrm{T}}{[\text{value of } a \text{ in Å}]^2}$$

For $a = 3.8\,\text{Å}$ we get $B_0 \simeq 4.56 \times 10^3\,\mathrm{T}$, which is the value we use to express the magnetic field B in T. In order to fit the data, we choose to use the very same set of fermionic parameters which allowed us to fit resistivity data, namely:

$$t = 435\,\mathrm{meV} \qquad t' = -50\,\mathrm{meV} \qquad t'' = 38\,\mathrm{meV} \qquad p = 0.24$$

Our goal is to reproduce the magnetoresistance data for $La_{1.6-x}Nd_{0.4}Sr_xCuO_4$ using the expression for $\tau(\mathbf{k}_\mathrm{F})$ given by equation (5.9), we therefore have three fitting parameters available, namely τ_is, τ_an and ν. In order to take into account the inelastic component of the scattering we add to $1/\tau(\mathbf{k}_\mathrm{F})$ a term of the form $\alpha_\mathrm{in} k_\mathrm{B} T$ with $\alpha_\mathrm{in} = 1.2$, in complete analogy to what was done in reference [53]. The fit of the experimental data provided the following set of values:

$$\frac{1}{\tau_\mathrm{is}} = 17.7\,\mathrm{meV} \qquad \frac{1}{\tau_\mathrm{an}} = 39\,\mathrm{meV} \qquad \nu = 4$$

The result of the fit is graphically reported in figure 5.6. The set of parameters we have chosen not only allows a good fit of the experimental magnetoresistance curve, but is also consistent with the fit of the resistivity data at zero temperature in absence of magnetic field. In fact, at $T = 0$, the resistivity is fully determined by the elastic component of the quasiparticle scattering, which in this case is the one expressed by equation (5.9). In the case of the resistivity fit we had considered a completely momentum-independent elastic scattering, quantitatively described by the term Σ_0 that we had added to the imaginary part of the electronic self-energy. The value of ρ_{xx} we get at $T = 0$ and $B = 0$ that we obtain with the expression for $1/\tau(\mathbf{k}_\mathrm{F})$ given by (5.9) with the chosen parameters is the same as that obtained by setting $1/\tau(\mathbf{k}_\mathrm{F})$ equal to the constant value $2\Sigma_0$ with $\Sigma_0 = 13.7\,\mathrm{meV}$, which is the value we set to fit $La_{1.6-x}Nd_{0.4}Sr_xCuO_4$ resistivity.

With this chapter we conclude our discussion on the role of charge density fluctuations in the phenomenology of the strange-metal phase of cuprates. Once again, we stress that a crucial role within this model is given by the functional dependence of the parameter γ on the temperature and the doping level, quantitatively expressed by equation (3.8). This particular dependence does not have a microscopic origin within the theory, but was only assumed phenomenologically. In the next chapter we will provide a possible microscopic explanation for this abnormal behavior for damping.

Chapter 6

Microscopic origin of the abnormal damping

So far, we have addressed the problem of the phenomenology of the strange-metal phase in cuprates. In particular, we have shown how a strong damping of appropriate charge density collective modes is able to explain some of the most peculiar phenomena of this phase. However, the question remains open as to what microscopic mechanisms are responsible for this increase in dissipation.

In this chapter we will address exactly this still unresolved question. The explanation we are going to propose gives a central role to the interaction between the charge density fluctuations and the diffusion modes of electrons in two dimensions. Our study follows the discussion we presented in reference [142].

6.1 Coupling between charge density fluctuations and diffusive modes

Let's consider a regime in which charge density fluctuations have a rather short correlation length, namely at a doping level sufficiently larger than the critical one p_c (which we will identify with p^*). If we do not take into account any kind of interaction for charge density fluctuations, we can express their *bare* propagator (within Matsubara domain) in a form which is essentially analogous to that introduced in equation (2.2):

$$\mathcal{D}_b(\omega_n, \mathbf{k}) = \frac{1}{m_c^b + \nu|\mathbf{k} - \mathbf{q}_c|^2 + \gamma^b|\omega_n| + \dfrac{\omega_n^2}{\Omega}}$$

For simplicity, we considered its momentum dependence in the approximate form valid for $\mathbf{k}$ close to $\mathbf{q}_c$. The values of m_c^b and γ^b differ from those exhibited in (2.2) as they do not take into account any interaction. The Landau damping term γ^b for the bare charge density fluctuations quantitatively describes the tendency of these collective modes to decay into a particle-hole pair. Depending on the energy of the collective modes, the particle-hole pair produced in the decay may have a diffusive or a ballistic character. The energy scale that establishes which of the

two physical regimes we are in is the elastic scattering rate of the charge carriers on quenched impurities, which we denoted with Σ_0. From the study conducted so far, we know that the characteristic energy scale for charge density fluctuations (in this case, bare) is given by the m_c^b/γ^b ratio. Therefore, for $m_c^b/\gamma^b > \Sigma_0$ the charge density fluctuations will essentially decay into a ballistic particle-hole pair, while for $m_c^b/\gamma^b < \Sigma_0$ the decay will occur into a diffusive pair. In this latter case, according to standard theory of disordered electron systems [62], a diffusive collective mode is obtained by a ladder resummation of impurity scattering events which gives the electronic density-density response function the form of a diffusive pole:

$$\chi_{\rho\rho}(\mathbf{q}, \omega_n) = \frac{N_0 D q^2}{D q^2 + |\omega_n|}$$

Where D is the diffusion coefficient, which according to our units has the dimension of an energy, N_0 is the density of states at the Fermi level as usual, while q is simply the magnitude of the wave vector $\mathbf{q}$. This pole induces a momentum-independent self-energy correction to $\mathcal{D}_b(\omega_n, \mathbf{k})$, from which the original propagator is obtained:

$$\mathcal{D}(\omega_n, \mathbf{k}) = \frac{1}{m_c^b + \nu|\mathbf{k} - \mathbf{q}_c|^2 + \gamma^b|\omega_n| + \dfrac{\omega_n^2}{\Omega} - \Sigma(\omega_n)} \tag{6.1}$$

Of course, the self-energy $\Sigma(\omega_n)$ should not be confused with the electronic self-energy provided by charge density fluctuations introduced in chapter 2. This new self-energy is the charge density fluctuations self-energy provided by diffusive particle-hole pairs. From the point of view of Feynman diagrams, this self-energy can be seen as the (renormalized) bubble between the two bare charge density fluctuations lines:

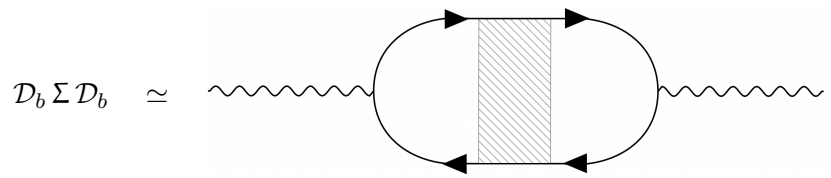

And, of course, the full charge density fluctuations propagator $\mathcal{D}(\omega_n, \mathbf{k})$ is simply the geometric resummation of such diagrams. The rectangle which appear in the renormalized bubble is simply the ladder resummation of elastic scattering on quenched impurities, graphically:

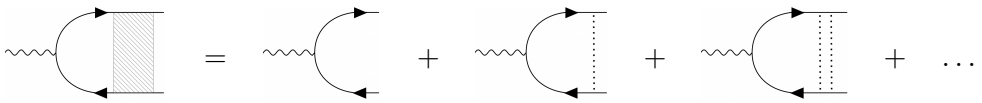

Where the dashed lines precisely represent this scattering mechanism. Since we are interested in the two-dimensional case, the explicit expression of the self-energy is given by:

$$\Sigma(\omega_n) = \tilde{g}^2 N_0 \int_{q_{\min}}^{q_{\max}} \frac{D q^2}{D q^2 + |\omega_n|} \frac{d^2 q}{(2\pi)^2} = \frac{\tilde{g}^2 N_0}{4\pi D} \int_{\Lambda_{\min}}^{\Lambda_{\max}} \left(1 - \frac{|\omega_n|}{D q^2 + |\omega_n|}\right) d(D q^2)$$

Here, $\tilde{g}$ denotes the coupling constant between bare charge density fluctuations and diffusive modes. For simplicity, we define the dimensionless constant Υ as the effective coupling constant for the self-energy $\Upsilon := \tilde{g}^2 N_0/(4\pi D)$. This expression directly provides the corrections to the terms m_c^b and γ^b which appear in expression (6.1):

$$\delta m_c = -\Upsilon(\Lambda_{\max} - \Lambda_{\min}) \qquad \delta\gamma(\omega_n) = \Upsilon \log\left(\frac{\Lambda_{\max} + |\omega_n|}{\Lambda_{\min} + |\omega_n|}\right)$$

As $\Lambda_{\max} > \Lambda_{\min}$, we clearly have $\delta m_c < 0$ and $\delta\gamma(\omega_n) > 0$. These identifications allow us to express $\Sigma(\omega_n)$ as $-\delta m_c - |\omega_n|\delta\gamma(\omega_n)$, therefore by comparison between (2.2) and (6.1) we get:

$$m_c = m_c^b + \delta m_c \qquad \gamma = \gamma^b + \delta\gamma(\omega_n)$$

In order for our description to be self-consistent, the condition $m_c^b/\gamma^b < \Sigma_0$ should be replaced with $m_c/\gamma < \Sigma_0$, however based on what we have shown so far the inequality $m_c/\gamma < m_c^b/\gamma^b$ holds, this clearly extends the range of validity of the diffusive regime. The mass renormalization δm_c is simply a constant shift and does not induce any non-trivial effects, such as a temperature dependence. Therefore m_c can be treated as a fixed parameter of the theory, as we did. What is remarkable is the fact that the Ladau damping renormalization actually depends on ω_n, and this can lead to some abnormal effects. In order to quantitatively evaluate these effects it is necessary, first of all, to establish the two cutoffs $\Lambda_{\max}$ and $\Lambda_{\min}$ of the theory. As usual, the upper energy cutoff for diffusive phenomena is of the order of the scattering rate, therefore we can fix $\Lambda_{\max} = \Sigma_0$. As for the lower cutoff, in the absence of other mechanisms the most reasonable thing is to simply set $\Lambda_{\min} = 0$.

$$\delta\gamma(\omega_n) = \Upsilon \log\left(1 + \frac{\Sigma_0}{|\omega_n|}\right)$$

This expression is ill-defined at $\omega_n = 0$, but this is not a problem as the product $|\omega_n|\delta\gamma(\omega_n)$ equals to zero for $\omega_n = 0$.

$$\mathcal{D}(\omega_n, \mathbf{k}) = \frac{1}{m_{\mathbf{k}} + \left[\gamma^b + \Upsilon \log\left(1 + \frac{\Sigma_0}{|\omega_n|}\right)\right]|\omega_n| + \frac{\omega_n^2}{\Omega}}$$

6.2 Calculations for the specific heat and the resistivity

The expression for the propagator we just found is the starting point for calculating the physical quantities of interest to us. First, it may be convenient to express it in the form of a retarded propagator in real frequency domain. In this regard, we apply the usual substitution $i\Omega_\ell \to \omega + i0^+$ and consider the negative x-semiaxis as the branch cut for the logarithm:

$$D_R(\omega, \mathbf{k}) = \frac{1}{m_{\mathbf{k}} - i\left[\gamma^b + \frac{1}{2}\,\Upsilon \log\left(1 + \frac{\Sigma_0^2}{\omega^2}\right)\right]\omega + \Upsilon\omega \arctan\left(\frac{\Sigma_0}{\omega}\right) - \frac{\omega^2}{\Omega}} \tag{6.2}$$

Where, of course, the term $m_{\mathbf{k}}$ already contains within it the renormalized mass m_c. The full calculation for the bosonic contribution to the specific heat gives the very same result exhibited in (4.2), provided the following substitutions in N_ω^{CDF} are made:

$$m_c \longrightarrow m_c + \frac{1}{2}\Upsilon\omega \arctan\Big(\frac{\Sigma_0}{\omega}\Big) \qquad \gamma \longrightarrow \gamma^b + \frac{1}{2}\Upsilon \log\Big(1+\frac{\Sigma_0^2}{\omega^2}\Big)$$
$$\frac{\omega}{\Omega} \longrightarrow \frac{\omega}{\Omega} - \frac{1}{2}\Upsilon \arctan\Big(\frac{\Sigma_0}{\omega}\Big)$$

Notice that the same substitutions connect the two expressions (2.2) and (6.2) for $D_R(\omega, \mathbf{k})$. The quantity N_0^{CDF} is not well defined due to the logarithmic divergence at $\omega = 0$, however it is possible to exhibit an asymptotic expression valid in the low frequency limit, which is very similar to the one given in (4.3):

$$N_\omega^{CDF} \simeq \frac{1}{\pi^2\nu}\Big[\gamma^b + \Upsilon \log\Big(\frac{\Sigma_0}{\omega}\Big)\Big] \log\Big(1+\frac{\pi\nu}{m_c}\Big) \qquad \text{for} \quad \omega \to 0^+$$

Which provides the following asymptotic behavior for the specific heat:

$$c_V^b \simeq \frac{k_B^2}{3\nu} T\Big[\gamma^b - c_0\Upsilon + \Upsilon \log\Big(\frac{\Sigma_0}{k_B T}\Big)\Big] \log\Big(1+\frac{\pi\nu}{m_c}\Big) \qquad \text{for} \quad T \to 0$$

Which clearly shows a logarithmic divergence at low temperature. The constant we denoted with c_0 is just the result of the following integral:

$$c_0 \coloneqq \frac{3}{\pi^2}\int_0^\infty \frac{x^2 e^x}{(e^x-1)^2}\,\log(x)\,dx = \frac{3}{2} + \log(2\pi) - 12\log(A_{GK}) \simeq 0.3528$$

Where $A_{GK} \simeq 1.282$ is the Glaisher-Kinkelin constant [143]. The full numerical calculation confirms this asymptotic trend and allows the fit of the experimental data available for $La_{1.6-x}Nd_{0.4}Sr_xCuO_4$ at a doping level of 24%, taken again from reference [55]. The procedure we follow is the same we exhibited in chapter 2.5: at first we estimate the fermionic contribution by means of Sommerfeld expression (2.18), then we subtract this contribution from the experimental data and finally fit the remaining part with the bosonic parameters. The fermionic parameters we choose for the description of the system under consideration are the following:

$$t = 350\,\text{meV} \qquad t' = -84\,\text{meV} \qquad t'' = 5.6\,\text{meV} \qquad p = 0.24$$

While for the bosonic parameters (including the ones which are involved in the Landau damping) we choose the following set:

$$m_c = 15\,\text{meV} \qquad \nu = 1.3\,\text{eV}/(\text{r.l.u.})^2 \qquad q_c = 1.95 \qquad \Omega = 30\,\text{meV}$$
$$\gamma^b = 5.5 \qquad \Upsilon = 6.5 \qquad \Sigma_0 = 16\,\text{meV}$$

The result of the fit is exhibited in figure 6.1. Similarly to what we did in chapter 2.5, in order to fit the resistivity data down to sufficiently low temperatures we were forced to uniformly overestimate the specific heat, in this case the amplification

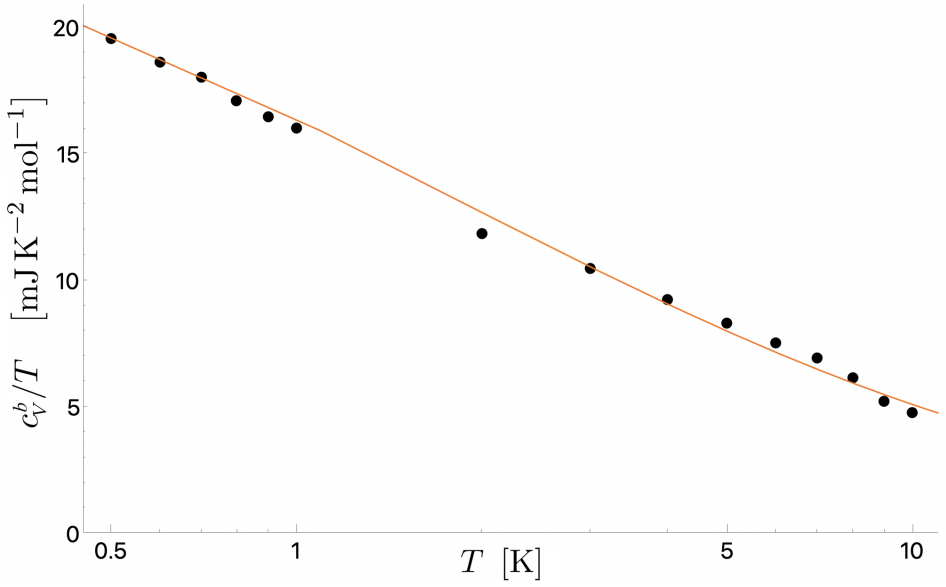

Figure 6.1. Plots of the bosonic contribution to the specific heat for $La_{1.6-x}Nd_{0.4}Sr_xCuO_4$, at $p = 0.24$. The black dots represent the result of subtracting the fermionic contribution from the experimental values reported in reference [55]. The orange curve is the result of our theoretical calculation with the parameters we have exhibited, it is uniformly rescaled by a factor of 1/43 in order to have a quantitative agreement with the experimental data.

factor is equal to 43.

From the comparison between the results of the present study and those exhibited in section 4 it clearly emerges that the two approaches used are essentially equivalent, at least as regards thermodynamics at low temperatures. The interaction between charge density fluctuations and diffusive modes self-consistently predicts a (logarithmically divergent) increase in damping at $p = p^*$, as a function of frequency. This behavior can be translated into an effective dependence of the damping parameter γ on the temperature, such as that described by equation (3.8).

As concerns resistivity, from the models we studied in chapters 3 and 4 we concluded that the main ingredient for having the extension of the linear regime at low temperatures is a *large* value of γ. This property is clearly provided by our model. For the explicit calculation of the resistivity we use linear response theory as usual, therefore we express ρ as $1/(e^2\Gamma_{11})$, where Γ_{11} is given by equation (5.3). For the calculation of the self-energy which appears inside the expression of Γ_{11} we use once again expression (2.4), the difference with the previous calculations is that in this case the propagator to be inserted in the self-energy expression is the one given by equation (6.2). The set of parameters we used for the calculation of the bosonic specific heat also allows for the fit of the resistivity data, we show the result in figure 6.2. This result is qualitatively and quantitatively similar to that found assuming that γ effectively depends on temperature through the expression $\gamma(T) = \max(\gamma_0 \log(T_0/T), 1)$.

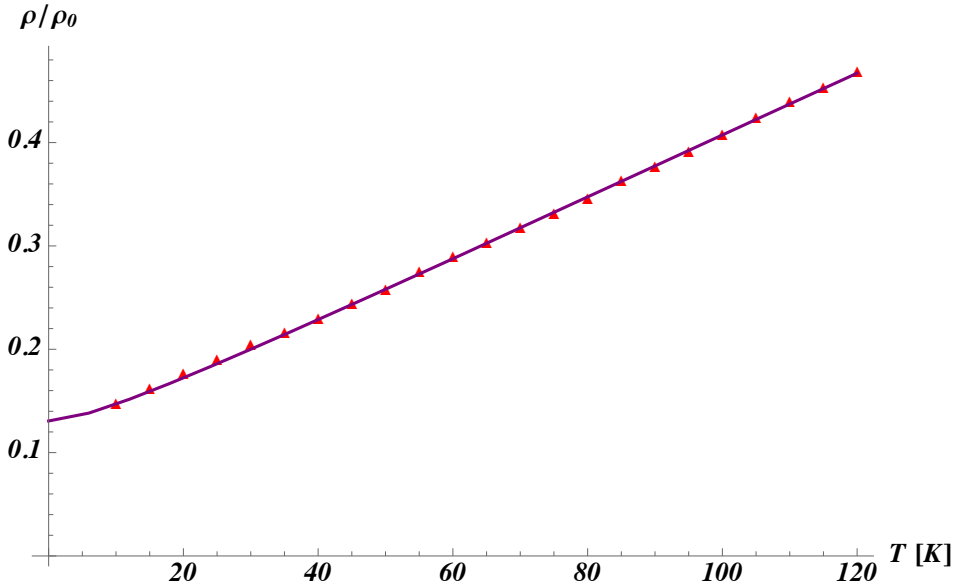

Figure 6.2. From [142], plots of the the resistivity for $La_{1.6-x}Nd_{0.4}Sr_xCuO_4$, at $p = 0.24$. The red triangles represent the experimental data reported in reference [55], while the purple curve is the result of our theoretical calculation with the parameters we have exhibited. Resistivity is expressed in units of $\rho_0 := \hbar a/e^2$, where a is the lattice spacing. In the reference mentioned, the value of a was set as 4.3 Å.

6.3 Role of the dimension and of the doping level

The ingredients underlying the mechanism we discussed in this chapter, namely the scattering by quenched impurities and the presence of two-dimensional short-ranged collective modes, are very general and can be extended to a broader class of physical systems in which the strange-metal behavior has been observed. Within our description, the logarithmic divergence of the specific heat emerges as a consequence of the logarithmic dependence of $\delta\gamma(\omega_n)$ on ω_n. The fact that this dependence is logarithmic (and divergent) crucially depends on the assumption that we are dealing with a two-dimensional system. The extension of this mechanism to a three-dimensional system would introduce a temperature scale T_{3D} below which the divergence of γ stops. Therefore, for the logarithmic divergence of c_V^b/T to be extended to temperatures below T_{3D}, the presence of some mechanism that can suppress this temperature scale is necessary.

In the calculations we made to reproduce the experimental data we assumed that we were already at the doping level at which the damping actually becomes singular, it is therefore necessary to equip our microscopic model with the range in p where the diffusive decay channel becomes effective. From the perspective in which the short-ranged collective modes are the precursors of a quantum criticality, the correlation length ξ will tend to diverge when p approaches p_c (from above) at $T = 0$. In this regime, the argument that charge density modes are short-ranged and nearly independent fails and physics is governed by Hertz-Millis theory [34, 35], we are therefore led to assume that the coupling between charge density fluctuations and

diffusive modes becomes negligible. On the other hand, if p is too large the condition $m_c^b/\gamma^b < \Sigma_0$ ceases to be valid, therefore the collective modes can decay only in ballistic particle-hole pairs, even in this case the two modes tend to decouple. Since the trend of the effective coupling between charge density fluctuations and diffusive modes is non-monotonic as a function of the doping level (higher than the critical doping level), we deduce that it has a maximum at a particular doping level value, which we identify with p^* which must be the only doping value at which the possible criticality is observed. Phenomenologically, this can be well described by assuming that the effective γ is given by a parallel sum between a logarithmically divergent T-function at zero temperature and a divergent p-function (not necessarily as a logarithm) at $p = p^*$. This is precisely the phenomenological expression (3.8) we chose for $\gamma = \gamma(T, p)$.

Despite its limitations, the model we have just exhibited provides an answer to the question regarding the origin of the temperature and doping dependence of the damping parameter, thus closing our current study on the stange-metal phase of cuprates. Before concluding this thesis, we want to exhibit the results of a parallel study that we carried out during our research, namely the one relating to the nematic properties observed in cuprate thin films.

Chapter 7

Interplay between nematicity and charge fluctuations

In the discussion we have presented so far, we have treated cuprates as two-dimensional systems with tetragonal symmetry. As we have discussed, this description is justified by experimental evidence that the in-plane transport properties in bulk systems are essentially isotropic (here, by *isotropy* we mean the discrete four-fold rotational symmetry, as it's common in the context of two-dimensional reticular systems), but they differ significantly from those observed along the orthogonal direction. These macroscopic properties clearly reflect the microscopic reticular structure of cuprates, which is tetragonal or at most slightly orthorhombic (as for the case of $YBa_2Cu_3O_{7-\delta}$). However, it should be stressed that this kind of structure is typical of three-dimensional bulk systems, and in general it is not preserved when thin films of the same compounds are considered. Examples of in-plane anisotropic transport properties have been observed in a number of cuprate thin films, providing evidence for a nematic state.

In this chapter we report the results of the analysis we conducted on recent experimental data for ultrathin $YBa_2Cu_3O_{7-\delta}$ films [20]. In these films, anisotropy is induced via strain engineering, leading to a suppression of charge density wave scattering along one axis and a concomitant enhancement of strange-metal behavior along the other axis.

7.1 Experimental evidence of nematicity in cuprate films

The anisotropy observed in $YBa_2Cu_3O_{7-\delta}$ thin films is evident from the different RIXS spectra and the different values of the in-plane resistivity measured along the two axial directions [20]. The cuprate samples that were analyzed have a thickness between 10 nm and 50 nm and each of the them was grown on two different substrates, namely MgO and $SrTiO_3$, which are characterized by a different morphology and different lattice parameters. Thinner films are clearly more likely to develop anisotropic properties, this is clearly visible for example from x-ray diffraction experiments, which show that the orthorhombic distortion intensifies as the thickness of the sample decreases, as shown in figure 7.1. Since in the presence of orthorhombic

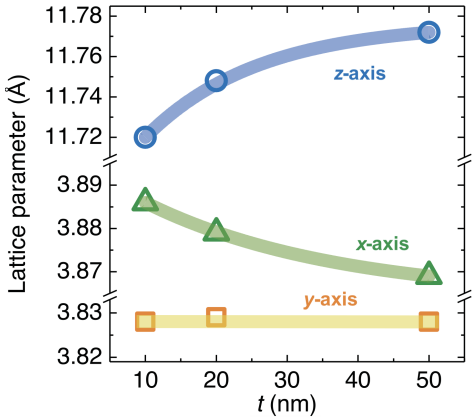

Figure 7.1. From [20], lattice parameters of $YBa_2Cu_3O_{7-\delta}$ films at $T = 300\,\mathrm{K}$ and $p \simeq 0.12$ grown on MgO as function of the thickness of films (here t represents the tickness, not to be confused with the hopping parameter), measured in x-ray diffraction experiments. The shapes represent the experimental data, while thick lines are guides to the eye. Remarkably, the total volume of the three-dimensional unit cell remains essentially unchanged as the thickness varies.

distortion the two planar directions are no longer equivalent, we indicate with x the direction in which the lattice spacing is larger while with y we indicate the other one. It is convenient to leave the two lattice parameters a_x and a_y explicit, which satisfy the inequality $a_x > a_y$ by construction.

The remarkable observation is that nematicity seems to be more intense in the samples grown on MgO compared to those grown on $SrTiO_3$. This clearly emerges from resistivity data, which show that the slope of the resistivity in the regime in which it is linear in temperature, as well as the range of validity of the linear regime itself, changes significantly between the two samples of different thickness if the substrate is MgO, while it is essentially unchanged if the substrate is $SrTiO_3$ (see figures 7.2 and 7.3). According to Kubo theory, the resistivity along an axial direction is inversely proportional to the average squared Fermi velocity component along that direction, consequently if the resistivity slopes are different then the Fermi

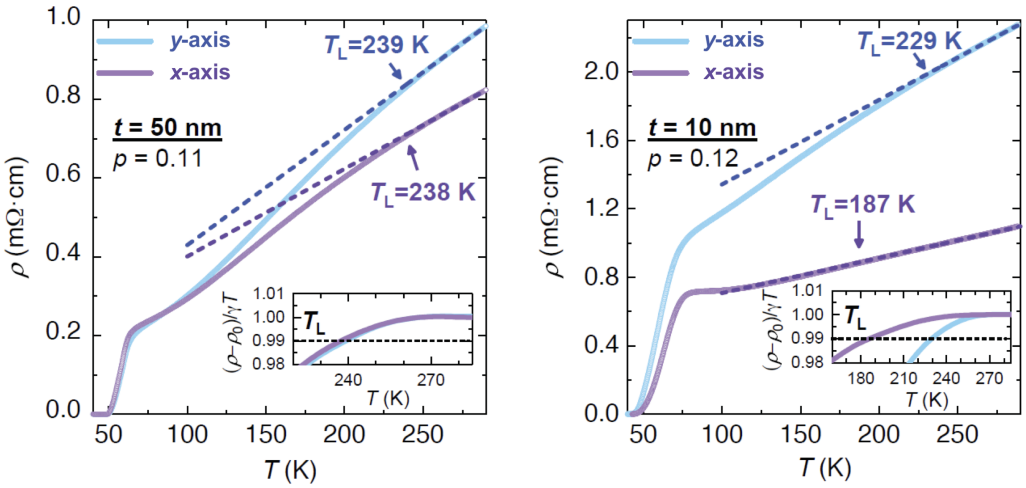

Figure 7.2. From [20], plots of the resistivity as a function of temperature for $YBa_2Cu_3O_{7-\delta}$ films grown on a MgO substrate. The dashed lines are the high-temperature linear fits of the curves. The inset shows the determination of T_L, defined as the temperature where the resistivity normalized to 290 K deviates by 1% from the linear fit.

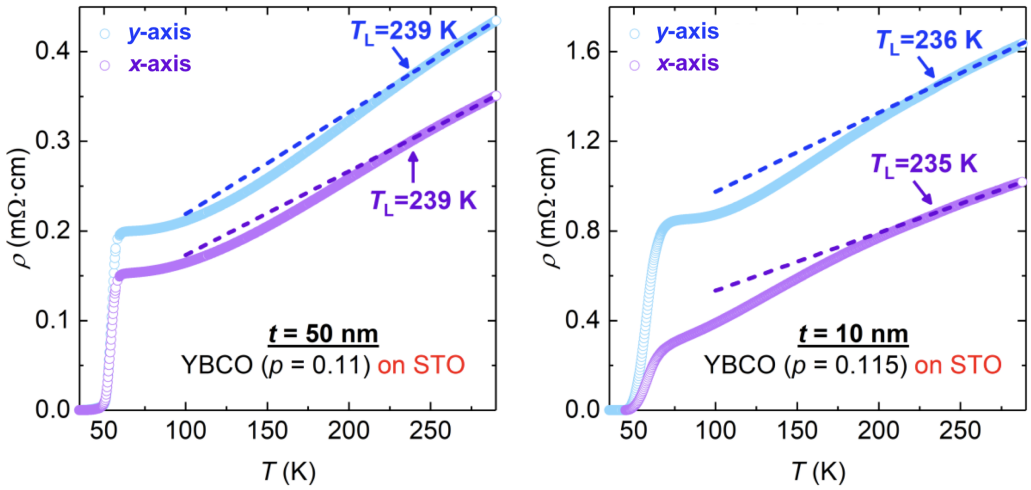

Figure 7.3. From supplementary information of reference [20], same plots as those of figure 7.2 but the substrate is $SrTiO_3$.

surface must be nematic, like that shown in figure 7.4. This latter property is well captured by our theoretical scheme, in fact the generalization of the conductivity tensor for a non-tetragonal system, all other hypotheses adopted in section 5.1 being the same, is given by the following equation:

$$\sigma^{\alpha\beta} = \mathrm{e}^2\Gamma_{11}^{\alpha\beta} = \frac{\widetilde{N}_0^{\alpha\beta}}{v_{\mathrm{uc}}}\int_{-\infty}^{+\infty}\frac{1}{2\left(\Sigma_0 - \mathrm{Im}\Sigma_R(\omega)\right)}\left(-\frac{\partial f(\omega)}{\partial\omega}\right)d\omega$$

Where each the indices α and β can be equal to x or y, but in our case the only components of the tensor different from zero are the diagonal ones, i.e. when $\alpha = \beta = x$ or $\alpha = \beta = y$. The tensor $\widetilde{N}_\xi^{\alpha\beta}$ is defined by:

$$\widetilde{N}_\xi^{\alpha\beta} := \frac{1}{N}\sum_{\mathbf{k},\sigma} v_{\mathbf{k},\alpha}v_{\mathbf{k},\beta}\delta(\xi - \xi_{\mathbf{k}} - \mathrm{Re}\Sigma_R(0)) = \frac{2}{N}\sum_{\mathbf{k}}\frac{\partial^2\xi_{\mathbf{k}}}{\partial k_\alpha \partial k_\beta}\theta(\xi - \xi_{\mathbf{k}} - \mathrm{Re}\Sigma_R(0))$$

For this tensor to not simply be a multiple of the identity the dispersion $\xi_{\mathbf{k}}$ must not have tetragonal symmetry. Of course, in the case of a tetragonal symmetry we simply recover the definition given in equation (5.2). We point out that, for such a system, it might not be a good approximation to consider electronic self-energy as momentum-independent, so it would be more appropriate to carry out the **k**-sum explicitly. However, the observation that $\sigma^{\alpha\beta}$ depends linearly on $v_{\mathbf{k},\alpha}v_{\mathbf{k},\beta}$ remains valid, as does the link between the resistivity slope and the shape of the Fermi surface.

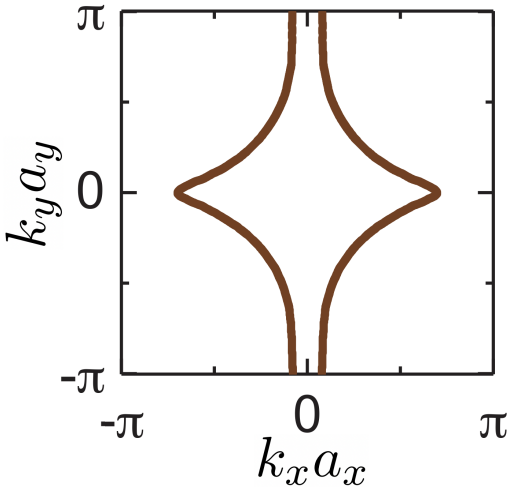

Figure 7.4. From [20], hypothetical Fermi surface which is compatible with the anisotropic transport of the 10 nm thick samples.

While the resistivity data suggest the presence of an electronic nematicity (whose intensity seems to depend crucially on the substrate), analysis of RIXS spectra shows that collective charge modes also have nematic behavior [20]. In fact, RIXS experiments carried out on $YBa_2Cu_3O_{7-\delta}$ samples at $p = 0.125$ with a thickness of 50 nm and 10 nm grown on the MgO substrate show a suppression of the charge density waves order along the solely y-direction for the thinner sample, while in the thicker one essentially the same signal is observed along the two axial directions (see figure 7.5). The same measurements conducted on $YBa_2Cu_3O_{7-\delta}$ grown on the $SrTiO_3$ substrate show that, in this case, the charge density waves signal is isotropic and essentially thickness-independent.

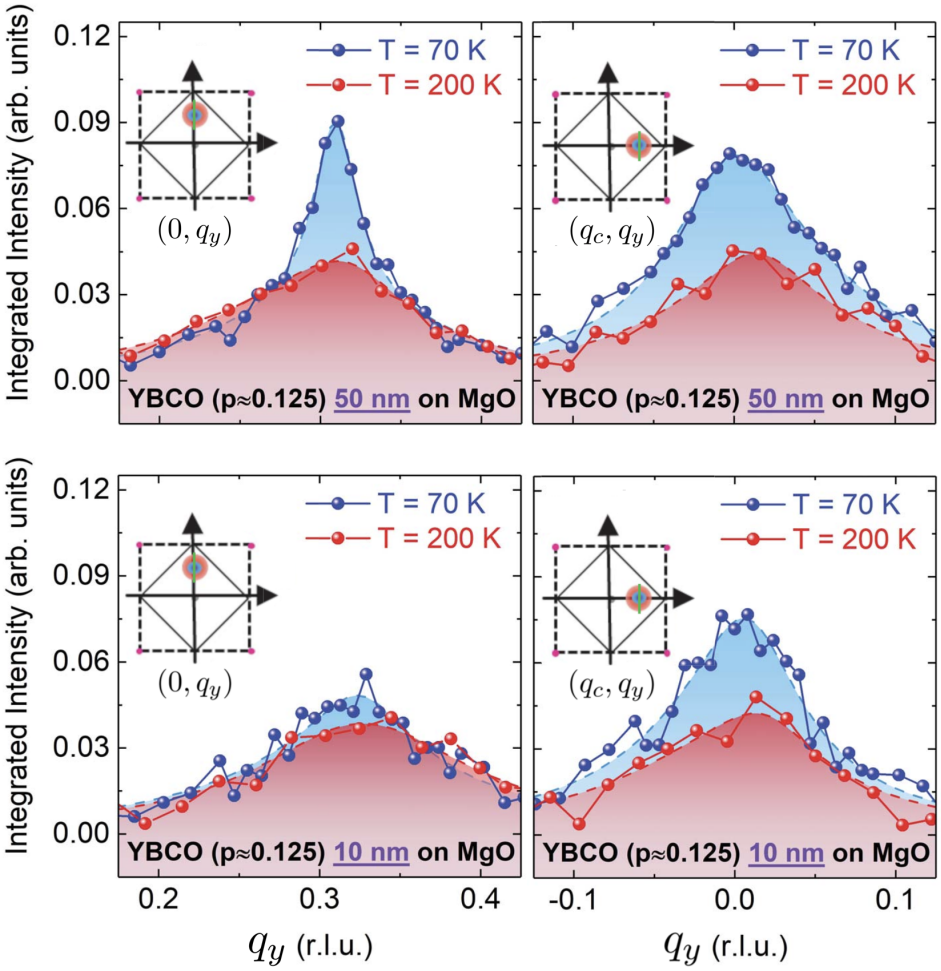

Figure 7.5. From [20], quasi-elastic scans measured at $T = 70\,\mathrm{K}$ and $T = 200\,\mathrm{K}$ on $YBa_2Cu_3O_{7-\delta}$ thin films on MgO substrate along the y-direction. Upper panels: scans centered on the charge density wave peak on the y-axis (left panel) and that on the x-axis (right panel) for the 50 nm thick sample. Lower panels: same as the upper panels, but for the 10 nm thick sample. Note that, in the 10 nm thick sample, the charge density wave intensity along the y-axis is almost negligible.

The fact that the observed anisotropy appears to be more marked in the system in contact with MgO compared to the system in contact with $SrTiO_3$ clearly suggests that the interaction between the $YBa_2Cu_3O_{7-\delta}$ film and the substrate may have a fundamental role in determining the physical properties observed. In order to better understand the effect of the interaction between sample and substrate in the two cases, a study of the surfaces of the two substrates was carried out using the tapping mode atomic force microscopy and peak force quantitative nanomechanics atomic force microscopy techniques [144]. These experiments show that the surface of MgO substrates is characterized by elongated nanofacets, which have an average heigth of 1.5 nm and a nearly triangular shape. The $YBa_2Cu_3O_{7-\delta}$ layer placed in contact

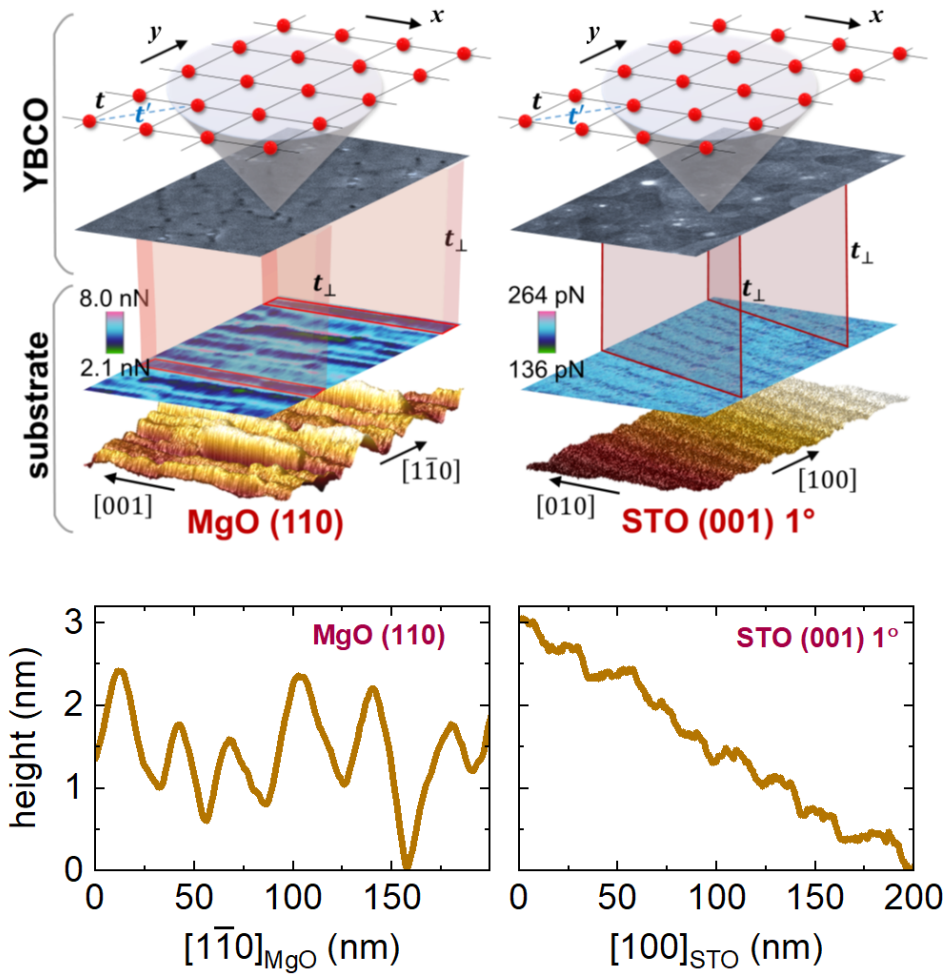

Figure 7.6. From [144], analysis of the substrate surface and modelization of the interface with the $YBa_2Cu_3O_{7-\delta}$ film. In the upper panels, the yellow-brown maps represent the tapping mode atomic force microscopy images of a $250 \times 250\,nm^2$ region of the substrate, while the bluish maps represent the peak force quantitative nanomechanics atomic force microscopy adhesion images of the very same areas. The planar tight-binding structure of the $YBa_2Cu_3O_{7-\delta}$ planes is the topmost enlargement at the interatomic scale. The lower panels represent the tapping mode atomic force microscopy linescans along the reported directions.

with this structure (see figure 7.6) is therefore subjected to a very anisotropic strain. On the contrary, atomic force microscopy study of the $SrTiO_3$ substrate show a surface characterized by markedly shallower steps, it is therefore natural to expect that this substrate will induce a much more isotropic strain than that of the previous case. In both cases, the lattice direction that we have denoted by x, i.e. the one in which the elongation of the lattice step occurs, is the one aligned with the facets (for MgO) or with the shallow steps (for $SrTiO_3$).

7.2 Microscopic model for the strain-induced nematicity

We are going to show a model that can take into account the interaction between cuprate film and substrate and that can consequently provide the right nematicity properties observed in the two systems. By adopting the second quantization formalism, we denote by $\hat{a}^{\dagger}_{i,\sigma}$ and $\hat{a}_{i,\sigma}$ respectively the creation and destruction operators for the $YBa_2Cu_3O_{7-\delta}$ electrons (in real space), while we use $\hat{c}^{\dagger}_{i,\sigma}$ and $\hat{c}_{i,\sigma}$ to denote the same operators for undercoordinated facet (or step) states on the substrate. The Hamiltonian for the system takes on the following form:

$$H = \sum_{ij,\sigma} t_{ij}\, \hat{a}^{\dagger}_{i,\sigma}\hat{a}_{j,\sigma} \; + \sum_{n,\sigma}\sum_{m=1}^{L} \hat{h}^{\mathrm{coup}}_{n,m,\sigma}$$

The first piece of this Hamiltonian is the standard tight-binding part, where for simplicity only the first two hopping terms t and t' will be considered (at this level, the tight-binding structure for this system has tetragonal symmetry). The second piece of this Hamiltonian includes all the information about the coupling with the substrate. The local coupling Hamiltonian $\hat{h}^{\mathrm{coup}}_{n,m,\sigma}$ can be expressed as follows:

$$\hat{h}^{\mathrm{coup}}_{n,m,\sigma} = \begin{pmatrix} \hat{a}^{\dagger}_{\mathbf{R}_n+m\mathbf{a}_x,\sigma} \\ \hat{c}^{\dagger}_{\mathbf{R}_n+m\mathbf{a}_x,\sigma} \end{pmatrix}^{\mathrm{T}} \begin{pmatrix} 0 & t_{\perp} \\ t_{\perp} & -V_{\mathrm{sub}} \end{pmatrix} \begin{pmatrix} \hat{a}_{\mathbf{R}_n+m\mathbf{a}_x,\sigma} \\ \hat{c}_{\mathbf{R}_n+m\mathbf{a}_x,\sigma} \end{pmatrix}$$

Here, the vectors $\mathbf{R}_n$ denote the starting sites of the one-dimensional structures on the substrate, which have length L (in units of lattice spacings along the x-direction) and local potentials $-V_{\mathrm{sub}}$. The vector $\mathbf{a}_x$ is simply the primitive vector along x-direction. A pictorial scheme of our model is shown in figure 7.7. Since we are only interested in the properties of the cuprate film, we can simplify the model by diagonalizing the Hamiltonian coupling and eliminating the substrate degrees of freedom. The result is the following effective Hamiltonian:

$$H = \sum_{ij,\sigma} t_{ij}\, \hat{a}^{\dagger}_{i,\sigma}\hat{a}_{j,\sigma} \; + \; V_{\mathrm{eff}} \sum_{n,\sigma}\sum_{m=1}^{L} \hat{a}^{\dagger}_{\mathbf{R}_n+m\mathbf{a}_x,\sigma}\hat{a}_{\mathbf{R}_n+m\mathbf{a}_x,\sigma}$$

Where the effective potential V_{eff} is given by:

$$V_{\mathrm{eff}} = \frac{1}{2}\left[\sqrt{V_{\mathrm{sub}}^2 + 4t_{\perp}^2} - V_{\mathrm{sub}}\right]$$

Due to the anisotropic shape of the facets (or steps) we are allowed to consider the limit $L \to \infty$, so that our model corresponds to charge carriers in the CuO_2

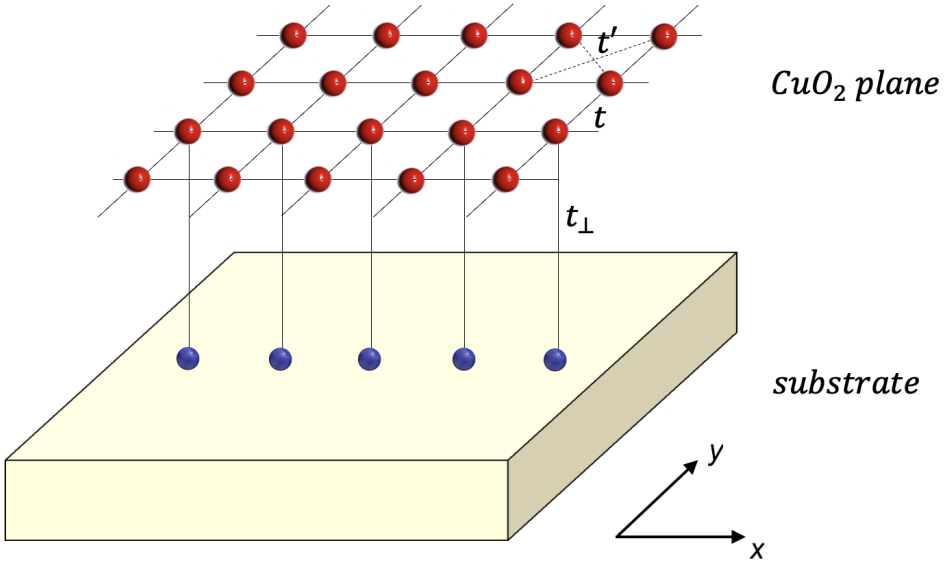

Figure 7.7. Schematic view of the planar tight-binding model with the CuO_2 layer (red dots) effectively coupled by the perpendicular hopping $t_\perp$ to the substrate facets or steps (blue dots).

layer which are subject to infinitely extended one-dimensional potentials along the x-direction and randomly distributed with an area fraction of nanofacets (steps) given by a parameter which we denote with δ. The resulting electronic structure can be most conveniently obtained from the coherent-potential approximation [145, 146] with a self-energy:

$$\Sigma_{CPA}(\omega, k_x) = \frac{\delta\, V_{\text{eff}}}{1 - \left(V_{\text{eff}} - \Sigma_{CPA}(\omega, k_x)\right) G_{CPA}(\omega - \Sigma_{CPA}(\omega, k_x), k_x)}$$

Where:

$$G_{CPA}(\omega, k_x) = \frac{1}{N}\sum_{k_y} \frac{1}{\omega + 2t\cos(k_x a_x) + 2t\cos(k_y a_y) + 4t'\cos(k_x a_x)\cos(k_y a_y) + \mu} =$$

$$= \frac{\operatorname{sgn}\left(\omega + 2t\cos(k_x a_x) + \mu\right)}{\sqrt{\left|\left(\omega + 2t\cos(k_x a_x) + \mu\right)^2 - \left(2t + 4t'\cos(k_x a_x)\right)^2\right|}}$$

From the previous two equations it is possible to make self-energy explicit. The expression for the resulting dispersion is the usual one, namely $\tilde{\omega}_{\mathbf{k}} = \xi_{\mathbf{k}} + \mathrm{Re}\Sigma_{CPA}(\omega, k_x)$. This dispersion is such as to provide a nematic Fermi surface like the one shown in figure 7.4, and therefore an average velocity greater along x than along y near the Fermi surface. This shows that our model is able to take into account, at least qualitatively, the anisotropy observed in transport. In our model, the morphological difference between the two different substrates analyzed is taken into account by the different value of the parameter V_{eff}. In agreement with the plots shown in figure 7.6, we deem that the value of V_{eff} describing MgO substrate must be significantly higher

than that for $SrTiO_3$ substrate, also taking into account the shape of the Fermi surfaces that we expect from the resistivity data in the two cases we deduce that $V_{\text{eff}} \simeq t$ for MgO and $V_{\text{eff}} \ll t$ for $SrTiO_3$.

This nematic Fermi surface can also be modeled within an effective one-band model, where the nearest-neighbor hopping parameter takes a different value depending on the axial direction:

$$\xi_{\mathbf{k}} = -2t(1+\alpha)\cos(k_x a_x) - 2t(1-\alpha)\cos(k_y a_y) - 4t'\cos(k_x a_x)\cos(k_y a_y) - \mu$$

Where α denotes the anisotropy parameter. In figure 7.8 we show a comparison between the nematic Fermi surface obtained from the coherent-potential approximation and the one fitted with this effective one-band anisotropic model.

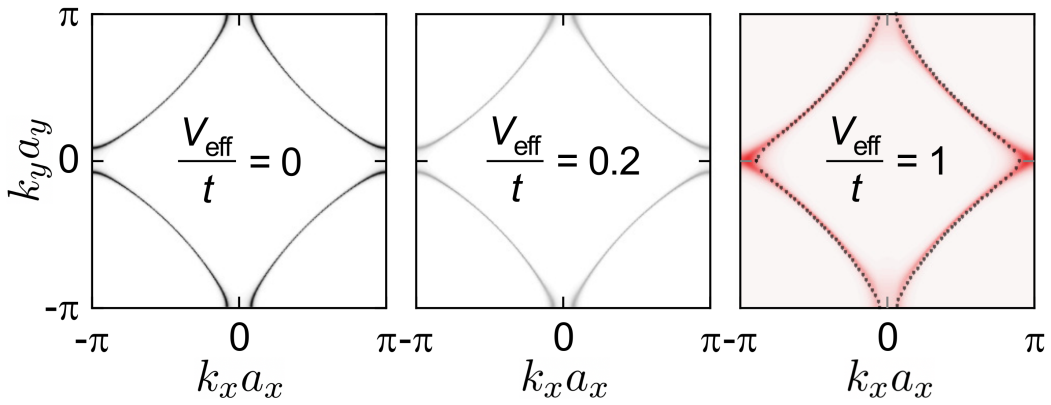

Figure 7.8. From [144], Fermi surface within the coherent-potential approximation for different values of the effective potential V_{eff}. In all cases, the concentration of one-dimensional strips is $\delta = 0.15$, the next-nearest neighbor hopping is $t' = 0.15\,t$ and the doping level is $p = 0.12$. The black dotted line in the third panel corresponds to an anisotropic tight-binding parametrization with anisotropy parameter $\alpha = 0.015$, notice that it is qualitatively compatible with the one in figure 7.4.

7.3 Frustrated phase separation scenario for charge instability

Having established that our microscopic model for the description of the interaction between substrate and $YBa_2Cu_3O_{7-\delta}$ film is able to predict an effective nematic dispersion for the latter, we are now going to show how this nematicity affects the resulting charge collective modes. For the description of charge instability we will use the already mentioned frustrated phase separation framework. Our starting point is the minimal model given by the following Hamiltonian:

$$H = \sum_{\mathbf{k},\sigma} \xi^{ren}_{\mathbf{k}} \hat{a}^{\dagger}_{\mathbf{k},\sigma} \hat{a}_{\mathbf{k},\sigma} - \frac{g_{\text{ph}}}{\sqrt{N}} \sum_{\mathbf{q}} (\hat{b}_{\mathbf{q}} + \hat{b}^{\dagger}_{-\mathbf{q}}) \hat{\rho}_{\mathbf{q}} + \omega_0 \sum_{\mathbf{q}} \hat{b}^{\dagger}_{\mathbf{q}} \hat{b}_{\mathbf{q}} + \frac{1}{2N} \sum_{\mathbf{q}} V_{\text{rep}}(\mathbf{q}) \hat{\rho}_{\mathbf{q}} \hat{\rho}_{-\mathbf{q}}$$

Where $\hat{b}^{\dagger}_{\mathbf{q}}$ and $\hat{b}_{\mathbf{q}}$ are the standard creation and annihilation operators for a dispersionless phonon mode with frequency ω_0, whose coupling with electrons is quantitatively

described by the coupling constant g_{ph}. The operator $\hat{\rho}_{\mathbf{q}}$ is the standard second-quantization density operator for fermions:

$$\hat{\rho}_{\mathbf{q}} \coloneqq \sum_{\mathbf{k},\sigma} \hat{a}^{\dagger}_{\mathbf{k},\sigma} \hat{a}_{\mathbf{k}+\mathbf{q},\sigma}$$

This Hamiltonian represents the standard Hubbard-Holstein model in the $U \to \infty$ limit, where the strong Hubbard repulsion was treated by means of slave-boson approach [7, 63, 92]. This technique, used in the $U \to \infty$ limit, allows the local repulsion term to be converted into two distinct effects: on the one hand the original dispersion $\xi_{\mathbf{k}}$ (which is the nematic one, which also includes the anisotropy parameter α) is replaced by the renormalized one $\xi^{ren}_{\mathbf{k}} \coloneqq p\xi_{\mathbf{k}}$, on the other an effective repulsive potential $V_{\mathrm{sr}}(\mathbf{q})$ is generated, which is added to the Coulomb one $V_{\mathrm{c}}(\mathbf{q})$. The total repulsive potential $V_{\mathrm{rep}}(\mathbf{q})$ is just the sum of the two. The interaction between electrons and the Holstein phonon results in an effective attractive potential between the electronic quasiparticles $V_{\mathrm{ph}}(\mathbf{q}) = -\lambda_{\mathrm{ph}}$, where $\lambda_{\mathrm{ph}} \coloneqq g^2_{\mathrm{ph}}/\omega_0$. The overall interaction potential $V_{\mathrm{tot}}(\mathbf{q})$ acting on the electrons in this model is given by three distinct contributions:

$$V_{\mathrm{tot}}(\mathbf{q}) = V_{\mathrm{sr}}(\mathbf{q}) + V_{\mathrm{c}}(\mathbf{q}) + V_{\mathrm{ph}}(\mathbf{q})$$

The first two terms constitute the repulsive part of the interaction. The expression for the short-range residual repulsion is the following:

$$V_{\mathrm{sr}}(\mathbf{q}) = \frac{1}{2p}\frac{1}{N}\sum_{\mathbf{k},\sigma}(\xi_{\mathbf{k}+\mathbf{q}} - \xi_{\mathbf{k}})f(\xi_{\mathbf{k}})$$

It is possible to show that $V_{\mathrm{sr}}(\mathbf{q})$ is positive-definite and that it vanishes only at $\mathbf{q} = \mathbf{0}$. The calculation of the Coulomb repulsion in momentum space can be carried out similarly to what is explained in reference [63], the result is the following:

$$V_{\mathrm{c}}(\mathbf{q}) = \frac{\mathrm{e}^2 d}{2\,\varepsilon_z}\frac{1}{\sqrt{A(\mathbf{q})^2 - 1}}$$

$$\text{where} \quad A(\mathbf{q}) \coloneqq 1 + \frac{\varepsilon_x}{\varepsilon_z}\frac{d^2}{a_x^2}\left[1 - \cos(q_x a_x) + \frac{\varepsilon_y}{\varepsilon_x}\frac{a_x^2}{a_y^2}\Big(1 - \cos(q_y a_y)\Big)\right]$$

Here, ε_x, ε_y and ε_z are the (dimensional) permittivities along the three lattice directions, while d is the interplane distance, in accordance with the notation already used in section 4.3. We note that this expression diverges at $\mathbf{q} = \mathbf{0}$ as $1/|\mathbf{q}|$ rather than as $1/|\mathbf{q}|^2$, as would be expected for the Coulomb potential. The reason is that $V_{\mathrm{c}}(\mathbf{q})$ is not the full three-dimensional Coulomb potential, but only its two-dimensional projection on the lattice plane (i.e. integrated over the z-component of $\mathbf{q}$).

The term $V_{\mathrm{ph}}(\mathbf{q})$ is the only attractive contribution to the total interaction potential. According to random phase approximation, an ideal Fermi gas that interacts only through a momentum-independent attractive potential $V_{\mathrm{tot}}(\mathbf{q}) = -\lambda_{\mathrm{ph}}$ would undergo charge instability when the condition $1/\chi^0_{\rho\rho}(\mathbf{q}) = \lambda_{\mathrm{ph}}$ is met (to shorten the notation, we use $\chi^0_{\rho\rho}(\mathbf{q})$ to denote the static susceptibility $\chi^0_{\rho\rho}(\mathbf{q}, \omega_n = 0)$). In

this case, the charge instability would occur at the nesting wave vector, i.e. the wave vector at which $\chi^0_{\rho\rho}(\mathbf{q})$ reaches its absolute minimum. Within our scheme, the density-density, density-energy and energy-energy susceptibilities (respectively denoted with $\chi_{\rho\rho}$, $\chi_{\rho\varepsilon}$ and $\chi_{\varepsilon\varepsilon}$) are mixed together due to the interaction between transitive and local charges, which is another consequence of the slave-boson calculation. In this case, the random phase approximation takes the following matrix form:

$$\boldsymbol{\chi}(\mathbf{q}) = \boldsymbol{\chi}^0(\mathbf{q}) \Big[\mathbf{1}_{2\times 2} + \mathbf{V}(\mathbf{q}) \boldsymbol{\chi}^0(\mathbf{q}) \Big]^{-1}$$

The three symmetric matrices introduced in this expressions have the following explicit forms:

$$\boldsymbol{\chi}^0(\mathbf{q}) \coloneqq \begin{pmatrix} \chi^0_{\rho\rho}(\mathbf{q}) & \chi^0_{\rho\varepsilon}(\mathbf{q}) \\ \chi^0_{\rho\varepsilon}(\mathbf{q}) & \chi^0_{\varepsilon\varepsilon}(\mathbf{q}) \end{pmatrix} = -\frac{1}{N} \sum_{\mathbf{k},\sigma} \begin{pmatrix} 1 & \frac{\xi_{\mathbf{k}+\mathbf{q}}+\xi_{\mathbf{k}}}{2} \\ \frac{\xi_{\mathbf{k}+\mathbf{q}}+\xi_{\mathbf{k}}}{2} & \frac{\left(\xi_{\mathbf{k}+\mathbf{q}}+\xi_{\mathbf{k}}\right)^2}{4} \end{pmatrix} \frac{f(\xi^{ren}_{\mathbf{k}+\mathbf{q}}) - f(\xi^{ren}_{\mathbf{k}})}{\xi^{ren}_{\mathbf{k}+\mathbf{q}} - \xi^{ren}_{\mathbf{k}}}$$

$$\boldsymbol{\chi}(\mathbf{q}) \coloneqq \begin{pmatrix} \chi_{\rho\rho}(\mathbf{q}) & \chi_{\rho\varepsilon}(\mathbf{q}) \\ \chi_{\rho\varepsilon}(\mathbf{q}) & \chi_{\varepsilon\varepsilon}(\mathbf{q}) \end{pmatrix} \qquad \mathbf{V}(\mathbf{q}) \coloneqq \begin{pmatrix} V_{\text{tot}}(\mathbf{q}) & -1 \\ -1 & 0 \end{pmatrix}$$

We would like to clarify that our susceptibilities already have the right sign as they take into account the negative sign given by the fermionic loop (notice, in particular, that $\chi^0_{\rho\rho}(\mathbf{q})$ is positive definite), while each of the interaction lines that appears in the random phase resummation is associated with the quantity $-\mathbf{V}(\mathbf{q})$, where the additional minus sign emerges as a consequence of the usual cancellation of disconnected diagrams in the calculation of response functions [155]. The explicit computation of the quantity $\chi_{\rho\rho}(\mathbf{q})$ leads to:

$$\chi_{\rho\rho}(\mathbf{q}) = \frac{\chi^0_{\rho\rho}(\mathbf{q})}{\det\Big[\mathbf{1}_{2\times 2} + \mathbf{V}(\mathbf{q}) \boldsymbol{\chi}^0(\mathbf{q}) \Big]}$$

Of course, if the determinant of the matrix $\mathbf{1}_{2\times 2} + \mathbf{V}(\mathbf{q})\boldsymbol{\chi}^0(\mathbf{q})$ is strictly positive at any $\mathbf{q}$, no charge instability occurs, which is what happens if the interaction is completely repulsive. For our model to provide an instability it is necessary (but not sufficient) that the attraction λ_{ph} takes a finite (positive) value. We define the critical value of λ_{ph} as the smallest value that λ_{ph} must have for the determinant of $\mathbf{1}_{2\times 2} + \mathbf{V}(\mathbf{q})\boldsymbol{\chi}^0(\mathbf{q})$ to vanish at a particular value of $\mathbf{q}$ (which is unique up to equivalent vectors under group symmetries of the system) and to be strictly positive at any other wave vector. Within our framework, this particular wave vector is precisely the theoretical critical wave vector $\mathbf{q}_c$ for charge density waves.

Formally, it is possible to insert the effect of the interaction between local and transitive charges within an effective (susceptibility-dependent) potential, in such a way as to recover the standard structure of the random phase approximation:

$$\chi_{\rho\rho}(\mathbf{q}) = \frac{\chi^0_{\rho\rho}(\mathbf{q})}{1 + \widetilde{V}_{\text{tot}}(\mathbf{q})\chi^0_{\rho\rho}(\mathbf{q})} \qquad \text{where} \quad \widetilde{V}_{\text{tot}}(\mathbf{q}) := \frac{\det\left[\mathbf{1}_{2\times 2} + \mathbf{V}(\mathbf{q})\boldsymbol{\chi}^0(\mathbf{q})\right] - 1}{\chi^0_{\rho\rho}(\mathbf{q})}$$

A schematic representation of the frustrated phase mechanism is sketched in figure 7.9. The repulsive potential $V_{\text{rep}}(\mathbf{q}) = V_{\text{sr}}(\mathbf{q}) + V_{\text{c}}(\mathbf{q})$ is strictly positive and has a minimum at a finite value of $\mathbf{q}$, due to the complementary behaviors of the two contributions. In fact, while $V_{\text{sr}}(\mathbf{q})$ vanishes at $\mathbf{q} = \mathbf{0}$ and it is increasing with $|\mathbf{q}|$, $V_{\text{c}}(\mathbf{q})$ diverges at zero momentum and rapidly decreases with $|\mathbf{q}|$, the compromise between these two trends produces the absolute minimum at finite momentum. Of course, in order to have an instability it is necessary that the total effective potential has a negative sign for some $\mathbf{q}$ and that it "touches" the $-1/\chi^0_{\rho\rho}(\mathbf{q})$ curve in correspondence with a particular wave vector. The effect of phononic attraction is exactly to lower the curve of the effective potential and favor this touch.

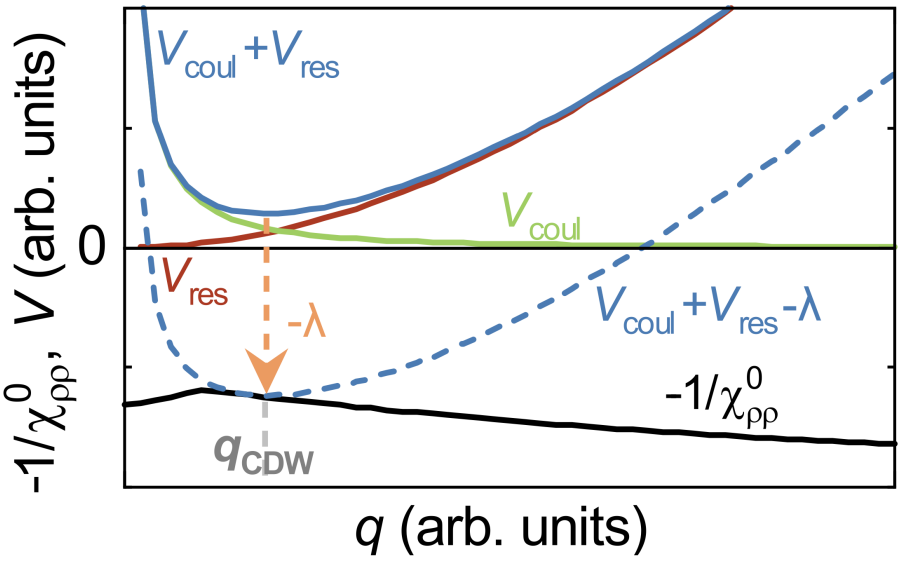

Figure 7.9. From [144], schematic representation of charge instability within frustrated phase separation scenario. Note that the instability condition is, in general, fulfilled away from the nesting condition which would occur at the minimum of $\chi^0_{\rho\rho}(\mathbf{q})$. For the sake of simplicity, we are not considering the effect of the interaciton with transitive charges in this picture, therefore $\widetilde{V}_{\text{tot}}(\mathbf{q}) = V_{\text{tot}}(\mathbf{q})$. However, this does not affect the qualitative observations we made about the roles of individual contributions to the total potential.

For the complete numerical calculation, we need to fix the relevant parameters of the theory. For the fermionic structure we have:

$$t' = -0.17\,t \qquad \alpha = 0.015 \tag{7.1}$$

Which are similar to the parameters that allowed us to fit the nematic Fermi surface at $p = 0.12$ obtained within coherent-potential approximation with $\delta = 0.15$ and $V_{\text{eff}} = t$. For the parameters which appear in the interaction we have:

$$\frac{e^2 d}{2\,\varepsilon_z} = 0.5\,t \qquad \frac{\varepsilon_x}{\varepsilon_z}\frac{d^2}{a_x^2} = 54 \qquad \frac{\varepsilon_y}{\varepsilon_x} = 1 \qquad \frac{a_y}{a_x} = 0.98$$

Since $V_{\rm sr}(\mathbf{q})$ and the bare susceptibility $\chi^0_{\rho\rho}(\mathbf{q})$ are doping-dependent we expect that, at least in principle, the critical wave vector itself may depend on momentum. We performed the full numerical calculation in a doping window between $p = 0.02$ and $p = 0.24$ with this set of parameters. From our numerical results, we were able to distinguish three distinct doping regimes:

- At low doping level, the anisotropy of $V_{\rm tot}(\mathbf{q})$ is dominated by the doping dependence of the residual repulsion $V_{\rm sr}(\mathbf{q})$, the latter being proportional to $1/p$. Within a standard slave-boson approach, $V_{\rm sr}(\mathbf{q})$ turns out to be proportional to the quasiparticle kinetic energy. Since the magnitude of the hopping along the x-axis is larger than the other one, the repulsion is stronger along the x-axis, so that this term forces the instability to occur along the y-axis.

- When increasing the doping, the contribution of $V_{\rm sr}(\mathbf{q})$ to $V_{\rm tot}(\mathbf{q})$ decreases so that the strongly enhanced $\chi^0_{\rho\rho}(\mathbf{q})$ along the x-axis, starting at $p \simeq 0.12$, leads to a rotation of the critical wave vector from the y-axis to the x-axis of the $YBa_2Cu_3O_{7-\delta}$ unit cell. For the considered parameters, the Fermi surface is closed at $(\pi, 0)$ while it is still open at $(0, \pi)$ (see violet curve in Fig. 5). As a consequence, the charge density waves modulation stays oriented along the x-direction in the doping range which roughly extends from 0.12 to 0.15.

- Finally, at $p \simeq 0.15$ the Fermi surface gets also closed at $(0, \pi)$ (while still being nematic, as it's evident from orange curve in Fig. 5) and upon increasing doping from $p = 0.15$ and $p = 0.2$ its topology favors a finite angle between $\mathbf{q}_c$ and the x-axis. Therefore the instability vector rotates from the x-axis

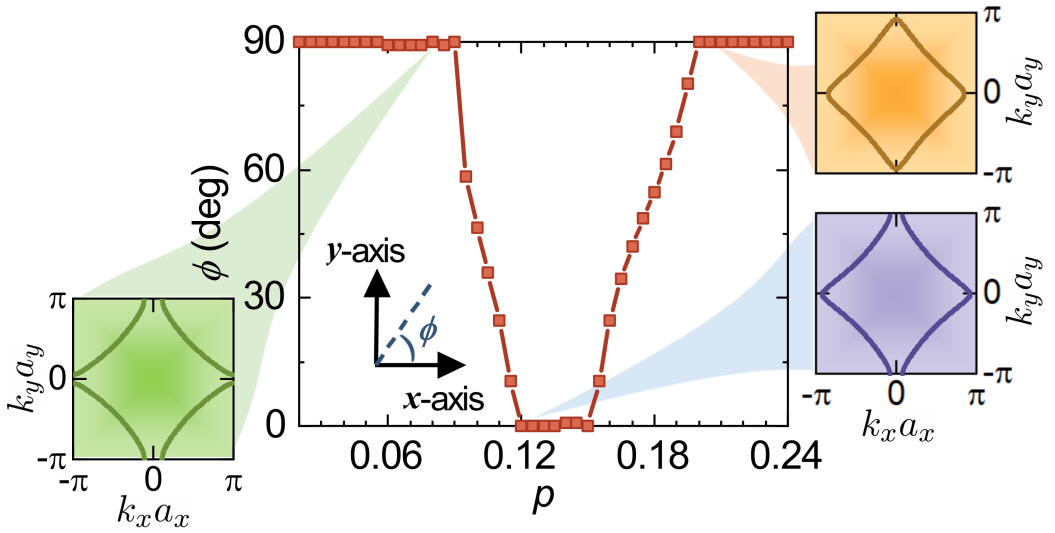

Figure 7.10. From [144], angle (with respect to the x-axis) of $\mathbf{q}_c$ as a function of doping for the chosen set of parameters. In the three insets, the nematic Fermi surfaces are shown as a function of doping, in cases $p = 0.08$, $p = 0.13$ and $p = 0.2$.

back to the y-axis, where it remains for $p \gtrsim 0.2$. In this regime the anisotropic interactions again dominate the orientation of $\mathbf{q}_c$ over the reduced nesting along the x-axis.

These considerations are collected in figure 7.10, where the orientation of the critical wave vector is reported as a function of the doping level. According with our results, the charge instability at $p = 0.125$ is oriented along the x-axis, which is in agreement with the experimental observation. Furthermore, our model predicts that this same orientation holds up to $p \simeq 0.15$.

In figure 7.11 we show instead the plot of the magnitude of $\mathbf{q}_c$ as a function of the doping level. What we observe is a continuous increase of $|\mathbf{q}_c|$ with doping which only deviates from an approximate linear behavior at doping $p \simeq 0.14$ and $p \simeq 0.2$. In these doping ranges the minimum of $V_{\text{tot}}(\mathbf{q})$ is close to a nesting vector so that the magnitude of $\mathbf{q}_c$ gets additionally influenced by the structure of the enhanced charge correlations $\chi^0_{\rho\rho}(\mathbf{q})$. Notably, the magnitude of $\mathbf{q}_c$ does not change significantly across the transition, as the minimum of $V_{\text{tot}}(\mathbf{q})$ is only weakly dependent on the orientation of $\mathbf{q}$.

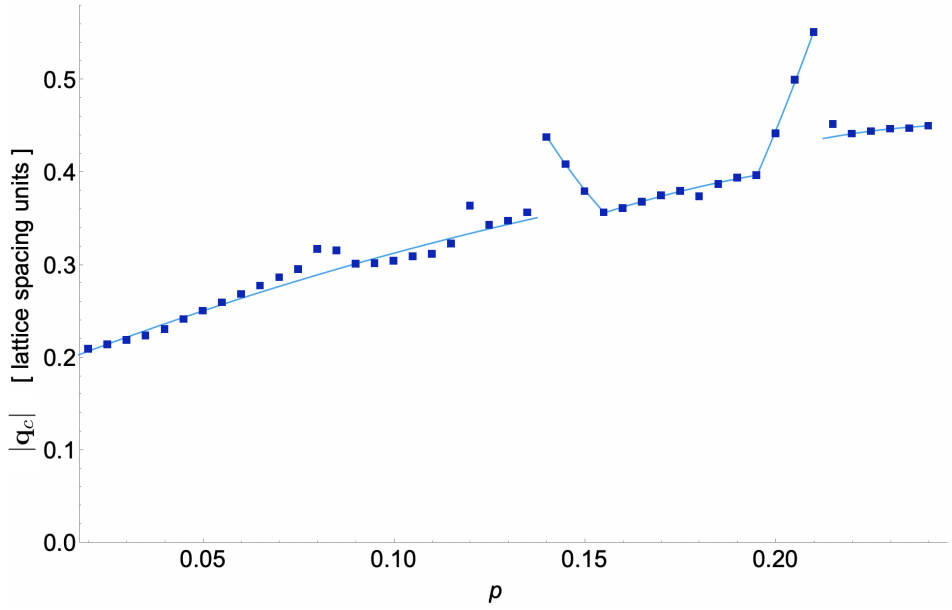

Figure 7.11. Magnitude of $\mathbf{q}_c$ as a function of the doping level for the chosen set of parameters. The square markers are the result of the numerical calculation, while the solid lines are just a guide to the eye. The lattice spacing units for $\mathbf{q}_c$ are referred separately to the two components of the vector, i.e. the quantity reported on the y-axis is $\sqrt{q_{c,x}^2 a_x^2 + q_{c,y}^2 a_y^2}$ (where $q_{c,x}$, $q_{c,y}$, a_x and a_y can be expressed in standard SI units).

As we have already mentioned in section 5.1, the value of $|\mathbf{q}_c|$ obtained from this calculation is significantly lower than that experimentally observed. In fact, according to figure 7.11, the magnitude of $\mathbf{q}_c$ should be around 0.3 r.l.u. (slightly less than 1 in lattice spacing units), while our calculation provides $|\mathbf{q}_c| \simeq 0.34$ in lattice spacing units. We believe that this discordance may be an artifact of random phase approximation, moreover amplified by the overestimation of the local repulsion, due

to the fact that we considered the $U \to \infty$ limit Hubbard model. According to our discussion, a reduction of the residual repulsion would not only increase the value of $|\mathbf{q}_c|$, but would extend the doping region where the criticality is along the x-direction. Moreover, the inclusion of more realistic electron-phonon couplings can support an agreement with experimentally determined charge density waves modulations. What is notable is that our theoretical value of $|\mathbf{q}_c|$ is consistent with the one that allowed us to correctly reproduce the Seebeck coefficient for optimally doped $La_{1.6-x}Nd_{0.4}Sr_xCuO_4$ compound, which gives our scheme internal coherence. We remind that we performed the Seebeck coefficient calculation in a perfectly tetragonal model, while here we are considering an orthorombic system. However, the orthorombic distortion we are considering is quite slight, in fact the tetragonal limit within our model is obtained by considering the following parameters:

$$\alpha = 0 \qquad \varepsilon_x = \varepsilon_y \qquad a_x = a_y$$

While the parameters we actually used differ only slightly from these. Of course, for a perfectly tetragonal symmetry, ask what the angle of the critical wave vector is would be pointless, as the two planar directions would become completely equivalent. However, the magnitude of this vector is well defined, which we deduce is very similar to those exhibited in figure 7.11, on the ground of our observations.

We also point out a further simplification envisaged by our model, namely having kept the hopping parameters fixed as the doping level varies. By taking into account the dependence of these parameters on doping, in principle, it could change the doping window in which the criticality is obtained along the x-axis. However, since our estimate for the hopping parameters is based on the sample data at $p = 0.12$ we believe that, even taking this further effect into account, the direction of the critical wave vector at $p = 0.125$ should not change.

Chapter 8

Conclusions

On the basis of what is addressed in this thesis work, it is evident that the main problem related to the full understanding of cuprates is due to the great variety of microscopic phenomena that occurs within them. The global phenomenology of cuprates is most likely due to a complicated superposition of these microscopic effects, this not only makes it difficult to distinguish the relevant phenomena underlying the behavior of these systems from the more marginal ones, but also makes it virtually impossible to delineate an accurate microscopic model. In this work we mainly focused on the effect of charge density fluctuation modes on some of the characteristic physical properties of cuprates. We tried to simulate the effects of these collective modes on our system starting from a phenomenological model and using calculation techniques based on the theory of many-body systems, equipped with numerical computations.

Based on the experimental evidence that the momentum distribution of charge density fluctuations is very broad, we opened our discussion by studying a preliminary model, in which the only mediator of the electronic interaction is a damped and strictly dispersionless Holstein phonon. Despite its simplicity, this model captures the main physical characteristics of charge density fluctuations, and describes with good approximation their effects on the macroscopic properties of the systems under consideration. From the study of this model, clear similarities and differences emerged with the Marginal Fermi liquid theory, which is one of the most commonly used paradigms for the explanation of strange-metal phenomenology. This interesting analogy suggests that charge density fluctuations may be a good candidate for the explanation of some important phenomena of the strange-metal phase of cuprates.

After analyzing the dispersionless damped Holstein model in detail, we tackled the study of actual charge density fluctuations. In particular, we applied our model to the description of some peculiar phenomena of the strange-metal phase, namely the behavior of the specific heat, the resistivity and the Seebeck coefficient as a function of temperature close to the critical doping level. We were able to show that our model is able to reproduce, quantitatively and/or qualitatively, the physical quantities of interest to us, at the cost of intervening on only one parameter of the theory, namely the Landau damping term γ. This last parameter plays a fundamen-

tal role in our theory. In fact from our study it emerged that, as γ increases, the temperature range in which the resistivity is linear extends to increasingly lower temperatures, furthermore it shows that the direct bosonic contribution to both the specific heat and the thermopower has good linearity in γ. Based on these observations, we phenomenologically postulated a functional dependence of this parameter on temperature and doping level, in such a way as to evolve logarithmically in temperature until possibly diverging at zero temperature in the case in which doping is set at the critical level. This functional dependence allowed us to quantitatively fit the resistivity data, as well as the qualitative trend of the specific heat up to an overall amplification factor. Furthermore, under the same hypotheses on the dependence of γ on temperature and doping it was possible to correctly fit the data of the Seebeck effect. Given the crucial role of the functional dependence of charge density fluctuations damping on temperature and doping, which was initially assumed purely phenomenologically, we investigated the possible origin of this abnormal damping. The mechanism we have proposed, as a possible rationale, is based on the interaction between the charge density collective modes and the diffusive particle-hole pairs. In two-dimensional systems, this mechanism precisely provides a logarithmic temperature dependence for damping.

In essence, the study we carried out shows that the presence of charge density fluctuations in the strange-metal phase of cuprates may be responsible, at least in part, for some of the most peculiar phenomena that characterize this phase. From this perspective, we believe that the recent observation of charge density fluctuations in cuprates [10] could be an important step forward in understanding these systems. Furthermore, a prediction of our model is that charge density fluctuations in the strange-metal phase should not be affected by the presence of a magnetic field. The RIXS experiments which detected these collective modes were carried out in the absence of magnetic field, so, below the superconducting critical temperature, superconductivity sets in, whereas our calculations were also aimed at described the extraction of the strange-metal behavior down to temperatures lower than the superconducting critical temperature, as it is observed when superconductivity is suppressed by a sufficiently strong magnetic field. With the technologies available nowadays, it is not possible to carry out RIXS experiments at such strong magnetic field, so our prediction is yet to be tested.

Another interesting aspect of our description lies in the fact that the critical behavior of our system is not associated with a divergence of the correlation length, but rather with the divergence of the relaxation time of these collective modes, thereby setting a new stage for the violation of the Fermi liquid behavior. Of course, our work has left some questions still open. For instance, the very origin of charge density fluctuations is not yet clear, nor what relationship they have with standard charge density waves. Furthermore, it is not yet clear what role charge density fluctuations play in the model we have adopted to calculate the magnetoresistance, nor what their effect is on other physical properties, such as optical conductivity or the Hall effect. Despite the still unresolved questions, we believe that our results are encouraging and can be a step forward in the general understanding of strange-metal behavior, possibly even in systems other than cuprates, provided similar conditions, namely the vicinity to

a quantum critical point and the occurrence of slow and short-ranged dynamical collective mode fluctuations associated to it, are met.

Beyond the issue of the strange-metal phase, another question we have addressed within our work concerns the nematic properties observed in cuprate thin films. This nematicity is experimentally evident from the different behavior of the resistivity along the two planar directions, as well as from the unidirectionality of the charge instability at low temperature. The model we have developed for the description of these phenomena accounts for the interaction between the cuprate sample and the substrate. We have shown that our model correctly predicts a nematic Fermi surface and a unidirectional charge instability observed in the experiment [20]. Since our analysis showed that the morphology of the substrates has a very relevant effect on the phenomenology of cuprate thin films, a possible line of research suggested by this work is the study of other types of patterns for the substrates, as well as their effect on the microscopic parameters of films. Moreover, this kind of study can also be extended to other physical phenomena, not addressed in our work that was focused on the properties of the metallic phase, such as superconductivity itself. Patterning and constraining the landscape on which superconductivity occurs may lead to a plethora of interesting phenomena, including the enhancement of the superconducting critical temperature [147, 148, 149, 150, 151, 152, 153, 154].

Appendix A

A note about Fourier transform

Conventions about the Fourier transform in time-frequency domain

Let $F(t)$ be a generic (sufficiently regular) function of the time variable $t \in \mathbb{R}$, and let's denote with $\hat{F}(\omega)$ its Fourier transform (here, $\omega \in \mathbb{R}$ is the frequency domain variable). The convention we use for the time-frequency Fourier transform is the following:

$$\hat{F}(\omega) = \int_{-\infty}^{+\infty} F(t) e^{i\omega t} dt \qquad F(t) = \int_{-\infty}^{+\infty} \hat{F}(\omega) e^{-i\omega t} \frac{d\omega}{2\pi}$$

For finite temperature calculations we will often adopt the Matsubara formalism in which both the time variables and the frequency variables are pure imaginary quantities. The notation we use is the following:

$$t \to -i\tau \qquad \omega \to i\omega_n \qquad \text{where} \quad \tau, \omega_n \in \mathbb{R}$$

For simplicity, we will not use a different notation for functions defined on the real axis and those defined on the imaginary axis. For instance, the analytic continuation of $F(t)$ on the imaginary axis will be expressed simply as $F(-i\tau)$. The domain of definition of the variables τ and ω_n (which is, in any case, a subset of the real numbers) depends on temperature and, for the second variable, also on the nature of the field to which they are associated:

$$\tau \in [-\beta, \beta] \qquad \omega_n = \begin{cases} \dfrac{2n\pi}{\beta} & \text{for bosons} \\ \dfrac{(2n+1)\pi}{\beta} & \text{for fermions} \end{cases}$$

The values that any physical function defined in the imaginary time domain assumes at $\tau < 0$ and those that it assumes at $\tau > 0$ are constrained to satisfy a well-defined connection condition, expressed by the following equation:

$$F(-i\tau) = \begin{cases} F(-i(\tau+\beta)) & \text{for bosons} \\ -F(-i(\tau+\beta)) & \text{for fermions} \end{cases} \qquad \text{where } \tau \in [-\beta, 0] \tag{A.1}$$

Since $\omega t = \omega_n \tau$, the exponentials appearing in the imaginary domain Fourier transform are formally the same as those for the real domain one. The difference between the two transforms lies only in the fact that τ is defined on a bounded domain, so the integral over frequencies is replaced by a discrete summation, in agreement with the fact that ω_n is defined only on a discrete set. Whether the sum is extended over even or odd frequencies depends on the nature (bosonic or fermionic) of the field described by the function. The notation we will use for imaginary frequencies is the same whether they are even or odd, their parity will be specified with the summation symbol:

$$\hat{F}(i\omega_n) = \frac{1}{2}\int_{-\beta}^{+\beta} F(-i\tau)e^{i\omega_n\tau}d\tau = \int_{0}^{+\beta} F(-i\tau)e^{i\omega_n\tau}d\tau$$

$$F(-i\tau) = \begin{cases} \dfrac{1}{\beta}\displaystyle\sum_{n\,\text{even}} \hat{F}(i\omega_n)\, e^{-i\omega_n\tau} & \text{for bosons} \\[2ex] \dfrac{1}{\beta}\displaystyle\sum_{n\,\text{odd}} \hat{F}(i\omega_n)\, e^{-i\omega_n\tau} & \text{for fermions} \end{cases}$$

The second equality in the first of these two equations is a direct consequence of identity (A.1) and it holds regardless the parity of Matsubara frequency.

Conventions about the Fourier transform in position-momentum domain

Let's consider a d-dimensional continuous and infinitely extended system, and let $\mathbf{x}$ and $\mathbf{k}$ be two vectors belonging to $\mathbb{R}^{\mathrm{d}}$ (of course, they are physically associated with a displacement and a momentum, respectively). Let $F(\mathbf{x})$ be a sufficiently regular scalar function of the displacement $\mathbf{x}$. In analogy to what was done previously, we use $\hat{F}(\mathbf{k})$ to indicate its Fourier transform:

$$\hat{F}(\mathbf{k}) = \int_{\mathbb{R}^{\mathrm{d}}} F(\mathbf{x})e^{-i\mathbf{k}\mathbf{x}}d^{\mathrm{d}}\mathbf{x} \qquad F(\mathbf{x}) = \int_{\mathbb{R}^{\mathrm{d}}} \hat{F}(\mathbf{k})e^{i\mathbf{k}\mathbf{x}}\frac{d^{\mathrm{d}}\mathbf{k}}{(2\pi)^{\mathrm{d}}}$$

Let's now consider the case of a finite and discrete system. We use V to denote the total volume of the system, while we use v_{uc} to denote the volume of the Wigner-Seitz cell of the coordinate space, the total number of sites of the system $N \gg 1$ is simply given by the ratio V/v_{uc}. It should be stressed that, at this level, the discrete structure is not just a substructure of the system (as it is usually considered in crystallography) but is the very structure of the space considered. In the case of a crystal system, for instance, despite the Bravais lattice substructure it makes sense to define functions of the space variable on a continuous domain, which are therefore well defined even outside the lattice sites and which can vary on even smaller scales

than the lattice spacing. This is the case, for example, of the electronic wavefunctions predicted by Bloch's theorem. Within this context, by "discrete structure" we mean that the domain itself for the space variable functions is discrete. However, for the sake of simplicity, we adopt a nomenclature similar to that commonly used to describe lattice systems in condensed matter physics.

For the (finite) volume of the system, Born-von Karman periodic conditions are always considered. Of course, the fact that the volume of the system is finite implies that the **k**-space is discrete on a scale inversely proportional to the volume itself. We use the notation *FBZ* to indicate the Wigner-Seitz cell in **k**-space, as it coincides with the well-known *First Brillouin Zone* of the reciprocal lattice. In order to switch to a discrete description it is necessary to replace the integrals with summations and to consider the following identifications:

$$d^{\mathrm{d}}\mathbf{x} \sim v_{\mathrm{uc}} \qquad d^{\mathrm{d}}\mathbf{k} \sim \frac{(2\pi)^{\mathrm{d}}}{V} \qquad \text{where} \quad V = N v_{\mathrm{uc}} \tag{A.2}$$

The position-momentum Fourier transform is therefore defined as:

$$\hat{F}(\mathbf{k}) = v_{\mathrm{uc}} \sum_{\mathbf{x}\in V} F(\mathbf{x}) e^{-i\mathbf{k}\mathbf{x}} \qquad F(\mathbf{x}) = \frac{1}{V} \sum_{\mathbf{k}\in FBZ} \hat{F}(\mathbf{k}) e^{i\mathbf{k}\mathbf{x}} \tag{A.3}$$

Here, both $F(\mathbf{x})$ and $\hat{F}(\mathbf{k})$ are defined only on a discrete set, these two sets are clearly distinct but have the very same finite cardinality (which is N). It is worth noting that the notation we use for vectors (both in coordinate and momentum space) is the same whether they are defined in a discrete set or if they are defined in a continuous set. The discrete or continuous nature of the vectors is signaled by whether they appear as sum variables or integration variables, respectively. In any case, the scales on which the discretization takes place are those set by (A.2).

There are two interesting limits of equations (A.3), namely the thermodynamic limit ($V \to \infty$) and the continuum limit ($v_{\mathrm{uc}} \to 0$), both of which separately imply $N \to \infty$. The thermodynamic limit (at finite v_{uc}) leads to:

$$\hat{F}(\mathbf{k}) = v_{\mathrm{uc}} \sum_{\mathbf{x}\in\mathbb{R}^{\mathrm{d}}} F(\mathbf{x}) e^{-i\mathbf{k}\mathbf{x}} \qquad F(\mathbf{x}) = \int_{FBZ} \hat{F}(\mathbf{k}) e^{i\mathbf{k}\mathbf{x}} \frac{d^{\mathrm{d}}\mathbf{k}}{(2\pi)^{\mathrm{d}}}$$

Conversely, the continuum limit (at finite V) leads to:

$$\hat{F}(\mathbf{k}) = \int_V F(\mathbf{x}) e^{-i\mathbf{k}\mathbf{x}} d^{\mathrm{d}}\mathbf{x} \qquad F(\mathbf{x}) = \frac{1}{V} \sum_{\mathbf{k}\in\mathbb{R}^{\mathrm{d}}} \hat{F}(\mathbf{k}) e^{i\mathbf{k}\mathbf{x}} \tag{A.4}$$

Finally, considering both limits simultaneously allows us to reproduce the actual Fourier transform.

In this thesis work, we have chosen to work with a finite volume system, for which the Born-von Karman boundary conditions hold, under the usual hypothesis that this volume is very *large*. Moreover, we have chosen to use the continuum formalism, as it allows us to give a broader and more general description of our systems. Therefore,

the Fourier transform we will use is the one defined by equations (A.4). It is worth providing here the delta functions spectral representations compatible with relations this formalism:

$$\delta_{\mathbf{k},\mathbf{k}'} = \frac{1}{V}\int_V e^{-i(\mathbf{k}-\mathbf{k}')\mathbf{x}} d^{\mathrm{d}}\mathbf{x} \qquad \delta(\mathbf{x}-\mathbf{y}) = \frac{1}{V}\sum_{\mathbf{k}\in\mathbb{R}^{\mathrm{d}}} e^{i\mathbf{k}(\mathbf{x}-\mathbf{y})}\Big|_{\mathbf{x}-\mathbf{y}\,\in V}$$

Where $\delta_{\mathbf{k},\mathbf{k}'}$ is a Kronecker delta (which is well defined, as $\mathbf{k}$-space is discrete), while $\delta(\mathbf{x}-\mathbf{y})$ is a Dirac delta, which is restricted to the V set. The boundary conditions we have imposed on V ensure that there is no loss of generality in considering $\mathbf{x}-\mathbf{y}\in V$. We also provide the expressions for second quantization field operators in terms of plane waves:

$$\hat{a}_{\mathbf{k}} = \frac{1}{\sqrt{V}}\int_V e^{-i\mathbf{k}\mathbf{x}}\psi(\mathbf{x})d^{\mathrm{d}}\mathbf{x} \qquad \psi(\mathbf{x}) = \frac{1}{\sqrt{V}}\sum_{\mathbf{k}\in\mathbb{R}^{\mathrm{d}}} e^{i\mathbf{k}\mathbf{x}}\hat{a}_{\mathbf{k}} \tag{A.5}$$

In order to soften the notation, we avoid making explicit the domain of summations and integrations, this should be clear from time to time based on the framework. For this reason, equations (A.4) are simply expressed as:

$$\hat{F}(\mathbf{k}) = \int F(\mathbf{x})e^{-i\mathbf{k}\mathbf{x}}d^{\mathrm{d}}\mathbf{x} \qquad F(\mathbf{x}) = \frac{1}{V}\sum_{\mathbf{k}}\hat{F}(\mathbf{k})e^{i\mathbf{k}\mathbf{x}}$$

Within this work, expressions involving $\mathbf{k}$-sums are relatively frequent, however we want to stress they not always have the meaning of a Fourier transform. For physical reasons, most of these $\mathbf{k}$-sums are restricted only on the First Brillouin Zone rather than $\mathbb{R}^{\mathrm{d}}$. Even in this case, we will not make explicit the domain on which the sum runs, unless it is unclear from the context.

The case of a three-dimensional layered system

As we have already emphasized, the continuum description does not preclude systems under consideration from having a lattice structure: for such systems, a finite unitary volume v_{uc} is well defined, it is simply not to be identified with the volume that we have set to zero to get the continuum limit in coordinate space. In this case, N (which is finite, although very large) represents the total number of Bravais lattice sites, which has nothing to do with the cardinality of the sets on which $\mathbf{x}$ and $\mathbf{k}$ variables are defined, which instead are countably infinite. Most of the systems analyzed in this work are three-dimensional crystals, however such as to have a trivial behavior along the z-direction, so that most of the physical phenomena that characterize them can be well described by essentially two-dimensional models. According to the notation used within this work, N denotes the total number of lattice sites *on a single lattice plane* (therefore, if V_{3D} is the total three-dimensional volume of the system, the identity $V_{3D} = Nv_{\mathrm{uc}}$ is *not* valid), while the volume of the three-dimensional unit cell v_{uc} is equal to a^2d in the tetragonal case, or to $a_x a_y d$ in the case with orthorhombic distortion (of course, the interplane distance d should not be confused with the dimensionality d). Due to the very nature of the systems under examination, vector quantities such as displacement or momentum are to be

considered two-dimensional, belonging to the single lattice plane. This means, for instance, that a generic function of the momentum $F(\mathbf{k})$ actually depends on k_x and k_y but not on k_z, therefore if we consider the sum of $F(\mathbf{k})$ over all momenta in the three-dimensional Brillouin Zone, the sum over the z-components simply gives the number of lattice planes. In many cases, this simplifies the number of lattice planes inside the term V_{3D}, leaving explicit only the number of sites on the lattice plane N and the volume of the unit cell v_{uc}:

$$\frac{1}{V_{3D}} \sum_{k_z} \sum_{\mathbf{k}} \hat{F}(\mathbf{k}) = \frac{1}{v_{\mathrm{uc}}} \frac{1}{N} \sum_{\mathbf{k}} \hat{F}(\mathbf{k})$$

For the tetragonal case, we have adopted the convention $a = 1$, therefore we simply have $v_{\mathrm{uc}} = d$. The dimensionless factor $1/v_{\mathrm{uc}}$ (or $1/d$) should be included in front of the sums over momenta which are originally normalized with the total three-dimensional volume.

Appendix B

Spectral decomposition of correlation functions

Equivalence of correlation functions within real and imaginary time domain

Given a system described by a (time-independent) Hamiltonian H_0, it is possible to define the thermal average of a generic operator $\mathcal{O}$ as follows:

$$\langle \mathcal{O} \rangle \coloneqq \frac{1}{\mathcal{Z}_G} \sum_n \langle n | \, e^{-\beta H_0} \mathcal{O} \, | n \rangle \qquad \text{where} \qquad \mathcal{Z}_G \coloneqq \sum_n \langle n | \, e^{-\beta H_0} \, | n \rangle$$

Here, the set of vectors $|n\rangle$ is the complete basis of eigenstates of H_0:

$$H_0 \, | n \rangle = E_n \, | n \rangle \qquad \sum_n | n \rangle \, \langle n | = \mathrm{Id}$$

We consider two space and time dependent operators (within interaction picture) $A(\mathbf{r}, t)$ and $B(\mathbf{r}, t)$, for which bosonic commutation relations apply, and we denote by $\chi_{AB}(\mathbf{r}, t)$ the response function provided by Kubo formula (2.10). The spectral decomposition (or representation) of a correlation function of the form $\langle A(\mathbf{r}, t) B(\mathbf{0}, 0) \rangle$ consists in expressing this function in terms of the matrix elements of the two operators. It is customarily performed as follows:

$$\begin{aligned} \langle A(\mathbf{r}, t) B(\mathbf{0}, 0) \rangle &= \frac{1}{\mathcal{Z}_G} \sum_n \langle n | \, e^{-\beta H_0} A(\mathbf{r}, t) B(\mathbf{0}, 0) \, | n \rangle \\ &= \frac{1}{\mathcal{Z}_G} \sum_{n,m} \langle n | \, e^{-\beta H_0} A(\mathbf{r}, t) \, | m \rangle \, \langle m | \, B(\mathbf{0}, 0) \, | n \rangle = \\ &= \frac{1}{\mathcal{Z}_G} \sum_{n,m} e^{-\beta E_n} e^{i(E_n - E_m)t} \, \langle n | \, A(\mathbf{r}) \, | m \rangle \, \langle m | \, B(\mathbf{0}) \, | n \rangle \end{aligned}$$

A similar relation holds for the imaginary time correlation functions:

$$\langle A(\mathbf{r}, \tau) B(\mathbf{0}, 0) \rangle = \frac{1}{\mathcal{Z}_G} \sum_{n,m} e^{-\beta E_n} e^{(E_n - E_m)\tau} \, \langle n | \, A(\mathbf{r}) \, | m \rangle \, \langle m | \, B(\mathbf{0}) \, | n \rangle$$

Let's consider the spectral decomposition of the function $\langle[A(\mathbf{r},t)B(\mathbf{0},0)]\rangle$ and the Fourier transform of $i\theta(t)\langle[A(\mathbf{r},t)B(\mathbf{0},0)]\rangle$:

$$\langle[A(\mathbf{r},t)B(\mathbf{0},0)]\rangle = \frac{1}{\mathcal{Z}_G}\sum_{n,m}(e^{-\beta E_n} - e^{-\beta E_m})e^{i(E_n-E_m)t}\,\langle n|\,A(\mathbf{r})\,|m\rangle\,\langle m|\,B(\mathbf{0})\,|n\rangle$$

$$\mathcal{F}_t\Big[i\theta(t)\langle[A(\mathbf{r},t)B(\mathbf{0},0)]\rangle\Big] = -\frac{1}{\mathcal{Z}_G}\sum_{n,m}\frac{e^{-\beta E_n} - e^{-\beta E_m}}{E_n - E_m + \omega + i0^+}\,\langle n|\,A(\mathbf{r})\,|m\rangle\,\langle m|\,B(\mathbf{0})\,|n\rangle$$

If we do the same with the function $\langle T_\tau A(\mathbf{r},\tau)B(\mathbf{0},0)\rangle$ we get:

$$\langle T_\tau A(\mathbf{r},\tau)B(\mathbf{0},0)\rangle = \begin{cases} \dfrac{1}{\mathcal{Z}_G}\displaystyle\sum_{n,m} e^{-\beta E_n}e^{(E_n-E_m)\tau}\langle n|A(\mathbf{r})|m\rangle\langle m|B(\mathbf{0})|n\rangle & 0<\tau<\beta \\ \dfrac{1}{\mathcal{Z}_G}\displaystyle\sum_{n,m} e^{-\beta E_m}e^{(E_n-E_m)\tau}\langle n|A(\mathbf{r})|m\rangle\langle m|B(\mathbf{0})|n\rangle & -\beta<\tau<0 \end{cases}$$

$$\mathcal{F}_\tau\Big[\langle T_\tau A(\mathbf{r},\tau)B(\mathbf{0},0)\rangle\Big] = -\frac{1}{\mathcal{Z}_G}\sum_{n,m}\frac{e^{-\beta E_n} - e^{-\beta E_m}}{E_n - E_m + i\omega_n}\,\langle n|\,A(\mathbf{r})\,|m\rangle\,\langle m|\,B(\mathbf{0})\,|n\rangle$$

Therefore, we deduce the fundamental property:

$$\mathcal{F}_\tau\Big[\langle T_\tau A(\mathbf{r},\tau)B(\mathbf{0},0)\rangle\Big]\Big|_{i\omega_n\to\omega+i0^+} = \mathcal{F}_t\Big[i\theta(t)\langle[A(\mathbf{r},t)B(\mathbf{0},0)]\rangle\Big]$$

Which is one of the main reason why Matsubara correlation functions are so useful. Of course, the same result is valid even if the operators depend only on the time variable. Notice that the right hand side of the last equation is equal to the Fourier transform of $\chi_{AB}(\mathbf{r},t)$ by virtue of Kubo formula. For this reason, it is convenient to *define* the response function in imaginary time domain as follows:

$$\chi_{AB}(\mathbf{r},\tau) \coloneqq \langle T_\tau A(\mathbf{r},\tau)B(\mathbf{0},0)\rangle$$

So that the following useful identity holds:

$$\chi_{AB}(\mathbf{q}, i\omega_n \to \omega + i0^+) = \chi_{AB}(\mathbf{q},\omega)$$

Reactive and dissipative part of the response function

Given the correlation function $\langle A(\mathbf{r},t)B(\mathbf{0},0)\rangle$ we use the notation $\langle AB\rangle(\mathbf{q},\omega)$ to denote its Fourier transform, both in momentum and frequency domain:

$$\langle AB\rangle(\mathbf{q},\omega) \coloneqq \mathcal{F}_{\mathbf{r},t}\Big[\langle A(\mathbf{r},t)B(\mathbf{0},0)\rangle\Big]$$

For simplicity, we apply an analogous notation also for the retarded correlation function, defined as:

$$\langle AB\rangle_R(\mathbf{q},\omega) \coloneqq \mathcal{F}_{\mathbf{r},t}\Big[i\theta(t)\langle[A(\mathbf{r},t)B(\mathbf{0},0)]\rangle\Big]$$

A similar notation is also used when the Fourier transform involves only the time variable. With this definition, Kubo formula can be expressed in momentum and frequency domain as follows:

$$\chi_{AB}(\mathbf{q},\omega) = \langle AB\rangle_R(\mathbf{q},\omega) \tag{B.1}$$

At first sight, the function to which we are applying the Fourier transform can be, in general, complex. However, from spectral representation the following identity is evident:

$$\langle AB\rangle_R(\mathbf{q},\omega)^* = \langle AB\rangle_R(-\mathbf{q},-\omega)$$

Which implies that the inverse Fourier transform of $\langle AB\rangle_R(\mathbf{q},\omega)$ is actually a real function of time and space, as we expect since it coincides with the response function. The following trivial properties hold:

$$\mathrm{Re}\big[\langle AB\rangle_R(\mathbf{q},\omega)\big] = \frac{\langle AB\rangle_R(\mathbf{q},\omega) + \langle AB\rangle_R(-\mathbf{q},-\omega)}{2}$$

$$\mathrm{Im}\big[\langle AB\rangle_R(\mathbf{q},\omega)\big] = \frac{\langle AB\rangle_R(\mathbf{q},\omega) - \langle AB\rangle_R(-\mathbf{q},-\omega)}{2i}$$

Namely, the real part of $\langle AB\rangle_R(\mathbf{r},\omega)$ is an even function for the simultaneous change of sign of ω and $\mathbf{q}$, while the imaginary part is odd. It is often convenient to work with functions $\chi'_{AB}(\mathbf{q},\omega)$ and $\chi''_{AB}(\mathbf{q},\omega)$, defined as follows:

$$\chi'_{AB}(\mathbf{q},\omega) \coloneqq \frac{\langle AB\rangle_R(\mathbf{q},\omega) + \langle BA\rangle_R(-\mathbf{q},-\omega)}{2}$$

$$\chi''_{AB}(\mathbf{q},\omega) \coloneqq \frac{\langle AB\rangle_R(\mathbf{q},\omega) - \langle BA\rangle_R(-\mathbf{q},-\omega)}{2i}$$

The first of these two functions is known as *reactive part* of the response function, while the second is called *dissipative part*. It is possible to show that they reduce respectively to the real and the imaginary part of $\langle AB\rangle_R(\mathbf{q},\omega)$ under suitable conditions involving time-reversal symmetry of the operators, for instance the condition that both operators are symmetric under time-reversal is sufficient. Also notice that:

$$\mathrm{Re}\big[\langle AB\rangle_R(\mathbf{q},\omega)\big] + i\,\mathrm{Im}\big[\langle AB\rangle_R(\mathbf{q},\omega)\big] = \chi'_{AB}(\mathbf{q},\omega) + i\chi''_{AB}(\mathbf{q},\omega) = \chi_{AB}(\mathbf{q},\omega)$$

The fluctuation-dissipation theorem

Let's consider the spectral representation of $\langle AB\rangle(\mathbf{q},\omega)$, obtained simply by applying the Fourier transform directly to the expression for the spectral decomposition of $\langle A(\mathbf{r},t)B(\mathbf{0},0)\rangle$:

$$\langle AB\rangle(\mathbf{r},\omega)=\frac{1}{\mathcal{Z}_G}\sum_{n,m}e^{-\beta E_n}2\pi\delta(E_n-E_m+\omega)\langle n|A(\mathbf{r})|m\rangle\langle m|B(\mathbf{0})|n\rangle$$

From the spectral representation of $\mathcal{F}_t\Big[i\theta(t)\langle[A(\mathbf{r},t)B(\mathbf{0},0)]\rangle\Big]$ and the definition of $\langle AB\rangle_R(\mathbf{r},\omega)$ we have:

$$\langle AB\rangle_R(\mathbf{r},\omega)=-\frac{1}{\mathcal{Z}_G}\sum_{n,m}\frac{e^{-\beta E_n}-e^{-\beta E_m}}{E_n-E_m+\omega+i0^+}\langle n|A(\mathbf{r})|m\rangle\langle m|B(\mathbf{0})|n\rangle$$

We can also explicit the spectral representation of $\chi''_{AB}(\mathbf{r},\omega)$:

$$\begin{aligned}\chi''_{AB}(\mathbf{r},\omega)&=-\frac{1}{2i}\Bigg[\frac{1}{\mathcal{Z}_G}\sum_{n,m}\frac{e^{-\beta E_n}-e^{-\beta E_m}}{E_n-E_m+\omega+i0^+}\langle n|A(\mathbf{r})|m\rangle\langle m|B(\mathbf{0})|n\rangle+\\&\quad-\frac{1}{\mathcal{Z}_G}\sum_{n,m}\frac{e^{-\beta E_n}-e^{-\beta E_m}}{E_n-E_m-\omega+i0^+}\langle n|B(-\mathbf{r})|m\rangle\langle m|A(\mathbf{0})|n\rangle\Bigg]=\\&=-\frac{1}{\mathcal{Z}_G}\sum_{n,m}\mathrm{Im}\left[\frac{e^{-\beta E_n}-e^{-\beta E_m}}{E_n-E_m+\omega+i0^+}\right]\langle n|A(\mathbf{r})|m\rangle\langle m|B(\mathbf{0})|n\rangle=\\&=\frac{1-e^{-\beta\omega}}{2}\frac{1}{\mathcal{Z}_G}\sum_{n,m}e^{-\beta E_n}2\pi\delta(E_n-E_m+\omega)\langle n|A(\mathbf{r})|m\rangle\langle m|B(\mathbf{0})|n\rangle\end{aligned}$$

Which coincides with the spectral representation of $\langle AB\rangle(\mathbf{r},\omega)$ except for the prefactor. This proves fluctuation-dissipation theorem, which is usually expressed in momentum domain:

$$\chi''_{AB}(\mathbf{q},\omega)=\frac{1-e^{-\beta\omega}}{2}\langle AB\rangle(\mathbf{q},\omega)$$

Onsager relations for current operators

Spectral decomposition also allows us to show two important properties of Onsager coefficients, namely that they are real and that they obey Onsager relations. Let's start by applying the spectral decomposition to the term $\langle J_\alpha(\mathbf{r},-t-i\lambda)J_\beta(\mathbf{0},0)\rangle$ inside expression (2.11). By performing this decomposition, both integrals in $d\lambda$ and in dt can be analytically solved. The result is:

$$\begin{aligned}Z_{\alpha\beta}=\lim_{\epsilon\to0^+}\frac{1}{\mathcal{Z}_G}\sum_{n,m}\frac{1}{\epsilon-i(E_n-E_m)}\left(-\frac{e^{-\beta E_n}-e^{-\beta E_m}}{\beta(E_n-E_m)}\right)\times\\\times\int_{\mathbb{R}^\mathrm{d}}\langle n|J_\alpha(\mathbf{r})|m\rangle\langle m|J_\beta(\mathbf{0})|n\rangle\,d^\mathrm{d}\mathbf{r}\end{aligned}$$

By applying complex conjugation to both members of this equation, relation $Z^*_{\alpha\beta}=Z_{\alpha\beta}$ evident, which proves that $Z_{\alpha\beta}\in\mathbb{R}$ consistently with what we expect. This

observation allows us to express $Z_{\alpha\beta}$ as $\mathrm{Re}Z_{\alpha\beta}$, leading to the following simpler form:

$$Z_{\alpha\beta} = \mathrm{Re}Z_{\alpha\beta} = \frac{1}{\mathcal{Z}_G}\sum_{n,m}\pi\,\delta(E_n - E_m)e^{-\beta E_n}\left(\int_{\mathbb{R}^{\mathrm{d}}}\langle n|\,J_\alpha(\mathbf{r})\,|m\rangle\,\langle m|\,J_\beta(\mathbf{0})\,|n\rangle\,d^{\mathrm{d}}\mathbf{r}\right)$$

In order to show the validity of Onsager relations we have to introduce the concept of parity under time-reversal symmetry. For the case of our interest, time-reversal symmetry can be expressed through the following relation:

$$\langle J_\alpha(\mathbf{r}, -t - i\lambda)J_\beta(\mathbf{0}, 0)\rangle = \pm\langle J_\alpha(\mathbf{r}, t - i\lambda)J_\beta(\mathbf{0}, 0)\rangle^* \tag{B.2}$$

Of course, the positive sign applies to symmetric functions while the negative one applies to antisymmetric functions. By applying spectral decomposition to both sides of this equation we get:

$$\begin{aligned}&\sum_{n,m} e^{-\beta E_m}e^{i(E_n-E_m)t}e^{(E_m-E_n)\lambda}\,\langle n|\,J_\alpha(\mathbf{r})\,|m\rangle\,\langle m|\,J_\beta(\mathbf{0})\,|n\rangle = \\ &= \pm\sum_{n,m} e^{-\beta E_n}e^{-i(E_n-E_m)t}e^{-(E_m-E_n)\lambda}\,\langle n|\,J_\alpha(\mathbf{r})\,|m\rangle\,\langle m|\,J_\beta(\mathbf{0})\,|n\rangle\end{aligned}$$

In light of what we have seen so far, we can write the following chain of equalities:

$$\begin{aligned}&e^{(\epsilon - iE_n + iE_m)t}\left[\frac{e^{-\beta E_n}}{\beta}\int_0^\beta e^{(E_n-E_m)\lambda}\left(\int_{\mathbb{R}^{\mathrm{d}}}\langle n|\,J_\beta(\mathbf{r})\,|m\rangle\,\langle m|\,J_\alpha(\mathbf{0})\,|n\rangle\,d^{\mathrm{d}}\mathbf{r}\right)d\lambda\right] = \\ &= e^{(\epsilon - iE_m + iE_n)t}\left[\frac{e^{-\beta E_m}}{\beta}\int_0^\beta e^{(E_m-E_n)\lambda}\left(\int_{\mathbb{R}^{\mathrm{d}}}\langle n|\,J_\alpha(\mathbf{r})\,|m\rangle\,\langle m|\,J_\beta(\mathbf{0})\,|n\rangle\,d^{\mathrm{d}}\mathbf{r}\right)d\lambda\right] = \\ &= \pm\, e^{(\epsilon - iE_n + iE_m)t}\left[\frac{e^{-\beta E_n}}{\beta}\int_0^\beta e^{(E_n-E_m)\lambda}\left(\int_{\mathbb{R}^{\mathrm{d}}}\langle n|\,J_\alpha(\mathbf{r})\,|m\rangle\,\langle m|\,J_\beta(\mathbf{0})\,|n\rangle\,d^{\mathrm{d}}\mathbf{r}\right)d\lambda\right]\end{aligned}$$

From first to second line, we just switched the $\mathbf{r}$ variable of the integral to $-\mathbf{r}$ and exploited translational invariance of the system, moreover we inverted the dummy indices m and n. From second to third line we simply exploited time-reversal relations. Given these equalities, it is now necessary to explicitly solve the integrals in $d\lambda$, then integrate the resulting expressions in dt (from $-\infty$ to 0) and finally consider the limit $\epsilon \to 0^+$. The equality between the first and third lines, at the end of the calculation, provides the identity $Z_{\beta\alpha} = \pm Z_{\alpha\beta}$, which is the form of the Onsager relations we were looking for.

Appendix C

Details about Kubo formalism

Perturbation theory: general remarks

In this appendix we will use all the notations and conventions introduced in section 2.3, including the decomposition of the Hamiltonian for the interacting system. The calculations that we will make in this section, as well as the notation adopted, are taken and reworked from references [98] and [155].

First of all, we recall that in absence of any perturbation it is possible to define the unperturbed density operator $\hat{\rho}_0$, along with the thermal average of a generic operator $\mathcal{O}$:

$$\hat{\rho}_0 \coloneqq \frac{e^{-\beta H_0}}{\mathcal{Z}_G} \qquad \langle \mathcal{O} \rangle \coloneqq \sum_n \langle n | \, \hat{\rho}_0 \mathcal{O} \, | n \rangle \qquad \text{where} \qquad \mathcal{Z}_G \coloneqq \sum_n \langle n | \, e^{-\beta H_0} \, | n \rangle$$

As usual, the set of vectors $|n\rangle$ is the complete basis of eigenstates of the unperturbed Hamiltonian. In the presence of perturbation $\delta H(t)$, the density operator will be altered by the perturbation, and will generally acquire a dependence on time. Within a perturbative approach, we can express the full density operator $\hat{\rho}(t)$ as a correction to the unperturbed one:

$$\hat{\rho}(t) \coloneqq \hat{\rho}_0 + \delta\hat{\rho}(t) \qquad \langle \mathcal{O}(t) \rangle_{\text{n.e.}} \coloneqq \sum_n \langle n | \, \hat{\rho}(t) \mathcal{O} \, | n \rangle$$

Within Schrödinger picture, the equation of motion for $\hat{\rho}(t)$ is provided by von Neumann equation [99, 156]:

$$i \frac{\partial \hat{\rho}(t)}{\partial t} = \big[H, \hat{\rho}(t) \big] = \big[H_0 + \delta H(t), \hat{\rho}_0 + \delta\hat{\rho}(t) \big] \simeq \big[H_0, \delta\hat{\rho}(t) \big] + \big[\delta H(t), \hat{\rho}_0 \big]$$

We have considered only the first order of perturbation. In order to solve the previous equation we use the following identity:

$$i e^{-iH_0 t} \frac{\partial \big(e^{iH_0 t} \, \delta\hat{\rho}(t) \, e^{-iH_0 t} \big)}{\partial t} e^{iH_0 t} = i \frac{\partial \delta\hat{\rho}(t)}{\partial t} - \big[H_0, \delta\hat{\rho}(t) \big]$$

Which allows us to manipulate von Neumann equation as follows:

$$[\delta H(t), \hat{\rho}_0] = i\frac{\partial \delta\hat{\rho}(t)}{\partial t} - [H_0, \delta\hat{\rho}(t)] = ie^{-iH_0t}\frac{\partial\big(e^{iH_0t}\,\delta\hat{\rho}(t)\,e^{-iH_0t}\big)}{\partial t}e^{iH_0t}$$
$$\frac{\partial\big(e^{iH_0t}\,\delta\hat{\rho}(t)\,e^{-iH_0t}\big)}{\partial t} = -i\big[e^{iH_0t}\delta H(t)e^{-iH_0t}, \hat{\rho}_0\big]$$

Notice that the product $e^{iH_0t}\delta H(t)e^{-iH_0t}$ can be interpreted as the perturbative part of the Hamiltonian evolving through interaction picture. In order to integrate the equation for $\delta\hat{\rho}(t)$ we set the usual initial condition:

$$\lim_{t\to-\infty}\delta\hat{\rho}(t) = 0$$

Therefore we get:

$$\delta\hat{\rho}(t) = -i\int_{-\infty}^{t}\big[e^{iH_0(t'-t)}\delta H(t')e^{-iH_0(t'-t)}, \hat{\rho}_0\big]dt'$$

Since we have an explicit expression for $\delta\hat{\rho}(t)$ we are able compute the expectation value $\langle\mathcal{O}(t)\rangle_{\text{n.e.}}$ explicitly:

$$\langle\mathcal{O}(t)\rangle_{\text{n.e.}} = \sum_n \langle n|\,\hat{\rho}(t)\mathcal{O}\,|n\rangle = \sum_n \langle n|\,\hat{\rho}_0\mathcal{O}\,|n\rangle + \sum_n \langle n|\,\delta\hat{\rho}(t)\mathcal{O}\,|n\rangle =$$
$$= \langle\mathcal{O}\rangle - i\sum_n\int_{-\infty}^{t}\langle n|\,\big[e^{iH_0(t'-t)}\delta H(t')e^{-iH_0(t'-t)}, \hat{\rho}_0\big]\mathcal{O}\,|n\rangle\,dt' =$$
$$= \langle\mathcal{O}\rangle - i\sum_n\int_{-\infty}^{t}\langle n|\,\hat{\rho}_0\big[e^{iH_0t}\mathcal{O}e^{-iH_0t}, e^{iH_0t'}\delta H(t')e^{-iH_0t'}\big]\,|n\rangle\,dt'$$

We exploited the cyclic property of trace, as well as commutativity between operators $\hat{\rho}_0$ and e^{iH_0t}. The relation we have just shown is a very general form (but, for the moment, not very convenient to use) of the Kubo formula, which is equivalent to the following equation:

$$\langle\mathcal{O}(t)\rangle_{\text{n.e.}} - \langle\mathcal{O}\rangle = -i\int_{-\infty}^{t}\Big\langle\big[e^{iH_0t}\mathcal{O}e^{-iH_0t}, e^{iH_0t'}\delta H(t')e^{-iH_0t'}\big]\Big\rangle dt' \tag{C.1}$$

The Kubo formula

Formally, equation (C.1) works for any kind of perturbation, as long as we limit ourselves to considering only the linear order in the perturbation itself. Within our description, the perturbation to the Hamiltonian is due to the ignition of external (in general, time-dependent) sources, therefore we choose to use the expression for $\delta H(t)$ exhibited in equation (2.7). In order to make the response function explicit, we start from the definition of $\delta\langle A_{\text{i}}(\mathbf{r},t)\rangle$ given by (2.8) and express its right-hand side through equation (C.1). We get:

$$\delta\langle A_{\mathrm{i}}(\mathbf{r},t)\rangle = -i\int_{-\infty}^{t}\Big\langle\big[e^{iH_0t}A_{\mathrm{i}}(\mathbf{r})e^{-iH_0t}, e^{iH_0t'}\delta H(t')e^{-iH_0t'}\big]\Big\rangle dt' =$$

$$= +i\sum_{\mathrm{j}}\int_{-\infty}^{t}\int_{\mathbb{R}^{\mathrm{d}}}\Big\langle\big[e^{iH_0t}A_{\mathrm{i}}(\mathbf{r})e^{-iH_0t}, e^{iH_0t'}A_{\mathrm{j}}(\mathbf{r}')e^{-iH_0t'}\big]\Big\rangle v_{\mathrm{j}}(\mathbf{r}',t')d^{\mathrm{d}}\mathbf{r}'dt' =$$

$$= +i\sum_{\mathrm{j}}\int_{\mathbb{R}^{\mathrm{d}+1}}\theta(t-t')\Big\langle\big[A_{\mathrm{i}}(\mathbf{r},t), A_{\mathrm{j}}(\mathbf{r}',t')\big]\Big\rangle v_{\mathrm{j}}(\mathbf{r}',t')d^{\mathrm{d}}\mathbf{r}'dt' =$$

$$= +i\sum_{\mathrm{j}}\int_{\mathbb{R}^{\mathrm{d}+1}}\theta(t-t')\Big\langle\big[A_{\mathrm{i}}(\mathbf{r}-\mathbf{r}',t-t'), A_{\mathrm{j}}(\mathbf{0},0)\big]\Big\rangle v_{\mathrm{j}}(\mathbf{r}',t')d^{\mathrm{d}}\mathbf{r}'dt'$$

Note that in the last step we used explicitly the hypothesis of translational invariance of the system. By comparison with the definition of $\chi_{AB}(\mathbf{r},t)$ given by (2.9) we conclude:

$$\chi_{\mathrm{ij}}(\mathbf{r},t) = +i\theta(t)\big\langle\big[A_{\mathrm{i}}(\mathbf{r},t), A_{\mathrm{j}}(\mathbf{0},0)\big]\big\rangle$$

Which is the form of Kubo formula most commonly used in the literature. It should be stressed that the overall minus sign in expression (2.7) is purely conventional, some authors define $\delta H(t)$ with an overall plus sign [157, 158], and consequently they obtain an expression for $\chi_{\mathrm{ij}}(\mathbf{r},t)$ similar to our one but which differs from it by an overall minus sign.

Current operators

As we mentioned in section 2.3, the formalism we adopt for the description of current-current response functions is based on the entropy production rate. First, we need to identify the internal energy variation due to ignition of the sources, which is precisely the expectation value of the perturbative part of the Hamiltonian:

$$U(t) = \langle\delta H(t)\rangle_{\mathrm{n.e.}} = -\sum_{\mathrm{i}}\int_{\mathbb{R}^{\mathrm{d}}}\langle A_{\mathrm{i}}(\mathbf{r},t)\rangle_{\mathrm{n.e.}}v_{\mathrm{i}}(\mathbf{r},t)d^{\mathrm{d}}\mathbf{r}$$

By differentiating with respect to time we get:

$$\frac{dU}{dt} = -\sum_{\mathrm{i}}\int_{\mathbb{R}^{\mathrm{d}}}\frac{d\langle A_{\mathrm{i}}(\mathbf{r},t)\rangle_{\mathrm{n.e.}}}{dt}v_{\mathrm{i}}(\mathbf{r},t)d^{\mathrm{d}}\mathbf{r} - \sum_{\mathrm{i}}\int_{\mathbb{R}^{\mathrm{d}}}\langle A_{\mathrm{i}}(\mathbf{r},t)\rangle_{\mathrm{n.e.}}\frac{\partial v_{\mathrm{i}}(\mathbf{r},t)}{\partial t}d^{\mathrm{d}}\mathbf{r} =$$

$$= -\sum_{\mathrm{i}}\int_{\mathbb{R}^{\mathrm{d}}}\frac{d\langle A_{\mathrm{i}}(\mathbf{r},t)\rangle_{\mathrm{n.e.}}}{dt}v_{\mathrm{i}}(\mathbf{r},t)d^{\mathrm{d}}\mathbf{r} + \left\langle\frac{\partial\,\delta H(t)}{\partial t}\right\rangle_{\mathrm{n.e.}}$$

The two terms of the sum in the last line can be interpreted, respectively, as the energy that the system loses in form of heat and that which it acquires through work exerted from external forces. While the latter is non-negative, the second is non-positive as it coincides (up to a minus sign and a temperature factor) with the irreversible entropy production rate:

$$T\frac{\partial S_{\mathrm{irr}}}{\partial t} = \sum_i \int_{\mathbb{R}^{\mathrm{d}}} \frac{d\langle A_{\mathrm{i}}(\mathbf{r},t)\rangle_{\mathrm{n.e.}}}{dt} v_{\mathrm{i}}(\mathbf{r},t) d^{\mathrm{d}}\mathbf{r}$$

Clearly, the first factor within the integral can be interpreted as a current while the second plays the role of a conjugate force. Since we are interested in the description of a stationary regime, it is convenient to take the following expression for the variation of the Hamiltonian due to the activation of external forces:

$$\delta H(t) \coloneqq -e^{\epsilon t}\hat{F}$$

Where $\hat{F}$ is an operator which does not have an explicit time dependence, therefore it is constant in time within Schrödinger picture. The prefactor $e^{\epsilon t}$ ensures that the sources are activated adiabatically and that the system respects the right boundary condition. We will take the limit $\epsilon \to 0^+$ at the end of the calculation, this limit will allows us to actually recover the stationarity condition. We choose the following ansatz for the expression of the density operator correction:

$$\delta\hat{\rho}(t) = e^{\epsilon t}\hat{f}$$

We can explicit $\hat{f}$ by using von Neumann equation:

$$e^{\epsilon t}\hat{f} = +i\int_{-\infty}^{t} e^{\epsilon t'}\big[e^{iH_0(t'-t)}\hat{F}e^{-iH_0(t'-t)},\hat{\rho}_0\big]dt' =$$
$$= i\int_{-\infty}^{t} e^{\epsilon t'}\big[\hat{F}(t'-t),\hat{\rho}_0\big]dt' = i\int_{-\infty}^{0} e^{\epsilon t}e^{\epsilon t'}\big[\hat{F}(t'),\hat{\rho}_0\big]dt'$$

We find that:

$$\hat{f} = i\int_{-\infty}^{0} e^{\epsilon t}\big[\hat{F}(t),\hat{\rho}_0\big]dt$$

In order to deal with the propagator which appears in the previous expression we need to show an important identity:

$$i\big[\hat{F}(t),\hat{\rho}_0\big] = i\frac{1}{\mathcal{Z}_G}\big(\hat{F}(t)e^{-\beta H_0} - e^{-\beta H_0}\hat{F}(t)\big) =$$
$$= i\frac{1}{\mathcal{Z}_G}\big(\hat{F}(t) - e^{-\beta H_0}\hat{F}(t)e^{+\beta H_0}\big)e^{-\beta H_0} = i\big(\hat{F}(t) - e^{+iH_0(i\beta)}\hat{F}(t)e^{-iH_0(i\beta)}\big)\hat{\rho}_0 =$$
$$= -i\big(\hat{F}(t+i\beta) - \hat{F}(t)\big)\hat{\rho}_0 = \int_0^{\beta}\frac{\partial\hat{F}(t+i\lambda)}{\partial t}d\lambda\,\hat{\rho}_0$$

Therefore we get:

$$\hat{f} = \int_{-\infty}^{0} e^{\epsilon t}\left(\int_0^{\beta}\frac{\partial\hat{F}(t+i\lambda)}{\partial t}d\lambda\,\hat{\rho}_0\right)dt$$

In equilibrium conditions we have no current flow, namely $\langle J_\alpha(\mathbf{r})\rangle = 0$. Therefore the expectation value of the current operator entirely comes from the correction to $\hat{\rho}_0$:

$$\langle J_\alpha(\mathbf{r})\rangle_{\text{n.e.}} = \lim_{\epsilon\to 0^+} e^{\epsilon t}\sum_n \langle n|\,\hat{f}J_\alpha(\mathbf{r})\,|n\rangle = \sum_n \langle n|\,\hat{f}J_\alpha(\mathbf{r})\,|n\rangle =$$
$$= \lim_{\epsilon\to 0^+}\int_{-\infty}^0 e^{\epsilon t'}\left(\int_0^\beta \sum_n \langle n|\,\hat{\rho}_0 J_\alpha(\mathbf{r})\frac{\partial\hat{F}(t'+i\lambda)}{\partial t'}\,|n\rangle\,d\lambda\right)dt'$$

Notice that the factor $e^{\epsilon t}$ in front of $\hat{f}$ is irrelevant and vanishes after taking the (first) limit $\epsilon\to 0^+$, this ensures that $\langle J_\alpha(\mathbf{r})\rangle_{\text{n.e.}}$ actually does not depend on time. On the contrary, the factor $e^{\epsilon t'}$ that appears inside the integral in dt' is crucial and therefore it is necessary to preserve its limit until the end of the calculation. At this point, we just need a reasonable expression for $\partial\hat{F}(t+i\lambda)/\partial t$. According to our previous discussion, the time derivative of $\hat{F}(t)$ is linked to entropy production rate as follows:

$$\frac{d\langle\hat{F}(t)\rangle_{\text{n.e.}}}{dt} = T\frac{\partial S_{\text{irr}}}{\partial t} = \frac{1}{\beta}\sum_\alpha\int_{\mathbb{R}^{\text{d}}}\langle J_\alpha(\mathbf{r})\rangle_{\text{n.e.}}X_\alpha(\mathbf{r})d^{\text{d}}\mathbf{r}$$

Therefore the corresponding operator, within interaction representation, must have the following form:

$$\frac{\partial\hat{F}(t)}{\partial t} = \frac{1}{\beta}\sum_\alpha\int_{\mathbb{R}^{\text{d}}} J_\alpha(\mathbf{r},t)X_\alpha(\mathbf{r})d^{\text{d}}\mathbf{r}$$

Our expression for the current becomes:

$$\langle J_\alpha(\mathbf{r})\rangle_{\text{n.e.}} = \lim_{\epsilon\to 0^+}\int_{-\infty}^0 e^{\epsilon t}\left(\int_0^\beta\sum_n\langle n|\,\hat{\rho}_0 J_\alpha(\mathbf{r})\frac{\partial\hat{F}(t+i\lambda)}{\partial t}\,|n\rangle\,d\lambda\right)dt =$$
$$= \lim_{\epsilon\to 0^+}\frac{1}{\beta}\sum_\beta\int_{\mathbb{R}^{\text{d}}}\left[\int_{-\infty}^0 e^{\epsilon t}\left(\int_0^\beta\sum_n\langle n|\,\hat{\rho}_0 J_\alpha(\mathbf{r},0)J_\beta(\mathbf{r}',t+i\lambda)\,|n\rangle\,d\lambda\right)dt\right]X_\beta(\mathbf{r}')d^{\text{d}}\mathbf{r}'$$

We used the trivial identity $J_\alpha(\mathbf{r}) = J_\alpha(\mathbf{r},0)$, which is a direct consequence of the equation of time evolution in interaction picture. By comparison with the definition of $Z_{\alpha\beta}(\mathbf{r}-\mathbf{r}')$ we deduce:

$$Z_{\alpha\beta}(\mathbf{r}-\mathbf{r}') = \lim_{\epsilon\to 0^+}\frac{1}{\beta}\int_{-\infty}^0 e^{\epsilon t}\left(\int_0^\beta\langle J_\alpha(\mathbf{r},0)J_\beta(\mathbf{r}',t+i\lambda)\rangle d\lambda\right)dt =$$
$$= \lim_{\epsilon\to 0^+}\frac{1}{\beta}\int_{-\infty}^0 e^{\epsilon t}\left(\int_0^\beta\langle J_\alpha(\mathbf{r}-\mathbf{r}',-t-i\lambda)J_\beta(\mathbf{0},0)\rangle d\lambda\right)dt$$

After integrating over space, we obtain exactly the expression for $Z_{\alpha\beta}$ exhibited in equation (2.11). Now we are going to express this relation in a more convenient form. First of all, let's introduce the Fourier transform of the current-current correlation function, in analogy with what was done previously:

$$\langle J_\alpha J_\beta\rangle(\mathbf{q},\omega) \coloneqq \mathcal{F}_{\mathbf{r},t}\Big[\langle J_\alpha(\mathbf{r},t)J_\beta(\mathbf{0},0)\rangle\Big]$$

By expliciting inverse Fourier transform:

$$\int_{\mathbb{R}^{\mathrm{d}}} \langle J_\alpha(\mathbf{r},t) J_\beta(\mathbf{0},0)\rangle d^{\mathrm{d}}\mathbf{r} = \int_{-\infty}^{+\infty} \langle J_\alpha J_\beta\rangle(\mathbf{q}=\mathbf{0},\omega) e^{-i\omega t}\frac{d\omega}{2\pi}$$

Therefore:

$$\begin{aligned} Z_{\alpha\beta} &= \lim_{\epsilon\to 0^+}\frac{1}{\beta}\int_{-\infty}^{0} e^{\epsilon t}\left[\int_0^\beta\left(\int_{-\infty}^{+\infty}\langle J_\alpha J_\beta\rangle(\mathbf{q}=\mathbf{0},\omega)e^{+i\omega t}e^{-\lambda\omega}\frac{d\omega}{2\pi}\right)d\lambda\right]dt = \\ &= \lim_{\epsilon\to 0^+}\frac{1}{\beta}\int_{-\infty}^{+\infty}\langle J_\alpha J_\beta\rangle(\mathbf{q}=\mathbf{0},\omega)\left(\int_{-\infty}^{0}e^{(\epsilon+i\omega)t}dt\right)\left(\int_0^\beta e^{-\lambda\omega}d\lambda\right)\frac{d\omega}{2\pi} = \\ &= \lim_{\epsilon\to 0^+}\frac{1}{\beta}\int_{-\infty}^{+\infty}\langle J_\alpha J_\beta\rangle(\mathbf{q}=\mathbf{0},\omega)\frac{1}{\epsilon+i\omega}\frac{1-e^{-\beta\omega}}{\omega}\frac{d\omega}{2\pi} = \\ &= \lim_{\epsilon\to 0^+}\frac{1}{\beta}\int_{-\infty}^{+\infty}\frac{1}{\epsilon+i\omega}\frac{\chi''_{\alpha\beta}(\mathbf{q}=\mathbf{0},\omega)}{\omega}\frac{d\omega}{\pi} = \end{aligned}$$

Notice that we used the fluctuation-dissipation relation. Finally, we exploit the fact that $Z_{\alpha\beta}\in\mathbb{R}$, so we get the very compact result:

$$Z_{\alpha\beta} = \frac{1}{\beta}\lim_{\omega\to 0}\frac{\chi''_{\alpha\beta}(\mathbf{q}=\mathbf{0},\omega)}{\omega}$$

First of all, notice that the limit in this equation is regular, as a consequence of $\chi''_{\alpha\beta}(\mathbf{q},\omega=0)=0$. Moreover, since $\omega\chi''_{\alpha\beta}(\mathbf{q},\omega)$ is a positive (semi)definite matrix, $Z_{\alpha\beta}$ must be positive (semi)definite as well, as we expected. Our calculation also clarifies why it is necessary to fix $\mathbf{q}=\mathbf{0}$ before taking the limit $\omega\to 0$. We remind that, if we had used the opposite convention for the sign in the definition of $\delta H(t)$, the fluctuation-dissipation relation would have differed from the one we exhibited by an overall minus sign, which would also appear in the expression for $Z_{\alpha\beta}$.

For the particular case of symmetric currents under time-reversal, we are allowed to substitute $\chi''_{\alpha\beta}(\mathbf{q}=\mathbf{0},\omega)$ with $\mathrm{Im}\chi_{\alpha\beta}(\mathbf{q}=\mathbf{0},\omega)$ in the calculation of $Z_{\alpha\beta}$. Our final result is therefore:

$$Z_{\alpha\beta} = \frac{1}{\beta}\lim_{\omega\to 0}\frac{\mathrm{Im}\chi_{\alpha\beta}(\mathbf{q}=\mathbf{0},\omega)}{\omega}$$

Appendix D

Regularization of some non-convergent bosonic Matsubara series

Standard Matsubara sums

Let's begin by considering the decomposition of two simple analytic functions, which are valid for any $z \in \mathbb{C}$:

$$\frac{\sin(z)}{z} = \prod_{n=1}^{\infty} \left(1 - \frac{z^2}{\pi^2 n^2}\right) \qquad \frac{\sinh(z)}{z} = \prod_{n=1}^{\infty} \left(1 + \frac{z^2}{\pi^2 n^2}\right)$$

By taking the logarithm of both sides of the second of these two equations, and by deriving both sides of the resulting expression with respect to z, we will get the following identity:

$$\sum_{n \in \mathbb{Z}} \frac{1}{z^2 + n^2\pi^2} = \frac{\cosh(z)}{z \sinh(z)}$$

This series converges for any $z \in \mathbb{Z}$ except for $z = 0$, where it has a double pole, and for $z = in\pi$ with $n \in \mathbb{Z} \setminus \{0\}$, where it has simple poles. It can be useful to express this series as a sum over Matsubara frequencies. The first step is to replace z with $\beta\omega$:

$$\frac{1}{\beta} \sum_{n \in \mathbb{Z}} \frac{1}{\omega^2 + \omega_n^2} = \frac{\cosh(\beta\omega)}{\omega \sinh(\beta\omega)}$$

Where we identified $\omega_n = \pi n/\beta$. Note that both ω and ω_n have the dimension of an energy. This equation does not represent a Matsubara sum, strictly speaking. The reason is that Matsubara sums are restricted only to even or odd integers, while our sum run over all integers. In order to restrict ourselves only to bosonic frequencies, it is sufficient to observe that the variable n of the sum always appears divided by β, so replacing β with $\beta/2$ has the effect of selecting only the even integers in the sum. In order to get the fermionic sum it is sufficient to consider the difference between the sum over all integers and the sum over only even integers. This is a quite general approach for selecting only even or odd frequencies in a sum that runs

over all integers, where the dependence on the integer number n is only through ω_n. The explicit calculation for our case provides:

$$\frac{1}{\beta}\sum_{n\,\mathrm{even}}\frac{1}{\omega^2+\omega_n^2}=\frac{\cosh\Big(\frac{\beta\omega}{2}\Big)}{2\omega\sinh\Big(\frac{\beta\omega}{2}\Big)}\qquad\frac{1}{\beta}\sum_{n\,\mathrm{odd}}\frac{1}{\omega^2+\omega_n^2}=\frac{\sinh\Big(\frac{\beta\omega}{2}\Big)}{2\omega\cosh\Big(\frac{\beta\omega}{2}\Big)}$$

It should be stressed that all the series we exhibited in this section are regular, in the sense that they actually converge at a finite value (except, of course, at poles). In quantum many-body theory, summations like these are often encountered:

$$\frac{1}{\beta}\sum_{n\,\mathrm{even}}\frac{1}{i\omega_n-\omega}\qquad\frac{1}{\beta}\sum_{n\,\mathrm{odd}}\frac{1}{i\omega_n-\omega}\tag{D.1}$$

These sums, unlike the previous ones, do not converge in the sense foreseen by the theory of numerical series. The standard regularization techniques for these kinds series usually involve the application of the residue theorem. The method we propose here consists of making the following identification:

$$\sum_{n\in\mathbb{Z}}\frac{1}{i\omega_n-\omega}=-\omega\sum_{n\in\mathbb{Z}}\frac{1}{\omega^2+\omega_n^2}$$

Strictly speaking, this identity is true only if the summation which appears on the left-hand side is interpreted as the $N\to\infty$ limit of the sum from $n=-N$ to N (where $N\in\mathbb{N}$) of the quantity $(i\omega_n-\omega)^{-1}$. By assuming that this identification has general validity, we can write:

$$\frac{1}{\beta}\sum_{n\,\mathrm{even}}\frac{1}{i\omega_n-\omega}=-\frac{\cosh\Big(\frac{\beta\omega}{2}\Big)}{2\sinh\Big(\frac{\beta\omega}{2}\Big)}=-\left(\frac{1}{e^{\beta\omega}-1}+\frac{1}{2}\right)$$

$$\frac{1}{\beta}\sum_{n\,\mathrm{odd}}\frac{1}{i\omega_n-\omega}=-\frac{\sinh\Big(\frac{\beta\omega}{2}\Big)}{2\cosh\Big(\frac{\beta\omega}{2}\Big)}=\frac{1}{e^{\beta\omega}+1}-\frac{1}{2}$$

Which are precisely the Bose and Fermi functions (up to an overall minus sign for the former) with the addition of the zero-point term. Of course, the calculation carried out with the residue theorem would have led to a completely similar result.

In the following paragraphs we will provide systematic techniques for carrying out some formally non-convergent infinite sums, such as those expressed by equations (D.1), focusing in particular on the case of bosonic sums. We would like to point out that many of the identities we will exhibit are only formal and should not be taken as equalities in the strict sense. Furthermore, it must be kept in mind that for some of the non-convergent summations that we will exhibit there is a margin of arbitrariness in assigning them a finite value. The scheme that we will exhibit does not claim to be universally valid, but only to have internal coherence and to reproduce the known results within the appropriate limits.

Regularization of divergent sums through the analytic continuation of the Riemann zeta function

The Riemann zeta function is a mathematical function of a complex variable z which, for $\mathrm{Re}(z) > 1$, is defined as follows:

$$\zeta(z) := \sum_{n=1}^{\infty} \frac{1}{n^z}$$

The definition of $\zeta(z)$ can be extended to the whole complex plane via analytic continuation, except for $z = 1$, where the function has a simple pole with residue 1. The idea behind the regularization technique that we have in mind is to express the divergent series in a Riemann zeta function form, in order to attribute to it the value foreseen by the latter's analytic continuation. However, we must be careful of the fact that $\zeta(z)$ is defined as a sum over the natural numbers, while the sums over the Matsubara frequencies run over both positive and negative integers. The following observation may help:

$$a_n = a_{-n} \quad \Longrightarrow \quad \sum_{n\,\in\,\mathbb{Z}} a_n = a_0 + 2\sum_{n=1}^{\infty} a_n$$

Where a_n is a generic function from $\mathbb{Z}$ to $\mathbb{C}$. Strictly speaking, this identity holds only if all the sums appearing in those expressions are convergent, however we will assume that it also holds for sums that do not converge, where possible. A case of interest, for instance, is the infinite summation of a constant quantity, which can be regularized as follows:

$$\sum_{n=1}^{\infty} k = k\sum_{n=1}^{\infty} 1 = k\,\zeta(0) = -\frac{1}{2}k \qquad \sum_{n\,\in\,\mathbb{Z}} k = k + 2\sum_{n=1}^{\infty} k = k\,(1 + 2\zeta(0)) = 0$$

Another sum of interest to us is the infinite summation of $\log(n)$, which is related to $\zeta(z)$ by the following relation:

$$\sum_{n=1}^{\infty} \log(n) = -\zeta'(0) = \frac{1}{2}\log(2\pi)$$

Which would imply, in particular:

$$\sum_{n=1}^{\infty} \log(2\pi n) = \sum_{n=1}^{\infty} \log(n) + \sum_{n=1}^{\infty} \log(2\pi) = \frac{1}{2}\log(2\pi) - \frac{1}{2}\log(2\pi) = 0$$

This last relation allows us to regularize another useful sum. Let's go back to our decomposition for $\sinh(z)/z$, replace z with $z/2$ and then take the logarithm of both sides. Finally, by exploiting the fact that the (regularized) sum of $\log(2\pi n)$ over all natural numbers is zero, we get the following identity:

$$\sum_{n=1}^{\infty} \log\Big((2\pi n)^2 + z^2\Big) = \log\Big(2\sinh\Big(\frac{z}{2}\Big)\Big) - \log(z) \tag{D.2}$$

When calculating logarithms, we will always use the convention $\mathrm{Arg}(z) \in (-\pi, \pi]$ for the phase of complex number z, this allows us to safely use the identity $\log(z^2) = 2\log(z)$ for $\mathrm{Re}(z) > 0$. By taking this observation into account, we can express the previous identity in a more compact way:

$$\frac{1}{2}\sum_{n\in\mathbb{Z}} \log\Big((2\pi n)^2 + z^2\Big) = \log\bigg(2\sinh\Big(\frac{z}{2}\Big)\bigg) \qquad \text{where} \quad \mathrm{Re}(z) > 0$$

With the identities we have exhibited so far we can regularize another interesting series, namely the sum of $\log(2\pi n + z)$ over all positive integers n. First of all, let's define the function $\varsigma(z)$ as:

$$\varsigma(z) \coloneqq \sum_{n=1}^{\infty} \log(n + z)$$

First of all, notice that $\varsigma(0) = -\zeta'(0)$. Moreover, if we treat the series that defines $\varsigma(z)$ as a convergent series, we can interpret the difference $\varsigma(z) - \varsigma(z-1)$ as a telescopic series with initial term $\log(z)$. These two properties can be expressed compactly through the following system:

$$\begin{cases} \varsigma(0) = \dfrac{1}{2}\log(2\pi) \\ \varsigma(z) - \varsigma(z-1) = -\log(z) \end{cases}$$

And the simplest analytic function which satisfies both equations is:

$$\varsigma(z) = -\log\Big(\Gamma(1+z)\Big) + \frac{1}{2}\log(2\pi)$$

By putting this result together with the definition of $\varsigma(z)$ in series form, and by using once again the regularized expression of the sum of $\log(2\pi n + z)$, we obtain the following useful identity:

$$\sum_{n=1}^{\infty} \log(2\pi n + z) = -\log\bigg(\Gamma\Big(1 + \frac{z}{2\pi}\Big)\bigg) \tag{D.3}$$

The coherence between equations (D.2) and (D.3) is ensured by the following identity, which is a direct consequence of the definition of $\Gamma(z)$ and the Euler's reflection formula [159]:

$$\Gamma\Big(1 + \frac{iz}{2\pi}\Big)\,\Gamma\Big(1 - \frac{iz}{2\pi}\Big) = \frac{z}{2\sinh\Big(\frac{z}{2}\Big)} \tag{D.4}$$

The usefulness of summations involving multiples of 2π is that they are closely related to bosonic Matsubara sums. In particular, the sum appearing in (D.2) is useful for the description of an undamped bosonic system, while the one appearing in (D.3) generalizes the previous one also to the damped case.

Removal of the zero-point energy

An immediate application of the equations we have just shown is the calculation of the internal energy of a system of free phonons with dispersion $\omega_{\mathbf{k}}$ such that $\omega_{\mathbf{k}} > 0$ at any wave vector $\mathbf{k}$:

$$\mathcal{D}(\omega_n, \mathbf{k}) = \frac{2\omega_{\mathbf{k}}}{\omega_n^2 + \omega_{\mathbf{k}}^2}$$

The Helmholtz free energy for this system is provided by equation (2.13), the Matsubara sum that appears can be treated by exploiting the relations we have shown so far:

$$F_b = \frac{1}{2\beta} \sum_{\mathbf{k}} \sum_{n\,\text{even}} \log\Big(\frac{\beta^2(\omega_n^2 + \omega_{\mathbf{k}}^2)}{2\pi\beta\omega_{\mathbf{k}}} \Big)$$
$$= \frac{1}{2\beta} \sum_{\mathbf{k}} \sum_{n\,\in\,\mathbb{Z}} \log\big[(2\pi n)^2 + (\beta\omega_{\mathbf{k}})^2\big] = \frac{1}{\beta} \sum_{\mathbf{k}} \log\Big(2\sinh\Big(\frac{\beta\omega_{\mathbf{k}}}{2}\Big)\Big)$$

And the internal energy is simply given by:

$$U_b = \frac{\partial}{\partial\beta}\,(\beta F_b) = \sum_{\mathbf{k}} \Big(\frac{1}{e^{\beta\omega_{\mathbf{k}}} - 1} + \frac{1}{2} \Big)\omega_{\mathbf{k}}$$

Which is a well-known result, and also includes the zero-point energy term. Although in this case the presence of the additional zero-point term is harmless, it becomes problematic when we consider a damped system described by a propagator of the form (2.2). For the sake of concreteness, let's consider the case of charge density fluctuations as an exemplary case for a damped collective mode. We can therefore repeat our calculations taking (2.2) as the expression for the bosonic propagator, let's strart from the expression for the generalized free energy:

$$F_b = \frac{1}{2\beta} \sum_{\mathbf{k}} \sum_{n\,\text{even}} \log\Big(\frac{\beta^2(\omega_n^2 + \gamma\Omega|\omega_n| + \Omega m_{\mathbf{k}})}{\pi\beta\Omega} \Big) =$$
$$= \frac{1}{\beta} \sum_{\mathbf{k}} \Big[\frac{1}{2} \log(\beta^2 \omega_{\mathbf{k}}^+ \omega_{\mathbf{k}}^-) + \sum_{n=1}^{\infty} \log(2\pi n + i\beta\omega_{\mathbf{k}}^+) + \sum_{n=1}^{\infty} \log(2\pi n - i\beta\omega_{\mathbf{k}}^-) \Big] =$$
$$= \frac{1}{\beta} \sum_{\mathbf{k}} \Big[\log\Big(\beta\sqrt{\omega_{\mathbf{k}}^+ \omega_{\mathbf{k}}^-}\Big) - \log\Big(\Gamma\Big(1 + i\frac{\beta\omega_{\mathbf{k}}^+}{2\pi}\Big)\Gamma\Big(1 - i\frac{\beta\omega_{\mathbf{k}}^-}{2\pi}\Big)\Big)\Big]$$

Where $\omega_{\mathbf{k}}^+$ and $\omega_{\mathbf{k}}^-$ are defined through relations analogous to (3.9) and (3.10), with the difference that M is replaced by $m_{\mathbf{k}}$, namely:

$$\omega_{\mathbf{k}}^+ := \sqrt{\Omega m_{\mathbf{k}} - \frac{\gamma^2\Omega^2}{4}} - i\frac{\gamma\Omega}{2} \qquad \omega_{\mathbf{k}}^- := \sqrt{\Omega m_{\mathbf{k}} - \frac{\gamma^2\Omega^2}{4}} + i\frac{\gamma\Omega}{2} \qquad \text{for } \gamma^2 < \frac{4m_{\mathbf{k}}}{\Omega}$$

$$i\omega_{\mathbf{k}}^+ = \frac{\gamma\Omega}{2}\left(1 - \sqrt{1 - \frac{4m_{\mathbf{k}}}{\gamma^2\Omega}}\right) \qquad i\omega_{\mathbf{k}}^- = -\frac{\gamma\Omega}{2}\left(1 + \sqrt{1 - \frac{4m_{\mathbf{k}}}{\gamma^2\Omega}}\right) \qquad \text{for } \gamma^2 \geq \frac{4m_{\mathbf{k}}}{\Omega}$$

Of course, both $m_{\mathbf{k}}$ and Ω are strictly positive. By construction, both $\omega_{\mathbf{k}}^{+}$ and $\omega_{\mathbf{k}}^{-}$ have non-negative real parts. Moreover, the inequalities $\mathrm{Re}(i\omega_{\mathbf{k}}^{+}) \geq 0$ and $\mathrm{Re}(-i\omega_{\mathbf{k}}^{-}) \geq 0$ hold. The expression for the generalized internal energy is:

$$U_b = \sum_{\mathbf{k}} \Big[\frac{1}{\beta} - \frac{i\omega_{\mathbf{k}}^{+}}{2\pi} \psi\Big(1 + i\frac{\beta\omega_{\mathbf{k}}^{+}}{2\pi}\Big) + \frac{i\omega_{\mathbf{k}}^{-}}{2\pi} \psi\Big(1 - i\frac{\beta\omega_{\mathbf{k}}^{-}}{2\pi}\Big) \Big]$$

The agreement with the undamped case is given by the following identity for the digamma function, which is a direct consequence of equation (D.4):

$$\frac{1}{z} + \frac{\psi\Big(1 + \frac{iz}{2\pi}\Big) - \psi\Big(1 - \frac{iz}{2\pi}\Big)}{2\pi i} = \frac{1}{e^z - 1} + \frac{1}{2} \tag{D.5}$$

This expression for U_b has the problem that is logarithmically divergent at low temperatures, inter alia with a negative prefactor. This is clearly a unphysical result, which directly follows from the inclusion of the zero-point energy.

In order to remove the zero point term we can proceed manually, by appropriately changing the results of the non-convergent sums. What we require is that the product βF_b vanishes in the low temperature limit ($\beta \to \infty$), so we need to correct by hand expressions (D.2) and (D.3) in such a way that the thermodynamic potentials they describe satisfy this condition, while maintaining an internal consistency. For the non-dissipative system it is sufficient to make the following substitution:

$$\frac{1}{2} \sum_{n \in \mathbb{Z}} \log\big[(2\pi n)^2 + z^2\big] \;\longrightarrow\; \log\Big(2\sinh\Big(\frac{z}{2}\Big)\Big) - \frac{z}{2} \tag{D.6}$$

Which is valid under the condition $\mathrm{Re}(z) > 0$, it is straightforward to observe that this substitution perfectly removes the term $+\omega_{\mathbf{k}}/2$ which appears in the $\mathbf{k}$ sum which provides U_b for the case without damping. The damped case is more delicate, the basic idea is to apply a substitution of this kind on the right-hand side of equation (D.3):

$$-\log\Big(\Gamma\Big(1 + \frac{z}{2\pi}\Big)\Big) \;\longrightarrow\; -\log\Big(\Gamma\Big(1 + \frac{z}{2\pi}\Big)\Big) + \phi\Big(\frac{z}{2\pi}\Big)$$

Where the function $\phi(z)$ must satisfy:

$$\begin{cases} \lim\limits_{\substack{|z|\to\infty \\ \mathrm{Re}(z)>0}} \Big[-\log(\Gamma(1+z)) + \phi(z) + \dfrac{1}{2}\log(2\pi z) \Big] = 0 \\[2ex] \phi\Big(\dfrac{iz}{2\pi}\Big) + \phi\Big(-\dfrac{iz}{2\pi}\Big) = -\dfrac{z}{2} \end{cases}$$

The first constraint is due to the requirement that the contribution to free energy given by a single mode (of course, with positive real part) must vanish at $\beta \to \infty$, and we require this to happen separately for the two poles of the propagator. The

second relation is a simple consequence of the consistency with substitution (D.6). The simplest function which satisfies both requirements is:

$$\phi(z) = z\,(\log(z) - 1)$$

Of course, this choice is not unique. However, we shall see that this function is the only one that is consistent with the calculation performed alternatively by means of residue theorem. Given this expression for $\phi(z)$, we conclude that the substitution to be applied to the sum (D.3) is the following:

$$\sum_{n=1}^{\infty} \log(2\pi n + z) \;\longrightarrow\; -\log\Big(\Gamma\Big(1+\frac{z}{2\pi}\Big)\Big) + \frac{z}{2\pi}\Big(\log\Big(\frac{z}{2\pi}\Big) - 1\Big)$$

With this substitution, the new expressions for F_b and U_b are the following:

$$\begin{aligned} F_b = \frac{1}{\beta}\sum_{\mathbf{k}}\Big[&-\log\Big(\Gamma\Big(1+i\frac{\beta\omega_{\mathbf{k}}^{+}}{2\pi}\Big)\Big) + i\frac{\beta\omega_{\mathbf{k}}^{+}}{2\pi}\Big(\log\Big(i\frac{\beta\omega_{\mathbf{k}}^{+}}{2\pi}\Big) - 1\Big) + \frac{1}{2}\log\Big(2\pi i\frac{\beta\omega_{\mathbf{k}}^{+}}{2\pi}\Big) + \\ &-\log\Big(\Gamma\Big(1-i\frac{\beta\omega_{\mathbf{k}}^{-}}{2\pi}\Big)\Big) - i\frac{\beta\omega_{\mathbf{k}}^{-}}{2\pi}\Big(\log\Big(-i\frac{\beta\omega_{\mathbf{k}}^{-}}{2\pi}\Big) - 1\Big) + \frac{1}{2}\log\Big(-2\pi i\frac{\beta\omega_{\mathbf{k}}^{-}}{2\pi}\Big)\Big] \end{aligned} \tag{D.7}$$

$$\begin{aligned} U_b = \frac{1}{\beta}\sum_{\mathbf{k}}\Big[&1 + i\frac{\beta\omega_{\mathbf{k}}^{+}}{2\pi}\Big(\log\Big(i\frac{\beta\omega_{\mathbf{k}}^{+}}{2\pi}\Big) - \psi\Big(1+i\frac{\beta\omega_{\mathbf{k}}^{+}}{2\pi}\Big)\Big) + \\ &-i\frac{\beta\omega_{\mathbf{k}}^{-}}{2\pi}\Big(\log\Big(-i\frac{\beta\omega_{\mathbf{k}}^{-}}{2\pi}\Big) - \psi\Big(1-i\frac{\beta\omega_{\mathbf{k}}^{-}}{2\pi}\Big)\Big)\Big] \end{aligned} \tag{D.8}$$

It is worth noticing that, by construction, the two following limits hold:

$$\lim_{\gamma\to 0^+} F_b = \frac{1}{\beta}\sum_{\mathbf{k}} \log\Big(1 - e^{-\beta\sqrt{\Omega m_{\mathbf{k}}}}\Big) \qquad \lim_{\gamma\to 0^+} U_b = \sum_{\mathbf{k}} \frac{\sqrt{\Omega m_{\mathbf{k}}}}{e^{\beta\sqrt{\Omega m_{\mathbf{k}}}} - 1}$$

These limits ensure that, in the undamped limit, our expressions for F_b and U_b perfectly reproduce the well-known case of the ideal phonon gas, with dispersion $\omega_{\mathbf{k}} = \sqrt{\Omega m_{\mathbf{k}}}$.

Regularization through the residue theorem

A similar way of carrying out the calculation consists in differentiating βF_b with respect to the temperature before performing the Matsubara sum, and then carrying out the sum by applying the residue theorem. First of all, let's express internal

energy in the form of Matsubara sum:

$$U_b = \frac{\partial}{\partial\beta}\left(\beta F_b\right) = -k_{\mathrm{B}}T^2\frac{\partial}{\partial T}\left(\beta F_b\right) =$$

$$= \frac{k_{\mathrm{B}}T}{2}\sum_{\mathbf{k}}\sum_{n\,\mathrm{even}}\left[1-\frac{\gamma|\omega_n|+\dfrac{2\omega_n^2}{\Omega}}{m_{\mathbf{k}}+\gamma|\omega_n|+\dfrac{\omega_n^2}{\Omega}}\right] = \frac{1}{2\beta}\sum_{\mathbf{k}}\sum_{n\,\mathrm{even}}\left[-1+\frac{2m_{\mathbf{k}}+\gamma|\omega_n|}{m_{\mathbf{k}}+\gamma|\omega_n|+\dfrac{\omega_n^2}{\Omega}}\right]$$

$$= \sum_{\mathbf{k}}\left[\frac{1}{\beta}\sum_{n\,\mathrm{even}}\frac{m_{\mathbf{k}}}{m_{\mathbf{k}}+\gamma|\omega_n|+\dfrac{\omega_n^2}{\Omega}}+\frac{1}{2\beta}\sum_{n\,\mathrm{even}}\frac{\gamma|\omega_n|}{m_{\mathbf{k}}+\gamma|\omega_n|+\dfrac{\omega_n^2}{\Omega}}\right]$$

Here, we got rid of the constant term in the ω_n by identifying it with $1+2\zeta(0)$, similarly to what we have already done in the previous calculation. Notice that the second sum is logarithmically divergent, unless $\gamma = 0$.

Since only rational functions of ω_n appear in the summations, the residue theorem can be conveniently applied. Of course, the calculation cannot give the second summation a finite result, however it is possible to formally convert the summation into an integral, which will also be logarithmically divergent. The expression found is the following:

$$U_b = \sum_{\mathbf{k}}\int_0^\infty\left(\frac{1}{e^{\beta\omega}-1}+\frac{1}{2}\right)\frac{\gamma\omega\left(m_{\mathbf{k}}+\dfrac{\omega^2}{\Omega}\right)}{\left(m_{\mathbf{k}}-\dfrac{\omega^2}{\Omega}\right)^2+\gamma^2\omega^2}\frac{d\omega}{\pi}$$

Although this expression has the inconvenience of still being in the form of an integral, the contribution of the zero-point energy clearly emerges from it, so it can be easily removed by hand. The expressions obtained for F_b and U_b using this approach, after removing the zero-point energy, are the following:

$$F_b = \frac{1}{\beta}\sum_{\mathbf{k}}\int_0^\infty\log(1-e^{-\beta\omega})\frac{\gamma\left(m_{\mathbf{k}}+\dfrac{\omega^2}{\Omega}\right)}{\left(m_{\mathbf{k}}-\dfrac{\omega^2}{\Omega}\right)^2+\gamma^2\omega^2}\frac{d\omega}{\pi}$$

$$U_b = \sum_{\mathbf{k}}\int_0^\infty\frac{1}{e^{\beta\omega}-1}\frac{\gamma\omega\left(m_{\mathbf{k}}+\dfrac{\omega^2}{\Omega}\right)}{\left(m_{\mathbf{k}}-\dfrac{\omega^2}{\Omega}\right)^2+\gamma^2\omega^2}\frac{d\omega}{\pi}$$

These two integrals are convergent and have the correct low temperature behavior. In order to show the coherence between these last expressions and those exhibited previously, we first observe that F_b can be written alternatively as follows:

$$F_b = \frac{1}{\beta}\sum_{\mathbf{k}}\int_0^\infty\log(1-e^{-x})\left[\frac{2i\dfrac{\beta\omega_{\mathbf{k}}^+}{2\pi}}{x^2+\left(2\pi i\dfrac{\beta\omega_{\mathbf{k}}^+}{2\pi}\right)^2}+\frac{-2i\dfrac{\beta\omega_{\mathbf{k}}^-}{2\pi}}{x^2+\left(-2\pi i\dfrac{\beta\omega_{\mathbf{k}}^-}{2\pi}\right)^2}\right]dx$$

Namely F_b can be splitted into two parts, each of which is the same function evaluated once at $i\beta\omega_{\mathbf{k}}^{+}/(2\pi)$ and the other time at $-i\beta\omega_{\mathbf{k}}^{-}/(2\pi)$. Since $\omega_{\mathbf{k}}^{+}$ and $\omega_{\mathbf{k}}^{-}$ are linearly independent of each other, this splitting is unique. The expression we found previously for F_b, provided by (D.7), is also split in a similar way, and even in this case the splitting is unique. The bridge between the two forms is provided by Binet's second integral formula [160], which is valid for any $z \in \mathbb{C}$ such that $\mathrm{Re}(z) > 0$:

$$\int_0^\infty \log(1-e^{-x})\frac{2z}{x^2+(2\pi z)^2}dx = -\log\big(\Gamma(1+z)\big) + z\left(\log(z)-1\right) + \frac{1}{2}\log(2\pi z)$$

This identity clearly shows that the expression we have chosen for $\phi(z)$ is the only one possible. Indeed, if we had added to $\phi(z)$ a non-trivial function of z in accordance with our constraints we would have found a discrepancy between the two forms we found for F_b. Obviously, the coherence between the two forms we found for F_b implies coherence for the two forms for U_b.

It is worth noticing that, for our purposes, the $\mathrm{Re}(z) > 0$ request is not restrictive. In fact, the quantity on the right side of Binet's formula will always be evaluated in either $z = i\omega_{\mathbf{k}}^{+}$ or $z = -i\omega_{\mathbf{k}}^{-}$, and both satisfy $\mathrm{Re}(z) > 0$ for $\gamma > 0$, regardless of the damping regime. The only case that must be treated separately is the one in which γ is strictly equal to zero, but in this case we are allowed to use all the relations we have shown for the undamped case, taking care to apply substitution (D.6) to remove the zero-point energy. Relation (D.4) guarantees continuity between the natively undamped case and the case where the absence of damping is reached through $\gamma \to 0^+$ limit.

Appendix E

Calculations for the bosonic effective density of states

Here we show some details behind the calculations for the effective density of states N_ω^{CDF} introduced in section 4.2. First of all, it is convenient to express N_ω^{CDF} in terms of the function $\varrho(\varepsilon)$, for which we recall the definition:

$$N_\omega^{CDF} \coloneqq \frac{\theta(\omega)}{\pi}\int_{-\infty}^{+\infty}\frac{\gamma\left(\varepsilon+m_c+\dfrac{\omega^2}{\Omega}\right)}{\left(\varepsilon+m_c-\dfrac{\omega^2}{\Omega}\right)^2+\gamma^2\omega^2}\varrho(\varepsilon)d\varepsilon \qquad \varrho(\varepsilon)\coloneqq\frac{1}{N}\sum_{\mathbf{q}}\delta(\varepsilon+m_c-m_{\mathbf{q}})$$

Strictly speaking, this definition of the function $\varrho(\varepsilon)$ is only valid in the case in which there is no dispersion along z-axis. In this case, according to the approximation described in section 4.2, we can express $\varrho(\varepsilon)$ in the following simple form:

$$\varrho(\varepsilon)=\frac{\theta(\varepsilon)\,\theta(\pi\nu-\varepsilon)}{\pi\nu} \tag{E.1}$$

In order to prove this relation, it is convenient to consider the more general case in which there is also dispersion along the z-axis, then the two-dimensional case will be recovered in the $\nu_\perp \to 0$ limit, which can be taken at the end of the calculation. In this case we have:

$$\varrho(\varepsilon)\coloneqq\frac{v_{\text{uc}}}{V_{3D}}\sum_{\mathbf{q},\,q_z}\delta(\varepsilon+m_c-m_{\mathbf{q},q_z})=v_{\text{uc}}\int_{-\frac{\pi}{d}}^{+\frac{\pi}{d}}\left[\iint_{FBZ}\delta(\varepsilon+m_c-m_{\mathbf{q},q_z})\frac{dq_xdq_y}{4\pi^2}\right]\frac{dq_z}{2\pi}$$

Where *FBZ* denotes the two-dimensional First Brillouin zone. As we explained in section 4.2, in order to carry out the double integral in dq_x and dq_y we divide the two-dimensional Brillouin zone into four regions along the two diagonals and approximate each of these four regions with a circle centered in each of the four wave vectors $\mathbf{q}_c$ and of radius $\sqrt{\pi}$, so that each of the circles has an area equal to 1/4 that of the Brillouin zone. Of course, we carry out the resulting integral in polar coordinates by considering only one of the circles, and by multiplying the result by a factor of 4. We get:

$$\varrho(\varepsilon) \simeq 4v_{\text{uc}} \int_{-\frac{\pi}{d}}^{+\frac{\pi}{d}} \left[\int_0^{\sqrt{\pi}} \delta(\varepsilon - \nu q^2 - \nu_\perp q_z^2) \frac{2\pi q\, dq}{4\pi^2} \right] \frac{dq_z}{2\pi} =$$
$$= \frac{v_{\text{uc}}}{\pi^2 \nu} \int_0^{+\frac{\pi}{d}} \theta(\varepsilon - \nu_\perp q_z^2)\, \theta(\pi\nu + \nu_\perp q_z^2 - \varepsilon)\, dq_z$$

By taking into account the fact that $v_{\text{uc}} = d$, the final result is the same we exhibited in section 4.2, namely:

$$\pi\nu\varrho(\varepsilon) = \begin{cases} \sqrt{\varepsilon/E} & \text{for } 0 < \varepsilon \leq E \\ 1 & \text{for } E < \varepsilon \leq \pi\nu \\ 1 - \sqrt{(\varepsilon - \pi\nu)/E} & \text{for } \pi\nu < \varepsilon \leq E + \pi\nu \\ 0 & \text{elsewhere} \end{cases} \tag{E.2}$$

Where $E \coloneqq \pi^2 \nu_\perp / d^2$, the constraint $0 \leq E \leq \pi\nu$ is implicit. In the limit $\nu_\perp \to 0$ (which also implies $E \to 0$), this relation reduces to that given by equation (E.1). Let's go back to the two-dimensional case, by explicitly solving the integral in $d\varepsilon$ which defines N_ω^{CDF} we get:

$$N_\omega^{CDF} = \theta(\omega) \frac{1}{\pi^2 \nu} \left[\frac{\gamma}{2} \log \left(\frac{\left(m_c + \pi\nu - \frac{\omega^2}{\Omega} \right)^2 + \gamma^2 \omega^2}{\left(m_c - \frac{\omega^2}{\Omega} \right)^2 + \gamma^2 \omega^2} \right) + \right.$$
$$\left. + \frac{2\omega}{\Omega} \left(\arctan \left(\frac{m_c + \pi\nu - \frac{\omega^2}{\Omega}}{\gamma\omega} \right) - \arctan \left(\frac{m_c - \frac{\omega^2}{\Omega}}{\gamma\omega} \right) \right) \right]$$

Which, in the case $\omega = 0$, exactly reproduces the result already shown in equation (4.3). In order to generalize this expression to the three-dimensional case it is necessary to consider expression (E.2) for $\varrho(\varepsilon)$ instead of (E.1). In this case, the expression which defines N_ω^{CDF} can be written in terms of suitable integrals:

$$N_\omega^{CDF} = \theta(\omega) \frac{\gamma}{\pi^2 \nu} \left[\int_E^{E+\pi\nu} \frac{\varepsilon + m_c + \frac{\omega^2}{\Omega}}{\left(\varepsilon + m_c - \frac{\omega^2}{\Omega} \right)^2 + \gamma^2 \omega^2} d\varepsilon + \right.$$
$$\left. + \int_0^E \sqrt{\frac{\varepsilon}{E}} \frac{\varepsilon + m_c + \frac{\omega^2}{\Omega}}{\left(\varepsilon + m_c - \frac{\omega^2}{\Omega} \right)^2 + \gamma^2 \omega^2} d\varepsilon - \int_0^E \sqrt{\frac{\varepsilon}{E}} \frac{\varepsilon + m_c + \pi\nu + \frac{\omega^2}{\Omega}}{\left(\varepsilon + m_c + \pi\nu - \frac{\omega^2}{\Omega} \right)^2 + \gamma^2 \omega^2} d\varepsilon \right]$$

All the integrals in this expression are analytically solvable, but the full expressions are quite complicated and not helpful for our purposes. We carry out the explicit calculation only in the case $\omega = 0$, which is the only case we are interested in:

$$N_0^{CDF} = \frac{\gamma}{2\pi^2\nu}\left[\int_E^{E+\pi\nu}\frac{1}{\varepsilon+m_c}d\varepsilon + \int_0^E\sqrt{\frac{\varepsilon}{E}}\frac{1}{\varepsilon+m_c}d\varepsilon - \int_0^E\sqrt{\frac{\varepsilon}{E}}\frac{1}{\varepsilon+m_c+\pi\nu}d\varepsilon\right] =$$

$$= \frac{\gamma}{\pi^2\nu}\left[\frac{1}{2}\log\left(1+\frac{\pi\nu}{m_c+E}\right) - \sqrt{\frac{m_c}{E}}\arctan\left(\sqrt{\frac{E}{m_c}}\right) + \sqrt{\frac{m_c+\pi\nu}{E}}\arctan\left(\sqrt{\frac{E}{m_c+\pi\nu}}\right)\right]$$

Which is exactly the expression we have shown in section 4.3.

Appendix F

Useful identities for Allen approximation

Let α_x, β_x, α_y and β_y be four real parameters, the following equations provide a generalization of equation (24) of reference [120], where AC electrical conductivity is discussed:

$$\int_{-\infty}^{+\infty} \frac{\alpha_x}{(\beta_x - z)^2 + \alpha_x^2} \frac{\alpha_y}{(\beta_y - z)^2 + \alpha_y^2} \frac{dz}{\pi} = \mathrm{sgn}(\alpha_x \alpha_y) \frac{|\alpha_x| + |\alpha_y|}{(\beta_x - \beta_y)^2 + \left(|\alpha_x| + |\alpha_y|\right)^2}$$

$$\int_{-\infty}^{+\infty} z \frac{\alpha_x}{(\beta_x - z)^2 + \alpha_x^2} \frac{\alpha_y}{(\beta_y - z)^2 + \alpha_y^2} \frac{dz}{\pi} = \mathrm{sgn}(\alpha_x \alpha_y) \frac{|\alpha_x|\beta_y + |\alpha_y|\beta_x}{(\beta_x - \beta_y)^2 + \left(|\alpha_x| + |\alpha_y|\right)^2}$$

$$\int_{-\infty}^{+\infty} z^2 \frac{\alpha_x}{(\beta_x - z)^2 + \alpha_x^2} \frac{\alpha_y}{(\beta_y - z)^2 + \alpha_y^2} \frac{dz}{\pi} = \mathrm{sgn}(\alpha_x \alpha_y) \frac{|\alpha_x|(\alpha_y^2 + \beta_y^2) + |\alpha_y|(\alpha_x^2 + \beta_x^2)}{(\beta_x - \beta_y)^2 + \left(|\alpha_x| + |\alpha_y|\right)^2}$$

The first of these three equations is exactly the one expressed in reference [120], provided the following identifications are made (in accordance with the notation used in the mentioned reference):

$$\alpha_x = \mathrm{Im}\Sigma_1 \qquad \beta_x = \omega_1 - \mathrm{Re}\Sigma_1 \qquad \alpha_y = \mathrm{Im}\Sigma_2 \qquad \beta_y = \omega_2 - \mathrm{Re}\Sigma_2$$

While this equation plays an important role in the calculation of electrical conductivity, the other two allow the same scheme to be extended to the calculation of the electronic contribution to thermopower and thermal conductivity. The proof of these three equations is a simple application of the residue theorem, we omit the explicit computation.

In chapter 5 we applied the first two of these three equations respectively for the calculation of coefficients Γ_{11} and Γ_{12}. In that case, the identifications we made are the following:

$$\alpha_x = \alpha_y = \Sigma_0 - \mathrm{Im}\Sigma_R(\omega) \qquad \beta_x = \beta_y = \omega - \mathrm{Re}\Sigma_R(\omega) + \mathrm{Re}\Sigma_R(0)$$

Appendix G

Explicit calculation of the drag diagram

Our goal is to explicitly calculate the coefficient Γ_{12}^{drag} starting from the diagram (5.6) associated with the charge density fluctuations drag [136]. We start from the general case where it is calculated at finite momentum $\mathbf{q}$ and finite frequency $i\Omega_\ell$:

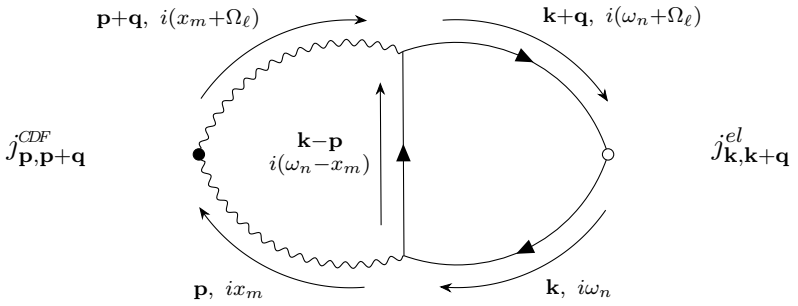

We denote by $\chi_{drag}(\mathbf{q}, i\Omega_\ell)$ the response function associated with this diagram. Our goal is to calculate the response function in the static limit, so first we will do the analytic continuation in frequency domain $i\Omega_\ell \to \omega + i0^+$, then we will fix $\mathbf{q} = \mathbf{0}$ and finally we will do the limit of $\mathrm{Im}\chi_{drag}(\mathbf{q}, \omega + i0^+)/\omega$ of ω as $\omega \to 0$.

An important property of $\chi_{drag}(\mathbf{q}, i\Omega_\ell)$ is that it is an even function of $\mathbf{q}$. In fact, since $\mathbf{k}$ and $\mathbf{p}$ are just sum variables, the change $\mathbf{q} \to -\mathbf{q}$ can be offset by the changes $\mathbf{k} \to -\mathbf{k}$ and $\mathbf{p} \to -\mathbf{p}$. The overall sign does not change, since the propagators are even functions of momentum, while the vertices are both odd.

Response function in Matsubara domain

Before making the expression for the response function explicit, we exhibit two important identities valid for Matsubara sums, respectively for the even and odd frequencies:

$$\frac{1}{\beta}\sum_{m\,\mathrm{even}} \frac{1}{A - ix_m}\frac{1}{B - ix_m}\frac{1}{C - ix_m} = \frac{1}{A-B}\left[\frac{b(A) - b(C)}{A - C} - \frac{b(B) - b(C)}{B - C}\right] \quad \text{(G.1a)}$$

$$\frac{1}{\beta}\sum_{n\,\mathrm{odd}}\frac{1}{i\omega_n - A}\frac{1}{i\omega_n - B}\frac{1}{i\omega_n - C} = \frac{1}{A-B}\left[\frac{f(A)-f(C)}{A-C} - \frac{f(B)-f(C)}{B-C}\right] \tag{G.1b}$$

Where A, B and C are, in general, complex quantities which have the dimension of a frequency (note the difference in overall sign between the two expressions). As usual, $b(\omega)$ and $f(\omega)$ denote the Bose function and the Fermi function, respectively. The full expression for the response function associated to our diagram is the following:

$$\chi_{drag}(\mathbf{q}, i\Omega_\ell) = \frac{1}{v_{\mathrm{uc}}}\frac{2g^2}{N^2}\sum_{\mathbf{k},\mathbf{p}}\left[\frac{1}{\beta}\sum_{m\,\mathrm{even}} B(\mathbf{p}, ix_m; \mathbf{q}, i\Omega_\ell)\Lambda(\mathbf{k}, \mathbf{p}, ix_m; \mathbf{q}, i\Omega_\ell)\right] \tag{G.2}$$

Where we have introduced the boson and fermion vertex functions:

$$\begin{aligned} B(\mathbf{p}, ix_m; \mathbf{q}, i\Omega_\ell) &\coloneqq j^{CDF}_{\mathbf{p},\mathbf{p}+\mathbf{q}}\mathcal{D}(ix_m, \mathbf{p})\mathcal{D}(ix_m + i\Omega_\ell, \mathbf{p}+\mathbf{q}) = \\ &= j^{CDF}_{\mathbf{p},\mathbf{p}+\mathbf{q}}\iint \mathrm{Im}D_R(x,\mathbf{p})\mathrm{Im}D_R(y,\mathbf{p}+\mathbf{q})\frac{1}{x-ix_m}\frac{1}{y-i(x_m+\Omega_\ell)}\frac{dx}{\pi}\frac{dy}{\pi} \end{aligned} \tag{G.3}$$

$$\begin{aligned} \Lambda(\mathbf{k}, \mathbf{p}, ix_m; \mathbf{q}, i\Omega_\ell) &\coloneqq -\frac{1}{\beta}\sum_{n\,\mathrm{odd}}\mathcal{G}_0(i\omega_n, \mathbf{k})\times \\ &\times\mathcal{G}_0(i\omega_n + i\Omega_\ell, \mathbf{k}+\mathbf{q})\mathcal{G}_0(i\omega_n - ix_m, \mathbf{k}-\mathbf{p})j^{el}_{\mathbf{k},\mathbf{k}+\mathbf{q}} = \\ &= -\frac{1}{\xi_{\mathbf{k}+\mathbf{q}} - \xi_{\mathbf{k}} - i\Omega_\ell}\left[\frac{f(\xi_{\mathbf{k}+\mathbf{q}}) - f(\xi_{\mathbf{k}-\mathbf{p}})}{\xi_{\mathbf{k}+\mathbf{q}} - \xi_{\mathbf{k}-\mathbf{p}} - ix_m - i\Omega_\ell} - \frac{f(\xi_{\mathbf{k}}) - f(\xi_{\mathbf{k}-\mathbf{p}})}{\xi_{\mathbf{k}} - \xi_{\mathbf{k}-\mathbf{p}} - ix_m}\right]j^{el}_{\mathbf{k},\mathbf{k}+\mathbf{q}} \end{aligned} \tag{G.4}$$

The factor of 2 in front of equation (G.2) is due to the spin multiplicity, while the overall minus sign in (G.1b) comes from the fermionic loop. Note that in equation (G.3) we used the spectral representation for $\mathcal{D}(p, ix_m)$, which is the following:

$$\mathcal{D}(ix_m, \mathbf{p}) = \fint \frac{\mathrm{Im}D_R(x,\mathbf{p})}{x - ix_m}\frac{dx}{\pi}$$

The proof of this relation is just an application of the residue theorem. By virtue of this relation, both integrals in dx and dy in equation (G.3) are to be understood as Cauchy principal value integrals. For equation (G.4) we exploited identity (G.1b) with $A = \xi_{\mathbf{k}+\mathbf{q}} - i\Omega_\ell$, $B = \xi_{\mathbf{k}}$ and $C = \xi_{\mathbf{k}-\mathbf{p}} + ix_m$ in order to carry out the sum over fermionic frequencies $i\omega_n$. By substituting these two expressions inside (G.2) we can perform the sum over x_m exactly. In fact, the full sum in x_m will be reduced to the only two following two sums, which can be performed by using relation (G.1a):

$$\begin{aligned} &\frac{1}{\beta}\sum_{m\,\mathrm{even}}\frac{1}{x-ix_m}\frac{1}{y-i(x_m+\Omega_\ell)}\frac{1}{\xi_{\mathbf{k}} - \xi_{\mathbf{k}-\mathbf{p}} - ix_m} = \\ &= \frac{1}{x - (\xi_{\mathbf{k}} - \xi_{\mathbf{k}-\mathbf{p}})}\left[\frac{b(y)-b(x)}{y-x-i\Omega_\ell} - \frac{b(y)-b(\xi_{\mathbf{k}} - \xi_{\mathbf{k}-\mathbf{p}})}{y - (\xi_{\mathbf{k}} - \xi_{\mathbf{k}-\mathbf{p}}) - i\Omega_\ell}\right] \\ &\frac{1}{\beta}\sum_{m\,\mathrm{even}}\frac{1}{x-ix_m}\frac{1}{y-i(x_m+\Omega_\ell)}\frac{1}{\xi_{\mathbf{k}+\mathbf{q}} - \xi_{\mathbf{k}-\mathbf{p}} - i(x_m+\Omega_\ell)} = \\ &= \frac{1}{y - (\xi_{\mathbf{k}+\mathbf{q}} - \xi_{\mathbf{k}-\mathbf{p}})}\left[\frac{b(x)-b(y)}{x-y+i\Omega_\ell} - \frac{b(x)-b(\xi_{\mathbf{k}+\mathbf{q}} - \xi_{\mathbf{k}-\mathbf{p}})}{x - (\xi_{\mathbf{k}+\mathbf{q}} - \xi_{\mathbf{k}-\mathbf{p}}) + i\Omega_\ell}\right] \end{aligned}$$

Therefore, the response function becomes:

$$\chi_{drag}(\mathbf{q}, i\Omega_\ell) = -\frac{1}{v_{\rm uc}}\frac{2g^2}{N^2}\sum_{\mathbf{k},\mathbf{p}}\frac{j^{CDF}_{\mathbf{p},\mathbf{p}+\mathbf{q}}\, j^{el}_{\mathbf{k},\mathbf{k}+\mathbf{q}}}{\xi_{\mathbf{k}+\mathbf{q}} - \xi_{\mathbf{k}} - i\Omega_\ell}\Bigg[\iint \mathrm{Im}D_R(x,\mathbf{p})\mathrm{Im}D_R(y,\mathbf{p}+\mathbf{q})\times$$
$$\times\Bigg[\frac{f(\xi_{\mathbf{k}+\mathbf{q}}) - f(\xi_{\mathbf{k}-\mathbf{p}})}{y - (\xi_{\mathbf{k}+\mathbf{q}} - \xi_{\mathbf{k}-\mathbf{p}})}\Bigg(\frac{b(y)-b(x)}{y-x-i\Omega_\ell} - \frac{b(x) - b(\xi_{\mathbf{k}+\mathbf{q}} - \xi_{\mathbf{k}-\mathbf{p}})}{x - (\xi_{\mathbf{k}+\mathbf{q}} - \xi_{\mathbf{k}-\mathbf{p}}) + i\Omega_\ell}\Bigg) +$$
$$-\frac{f(\xi_{\mathbf{k}}) - f(\xi_{\mathbf{k}-\mathbf{p}})}{x - (\xi_{\mathbf{k}} - \xi_{\mathbf{k}-\mathbf{p}})}\Bigg(\frac{b(y)-b(x)}{y-x-i\Omega_\ell} - \frac{b(y) - b(\xi_{\mathbf{k}} - \xi_{\mathbf{k}-\mathbf{p}})}{y - (\xi_{\mathbf{k}} - \xi_{\mathbf{k}-\mathbf{p}}) - i\Omega_\ell}\Bigg)\Bigg]\frac{dx}{\pi}\frac{dy}{\pi}\Bigg] \tag{G.5}$$

Since we are going to perform the analytic continuation in frequency domain, we need to decompose this expression into simple poles. We can do this by exploiting the following identities:

$$\frac{b(y)-b(x)}{(\xi_{\mathbf{k}+\mathbf{q}} - \xi_{\mathbf{k}} - i\Omega_\ell)(y-x-i\Omega_\ell)} = \frac{b(y)-b(x)}{y-x-(\xi_{\mathbf{k}+\mathbf{q}} - \xi_{\mathbf{k}})}\times$$
$$\times\Bigg[\frac{1}{\xi_{\mathbf{k}+\mathbf{q}} - \xi_{\mathbf{k}} - i\Omega_\ell} - \frac{1}{y-x-i\Omega_\ell}\Bigg]$$

$$\frac{b(\xi_{\mathbf{k}+\mathbf{q}} - \xi_{\mathbf{k}-\mathbf{p}}) - b(x)}{(\xi_{\mathbf{k}+\mathbf{q}} - \xi_{\mathbf{k}} - i\Omega_\ell)(\xi_{\mathbf{k}+\mathbf{q}} - \xi_{\mathbf{k}-\mathbf{p}} - x - i\Omega_\ell)} = \frac{b(\xi_{\mathbf{k}+\mathbf{q}} - \xi_{\mathbf{k}-\mathbf{p}}) - b(x)}{\xi_{\mathbf{k}} - \xi_{\mathbf{k}-\mathbf{p}} - x}\times$$
$$\times\Bigg[\frac{1}{\xi_{\mathbf{k}+\mathbf{q}} - \xi_{\mathbf{k}} - i\Omega_\ell} - \frac{1}{\xi_{\mathbf{k}+\mathbf{q}} - \xi_{\mathbf{k}-\mathbf{p}} - x - i\Omega_\ell}\Bigg]$$

$$\frac{b(\xi_{\mathbf{k}} - \xi_{\mathbf{k}-\mathbf{p}}) - b(y)}{(\xi_{\mathbf{k}+\mathbf{q}} - \xi_{\mathbf{k}} - i\Omega_\ell)(\xi_{\mathbf{k}} - \xi_{\mathbf{k}-\mathbf{p}} - y + i\Omega_\ell)} = \frac{b(\xi_{\mathbf{k}} - \xi_{\mathbf{k}-\mathbf{p}}) - b(y)}{\xi_{\mathbf{k}+\mathbf{q}} - \xi_{\mathbf{k}-\mathbf{p}} - y}\times$$
$$\times\Bigg[\frac{1}{\xi_{\mathbf{k}+\mathbf{q}} - \xi_{\mathbf{k}} - i\Omega_\ell} + \frac{1}{\xi_{\mathbf{k}} - \xi_{\mathbf{k}-\mathbf{p}} - y + i\Omega_\ell}\Bigg]$$

In inserting these three identities inside equation (G.5), we observe that half of the terms we find are proportional to $(\xi_{\mathbf{k}+\mathbf{q}} - \xi_{\mathbf{k}} - i\Omega_\ell)^{-1}$, so it is convenient to separate $\chi_{drag}(\mathbf{q}, i\Omega_\ell)$ into two pieces, one that contains the terms with $(\xi_{\mathbf{k}+\mathbf{q}} - \xi_{\mathbf{k}} - i\Omega_\ell)^{-1}$ and the other that does not contain them. We will denote these terms respectively with $\chi^{I}_{drag}(\mathbf{q}, i\Omega_\ell)$ and $\chi^{II}_{drag}(\mathbf{q}, i\Omega_\ell)$, so we get:

$$\chi_{drag}(\mathbf{q}, i\Omega_\ell) = \chi^{I}_{drag}(\mathbf{q}, i\Omega_\ell) + \chi^{II}_{drag}(\mathbf{q}, i\Omega_\ell) \tag{G.6}$$

Where:

$$\chi^{I}_{drag}(\mathbf{q}, i\Omega_\ell) \coloneqq -\frac{1}{v_{\rm uc}}\frac{2g^2}{N^2}\sum_{\mathbf{k},\mathbf{p}}\frac{j^{CDF}_{\mathbf{p},\mathbf{p}+\mathbf{q}}\, j^{el}_{\mathbf{k},\mathbf{k}+\mathbf{q}}}{\xi_{\mathbf{k}+\mathbf{q}} - \xi_{\mathbf{k}} - i\Omega_\ell}\Bigg[\iint \mathrm{Im}D_R(x,\mathbf{p})\mathrm{Im}D_R(y,\mathbf{p}+\mathbf{q})\times$$
$$\times\Bigg[\frac{f(\xi_{\mathbf{k}+\mathbf{q}}) - f(\xi_{\mathbf{k}-\mathbf{p}})}{y - (\xi_{\mathbf{k}+\mathbf{q}} - \xi_{\mathbf{k}-\mathbf{p}})}\Bigg(\frac{b(y)-b(x)}{y-x-(\xi_{\mathbf{k}+\mathbf{q}} - \xi_{\mathbf{k}})} - \frac{b(\xi_{\mathbf{k}+\mathbf{q}} - \xi_{\mathbf{k}-\mathbf{p}}) - b(x)}{\xi_{\mathbf{k}} - \xi_{\mathbf{k}-\mathbf{p}} - x}\Bigg) +$$
$$-\frac{f(\xi_{\mathbf{k}}) - f(\xi_{\mathbf{k}-\mathbf{p}})}{x - (\xi_{\mathbf{k}} - \xi_{\mathbf{k}-\mathbf{p}})}\Bigg(\frac{b(y)-b(x)}{y-x-(\xi_{\mathbf{k}+\mathbf{q}} - \xi_{\mathbf{k}})} - \frac{b(\xi_{\mathbf{k}} - \xi_{\mathbf{k}-\mathbf{p}}) - b(y)}{\xi_{\mathbf{k}+\mathbf{q}} - \xi_{\mathbf{k}-\mathbf{p}} - y}\Bigg)\Bigg]\frac{dx}{\pi}\frac{dy}{\pi}\Bigg] \tag{G.7}$$

$$\chi^{II}_{drag}(\mathbf{q}, i\Omega_\ell) \coloneqq + \frac{1}{v_{\text{uc}}} \frac{2g^2}{N^2} \sum_{\mathbf{k},\mathbf{p}} \frac{j^{CDF}_{\mathbf{p},\mathbf{p}+\mathbf{q}}\, j^{el}_{\mathbf{k},\mathbf{k}+\mathbf{q}}}{\xi_{\mathbf{k}+\mathbf{q}} - \xi_{\mathbf{k}} - i\Omega_\ell} \Bigg[\iint \text{Im}D_R(x,\mathbf{p}) \text{Im}D_R(y,\mathbf{p}+\mathbf{q}) \times$$
$$\times \Bigg[\frac{f(\xi_{\mathbf{k}+\mathbf{q}}) - f(\xi_{\mathbf{k}-\mathbf{p}})}{y - (\xi_{\mathbf{k}+\mathbf{q}} - \xi_{\mathbf{k}-\mathbf{p}})} \Bigg(\frac{b(y) - b(x)}{(y - x - (\xi_{\mathbf{k}+\mathbf{q}} - \xi_{\mathbf{k}}))(y - x - i\Omega_\ell)} +$$
$$- \frac{b(\xi_{\mathbf{k}+\mathbf{q}} - \xi_{\mathbf{k}-\mathbf{p}}) - b(x)}{(\xi_{\mathbf{k}} - \xi_{\mathbf{k}-\mathbf{p}} - x)(\xi_{\mathbf{k}+\mathbf{q}} - \xi_{\mathbf{k}-\mathbf{p}} - x - i\Omega_\ell)} \Bigg) - \frac{f(\xi_{\mathbf{k}}) - f(\xi_{\mathbf{k}-\mathbf{p}})}{x - (\xi_{\mathbf{k}} - \xi_{\mathbf{k}-\mathbf{p}})} \times$$
$$\times \Bigg(\frac{b(y) - b(x)}{(y - x - (\xi_{\mathbf{k}+\mathbf{q}} - \xi_{\mathbf{k}}))(y - x - i\Omega_\ell)} +$$
$$+ \frac{b(\xi_{\mathbf{k}} - \xi_{\mathbf{k}-\mathbf{p}}) - b(y)}{(\xi_{\mathbf{k}+\mathbf{q}} - \xi_{\mathbf{k}-\mathbf{p}} - y)(\xi_{\mathbf{k}} - \xi_{\mathbf{k}-\mathbf{p}} - y + i\Omega_\ell)} \Bigg) \Bigg] \frac{dx}{\pi} \frac{dy}{\pi} \Bigg] \tag{G.8}$$

By substituting expressions (G.7) and (G.8) inside (G.6), we get the expression we were looking for within Matsubara domain.

Static limit

Up to this point, we have not applied any approximation. Moreover, this expression is valid at any generic frequency $i\Omega_\ell$ and momentum $\mathbf{q}$. Again, since we are interested in the static response function to a uniform field, we have to work on the full expression of $\chi_{drag}(\mathbf{q}, i\Omega_\ell)$ by following these steps:

- We perform the analytic continuation in frequency domain $i\Omega_\ell \to \omega + i0^+$ and then we consider only the imaginary part of the found function
- We fix $\mathbf{q} = \mathbf{0}$
- We divide the found expression by ω
- We consider the limit $\omega \to 0$

Let's begin by calculating $\text{Im}\chi^I_{drag}(\mathbf{q}, \omega)$:

$$\text{Im}\chi^I_{drag}(\mathbf{q},\omega) \coloneqq \text{Im}\chi^I_{drag}(\mathbf{q}, i\Omega_\ell \to \omega + i0^+) = -\frac{1}{v_{\text{uc}}} \frac{2g^2}{N^2} \sum_{\mathbf{k},\mathbf{p}} j^{CDF}_{\mathbf{p},\mathbf{p}+\mathbf{q}}\, j^{el}_{\mathbf{k},\mathbf{k}+\mathbf{q}} \times$$
$$\times \pi\delta(\xi_{\mathbf{k}+\mathbf{q}} - \xi_{\mathbf{k}} - \omega) \Bigg[\iint \text{Im}D_R(x,\mathbf{p}) \text{Im}D_R(y,\mathbf{p}+\mathbf{q}) \frac{b(y) - b(x)}{y - x - (\xi_{\mathbf{k}+\mathbf{q}} - \xi_{\mathbf{k}})} \times$$
$$\times \Bigg(\frac{f(\xi_{\mathbf{k}+\mathbf{q}}) - f(\xi_{\mathbf{k}-\mathbf{p}})}{y - (\xi_{\mathbf{k}+\mathbf{q}} - \xi_{\mathbf{k}-\mathbf{p}})} - \frac{f(\xi_{\mathbf{k}}) - f(\xi_{\mathbf{k}-\mathbf{p}})}{x - (\xi_{\mathbf{k}} - \xi_{\mathbf{k}-\mathbf{p}})} \Bigg) \frac{dx}{\pi} \frac{dy}{\pi} +$$
$$- \iint \text{Im}D_R(x,\mathbf{p}) \text{Im}D_R(y,\mathbf{p}+\mathbf{q}) \Bigg(\frac{f(\xi_{\mathbf{k}+\mathbf{q}}) - f(\xi_{\mathbf{k}-\mathbf{p}})}{y - (\xi_{\mathbf{k}+\mathbf{q}} - \xi_{\mathbf{k}-\mathbf{p}})} \frac{b(\xi_{\mathbf{k}+\mathbf{q}} - \xi_{\mathbf{k}-\mathbf{p}}) - b(x)}{\xi_{\mathbf{k}} - \xi_{\mathbf{k}-\mathbf{p}} - x} +$$
$$- \frac{f(\xi_{\mathbf{k}}) - f(\xi_{\mathbf{k}-\mathbf{p}})}{x - (\xi_{\mathbf{k}} - \xi_{\mathbf{k}-\mathbf{p}})} \frac{b(\xi_{\mathbf{k}} - \xi_{\mathbf{k}-\mathbf{p}}) - b(y)}{\xi_{\mathbf{k}+\mathbf{q}} - \xi_{\mathbf{k}-\mathbf{p}} - y} \Bigg) \frac{dx}{\pi} \frac{dy}{\pi} \Bigg]$$

By fixing $\mathbf{q}=\mathbf{0}$ we find:

$$\begin{aligned}\mathrm{Im}\chi^{I}_{drag}(\mathbf{q}=\mathbf{0},\omega)=-\frac{1}{v_{\mathrm{uc}}}\frac{2g^2}{N^2}\sum_{\mathbf{k},\mathbf{p}} j^{CDF}_{\mathbf{p}}\, j^{el}_{\mathbf{k}}\delta(\omega)\Bigg[\iint \mathrm{Im}D_R(x,\mathbf{p})\mathrm{Im}D_R(y,\mathbf{p})\times\\ \times\frac{b(y)-b(x)}{y-x}\Bigg(\frac{f(\xi_{\mathbf{k}})-f(\xi_{\mathbf{k}-\mathbf{p}})}{y-(\xi_{\mathbf{k}}-\xi_{\mathbf{k}-\mathbf{p}})}-\frac{f(\xi_{\mathbf{k}})-f(\xi_{\mathbf{k}-\mathbf{p}})}{x-(\xi_{\mathbf{k}}-\xi_{\mathbf{k}-\mathbf{p}})}\Bigg)\frac{dx}{\pi}\frac{dy}{\pi}+\\ -\iint \mathrm{Im}D_R(x,\mathbf{p})\mathrm{Im}D_R(y,\mathbf{p})\Bigg(\frac{f(\xi_{\mathbf{k}})-f(\xi_{\mathbf{k}-\mathbf{p}})}{y-(\xi_{\mathbf{k}}-\xi_{\mathbf{k}-\mathbf{p}})}\frac{b(\xi_{\mathbf{k}}-\xi_{\mathbf{k}-\mathbf{p}})-b(x)}{\xi_{\mathbf{k}}-\xi_{\mathbf{k}-\mathbf{p}}-x}+\\ -\frac{f(\xi_{\mathbf{k}})-f(\xi_{\mathbf{k}-\mathbf{p}})}{x-(\xi_{\mathbf{k}}-\xi_{\mathbf{k}-\mathbf{p}})}\frac{b(\xi_{\mathbf{k}}-\xi_{\mathbf{k}-\mathbf{p}})-b(y)}{\xi_{\mathbf{k}}-\xi_{\mathbf{k}-\mathbf{p}}-y}\Bigg)\frac{dx}{\pi}\frac{dy}{\pi}\Bigg]\end{aligned}\tag{G.9}$$

We immediately notice that this object is identically equal to zero at each frequency ω. The reason is that the integrand functions appearing in the two integrals of expression (G.9) are both odd functions by switching x and y, and the integration domain is the same for each variable. We deduce that the limit of $\mathrm{Im}\chi^{I}_{drag}(\mathbf{q}=\mathbf{0},\omega)/\omega$ as $\omega\to 0$ is zero.

Let's now look at the computation of $\mathrm{Im}\chi^{II}_{drag}(\mathbf{q},\omega)$:

$$\begin{aligned}\mathrm{Im}\chi^{II}_{drag}(\mathbf{q},\omega)\coloneqq\mathrm{Im}\chi^{II}_{drag}(\mathbf{q},i\Omega_\ell\to\omega+i0^+)=+\frac{1}{v_{\mathrm{uc}}}\frac{2g^2}{N^2}\sum_{\mathbf{k},\mathbf{p}} j^{CDF}_{\mathbf{p},\mathbf{p}+\mathbf{q}}\, j^{el}_{\mathbf{k},\mathbf{k}+\mathbf{q}}\times\\ \times\pi\Bigg[\iint \mathrm{Im}D_R(x,\mathbf{p})\mathrm{Im}D_R(y,\mathbf{p}+\mathbf{q})\frac{(b(y)-b(x))\delta(y-x-\omega)}{y-x-(\xi_{\mathbf{k}+\mathbf{q}}-\xi_{\mathbf{k}})}\times\\ \times\Bigg(\frac{f(\xi_{\mathbf{k}+\mathbf{q}})-f(\xi_{\mathbf{k}-\mathbf{p}})}{y-(\xi_{\mathbf{k}+\mathbf{q}}-\xi_{\mathbf{k}-\mathbf{p}})}-\frac{f(\xi_{\mathbf{k}})-f(\xi_{\mathbf{k}-\mathbf{p}})}{x-(\xi_{\mathbf{k}}-\xi_{\mathbf{k}-\mathbf{p}})}\Bigg)\frac{dx}{\pi}\frac{dy}{\pi}+\\ -\iint \mathrm{Im}D_R(x,\mathbf{p})\mathrm{Im}D_R(y,\mathbf{p}+\mathbf{q})\Bigg(\frac{f(\xi_{\mathbf{k}+\mathbf{q}})-f(\xi_{\mathbf{k}-\mathbf{p}})}{y-(\xi_{\mathbf{k}+\mathbf{q}}-\xi_{\mathbf{k}-\mathbf{p}})}\frac{b(\xi_{\mathbf{k}+\mathbf{q}}-\xi_{\mathbf{k}-\mathbf{p}})-b(x)}{\xi_{\mathbf{k}}-\xi_{\mathbf{k}-\mathbf{p}}-x}\times\\ \times\delta(\xi_{\mathbf{k}+\mathbf{q}}-\xi_{\mathbf{k}-\mathbf{p}}-x-\omega)-\frac{f(\xi_{\mathbf{k}})-f(\xi_{\mathbf{k}-\mathbf{p}})}{x-(\xi_{\mathbf{k}}-\xi_{\mathbf{k}-\mathbf{p}})}\frac{b(\xi_{\mathbf{k}}-\xi_{\mathbf{k}-\mathbf{p}})-b(y)}{\xi_{\mathbf{k}+\mathbf{q}}-\xi_{\mathbf{k}-\mathbf{p}}-y}\times\\ \times\delta(\xi_{\mathbf{k}}-\xi_{\mathbf{k}-\mathbf{p}}-y+\omega)\Bigg)\frac{dx}{\pi}\frac{dy}{\pi}\Bigg]\end{aligned}$$

Again, let's fix $\mathbf{q}=\mathbf{0}$:

$$\begin{aligned}\mathrm{Im}\chi^{II}_{drag}(\mathbf{q}=\mathbf{0},\omega)=+\frac{1}{v_{\mathrm{uc}}}\frac{2g^2}{N^2}\sum_{\mathbf{k},\mathbf{p}} j^{CDF}_{\mathbf{p}}\, j^{el}_{\mathbf{k}}\pi\Bigg[\iint \mathrm{Im}D_R(x,\mathbf{p})\mathrm{Im}D_R(y,\mathbf{p})\frac{b(y)-b(x)}{y-x}\times\\ \times\Bigg(\frac{f(\xi_{\mathbf{k}})-f(\xi_{\mathbf{k}-\mathbf{p}})}{y-(\xi_{\mathbf{k}}-\xi_{\mathbf{k}-\mathbf{p}})}-\frac{f(\xi_{\mathbf{k}})-f(\xi_{\mathbf{k}-\mathbf{p}})}{x-(\xi_{\mathbf{k}}-\xi_{\mathbf{k}-\mathbf{p}})}\Bigg)\delta(y-x-\omega)\frac{dx}{\pi}\frac{dy}{\pi}-\iint \mathrm{Im}D_R(x,\mathbf{p})\times\\ \times\mathrm{Im}D_R(y,\mathbf{p})\Bigg(\frac{f(\xi_{\mathbf{k}})-f(\xi_{\mathbf{k}-\mathbf{p}})}{y-(\xi_{\mathbf{k}}-\xi_{\mathbf{k}-\mathbf{p}})}\frac{b(\xi_{\mathbf{k}}-\xi_{\mathbf{k}-\mathbf{p}})-b(x)}{\xi_{\mathbf{k}}-\xi_{\mathbf{k}-\mathbf{p}}-x}\delta(\xi_{\mathbf{k}}-\xi_{\mathbf{k}-\mathbf{p}}-x-\omega)+\\ -\frac{f(\xi_{\mathbf{k}})-f(\xi_{\mathbf{k}-\mathbf{p}})}{x-(\xi_{\mathbf{k}}-\xi_{\mathbf{k}-\mathbf{p}})}\frac{b(\xi_{\mathbf{k}}-\xi_{\mathbf{k}-\mathbf{p}})-b(y)}{\xi_{\mathbf{k}}-\xi_{\mathbf{k}-\mathbf{p}}-y}\delta(\xi_{\mathbf{k}}-\xi_{\mathbf{k}-\mathbf{p}}-y+\omega)\Bigg)\frac{dx}{\pi}\frac{dy}{\pi}\Bigg]=\end{aligned}$$

$$= +\frac{1}{v_{\rm uc}}\frac{2g^2}{N^2}\sum_{\mathbf{k},\mathbf{p}} j^{CDF}_{\mathbf{p}}\, j^{el}_{\mathbf{k}}(f(\xi_{\mathbf{k}}) - f(\xi_{\mathbf{k}-\mathbf{p}}))\Bigg[-\fint_{-\infty}^{+\infty}\frac{\mathrm{Im}D_R(x,\mathbf{p})}{x-(\xi_{\mathbf{k}}-\xi_{\mathbf{k}-\mathbf{p}})}\times$$
$$\times\Bigg(\frac{b(x+\omega)-b(x)}{\omega}\mathrm{Im}D_R(x+\omega,\mathbf{p}) - \frac{b(x)-b(x-\omega)}{\omega}\mathrm{Im}D_R(x-\omega,\mathbf{p})\Bigg)\frac{dx}{\pi}+$$
$$+\Bigg(\frac{b(\xi_{\mathbf{k}}-\xi_{\mathbf{k}-\mathbf{p}}+\omega)-b(\xi_{\mathbf{k}}-\xi_{\mathbf{k}-\mathbf{p}})}{\omega}\mathrm{Im}D_R(\xi_{\mathbf{k}}-\xi_{\mathbf{k}-\mathbf{p}}+\omega,\mathbf{p})+$$
$$-\frac{b(\xi_{\mathbf{k}}-\xi_{\mathbf{k}-\mathbf{p}})-b(\xi_{\mathbf{k}}-\xi_{\mathbf{k}-\mathbf{p}}-\omega)}{\omega}\mathrm{Im}D_R(\xi_{\mathbf{k}}-\xi_{\mathbf{k}-\mathbf{p}}-\omega,\mathbf{p})\Bigg)\fint_{-\infty}^{+\infty}\frac{\mathrm{Im}D_R(x,\mathbf{p})}{x-(\xi_{\mathbf{k}}-\xi_{\mathbf{k}-\mathbf{p}})}\frac{dx}{\pi}\Bigg]$$

Since $\mathrm{Im}\chi^{I}_{drag}(\mathbf{q}=\mathbf{0},\omega)=0$ identically, the Onsager coefficient Γ^{drag}_{12} is entirely determined by the expression above:

$$\Gamma^{drag}_{12} \coloneqq \lim_{\omega\to 0}\frac{\mathrm{Im}\chi_{drag}(\mathbf{q}=\mathbf{0},\omega)}{\omega} = \lim_{\omega\to 0}\frac{\mathrm{Im}\chi^{II}_{drag}(\mathbf{q}=\mathbf{0},\omega)}{\omega}$$

The following limit may be helpful:

$$\lim_{\omega\to 0}\frac{(b(\xi+\omega)-b(\xi))\mathrm{Im}D_R(\xi+\omega,\mathbf{p}) - (b(\xi)-b(\xi-\omega))\mathrm{Im}D_R(\xi-\omega,\mathbf{p})}{\omega^2} =$$
$$= \frac{1}{\mathrm{Im}D_R(\xi,\mathbf{p})}\frac{\partial}{\partial\xi}\Big[\Big(\mathrm{Im}D_R(\xi,\mathbf{p})\Big)^2 b'(\xi)\Big]$$

This allows us to write Γ^{drag}_{12} as:

$$\Gamma^{drag}_{12} = \lim_{\omega\to 0}\frac{\mathrm{Im}\chi^{II}_{drag}(\mathbf{q}=\mathbf{0},\omega)}{\omega} = \frac{1}{v_{\rm uc}}\frac{2g^2}{N^2}\sum_{\mathbf{k},\mathbf{p}} j^{CDF}_{\mathbf{p}}\, j^{el}_{\mathbf{k}}(f(\xi_{\mathbf{k}}) - f(\xi_{\mathbf{k}-\mathbf{p}}))\times$$
$$\times\Bigg[-\fint_{-\infty}^{+\infty}\frac{\frac{\partial}{\partial x}\Big[\Big(\mathrm{Im}D_R(x,\mathbf{p})\Big)^2 b'(x)\Big]}{x-(\xi_{\mathbf{k}}-\xi_{\mathbf{k}-\mathbf{p}})}\frac{dx}{\pi}+$$
$$+\frac{\frac{\partial}{\partial\xi}\Big[\Big(\mathrm{Im}D_R(\xi,\mathbf{p})\Big)^2 b'(\xi)\Big]}{\mathrm{Im}D_R(\xi,\mathbf{p})}\Bigg|_{\xi=\xi_{\mathbf{k}}-\xi_{\mathbf{k}-\mathbf{p}}}\fint_{-\infty}^{+\infty}\frac{\mathrm{Im}D_R(x,\mathbf{p})}{x-(\xi_{\mathbf{k}}-\xi_{\mathbf{k}-\mathbf{p}})}\frac{dx}{\pi}\Bigg]$$

It may be convenient to express this coefficient in the following form, which is the same that we exhibited in section 5.3:

$$\Gamma^{drag}_{12} = \frac{1}{v_{\rm uc}}\frac{2g^2}{N^2}\sum_{\mathbf{k},\mathbf{p}} j^{CDF}_{\mathbf{p}}\, j^{el}_{\mathbf{k}}(f(\xi_{\mathbf{k}}) - f(\xi_{\mathbf{k}-\mathbf{p}}))(I^a_{\mathbf{k},\mathbf{p}} + I^b_{\mathbf{k},\mathbf{p}})$$

With the definitions:

$$I^a_{\mathbf{k},\mathbf{p}} \coloneqq -\fint_{-\infty}^{+\infty} \frac{\dfrac{\partial}{\partial x}\left[\left(\mathrm{Im}D_R(x,\mathbf{p})\right)^2 b'(x)\right]}{x-(\xi_{\mathbf{k}}-\xi_{\mathbf{k}-\mathbf{p}})}\frac{dx}{\pi}$$

$$I^b_{\mathbf{k},\mathbf{p}} \coloneqq \left.\frac{\dfrac{\partial}{\partial \xi}\left[\left(\mathrm{Im}D_R(\xi,\mathbf{p})\right)^2 b'(\xi)\right]}{\mathrm{Im}D_R(\xi,\mathbf{p})}\right|_{\xi=\xi_{\mathbf{k}}-\xi_{\mathbf{k}-\mathbf{p}}} \fint_{-\infty}^{+\infty} \frac{\mathrm{Im}D_R(x,\mathbf{p})}{x-(\xi_{\mathbf{k}}-\xi_{\mathbf{k}-\mathbf{p}})}\frac{dx}{\pi}$$

Interestingly, the integral which appear inside the expression for $I^b_{\mathbf{k},\mathbf{p}}$ is exactly solvable through a Kramers-Kronig relation:

$$\fint_{-\infty}^{+\infty} \frac{\mathrm{Im}D_R(x,\mathbf{p})}{x-\xi}\frac{dx}{\pi} = \mathrm{Re}D_R(\xi,\mathbf{p}) = \frac{m_{\mathbf{p}}-\dfrac{\xi^2}{\Omega}}{\left(m_{\mathbf{p}}-\dfrac{\xi^2}{\Omega}\right)^2+\gamma^2\xi^2}$$

Notice that in our expression for Γ_{12}^{drag} the impurity scattering term Σ_0 plays no role, we therefore deduce that this result is valid both in the case of a perfect metal and in the case of a standard metal.

Bibliography

[1] H. K. Onnes, "Further experiments with liquid helium. C. On the change of electric resistance of pure metals at very low temperatures etc. IV. The resistance of pure mercury at helium temperatures", *Proceedings of the Section of Sciences* **13** (2), 1274 (1911)

[2] J. Bardeen, L. Cooper, J. R. Schriffer, "Theory of Superconductivity", *Physical Review* **108**, 1175 (1957)

[3] J. G. Bednorz, K. A. Müller, "Possible high-T_c superconductivity in the BaLaCuO system", *Z. Physik B - Condensed Matter* **64**, 189 (1986)

[4] S. A. Wolf, V. Z. Kresin, *Novel Superconductivity*, Springer (1987)

[5] M. K. Wu, J. R. Ashburn, C. J. Torng, *et al.* "Superconductivity at 93 K in a New Mixed-Phase Y-Ba-Cu-O Compound System at Ambient Pressure", *Phys. Rev. Lett.* **58**, 908 (1987)

[6] A. Schilling, M. Cantoni, J. D. Guo, H. R. Ott, "Superconductivity above 130 K in the Hg-Ba-Ca-Cu-O system", *Nature Physics* **363** (6424), 5658 (1993)

[7] C. Castellani, C. Di Castro, M. Grilli, "Singular Quasiparticle Scattering in the Proximity of Charge Instabilities", *Phys. Rev. Lett.* **75**, 4650 (1995)

[8] A. Abanov, A. V. Chubukov, J. Schmalian, "Quantum-critical theory of the spin- fermion model and its application to cuprates: Normal state analysis", *Adv. Phys.* **52**, 119 (2001)

[9] V. Aji, C. M. Varma, "Theory of the Quantum Critical Fluctuations in Cuprate Superconductors", *Phys. Rev. Lett.* **99**, 067003 (2007)

[10] R. Arpaia, S. Caprara, R. Fumagalli, *et al.* "Dynamical charge density fluctuations pervading the phase diagram of a Cu-based high-T_c superconductor", *Science* **365**, 906 (2019)

[11] P. Walmsley, C. Putzke, L. Malone, *et al.* "Quasiparticle mass enhancement close to the quantum critical point in $BaFe_2(As_{1-x}P_x)_2$", *Phys. Rev. Lett.* **110**, 257002 (2013)

[12] G. R. Stewart, "Non-Fermi-liquid behavior in d- and f-electron metals", *Rev. Mod. Phys.* **73**, 797 (2001)

[13] Y. Cao, D. Chowdhury, D. Rodan-Legrain, *et al.* "Strange metal in magic-angle graphene with near Planckian dissipation", *Phys. Rev. Lett.* **124**, 076801 (2020)

[14] A. Damascelli, Z. Hussain, Z. Shen, "Angle-resolved photoemission studies of the cuprate superconductors", *Reviews of Modern Physics* **75** (2), 473 (2003)

[15] E. Dagotto, "Correlated electrons in high-temperature superconductors", *Reviews of Modern Physics* **66** (3), 463 (1994)

[16] Y. Nakamura, S. Uchida, "Anisotropic transport properties of single-crystal $La_{2x}Sr_xCuO_4$: Evidence for the dimensional crossover", *Phys. Rev. B* **47**, 8369 (1993)

[17] W. C. Wu, J. P. Carbotte, "Absence of anisotropic universal transport in YBCO", *Physica C* **322**, 1-2, 123 (1999)

[18] A. Harabor, P. Rotaru, N. A. Harabor, *et al.* "Orthorhombic YBCO-123 ceramic oxide superconductor: Structural, resistive and thermal properties", *Ceramics International* **45** (2B), 2899 (2019)

[19] M. Bluschke, A. Frano, E. Schierle, *et al.* "Stabilization of three-dimensional charge order in $YBa_2Cu_3O_{6+x}$ via epitaxial growth", *Nat. Comm.* **9**, 2978 (2018)

[20] E. Wahlberg, R. Arpaia, G. Seibold, *et al.* "Restored strange metal phase through suppression of charge density waves in underdoped $YBa_2Cu_3O_{7-\delta}$", *Science* **373**, 1506 (2021)

[21] T. Ito, H. Takagi, T. Ishibashi, S. Uchida, "Normal-state conductivity between CuO2 planes in copper oxide superconductors", *Nature (London)* **350**, 596 (1991)

[22] K. Takenaka, K. Mizuhashi, H. Takagi, S. Uchida, "Interplane charge transport in $YBa_2Cu_3O_{7-\delta}$: Spin-gap effect on in-plane and out-of-plane resistivity", *Phys. Rev. B* **50**, 6534 (1994)

[23] H. Wagner, N. D. Mermin, "Absence of ferromagnetism or antiferromagnetism in one- or two-dimensional isotropic Heisenberg models", *Phys. Rev. Lett.* **17**, 1133 (1966)

[24] D. Barišic, M. K. Chana, Y. Li, *et al.* "Universal sheet resistance and revised phase diagram of the cuprate high-temperature superconductors", *PNAS* **110** (30), 12235 (2013)

[25] B. Keimer, S. A. Kivelson, M. R. Norman, *et al.* "From quantum matter to high-temperature superconductivity in copper oxides", *Nature* **518**, 179 (2015)

[26] P. A. Lee, N. Nagaosa, X. Wen, "Doping a Mott Insulator: Physics of High Temperature Superconductivity", *Rev. of Mod. Phys.* **78** (1), 17 (2006)

[27] H. A. Kramers, "L'interaction Entre les Atomes Magnétogènes dans un Cristal Paramagnétique", *Physica* **1** (1-6): 182 (1934)

[28] P. W. Anderson, "Antiferromagnetism. Theory of Superexchange Interaction", *Phys. Rev.* **79** (2): 350 (1950)

[29] N. E. Bickers, D. J. Scalapino, R. T. Scalettar, "CDW and SDW mediated pairing interactions", *Int. Journ. of Mod. Phys. B* **1**, 687 (1987)

[30] M. Inui, S. Doniach, P. J. Hirschfeld, *et al.* "Coexistence of antiferromagnetism and superconductivity in a mean-field theory of high-T_c superconductors", *Phys. Rev. B* **37** (10), 5182 (1988)

[31] C. Gros, D. Poilblanc, T. M. Rice, F. C. Zhang, "Superconductivity in correlated wavefunctions", *Physica C* **153-155** (1), 543 (1988)

[32] B. O. Wells, Z. X. Shen, D. S. Dessau, *et al.* "Evidence for k-dependent, in-plane anisotropy of the superconducting gap in $Bi_2Sr_2CaCu_2O_{8+\delta}$", *Phys. Rev. B*, **46** (18), 11830 (1992)

[33] Z. Shen, D. S. Dessau, B. O. Wells, *et al.* "Anomalously Large Gap Anisotropy in the a-b Plane of $Bi_2Sr_2CaCu_2O_{8+\delta}$", *Phys. Rev. Lett.* **70**, 1553 (1993)

[34] J. A. Hertz, "Quantum critical phenomena", *Phys. Rev. B* **14**, 1165 (1976)

[35] A. J. Millis, "Effect of a nonzero temperature on quantum critical points in itinerant fermion systems", *Phys. Rev. Lett.* **48**, 7183 (1993)

[36] J. L. Tallon, J. W. Loram, "The doping dependence of T^* - what is the real high-T_c phase diagram?", *Physica C*, **349**, 53 (2001)

[37] B. J. Ramshaw, S. E. Sebastian, R. D. McDonald, *et al.* "Quasiparticle mass enhancement approaching optimal doping in a high-T_c superconductor", *Science* **348**, 317 (2015)

[38] S. Badoux, W. Tabis, F. Laliberté, *et al.* "Change of carrier density at the pseudogap critical point of a cuprate superconductor", *Nature* **531**, 210 (2016)

[39] A. Perali, C. Castellani, C. Di Castro, M. Grilli, "d-wave superconductivity near charge instabilities", *Phys. Rev. B* **54**, 16216 (1996)

[40] N. W. Ashcroft, N. D. Mermin, *Solid State Physics*, Thomson Press (India) Ltd (2003)

[41] O. Gunnarsson, M. Calandra, J. E. Han, "Colloquium: Saturation of electrical resistivity", *Rev. of Mod. Phys.* **75**, 1085 (2003)

[42] N. E. Hussey, K. Takenaka, H. Takagi, "Universality of the Mott-Ioffe-Regel limit in metals", *Phil. Mag.* **84**, 2847 (2004)

[43] S. Martin, A. T. Fiory, R. M. Fleming, *et al.* "Normal-state transport properties of $Bi_{2+x}Sr_{2-y}CuO_{6+\delta}$ single crystals", *Phys. Rev. B* **41**, 846 (1990)

[44] R. Daou, O. Cyr-Choinière, F. Laliberté, *et al.* "Linear temperature dependence of resistivity and change in the Fermi surface at the pseudogap critical point of a high-T_c superconductor", *Nat. Phys.* **5**, 31 (2009)

[45] R. A. Cooper, Y. Wang, B. Vignolle, *et al.* "Anomalous criticality in the electrical resistivity of $La_{2-x}Sr_xCuO_4$", *Science* **323**, 603 (2009)

[46] J. Zaanen, "Why the temperature is high", *Nature* **430**, 512 (2004)

[47] A. Legros, S. Benhabib, W. Tabis, "Universal T-linear resistivity and Planckian dissipation in overdoped cuprates", *Nature Physics* **15**, 142 (2019)

[48] H. Jones, C. Zener, "The Theory of the Change in Resistance in a Magnetic Field", *Proc. R. Soc. Lond. A* **145** 268 (1934)

[49] N. E. Hussey, "The normal state scattering rate in high-T_c cuprates", *Eur. Phys. J. B* **31**, 495 (2003)

[50] I. M. Hayes, R. D. McDonald, N. P. Breznay*et al.* "Scaling between magnetic field and temperature in the high-temperature superconductor $BaFe_2(As_{1-x}P_x)_2$", *Nat. Phys.* **12**, 916 (2016)

[51] P. Giraldo-Gallo, J. A. Galvis, Z. Stegen, *et al.* "Scale-invariant magnetoresistance in a cuprate superconductor", *Science* **361**, 479 (2018)

[52] J. Ayres, M. Berben, M. Čulo, *et al.* "Incoherent transport across the strange-metal regime of overdoped cuprates", *Nature* **595**, 661 (2021)

[53] A. Ataei, A. Gourgout, G. Grissonnanche, *et al.* "Electrons with Planckian scattering obey standard orbital motion in a magnetic field", *Nat. Phys.* **18**, 1420 (2022)

[54] A. Gourgout, G. Grissonnanche, F. Laliberté, *et al.* "Seebeck Coefficient in a Cuprate Superconductor: Particle-Hole Asymmetry in the Strange Metal Phase and Fermi Surface Transformation in the Pseudogap Phase", *Phys. Rev. X*, **12**, 011037 (2022)

[55] B. Michon, C. Girod, S. Badoux, *et al.* "Thermodynamic signatures of quantum criticality in cuprate superconductors", *Nature* **567** (7747), 218 (2019)

[56] A. A. Rudnitskii, "Thermoelectric Properties of the Noble Metals and Their Alloys", *U. S. AEC, Division of Technical Information, Oak Ridge, Tenn.* (1959)

[57] S. H. Tang, P. P. Craig, T. A. Kitchens, "Seebeck Coefficient at the Curie Temperature: Specific Heat of Charge Carriers in Ferromagnets", *Phys. Rev. Lett.* **27**, 593 (1971)

[58] C. Collignon, A. Ataei, A. Gourgout, *et al.* "Thermopower across the phase diagram of the cuprate $La_{2-x}Sr_xCuO_4$: Signatures of the pseudogap and charge density wave phases", *Phys. Rev. B* **103**, 155102 (2021)

[59] C. E. Matt, C. G. Fatuzzo, Y. Sassa, *et al.* "Electron scattering, charge order, and pseudogap physics in $La_{1.6-x}Nd_{0.4}Sr_xCuO_4$: an angle-resolved photoemission spectroscopy study", *Phys. Rev. B* **92**, 134524 (2015)

[60] J. M. Tranquada, B. J. Sternlieb, J. D. Axe, *et al.* "Evidence for stripe correlations of spins and holes in copper oxide", *Nature* **375**, 561 (1995)

[61] J. M. Tranquada, J. D. Axe, N. Ichikawa, *et al.* "Neutron-scattering study of stripe-phase order of holes and spins in $La_{1.48}Nd_{0.4}Sr_{0.12}CuO_4$", *Phys. Rev. B* **54** (10), 7489 (1996)

[62] R. Raimondi, C. Castellani, M. Grilli, *et al.* "Charge collective modes and dynamic pairing in the three-band Hubbard model. II. Strong-coupling limit", *Phys. Rev. B* **47**, 3331 (1993)

[63] F. Becca, M. Tarquini, M. Grilli, C. Di Castro, "Charge-density waves and superconductivity as an alternative to phase separation in the infinite-U Hubbard-Holstein model", *Phys. Rev. B* **54**, 17 (1996)

[64] S. Caprara, M. Sulpizi, A. Bianconi, *et al.* "Single-particle properties of a model for coexisting charge and spin quasi-critical fluctuations coupled to electrons", *Phys. Rev. B* **59**, 14980 (1999)

[65] N. L. Saini, J. Avila, A. Bianconi, *et al.* "Topology of the pseudogap and shadow bands in $Bi_2Sr_2CaCu_2O_{8+\delta}$ at optimum doping", *Phys. Rev. Lett.* **79**, 3467 (1997)

[66] S. Caprara, C. Di Castro, M. Grilli, D. Suppa, "Charge-fluctuation contribution to the Raman response in superconducting cuprates", *Phys. Rev. Lett.* **95**, 117004 (2005)

[67] V. Hinkov, D. Haug, B. Fauqué, *et al.* "Electronic liquid crystal state in the high-temperature superconductor $YBa_2Cu_3O_{6.45}$", *Science* **319** 597 (2008)

[68] G. Ghiringhelli, M. Le Tacon, M. Minola, *et al.* "Long-range incommensurate charge fluctuations in (Y,Nd)$Ba_2Cu_3O_{6+x}$", *Science* **337**, 821 (2012)

[69] J. Chang, E. Blackburn, A. T. Holmes, *et al.* "Direct observation of competition between superconductivity and charge density wave order in $YBa_2Cu_3O_{6.67}$", *Nat. Phys.* **8**, 871 (2012)

[70] R. Comin, A. Frano, M. M. Yee, *et al.* "Charge order driven by Fermi-arc instability in $Bi_2Sr_{2-x}La_xCuO_{6+\delta}$", *Science* **343**, 390 (2014)

[71] S. Blanco-Canosa, A. Frano, E. Schierle, *et al.* "Resonant X-ray scattering study of charge-density- wave correlations in $YBa_2Cu_3O_{6+x}$", *Phys. Rev. B* **90**, 054513 (2014)

[72] T. Wu, H. Mayaffre, S. Krämer, *et al.* "Magnetic-field-induced charge-stripe order in the high temperature superconductor $YBa_2Cu_3O_y$", *Nature* **477**, 191 (2011)

[73] T. Wu, H. Mayaffre, S. Krämer, *et al.* "Emergence of charge order from the vortex state of a high-temperature superconductor", *Nat. Commun.* **4**, 2113 (2013)

[74] T. P. Croft, C. Lester, M. S. Senn, *et al.* "Charge density wave fluctuations in $La_{2-x}Sr_xCuO_4$ and their competition with superconductivity", *Phys. Rev. B* **89**, 224513 (2014)

[75] T. Wu, H. Mayaffre, S. Krämer, *et al.* "Incipient charge order observed by NMR in the normal state of $YBa_2Cu_3O_y$", *Nat. Comm.* **6**, 6438 (2015)

[76] S. Gerber, H. Jang, H. Nojiri, "Three-dimensional charge density wave order in $YBa_2Cu_3O_{6.67}$ at high magnetic fields", *Science* **350** (6263), 949 (2015)

[77] S. Caprara, M. Grilli, J. Lorenzana, B. Leridon, "Doping-dependent competition between superconductivity and polycrystalline charge density waves", *SciPost Phys.* **8**, 003 (2020)

[78] B. Leridon, S. Caprara, J. Vanacken, *et al.* "Protected superconductivity at the boundaries of charge-density-wave domains", *New Journ. of Phys.* **22** (7), 073025 (2020)

[79] Q. Chena, J. Stajicb, S. Tanb, K. Levin, "BCS-BEC crossover: From high temperature superconductors to ultracold superfluids", *Phys. Rep.* **412**, 1 (2005)

[80] R. Hlubina, T. M. Rice, "Resistivity as a function of temperature for models with hot spots on the Fermi surface", *Phys. Rev. B* **51**, 9253 (1995)

[81] G. Seibold, R. Arpaia, Y. Y. Peng, *et al.* "Strange metal behaviour from charge density fluctuations in cuprates", *Comm. Phys.* **4**, 7 (2021)

[82] P. Nozières, *Theory of Interacting Fermi Systems*, Perseus (1997)

[83] G. Baym, C. Pethick, *Landau Fermi-Liquid Theory*, Wiley-Interscience (1992)

[84] A. A. Abrikosov, L. P. Gorkov, I. E. Dzyaloshinski, *Methods of Quantum Field Theory in Statistical Physics*, Dover Pubns (1975)

[85] M. Fabrizio, *A Course in Quantum Many-body Theory*, Springer Nature (2022)

[86] R. de L. Kronig, "On the theory of the dispersion of X-rays", *J. Opt. Soc. Am.* **12** (6), 547 (1926)

[87] H. A. Kramers, "La diffusion de la lumière par les atomes", *Atti Cong. Intern. Fisici, (Transactions of Volta Centenary Congress) Como* **2** 545 (1927)

[88] A. C. Pipkin, *A Course on Integral Equations (Texts in Applied Mathematics, 9)*, Springer Nature (1991)

[89] J. Huang, T. Timusk, G. D. Gu, "High transition temperature superconductivity in the absence of the magnetic resonance mode", *Nature* **427**, 714 (2004)

[90] C. Castellani, C. Di Castro, M. Grilli, "Non-Fermi-liquid behavior and d-wave superconductivity near the charge-density-wave quantum critical point", *Z. Phys. B* **103**, 137 (1996)

[91] S. Andergassen, S. Caprara, C. Di Castro, M. Grilli, "Anomalous Isotopic Effect Near the Charge-Ordering Quantum Criticality", *Phys. Rev. Lett.* **87**, 056401 (2001)

[92] S. Caprara, C. Di Castro, G. Seibold, M. Grilli, "Dynamical charge density waves rule the phase diagram of cuprates", *Phys. Rev. B* **95**, 224511 (2017)

[93] M. E. Fisher, "Correlation Functions and the Critical Region of Simple Fluids", *J. Math. Phys.* **5**, 944 (1964)

[94] S. T. Carr, *Quantum Field Theory II: An introduction to Feynman diagrams*, A course for MPAGS, University of Birmingham (2009)

[95] G. Mazza, M. Grilli, C. Di Castro, *et al.* "Evidence for phonon-like charge and spin fluctuations from an analysis of angle-resolved photoemission spectra of $La_{2-x}Sr_xCuO_4$ superconductors", *Phys. Rev. B* **87**, 014511 (2021)

[96] G. Mirarchi, G. Seibold, C. Di Castro, *et al.* "The Strange-Metal Behavior of Cuprates", *Condens. Matter* **7**, 29 (2022)

[97] J. M. Luttinger, "Theory of Thermal Transport Coefficients", *Phys. Rev.* **135**, A1505 (1964)

[98] G. D. Mahan, *Many-Particle Physics (3rd edition)*, Springer (2000)

[99] J. J. Sakurai, J. Napolitano, *Modern Quantum Mechanics (2nd edition)*, Cambridge University Press (2017)

[100] R. Kubo, "Statistical-Mechanical Theory of Irreversible Processes. I. General Theory and Simple Applications to Magnetic and Conduction Problems", *J. Phys. Soc. Jpn.* **12** (6), 570 (1957)

[101] R. Kubo, M. Yokota, S. Nakajima, "Statistical-Mechanical Theory of Irreversible Processes. II. Response to Thermal Disturbance", *J. Phys. Soc. Jpn.* **12** (11), 1203 (1957)

[102] L. Onsager, "Reciprocal Relations in Irreversible Processes. I.", *Phys. Rev.* **37**, 405 (1931)

[103] R. K. Pathria, P. D. Beale, *Statistical Mechanics (3rd edition)*, Academic Press (2011)

[104] K. R. Symons, *Mechanics (3rd edition)*, Addison-Wesley (1971)

[105] P. L. Bhatnagar, E. P. Gross, M. Krook, "A Model for Collision Processes in Gases. I. Small Amplitude Processes in Charged and Neutral One-Component Systems", *Phys. Rev.* **94**, 511 (1954)

[106] J. L. Anderson, H. R. Witting, "A relativistic relaxation-time model for the Boltzmann equation", *Physica* **74** (3), 466 (1974)

[107] J. W. Negele, H. Orland, *Quantum Many-particle Systems*, Perseus (1998)

[108] G. M. Eliashberg, "Interactions between electrons and lattice vibrations in a superconductor", *Sov. Phys. JETP* **11**, 696 (1960)

[109] S. Zhang, E. Berg, A. V. Chubukov, "Free energy and specific heat near a quantum critical point of a metal", *Phys. Rev. B* **107**, 144507 (2023)

[110] C. M. Varma, Z. Nussinov, W. van Saarloos, "Singular or non-Fermi liquids", *Physics Reports* **361**, 267 (2002)

[111] G. Mirarchi, M. Grilli, G. Seibold, *et al.* "The Shrinking Fermi Liquid Scenario for Strange-Metal Behavior from Overdamped Optical Phonons", *Condens. Matter* **9** (1), 14 (2024)

[112] S. Engelsberg, J. R. Schrieffer, "Soupled Electron-Phonon System", *Phys. Rev.* **131**, 993 (1963)

[113] C. M. Varma, P. B. Littlewood, S. Schmitt-Rink, *et al.* "Phenomenology of the Normal State of Cu-O High-Temperature Superconductors", *Phys. Rev. Lett.* **64**, 497 (1990)

[114] B. Michon, C. Berthod, C. W. Rischau, *et al.* "Reconciling scaling of the optical conductivity of cuprate superconductors with Planckian resistivity and specific heat", *Nature Communications* **14**, 3033 (2023)

[115] S. Caprara, C. Di Castro, G. Mirarchi, *et al.* "Dissipation-driven strange metal behavior", *Comm. Phys.* **5**, 10 (2022)

[116] W. Meevasana, X. J. Zhou, S. Sahrakorpi, *et al.* "Hierarchy of multiple many-body interaction scales in high-temperature superconductors", *Phys. Rev. B* **75**, 174506 (2007)

[117] J. M. Bernardo, "Algorithm AS 103 psi(digamma function) computation", *Applied Statistics* **25**, 315 (1976)

[118] J. C. Ward, "An Identity in Quantum Electrodynamics", *Phys. Rev.* **78** (2), 182 (1950)

[119] Y. Takahashi, "On the Generalized Ward Identity", *Il Nuovo Cimento* **6** (2), 371 (1957)

[120] P. B. Allen, "Electron self-energy and generalized Drude formula for infrared conductivity of metals", *Phys. Rev. B* **92**, 054305 (2015)

[121] N. Biškup, S. Das, J. M. Gonzalez-Calbet, *et al.* "Atomic-resolution studies of epitaxial strain release mechanisms in $La_{1.85}Sr_{0.15}CuO_4$/ $La_{0.67}Ca_{0.33}MnO_3$ superlattices", *Phys. Rev. B* **91**, 205132 (2015)

[122] M. Dragomir, Q. Ma, J. P. Clancy, *et al.* "Materials preparation, single-crystal growth, and the phase diagram of the cuprate high-temperature superconductor $La_{2-x}Sr_xCuO_4$", *Phys. Rev. Materials* **4**, 114801 (2020)

[123] M. Horio, K. Hauser, Y. Sassa, *et al.* "Three-Dimensional Fermi Surface of Overdoped La-Based Cuprates", *Phys. Rev. Lett.* **121**, 077004 (2018)

[124] L. Gurevich, "Thermoelectric properties of conductors. I.", *J. Phys.* **9**, 477 (1945)

[125] L. Gurevich, "Thermoelectric properties of conductors. II.", *J. Phys.* **10**, 67 (1946)

[126] R. J. Hardy, "Energy-Flux Operator for a Lattice", *Phys. Rev.* **132**, 168 (1963)

[127] L. G. MacDowell, "On the calculation of the frequency sum rules of the heat flux correlation function", *Mol. Phys.* **96**, 881 (1999)

[128] C. Carbogno, R. Ramprasad, M. Scheffler, "*Ab Initio* Green-Kubo Approach for the Thermal Conductivity of Solids", *Phys. Rev. Lett.* **118**, 175901 (2017)

[129] E. Helfand, "Transport Coefficients from Dissipation in a Canonical Ensemble", *Phys. Rev.* **119**, 1 (1960)

[130] P. L. Taylor, O. Heinonen *A Quantum Approach to Condensed Matter*, Cambridge University Press (2002)

[131] A. Georges, J. Mravlje, "Skewed non-Fermi liquids and the Seebeck effect", *Phys. Rev. Research* **3**, 043132 (2021)

[132] M. Cutler, N. F. Mott, "Observation of Anderson Localization in an Electron Gas", *Phys. Rev.* **181**, 1336 (1969)

[133] I. I. Hanna, E. H. Sondheimer, "Electron and lattice conduction in metals", *Proc. R. Soc. Lond. A* **239** 247 (1957)

[134] J. Ziman, "The thermoelectric power of the alkali metals at low temperatures", *Phil. Mag.* **4**, 371 (1959)

[135] G. Mirarchi, G. Seibold, C. Di Castro, *et al.* "Anomalous thermopower from the drag of overdamped collective modes", in preparation.

[136] K. Baumann, "Quantum theory of transport coefficients. II", *Ann. of Phys.* **23** (2), 221-232 (1963)

[137] R. Peierls, "Zur kinetischen Theorie der Wärmeleitung in Kristallen", *Annalen der Physik* **395** (8), 1055 (1929)

[138] G. Grissonnanche, Y. Fang, A. Legros, *et al.* "Linear-in temperature resistivity from an isotropic Planckian scattering rate", *Nature* **595**, 667-672 (2021)

[139] E. Abrahams, C. M. Varma, "What angle-resolved photoemission experiments tell about the microscopic theory for high-temperature superconductors", *Proc. Natl Acad. Sci. USA* **97**, 5714-5716 (2000)

[140] G. Mirarchi, S. Caprara, M. Grilli *et al.* "Linear magnetoresistance induced by local impurity scattering in cuprates", in preparation.

[141] R. G. Chambers, "The Kinetic Formulation of Conduction Problems", *Proc. Phys. Soc. A* **65**, 458 (1952)

[142] M. Grilli, C. Di Castro, G. Mirarchi, *et al.* "Dissipative Quantum Criticality as a Source of Strange Metal Behavior", *Symm.* **15** (3), 569 (2023)

[143] S. R. Finch, *Mathematical Constants*, Cambridge University Press (2003)

[144] G. Mirarchi, R. Arpaia, E. Wahlberg, *et al.* "Tuning the ground state of cuprate high-critical-temperature superconducting thin films by nanofaceted substrates", arXiv:2306.12335 [cond-mat.supr-con] (2023)

[145] B. Velický, S. Kirkpatrick, H. Ehrenreich, "Single-Site Approximations in the Electronic Theory of Simple Binary Alloys", *Phys. Rev.* **175**, 747 (1968)

[146] F. Yonezawa, K. Morigaki, "Coherent Potential Approximation. Basic concepts and applications", *Prog. of Theor. Phys. Suppl.* **53**, 1 (1973)

[147] A. Perali, A. Bianconi, A. Lanzara, N. L. Saini, "The gap amplification at a shape resonance in a superlattice of quantum stripes: a mechanism for high T_c", *Solid State Commun.* **100**, 181 (1996)

[148] A. Bianconi, A. Valletta, A. Perali, N. L. Saini, "High-T_c superconductivity in a superlattice of quantum stripes", *Solid State Commun.* **102**, 369 (1997)

[149] A. Valletta, A. Bianconi, A. Perali, N. L. Saini, "Electronic and superconducting properties of a superlattice of quantum stripes at the atomic limit", *Z. Physik B - Condensed Matter* **104**, 707 (1997)

[150] A. Bianconi, A. Valletta, A. Perali, N. L. Saini, "Superconductivity of a striped phase at the atomic limit", *Physica C: Superconductivity* **296**, 269 (1998)

[151] D. Innocenti, N. Poccia, A. Ricci, *et al.* "Resonant and crossover phenomena in a multiband superconductor: tuning the chemical potential near a band edge", *Phys. Rev. B* **82**, 184528 (2010)

[152] D. Innocenti, S. Caprara, N. Poccia, *et al.* "Shape resonance for the anisotropic superconducting gaps near a Lifshitz transition: the effect of electron hopping between layers", *Supercond. Sci. Technol.* **24**, 015012 (2010)

[153] A. Bianconi, "Shape resonances in superstripes", *Nat. Phys.* **9**, 536 (2013)

[154] A. Bianconi, "Superconductivity in Quantum Complex Matter: the Superstripes Landscape", *J. Supercond. Nov. Magn.* **33**, 2269 (2020)

[155] H. Bruus, K. Flensberg, *Many-Body Quantum Theory in Condensed Matter Physics*, Cambridge University Press (2004)

[156] H. P. Breuer, F. Petruccione *The Theory of Open Quantum Systems*, OUP Oxford (2002)

[157] A. Altland, B. D. Simons, *Condensed Matter Field Theory (2nd edition)*, Cambridge University Press (2010)

[158] D. Tong, *Kinetic Theory*, University of Cambridge Graduate Course (2012)

[159] I. S. Gradshteyn, I. M. Ryzhik, *Table of Integrals, Series, and Products (7th edition)*, Academic Press (2007)

[160] E. T. Whittaker, G. N. Watson, *A Course of Modern Analysis (3rd edition)*, Dover Pubns (2020)

Acknowledgments

First of all, the author wants to express his deepest gratitude towards Sergio Caprara, for having followed his Ph.D. path with attention and dedication. The author also thanks Marco Grilli for always being present in this path, and Götz Seibold for all the precious help he gave. Thanks also to Carlo Di Castro for stimulating discussions.

Moreover, the author warmly thanks Sabine Andergassen and Andrea Perali for appreciating his work and for their precious comments and suggestions.

Finally, the author acknowledges financial support from the "Ateneo Research Projects" of "La Sapienza" University of Rome: "Competing phases and non-equilibrium phenomena in low-dimensional systems with microscopic disorder and nanoscale inhomogeneities" (grant n. RM12117A4A7FD11B), "Models and theories from anomalous diffusion to strange-metal behavior" (grant n. RM12218162CF9D05) and "Non-conventional aspects for transport phenomena and non-equilibrium statistical mechanics" (grant n. RM123188E830D258).

Acknowledgments (Another One With Love)

It's not the first time I've had to write a thesis, but without a doubt the work I had to do this time was much more challenging than what I've done in the past. Organizing and coherently displaying the material I produced in my first three years of research was definitely not an easy job. I had a lot of things to say, but deciding exactly what to say and what was the best way to do it paralyzed me more than once during the writing phase. Despite having accomplished this task, now that I find myself writing the acknowledgments I feel that I'm having a completely similar experience. Once again, I feel like I have so many things to say but I don't really know where to start, or exactly what to say. Undoubtedly, these last three (and a half) years that I have spent have been among the most intense and eventful of my entire life so far, also (and especially) beyond the academic sphere, and the heritage they left me is priceless. I think it is important that I do my best even in writing these last pages, as I am aware that these years would not have been the same without all the beautiful people who have stood by me.

Perhaps the most logical choice is to start by thanking my family from the bottom of my heart, for giving me their greatest support in everything I have done, and for never letting me lack anything. I would like to express special thanks to my sister Marta, for being the best sister and friend I could wish for. I know it sounds quite weird in English, but know that I love you. Of course, my lovely cats are included as a part of the family.

I also want to thank my added family, made up of my closest friends, both "historical" and more recent ones. I would like to start by thanking the "Pern Maiden" group, made up of Adriano Testa, Alessandro Cancellieri, Edoardo Mollica, Filippo Sacco, Lorenzo Remigi, Ludovico Sulpizii and Ugo Sofia, for being a solid presence in my life that I could always count on, and for all the beautiful moments and emotions we shared. Furthermore, I thank the group of friends that I share with my sister and that I met thanks to her, in particular Flavio Simoncini, Lorenzo Quarta, Marco Martinelli, Matteo Amororso, Matteo Pazzini and Tiziano Lupi. Thank you for making me feel part of the family straight away, and for being close to me in the last part of my path. I would also like to thank Alessio Masturzi and Francesca Ballarini, two very long-time friends with whom I have been lucky enough to never lose contact until today. I thank my dear friend Giulia Maniccia with whom I shared my university journey from the beginning up to this moment. Thank you for always being by my side and for helping me in the moments when I needed it, my whole university experience would have been very different without you. I also wish to thank Arianna Paolini, even though we have only known each other for a short time. Thank you for giving me a reason to actively dedicate myself to music (again) and for making me rediscover the beauty of sharing music with someone with whom you feel a strong musical affinity.

At this point I would like to thank, once again, the research group I have worked with during these years. In particular, I warmly thank my professor Sergio Caprara, not only for following my work with care and patience, but above all for always supporting me and making me feel at ease in the most delicate moments of my Ph.D. path (and even before). I feel so lucky to have had someone like you as Thesis Director.

Finally, it seems appropriate to mention a fundamental element in my university and doctoral experience, as well as in my whole life: Music. All the work I have done that has allowed me to get this far has been constantly accompanied by listening to meticulously chosen albums, many of which still occupy a special place in my heart. I can't imagine how different my Ph.D. journey would have been without the beneficial presence of music in my ears. An exhaustive list of the artists, as well as their staff, that I feel the need to thank is unfortunately too long to include here, and I honestly don't like the idea of selecting just a few of them by way of example. Although none of you will ever read these words, I would like to take this opportunity to tell you that each of you has improved the quality of my life and, in some way, has changed this very life of mine. I am and I will be forever grateful.

Okay... at this point, I'm probably supposed to end this section with some catchphrase or similar, and unfortunately I'm pretty bad at this stuff. I would just like to add that this important step was another opportunity to stop for a moment, take a deep breath and think about where I am now, who is around me and what I have with me. Although I still have quite a few doubts about my life and my future, one of my few certainties is the love of the people who are beside me in this particular phase of my life. I feel so lucky to have found these wonderful souls in my life's journey so far, and to still have them by my side. I love all of you.